

UC San Diego

UC San Diego Electronic Theses and Dissertations

Title

Characterizing the influence of iron on the cellular processes of marine phytoplankton

Permalink

<https://escholarship.org/uc/item/41h9v2n4>

Author

Coale, Tyler

Publication Date

2020

Peer reviewed|Thesis/dissertation

UNIVERSITY OF CALIFORNIA SAN DIEGO

Characterizing the influence of iron on the cellular processes of marine
phytoplankton

A dissertation submitted in partial satisfaction of the requirements for the degree
Doctor of Philosophy

in

Marine Biology

By

Tyler Hamilton Coale

Committee in Charge:

Professor Andrew Allen, Chair

Professor Katherine Barbeau

Professor Mark Ellisman

Professor Michael Landry

Professor Brian Palenik

2020

Copyright

Tyler Hamilton Coale, 2020

All rights reserved.

The dissertation of Tyler Hamilton Coale is approved, and it is acceptable in quality and form for publication on microfilm and electronically:

Chair

University of California San Diego

2020

DEDICATION
For my family.

TABLE OF CONTENTS

SIGNATURE PAGE	iii
DEDICATION	iv
TABLE OF CONTENTS	v
LIST OF FIGURES	ix
LIST OF TABLES	xii
ACKNOWLEDGEMENTS	xiii
VITA.....	xvi
ABSTRACT OF THE DISSERTATION	xvii
CHAPTER 1: A DIVERSITY OF RESPONSES TO IRON AVAILABILITY BY PHYTOPLANKTON OF THE CALIFORNIA CURRENT ECOSYSTEM	1
1.1 ABSTRACT	2
1.2 INTRODUCTION	3
1.3 METHODS.....	19
1.3.1 Experimental design.....	19
1.3.2 Sampling and incubations.....	20
1.3.3 RNA extraction, cDNA synthesis, PCR, library preparation, and sequencing.....	20
1.3.4 Chlorophyll	23
1.3.5 Pigments	23
1.3.6 Flow cytometry	24
1.3.7 Dissolved iron measurements.....	24
1.3.8 Macronutrients.....	25
1.3.9 POC/PON	25
1.4 RESULTS AND DISCUSSION.....	26
1.4.1 Oceanographic setting.....	26
1.4.2 Coastal DCM diatoms.....	30
1.4.3 Transition DCM <i>Pelagomonas calceolata</i>	32

1.4.4 Transition DCM <i>Bathycoccus prasinos</i>	34
1.4.5 Transition DCM <i>Phaeocystis</i>	36
1.4.6 Offshore <i>Prochlorococcus</i>	37
1.4.7 pTF expression.....	40
1.4.8 Phytoplankton diversity in an anomalous year.....	43
1.5 CONCLUSIONS.....	46
1.6 FIGURES AND TABLES.....	50
1.7 ACKNOWLEDGEMENTS.....	82
1.8 REFERENCES.....	82
CHAPTER 2: IRON/LIGHT CO-LIMITATION IN A GLOBALLY SIGNIFICANT PELAGOPHYTE.....	102
2.1 ABSTRACT.....	103
2.2 INTRODUCTION.....	104
2.3 METHODS.....	110
2.3.1 Low iron culturing.....	110
2.3.2 Transcriptomics.....	111
2.3.3 Proteomics.....	112
2.3.4 Photophysiology.....	117
2.3.5 Cell counts.....	118
2.3.6 Carbon and nitrogen cellular quotas.....	118
2.3.7 Chlorophyll measurements.....	118
2.3.8 Inductively coupled plasma mass spectrometry.....	118
2.4 RESULTS AND DISCUSSION.....	119
2.4.1 Low iron physiology of <i>P. calceolata</i>	119
2.4.2 Transcriptomic analysis.....	122
2.4.3 Proteomic analysis.....	129
2.5 CONCLUSIONS.....	134

2.6 FIGURES.....	138
2.7 ACKNOWLEDGEMENTS.....	161
2.8 REFERENCES	161
CHAPTER 3: REDUCTION-DEPENDENT SIDEROPHORE ASSIMILATION IN A MODEL PENNATE DIATOM	176
3.1 ABSTRACT	177
3.2 SIGNIFICANCE.....	178
3.3 INTRODUCTION	178
3.4 MATERIALS AND METHODS	187
3.4.1 Gene knockouts, fusion proteins and complementation	187
3.4.2 Low iron culturing.....	189
3.4.3 Iron speciation calculations	190
3.4.4 Growth rates	191
3.4.5 Benthic boundary layer	191
3.4.6 Iron uptake assays	192
3.4.7 Ga siderophore analogs.....	192
3.4.8 Ferric reductase activity	193
3.4.9 Phylogenetics.....	194
3.5 RESULTS	195
3.5.1 Knockout growth curves.....	195
3.5.2 Localizations.....	197
3.5.3 Iron uptake rates.....	197
3.5.4 Growth rates in natural seawater	198
3.5.5 Gallium uptake rates.....	199
3.5.6 Ferric reductase activity	200
3.5.7 Phylogenetic analysis.....	200
3.6 DISCUSSION.....	202
3.6.1 Advantages of direct siderophore uptake	202

3.6.2 Reduction matters	204
3.6.3 Roles of uptake proteins in accessing environmentally significant iron sources	209
3.6.4 Origin of siderophore acquisition proteins in diatoms	210
3.7 CONCLUSIONS	213
3.8 FIGURES AND TABLES	215
3.9 ACKNOWLEDGEMENTS	232
3.10 REFERENCES	233

LIST OF FIGURES

Figure 1.1: Experimental design of <i>in situ</i> array incubation experiments.	53
Figure 1.2: Average satellite derived sea surface chlorophyll and temperature measurements from August 2014 obtained from the NASA MODIS spectroradiometer.....	54
Figure 1.3: Vertical profiles of fluorescence derived chlorophyll, temperature and salinity.....	55
Figure 1.4: Ratios of pigments to chlorophyll a in surface seawater at each station.....	56
Figure 1.5: Pigment-based taxonomy based on HPLC pigment data.....	57
Figure 1.6: Size-fractionated chlorophyll measurements.....	58
Figure 1.7: Abundances of <i>Prochlorococcus</i> , <i>Synechococcus</i> , and picoeukaryotes measured by flow cytometry.....	59
Figure 1.8: Particulate organic carbon (POC), particulate organic nitrogen (PON), and particulate C:N ratios for each station.....	60
Figure 1.9: Average proportions of mRNA reads attributed to different eukaryotic groups from all incubation samples collected from each station.....	61
Figure 1.10: Transcriptional response of centric diatoms in the coastal DCM.....	62
Figure 1.11: Transcriptional response of pennate diatoms in the coastal DCM...	64
Figure 1.12: Average proportion of mRNA assigned to phytoplankton taxonomic groups for each station and depth	66
Figure 1.13: Transcriptional response of <i>P. calceolata</i> in the transition DCM.....	67
Figure 1.14: Transcriptional response of <i>B. prasinos</i> in the transition DCM	69
Figure 1.15: Phytotransferrin (pTF) expression at CCE stations	71
Figure 1.16: Transcriptional response of <i>Phaeocystis</i> in the transition DCM.....	72
Figure 1.17: Average percentage of <i>Prochlorococcus</i> counts attributed to high light or low light adapted ecotypes in all samples from the offshore station	74
Figure 1.18: Transcriptional response of low light adapted <i>Prochlorococcus</i> ecotypes in the offshore DCM.....	75
Figure 1.19: Transcriptional response of high light adapted <i>Prochlorococcus</i> ecotypes in the offshore surface.....	77
Figure 1.20: Comparison of molecular based diversity metrics	79

Figure 1.21: Average relative 16S amplicon abundance in all samples from all depths and stations.	80
Figure 1.22: Conceptual diagram showing partitioning of phytoplankton ecotypes across the cross shelf gradients of the CCE.....	81
Figure 2.1: Experimental design of Fe/light co-limitation experiment	138
Figure 2.2: Cellular quotas at the three major time points for carbon, nitrogen, chlorophyll a, and Fe.....	139
Figure 2.3: Ratios of nitrogen, chlorophyll a, and Fe to carbon at the three major time points	140
Figure 2.4: Ratios of chlorophyll a to iron, cellular copper quotas, and ratios of copper to carbon at the three major time points.....	141
Figure 2.5: Principal component analysis plot of <i>P. calceolata</i> transcriptomes	142
Figure 2.6: Heatmap showing average standardized transcript abundance of photosynthesis related genes across the diel cycle	143
Figure 2.7: Heatmap showing average standardized transcript abundance of nitrogen metabolism, respiration, ribosome and iron-related related genes across the diel cycle.....	145
Figure 2.8: Dynein, kinesin and myosin motor protein gene expression across all conditions and time points	147
Figure 2.9: Glycolysis gene expression across all conditions and time points.....	149
Figure 2.10: Principal component analysis plot of <i>P. calceolata</i> proteomes.....	150
Figure 2.11: Scaled abundance of photosynthetic proteins.....	151
Figure 2.12: Scaled abundance of nitrogen metabolism proteins	153
Figure 2.13: Scaled abundance of iron-sensitive proteins.....	154
Figure 2.14: Scaled abundance of iron transport and storage related proteins	156
Figure 2.15: Global proteomic response of <i>P. calceolata</i> to iron starvation at high light and low light	157
Figure 2.16: Iron and light induced state changes in the cellular functioning of <i>P. calceolata</i>	159
Figure 3.1: Growth of WT, Δ FRE2 and Δ FBP1 <i>P. tricornutum</i> cells in low iron Aquil media.....	217
Figure 3.2: Complementation and localization	218

Figure 3.3: Short term iron uptake rates in Aquil media	219
Figure 3.4: Iron uptake rates from enterobactin in Aquil media	220
Figure 3.5: Specific growth rates of diatom cultures in natural seawater.....	221
Figure 3.6: Results of short-term uptake experiments and ferric reductase activity assays	222
Figure 3.7: Bayesian phylogenetic tree of FBP1 and homologs, with functional annotations	223
Figure 3.8: Bayesian phylogenetic tree of FBP1 and homologs.....	224
Figure 3.9: Bayesian phylogenetic tree of FRE2 and homologs.....	225
Figure 3.10: Alignment of <i>P. tricornutum</i> ferric reductase genes with human NOX2	227
Figure 3.11: Growth of WT and Δ FRE1 <i>P. tricornutum</i> cells in low iron Aquil media	228
Figure 3.12: Iron uptake of WT and Δ FRE1 <i>P. tricornutum</i> cells in low iron Aquil media	229
Figure 3.13: Iron uptake experiments with the Fe(II) trapping agent Ferrozine...230	
Figure 3.14: Proposed model of iron uptake in <i>P. tricornutum</i>	231

LIST OF TABLES

Table 1.1. Nitrate, phosphate, silicic acid and dissolved iron measured in surface and deep chlorophyll maximum seawater 50

Table 1.2. Comparison of average percentages of mRNA (eukaryotes only), 18Sv4 and 18Sv9 taxonomy estimates 51

Table 1.3. Comparison of estimates of *Prochlorococcus* and *Synechococcus* contributions to community composition 52

Table 3.1. *P. tricornutum* knockout cell lines 215

Table 3.2. *P. tricornutum* ferric reductase genes 216

ACKNOWLEDGEMENTS

Chapter one is currently being prepared for submission for publication of the material. Coale, T., Ruacho, A., Manck, L., Forsch, K., Barbeau, K., and Allen, A. A diversity of responses to iron availability by phytoplankton of the California Current ecosystem. The dissertation author was the primary investigator and author of this paper. Funding for chapter one was provided by the National Science Foundation, United States Department of Energy, The Gordon and Betty Moore Foundation. Thanks to the California Current Ecosystem Long Term Ecological Research site and the California Cooperative Oceanic Fisheries Investigation. Special thanks to the captain and crew of the *R/V Melville* and chief scientist Michael Landry. Thanks to Angel Ruacho and Lauren Manck for assistance with sampling, and Michael Stukel for array deployments. Many thanks to Bethany Kolody for programming expertise and Ariel Rabines for amplicon data analysis. Ralf Goericke provided pigment-based taxonomy estimates. Finally, thanks to Hong Zheng for her magic touch in preparing cDNA libraries.

Chapter two is currently being prepared for submission for publication of the material. Coale, T., Tan, M., Venepally, P., Rowland, E., Bertrand, E., and Allen, A. Iron/light co-limitation in a globally significant pelagophyte. The dissertation author was the primary investigator and author of this paper. Thanks to Hong Zheng for assistance with RNA and protein sample preparation, Maxine Tan for late night sampling heroics and Rob Franks for expert operation of the

ICP-MS at the University of California, Santa Cruz Marine Analytical Laboratory. Also to Pratap Venepally for assistance developing gene models, assembling and annotating transcriptomes.

Chapter three, in full, is a reprint of previously published material in Proceedings of the National Academy of Sciences of the United States of America Coale, T. H., Moosburner, M., Horák, A., Oborník, M., Barbeau, K. A., & Allen, A. E. (2019). Reduction-dependent siderophore assimilation in a model pennate diatom. The dissertation author was the primary investigator and author of this paper. Many thanks to Jeff McQuaid for ISIP2a TALEN plasmids and Maxine Tan for help with plasmid design. Miroslav Oborník and Ales Horák generated phylogenies, and Mark Moosburner designed CRISPR-Cas9 constructs. Kathy Barbeau helped immeasurably with experimental design, interpretation of results and writing. Thanks to UC Ship Funds for supporting BBL field work, the captain and crew of *R/V Sally Ride*, chief scientist Angel Ruacho, Kayleen Fulton for sampling assistance, and Kiefer Forsch for dissolved iron measurements. Additional thanks to Vince Bielinski for conjugation plasmids, Rob Franks for assistance with ICP-MS analyses, Randelle Bundy and *R/V Kilo Moana* personnel for Stn ALOHA water collection, and Jia Jia Zhang for *Salinispora* cultures. This study was supported by National Science Foundation (NSF-OCE-1756884, NSF-OCE-1756860, and NSF-MCB-1818390), United States Department of Energy Genomics Science program (DE-SC0018344), and Gordon and Betty

Moore Foundation (GBMF3828 and GBMF5006) grants to A.E.A., and the Czech Science Foundation, project 15-17643S (M.O. and A.H.).

VITA

2009: Bachelor of Science, University of California Santa Cruz

2020: Doctor of Philosophy, Scripps Institution of Oceanography,
University of California San Diego

PUBLICATIONS

Coale, T. H., Moosburner, M., Horák, A., Oborník, M., Barbeau, K. A., & Allen, A. E. (2019). Reduction-dependent siderophore assimilation in a model pennate diatom. *Proceedings of the National Academy of Sciences*, *116*(47), 23609-23617.

Till, C. P., Solomon, J. R., Cohen, N. R., Lampe, R. H., Marchetti, A., **Coale, T. H.**, & Bruland, K. W. (2019). The iron limitation mosaic in the California Current System: Factors governing Fe availability in the shelf/near-shelf region. *Limnology and Oceanography*, *64*(1), 109-123.

Boiteau, R. M., Till, C. P., **Coale, T. H.**, Fitzsimmons, J. N., Bruland, K. W., & Repeta, D. J. (2019). Patterns of iron and siderophore distributions across the California current system. *Limnology and Oceanography*, *64*(1), 376-389.

Biller, D. V., **Coale, T. H.**, Till, R. C., Smith, G. J., & Bruland, K. W. (2013). Coastal iron and nitrate distributions during the spring and summer upwelling season in the central California Current upwelling regime. *Continental Shelf Research*, *66*, 58-72.

Coale, T. H., Deveny, A. J., & Fox, L. R. (2011). Growth, fire history, and browsing recorded in wood rings of shrubs in a mild temperate climate. *Ecology*, *92*(5), 1020-1026.

ABSTRACT OF THE DISSERTATION

Characterizing the influence of iron on the cellular processes of marine
phytoplankton

by

Tyler Hamilton Coale

Doctor of Philosophy in Marine Biology

University of California San Diego, 2020

Professor Andrew E. Allen, Chair

Vanishingly low concentrations of iron in the sunlit surface ocean are one of the greatest challenges to marine phytoplankton which rely on this element to perform photosynthesis. The impacts of iron limitation are observed across the world's oceans and are imprinted in the genomes of photoautotrophic organisms. In chapter one, I present observations of native phytoplankton assemblages in the California Current ecosystem and characterize their molecular strategies for persisting in low and/or variable iron environments. I contrast the strategies of tiny cyanobacteria and picoeukaryotic phytoplankton with those of diatoms, which are considered keystone species in iron limited regions. These new insights into gene expression by the primary producing inhabitants of California current ecosystem reveal metabolic tactics which help determine gradients in community structure across the region.

In chapter two I subject the pelagophyte *Pelagomonas calceolata* to physiological, transcriptomic and proteomic scrutiny under a range of iron and light conditions. *P. calceolata* is globally distributed, tolerates low iron remarkably well, and is one of the most numerically abundant eukaryote species on the planet. This study is the first to sequence either transcriptomes or proteomes from *P. calceolata*, and revealed are novel utilization of motility and mixotrophy in response to impaired photosynthetic capabilities. Low iron/low light adaptations in this organism have consequences for marine ecosystems and biogeochemical cycles.

Chapter three investigates specific iron acquisition proteins in the model pennate diatom *Phaeodactylum tricornutum*. I used reverse genetics techniques to demonstrate that a siderophore assimilation pathway exists in diatoms, separate from other iron acquisition mechanisms. I characterize the substrate specificity of this system and its role in the marine environment. The proteins involved arrived in *P. tricornutum* as a result of different evolutionary histories. I show a prokaryotic receptor protein and a eukaryotic reductase working together to acquire organically complexed iron, survey their occurrence across diatom genomes, discuss the implication of this system for microbial interactions and refine our mechanistic understanding of iron acquisition in important marine primary producers.

**CHAPTER 1: A diversity of responses to iron availability by phytoplankton of the
California Current ecosystem**

1.1 ABSTRACT

Coastal upwelling injects significant nutrients into California's nearshore marine environment in a sporadic manner, which are subsequently advected offshore through a system of filaments and eddies. This imparts spatial and temporal heterogeneity to primary production by phytoplankton communities and leads to successional community dynamics as nutrient concentrations change quickly, favoring different functional groups. As nutrients are consumed, coastal diatom dominated communities yield to picoeukaryotes, which are then displaced by *Synechococcus*, and finally *Prochlorococcus* offshore in the California Current. Limitation in the supply of bioavailable iron can exert significant bottom-up pressure across the region and elicits a variety of physiological responses from phytoplankton. These can include upregulation of iron acquisition proteins, substitution of iron-containing proteins with iron-free alternatives, modification of carbon and nitrogen metabolisms, and remodeling of the photosynthetic apparatus. We profiled these responses using metatranscriptomics from ambient seawater samples and *in situ* drifting iron and chelator addition experiments performed in 2014 across gradients in iron and macronutrient concentrations. Our results highlight the diverse strategies employed by the dominant phytoplankton

groups to mitigate iron stress and respond to iron inputs in different oceanographic settings within the California Current ecosystem.

1.2 INTRODUCTION

The California Current ecosystem (CCE) entails the marine environment delineated to the east by the North American coastline and to the west by the offshore edge of the California Current. As this eastern boundary current extends from southern British Columbia to the southern end of the Baja California Peninsula, the true extent CCE is substantial; roughly 3000 kilometers long by 350 kilometers wide. The bulk of the oceanographic research conducted within the CCE has taken place off California in the region between the Scripps Institution of Oceanography's Ellen Browning Scripps Memorial Pier in La Jolla and Cape Mendocino in Humboldt County. This region has been surveyed regularly since 1949 by the California Cooperative Oceanic Fisheries Investigation timeseries (CalCOFI) (Bograd & Lynn, 2003) which is partnership between Scripps Institution of Oceanography, NOAA Fisheries and California Department of Fish and Wildlife. In 2004 the CCE Long Term Ecological Research (LTER) site was established which supports and expands on the CalCOFI mission and the region is also surveyed by periodic research expeditions external to timeseries programs. Given the history and breadth of research conducted, the CCE qualifies as one of the world's best characterized coastal upwelling biome.

Along the California coast, prevailing equator-ward winds drive extensive coastal upwelling in the spring and summer seasons (Checkley et al., 2009) which can result in surface mixed layer nitrate concentrations exceeding 25 μM (Biller et al., 2013). Nutrient-rich freshly upwelled seawater is also characterized by low temperature ($< 12^\circ \text{C}$), high salinity, high pCO_2 , low chlorophyll concentrations and low phytoplankton biomass (Bruland et al., 2001). As this water arrives in the euphotic zone, light limitation of phytoplankton growth is relieved, and photosynthesis commences. This requires the rapid assimilation of inorganic nutrients to fuel dividing cells, and consequently dissolved nutrient concentrations decline as upwelled seawater blooms. Over the progression of a coastal phytoplankton bloom, advection typically carries upwelled seawater away from the coast and the physicochemical properties of this water evolve. The water warms, chlorophyll and biomass concentrations increase, and pCO_2 decreases due to carbon fixation and exchange with the atmosphere. The phytoplankton community inhabiting this parcel of water is also in a constant state of flux. Initially favored are large eukaryotic phytoplankton which can quickly utilize the plentiful inorganic nutrients and escape grazing pressure by multiplying much faster than herbivorous metazoans (Smayda, 1997). As nutrients are consumed and grazing intensity increases, smaller picoeukaryotic phytoplankton increase in relative abundance as do *Synechococcus* cyanobacteria. Regions of the CCE unimpacted (or minimally impacted) by

coastal processes remain oligotrophic and primary production here is dominated by cyanobacteria of the *Prochlorococcus* genus. This conceptual model of phytoplankton community evolution in the CCE is highly generalized, and a high degree of variability exists between specific upwelling events.

In a systematic comparison of eastern boundary current ecosystems, Carr and Kearns (2003) noted the chlorophyll:PO₄ ratio typical of the CCE was half that of Atlantic upwelling regimes. Iron bioavailability likely explains this discrepancy in nutrient utilization. CCE upwelling frequently delivers insufficient iron to support the full utilization of accompanying nitrate, inevitably leading to iron limitation as nutrient drawdown occurs (Biller et al., 2013; Bruland et al., 2001). The concept of iron limitation in CCE waters was at first controversial; John Martin considered it impossible due to the proximity of benthic iron sources (Martin, 1990). Now it is widely accepted as an important bottom-up control on CCE primary productivity after decades of research (e.g. Biller et al. 2013; Biller & Bruland 2014; Brzezinski et al. 2015; Cohen et al. 2017; Elrod et al. 2008; Firme et al. 2003; Hogle et al. 2018; Hutchins et al. 1998; Hutchins & Bruland 1998; King & Barbeau 2007; King & Barbeau 2011; Lampe et al. 2018; Till et al. 2019). The spatial extent of iron limitation is patchy due to a variable iron supply derived from resuspended sediment deposits along the continental shelf (Johnson et al., 1999). Much of the labile iron is deposited on the shelf by winter runoff which flows into rivers

and out to sea (Wheatcroft et al., 1997; Xu et al., 2002). Shelf width in the region correlates roughly with seawater dissolved iron concentrations (Biller et al., 2013; Bruland et al., 2001; Chase et al., 2005; Firme et al., 2003; Hutchins et al., 1998), and phytoplankton biomass during the upwelling season is correlated with the previous winter's river flow (Chase et al., 2007).

The physiological manifestations of iron starvation have been characterized in model marine phytoplankton organisms which are closely related to key members of the California Current microbial community. Diatoms represent perhaps the best studied clade. The model pennate *Phaeodactylum tricornutum* has been extensively studied under laboratory conditions designed to arouse the iron stress response. Some of the earlier work failed to reasonably replicate marine iron concentrations, but nonetheless reported impaired photosynthetic capabilities including decreased cellular chlorophyll (Glover, 1977; Hayward, 1968). Later physiological investigations demonstrated that cells decreased their light harvesting pigment inventories along with chlorophyll when subjected to iron stress (Geider et al., 1993). Photoprotective pigments also increased in abundance. This results in a decrease in electrons flowing through the electron transport chain into the photosynthetic reaction centers. Photosynthetic competency (F_v/F_m) is impaired, presumably due to a lack of iron cofactors in the redox enzymes that make up the photosynthetic electron transport chain. Cytochromes, ferredoxins, NADH dehydrogenases and

midstream thylakoid oxidases all require iron cofactors (Behrenfeld & Milligan, 2011). Photosystem I reaction center proteins use iron sulfur clusters as electron acceptors which greatly increases the iron quota of PSI. 12 atoms of iron are required for each PSI photosystem. PSII circumvents this iron investment by utilizing quinone electron acceptors which contain no iron. As a result, PSII employs just three iron atoms per photosystem; two used in associated cytochromes and one used in electron transport between primary and secondary quinones. When cells are balancing their iron budgets, PSI reaction centers are large investments while PSII are relatively inexpensive. Consequently, the ratio of PSI:PSII increases during iron stress in diatoms (Greene et al., 1991; Strzepek & Harrison, 2004).

The high iron cost of photosynthesis could be partially circumvented by the use of light driven proton pumps known as proteorhodopsins (Béja et al., 2000; Fuhrman et al., 2008). Proton gradients maintained by these proteins could be used to synthesize ATP without the use of iron dependent electron transport. Oceanic diatoms overexpress proteorhodopsins during low iron conditions (Marchetti et al., 2012). This alternative form of phototrophy likely supports the endurance of diatom seed populations until iron becomes available blooms can initiate (Marchetti et al., 2015).

Decreases in F_v/F_m of iron starved phytoplankton are also attributed to light harvesting antennae which are energetically decoupled from photosynthetic reaction centers (Greene et al., 1991; Roncel et al., 2016). This

decoupling prevents electron overflow through thylakoid proteins and facilitates quick restoration of photosynthesis when iron stress is relieved. Disconnected light harvesting complexes contribute to initial (F_o) but not variable (F_v) fluorescence resulting in decreased F_v/F_m . This phenomenon could account for most of the decrease in F_v/F_m observed in iron limited phytoplankton, though limited iron supply to PSII electron transport proteins should also be considered (Behrenfeld & Milligan, 2011).

With diminished flow of energy through the light reactions of photosynthesis, the light independent Calvin-Benson cycle is necessarily impacted. A decrease in the supply of ATP and NADPH impairs carbon fixation, and iron stress results in the upregulation of Calvin-Benson cycle fructose 1,6-bisphosphate aldolase (FBA) (Allen et al., 2008, 2012; Bertrand et al., 2015; Cohen et al., 2017; Lommer et al., 2012; Smith et al., 2016). A satisfactory explanation for the upregulation of plastid-localized FBA in diatoms is enigmatic. It seems unlikely that increased abundance of one enzyme could be effective in forcing the regenerative phase of the Calvin-Benson cycle, though this may be the reason underlying its upregulation. Alternatively, under the conditions of iron limitation this enzyme may operate to produce glyceraldehyde 3-phosphate from fructose bisphosphate in order to temporarily fuel otherwise stymied respiration. FBAs catalyze conversion between carbon compounds required for carbon fixation and glycolysis, and the balance of these pools might be particularly important under iron

limitation. Diatoms contain multiple FBA genes of two classes (Allen et al., 2012). Class I and II FBAs have convergently evolved and operate by different mechanisms, with class II requiring a divalent metal cofactor (Marsh & Leberherz, 1992). It is thought that Zn^{2+} is the typical cofactor of class II FBAs, therefore favoring class I should not reduce iron demand. Nevertheless, diatoms (and other phytoplankton) overexpress class I when iron limited and class II when iron replete. Detection of an iron sensitive class I FBA associated with diatom iron processing vesicles could indicate a completely different role for this protein (Turnšek et al., 2019), although this does not explain the differential expression of class I and II FBAs in cyanobacteria which presumably utilize different iron uptake strategies (Ludwig & Bryant, 2012; Narayan et al., 2011). It is clear that multiple FBAs serve different functions within diatom cells (Allen et al., 2012), and it could be that they catalyze different functions.

The disruption of adequate electron transport through the thylakoid membrane leads to excessive production of problematic reactive oxygen species (ROS) (Wolfe-Simon et al., 2005). Iron limitation therefore may increase the susceptibility of photoautotrophs to photoinhibition. If a photosynthesis redox protein is missing its iron cofactor, abundant molecular oxygen in the vicinity can substitute as an electron acceptor in a derailment of the electron transport chain. Reduction of O_2 entails the formation of superoxide which is generally considered a toxic byproduct. Some plastidic

ROS generation is the inevitable result of electron transport through imperfect biological systems, and protective proteins are produced which neutralize these reactive molecules before photo-oxidative damage occurs (Niyogi, 1999). Superoxide dismutases and phytochelatins are known both to mitigate oxidative stress and to be expressed in iron limited diatoms (Peers & Price, 2004; Smith et al., 2016). Superoxide dismutases require metal cofactors (Cu, Fe, Mn, Ni, or Zn), and diatoms of the Bacillariophyceae and Fragilariophyceae classes have largely abandoned iron-containing metalloforms (Groussman et al., 2015).

Ferredoxins are a class of iron containing proteins that transfer electrons in biological redox reactions, primarily cyclic and linear electron flow (Schoepp et al., 1999; Sétif, 2001). Ferredoxin also participates as a reductant in some redox reactions of nitrogen metabolism including nitrate and nitrite reduction, and the synthesis of glutamate from glutamine. Ferredoxin proteins contain two to four iron atoms each, which are present in iron sulfur clusters bound to cysteine residues. Plant-type ferredoxins contain one [2Fe-2S] cluster, while bacterial-types can utilize [4Fe-4S] or [3Fe-4S] clusters. Soluble plant-type ferredoxins in the stroma of chloroplasts transfer electrons from PSI to ferredoxin NADP⁺-reductases (FNR) which produces NADPH. In many diatoms, the plant-type ferredoxin gene (*petF*) is encoded in the plastid genome, while in others it has migrated to the nuclear genome (Gueneau et al., 1998; Lommer et al., 2010; Oudot-Le Secq et al., 2007). Flavodoxins are

electron transfer flavoproteins that can substitute for ferredoxin in some reactions. Ferredoxin (plant-type) and flavodoxin can both achieve similar redox potentials, but flavodoxin requires two reduction steps to reach the potential that ferredoxin attains with one (Sétif, 2001). Under iron replete conditions, diatoms produce both proteins although ferredoxin is more abundant (Doucette et al., 1996). Low iron induces flavodoxin expression in diatom cultures and natural communities (Allen et al., 2008; Chappell et al., 2014; Lommer et al., 2012; Roche et al., 1995; Smith et al., 2016), and some diatoms are not observed to produce ferredoxin at all (Pankowski & McMinn, 2009b, 2009a). Additionally, phytoplankton contain two flavodoxin variants termed clade I and clade II or 'long' and 'short' (Whitney et al., 2011). Clade II 'short' flavodoxins are transcriptionally sensitive to environmental iron concentrations and presumed to substitute for ferredoxin, while the role of clade I flavodoxins is unknown.

Cytochromes are another class of electron transport protein which utilizes iron containing prosthetic groups, in this case heme. Cytochrome c_6 (also known as cytochrome c_{553}) delivers electrons to PSI from the cytochrome b_6f complex. This protein is isofunctional with the copper-containing metalloprotein plastocyanin (De la Rosa et al., 2002), which is one of the few constituents of linear photosynthetic electron transfer which does not utilize iron. Many photosynthetic organisms contain both genes and favor plastocyanin under iron limiting conditions, while others retain only on

plastocyanin. *Thalassiosira oceanica* is thought to rely exclusively on plastocyanin, essentially trading some of the iron cost of photosynthesis for a copper requirement (Peers & Price, 2006). Cytochrome c_6 is widespread in diatom transcriptomes, while plastocyanin is less common though multiple paralogs are found in diatoms native to low iron regions (Groussman et al., 2015). In iron-enrichment experiments using natural phytoplankton communities plastocyanin was expressed preferentially in the absence of iron, but expression exceeded cytochrome c_6 even in iron replete conditions (Marchetti et al., 2012).

Acquisition of exogenous iron sources by phytoplankton occurs via multiple mechanisms. Iron in seawater is present in a variety of chemical species and physical forms (Gledhill & Buck, 2012). The free Fe^{3+} ion is complexed by hydroxide to form primarily $Fe(OH)_2^+$ and $Fe(OH)_4^-$ (Price & Morel, 1998). Despite the oxidizing properties of seawater, some dissolved iron is also present as Fe(II) (Rose & Waite, 2002). The sum of dissolved inorganic iron species is termed Fe' . In addition, a heterogeneous pool of organic ligands naturally present in seawater bind to iron and enable dissolved iron concentrations to exceed the predicted solubility of ferric hydroxides (Liu & Millero, 2002). As a result, nearly all dissolved iron in seawater is part of an organic ligand complex (Hunter & Boyd, 2007). Still, studies of iron bioavailability to microbes have consistently demonstrated Fe' to be the preferred substrate, with roughly 1000 times greater uptake rates (Lis et al.,

2014; Shaked et al., 2020). The iron uptake capabilities of phytoplankton have been studied for decades using both inorganic (Anderson & Morel, 1982; Sunda & Huntsman, 1995) and organic (Horstmann & Soria-Dengg, 1995; M. T. Maldonado & Price, 2001) substrates. These studies have characterized uptake kinetics, but the underlying molecular mechanisms were speculated largely based on the iron uptake proteins from the yeast *Saccharomyces cerevisiae*. The extracellular ferric reductase proteins of *S. cerevisiae* reduce Fe(III) to Fe(II) which is then reoxidized and transported into the cell through a permease-oxidase complex (Lesuisse & Labbe, 1994). A parallel iron assimilation mechanism of *S. cerevisiae* can transport organically complexed iron prior to reduction (Lesuisse et al., 2001). Eukaryotic phytoplankton contain many putative iron uptake genes, but the specific function of most are unknown (Blaby-Haas & Merchant, 2012; Groussman et al., 2015; Morrissey & Bowler, 2012). Transcriptomic profiling of iron limited diatoms revealed overexpression of many genes which might participate in the uptake process (Allen et al., 2008; Goldman et al., 2019; Lommer et al., 2012; Smith et al., 2016). Among these, the ISIPs (iron starvation induced proteins), ferric reductases, multicopper oxidases, ferric permeases, NRAMPs and ZIPs were candidates.

In 2018, McQuaid et al. demonstrated in *P. tricornutum* that ISIP2a is an inorganic iron uptake protein related to transferrins (McQuaid et al., 2018). This protein, dubbed phytotransferrin (pTF), is present in many eukaryotic

phytoplankton including most diatoms (Morrissey et al., 2015). It binds Fe³⁺ synergistically with a carbonate ion and is subsequently internalized into vesicles via clathrin mediated endocytosis. pTF is responsible for more than 90% of Fe³⁺ uptake in *P. tricornutum* (McQuaid et al., 2018). The details of *P. tricornutum* pTF vesicle dynamics were studied using proximity proteomic techniques which revealed iron trafficking to the chloroplast and identified other involved proteins (Turnšek et al., 2019). The carbonate dependence of pTF iron uptake means ocean acidification may adversely impact iron acquisition by diatoms and other marine phytoplankton.

Phytoplankton contain other inorganic iron transporters including Fe(III) permeases and divalent metal transporters of the NRAMP and ZIP protein families (Blaby-Haas & Merchant, 2012). Transcription of some are sensitive to iron concentrations (Kustka et al., 2007; Yoshinaga et al., 2014), but their role in uptake and cellular localization have not been confirmed. Intracellular trafficking and mobilization of internal iron stores may explain some iron transporter upregulation in response to iron stress (Lampe et al., 2018).

Many microbes in the marine environment produce siderophores, which are strong iron binding ligands that facilitate iron acquisition (Hider & Kong, 2010; Vraspir & Butler, 2009). These compounds are released into the environment to bind iron and are then retrieved by specific uptake proteins. Eukaryotic phytoplankton are not believed to produce siderophores, but uptake of siderophore-associated iron has been observed (Horstmann &

Soria-Dengg, 1995; Maldonado & Price, 2001; Maldonado & Price, 1999; Soria-Dengg et al., 2001). In 2018, Kazamia et al. described the crucial role of ISIP1 in delivering siderophore iron to the chloroplast in *P. tricornutum* (Kazamia et al., 2018). Two other proteins, a siderophore receptor and a ferric reductase are required for siderophore uptake in *P. tricornutum* (Coale et al., 2019). This confirmed a long-standing hypothesis that ferric reductases are involved in siderophore utilization by diatoms (M. T. Maldonado & Price, 2001). These siderophore acquisition genes are present in the genomes of many low-iron adapted diatoms. Groussmann et al. identified multiple copies of ferric reductases in most diatoms, and revealed two major clades; FRE-I and FRE-II (Groussman et al., 2015). However, two ferric reductases proteins from *P. tricornutum* fall within FRE-I and have been shown to serve different functions (Coale et al., 2019) and thus the roles of these proteins are only beginning to be understood. As with Fe³⁺ uptake, endocytosis is required for iron internalization and while these uptake processes are independent, the two pathways likely converge during intracellular trafficking (Turnšek et al., 2019).

The ability to store iron benefits organisms that live in low iron environments with episodic iron inputs. Luxury uptake of iron, which is uptake beyond the immediate cellular requirement, can be used during periods of iron limitation if storage mechanisms are adequate. The utility of iron is due to its participation in redox reactions, but this activity is also potentially harmful. Free iron in the cell can generate toxic reactive oxygen species which

damage DNA, proteins and lipids (Halliwell, 1989). In order to safely store luxury iron many diatoms utilize the iron storage protein ferritin (Marchetti et al., 2009). Ferritin subunits assemble into a hollow protein complex inside which iron is oxidized, mineralized and stored as a ferric oxide nanoparticle (Chasteen & Harrison, 1999; Pfaffen et al., 2013). Iron is released as Fe(II) which implies a reductive mechanism (Harrison & Arosio, 1996), but the proteins involved in diatoms are unknown. Ferritin is distributed across diatom classes, but mainly absent from the Coscinodiscophyceae (Groussman et al., 2015), and may serve different roles in different lineages (Cohen et al., 2018). As an alternative, some diatoms appear to store iron inside vacuoles (Nuester et al., 2012). Vacuolar storage may serve as a stopgap in diatoms lacking ferritin, but does not effectively substitute during prolonged iron droughts (Lampe et al., 2018). Increasing cellular iron quotas and long-term iron storage may not be the primary roles of ferritin. During iron starvation, turnover rates of iron containing proteins may increase due to increased oxidative damage or reallocation of iron resources on a diel timescale. In other phytoplankton ferritin helps facilitate recycling of photosynthetic proteins (Botbol et al., 2015; Busch et al., 2008), and some diatom ferritins might share this function (Pfaffen et al., 2015).

Picoeukaryotic marine phytoplankton are an understudied category of organisms. Unlike many diatoms, they are poorly preserved in fixatives, are difficult to identify by light microscopy, and difficult to maintain in culture.

They also represent a hodgepodge of differentially related organisms lumped together solely on the bases of diminished size, possession of a nucleus, and some photosynthetic ability (Worden & Not, 2008). It is harder to apply generalized ideas of nutrient stress to this group, but the basic impacts on photosynthesis likely remain similar. Many diverse lineages make up the picoeukaryotic phytoplankton community found in the CCE, and the Pelagophyceae can be one of the most abundant (Dupont et al., 2014). The most intensively studied picoeukaryotic genera of the pelagophyte class are *Aureococcus* and *Pelagomonas*. *Aureococcus* species typically favor estuarine environments where iron limitation is rare (Gobler et al., 2011), and accordingly the physiology of this group under low iron conditions has received little attention. As of Chapter 2 of this thesis, *Pelagomonas calceolata* has undergone scrutiny under low iron culture conditions. Chlorophyta, a class of unicellular green algae, represent another major contributor to picoeukaryotic marine phytoplankton. The freshwater model organism *Chlamydomonas reinhardtii* is by far the best studied (Glaesener et al., 2013), and insights into the iron metabolism of this organism have been invaluable in understanding iron stress in marine microbes. The marine chlorophyte *Ostreococcus* has been studied under iron limitation revealing impacts on cell size (Botebol et al., 2017) and diel redistribution of iron stores in order to maintain critical functions with minimal iron (Lelandais et al., 2016), and is common in the CCE (Lucas et al., 2011). Haptophytes are also

contributors to the CCE's picoeukaryotic phytoplankton and the abundant Prymnesiophyceae class has historically been detected via the diagnostic pigment 19'-hexanoyloxyfucoxanthin or microscopy (Taylor et al., 2012). Of the prymnesiophyceae, the genus *Phaeocystis* is known primarily from high latitude ecosystems but is also very common in the CCE (Kolody et al., 2019; Venrick, 2012). The impact of iron limitation on *Phaeocystis* physiology and gene expression has been investigated due to its prominence in the Southern Ocean high nutrient low chlorophyll (HNLC) ecosystem (Alderkamp et al., 2012; DiTullio et al., 2007; Garcia et al., 2009; Koch et al., 2018; Stefels et al., 1998; Van Leeuwe & Stefels, 2007).

Cyanobacteria of the genera *Synechococcus* and *Prochlorococcus* are the predominant prokaryotic phytoplankton in the CCE (M. V Brown & Fuhrman, 2005; Dupont et al., 2014; Taylor et al., 2012; Zeigler Allen et al., 2012). Nearshore adapted *Synechococcus* ecotypes inhabit the coastal environment, while different ecotypes persist offshore of the continental shelf (Lucas et al., 2011). An abrupt shift to *Prochlorococcus* dominated cyanobacterial populations accompanies the transition from a mesotrophic to oligotrophic ecosystem as upwelled nutrients are consumed (Taylor et al., 2012). These smallest of photosynthetic cells still have iron requirements which can be higher than other photosynthetic organisms (Cheng & He, 2020), and in excess of the bioavailable iron supply in ocean ecosystems (Mackey et al., 2015; Mann & Chisholm, 2000). This is despite diminished size

which results in low cellular nutrient quotas that can be satisfied with relatively high cell volume normalized uptake rates (Marañón, 2015). The impact of iron stress on cyanobacteria is similar to other phytoplankton in that photosynthesis is acutely impaired, but these prokaryotes possess different iron transport proteins (Webb et al., 2001), siderophore production capabilities (Boiteau & Repeta, 2015; Ito & Butler, 2005; Trick & Kerry, 1992; Wilhelm et al., 1996), and iron metabolism regulation proteins (ferric uptake regulators; FURs) (Rocap et al., 2003; Zinser et al., 2009). High light and low light adapted *Prochlorococcus* ecotypes are typically segregated by depth (Moore et al., 1998), and exhibit different tolerances to iron stress with high light ecotypes being more susceptible (Thompson et al., 2011).

1.3 METHODS

1.3.1 Experimental design

Incubation experiments were conducted at each station in order to gauge the molecular response of microbial communities to iron stress and iron supply. Whole seawater was collected from surface and DCM depths using a rosette of external spring Niskin bottles (General Oceanics) prepared for trace metal sampling. Inside a clean lab environment, an initial metatranscriptomic sample was taken (T0) and then seawater was divided into treatments: no addition control, 10 nM FeCl₃, and 100 nM iron-free desferrioxamine b (DFOB). These treatment bottles were returned to the depths they were collected

from and incubated *in situ* on a drifting array. After 24 hours, the treatment bottles were collected and harvested for metatranscriptomics (Figure 1.1).

1.3.2 Sampling and incubations

Pre-dawn uncontaminated seawater samples were obtained from surface and DCM depths using acid cleaned 5L Niskin-X samplers (General Oceanics) depolyed using trace metal clean methodologies (e.g. . Subsampling of Niskin-X bottles occurred inside a mobile clean laboratory located on the fantail of the *R/V Melville*. T0 samples were filtered immediately onto polyethersulfone Sterivex filters of 0.22 μ m porosity (EMD Millipore, catalog number SVGP01050) using a peristaltic pump. Seawater was removed with a syringe, filter units were sealed with Cha-seal capillary tube sealing compound (Kimble, catalog number 43510) and flash frozen in liquid nitrogen. 1L acid cleaned polycarbonate incubation bottles were filled from Niskin-X samplers and amended as either 10nM FeCl₃, 100nM DFOB, or no addition controls in duplicate. All treatment bottles were returned to their collection depth in mesh bags attached to a surface-tethered drifting experimental array with a holey-sock drogue at 15 m (Landry et al., 2009). After 24 hours, the array was recovered and treatment bottles were filtered immediately 0.22 μ m Sterivex filters as above and flash frozen in liquid nitrogen. Filters were kept at -80°C until extraction.

1.3.3 RNA extraction, cDNA synthesis, PCR, library preparation and sequencing

RNA retained on Sterivex filters was extracted using a NucleoMag RNA kit (Macherey Nagel), with the lysis step performed inside the Sterivex unit. Lysate was transferred to a 96-well plate and the remainder of the protocol was performed on an epMotion liquid handling workstation (Eppendorf). RNA was analyzed on a TapeStation system (Agilent) using the high sensitivity RNA ScreenTape assay. cDNA was synthesized using the SuperScript III First-Strand Synthesis System (Life Technologies, catalog number 18080-051) using random hexamer primers.

cDNA was used as template for 16S and 18S PCR reactions which were conducted with the Azura TruFi DNA polymerase PCR system (catalog number AZ-1710). The V4-V5 regions of the 16S small subunit ribosomal RNA gene was amplified using the 515F (GTGYCAGCMGCCGCGGTAA) and 926R (GTGYCAGCMGCCGCGGTAA) primers. The 18S ribosomal RNA gene was amplified using primers 1389F (GTGYCAGCMGCCGCGGTAA) and 1510R (GTGYCAGCMGCCGCGGTAA) targeting the V9 region, and primers EukV4F1 (CCAGCASCYGC GGTAATCC) and EukV4R1 (ACTTTCGTTCTTGATYR) targeting the V4 region. All primers also included Illumina adaptor, barcode and linker regions. PCR amplicons were visualized by gel electrophoresis in a 1.5% agarose gel, purified with Agencourt AMPure XP beads, and quantified via fluorometric assay using PicoGreen dsDNA Quantitation Reagent (Molecular Probes, Inc.). PCR products were pooled and sequenced on the

Illumina MiSeq platform by the Institute for Genomic Medicine at the University of California, San Diego.

For metatranscriptomic samples, after RNA extraction ribosomal RNA was removed using RiboZero Magnetic kits (Epicenter) following manufacturer's low input protocol. cDNA was synthesized using the Ovation RNA-seq System V2 (NuGEN) and Agencourt RNAClean XP beads were used for cDNA purification. cDNA fragmentation was performed using the Covaris E210 focused ultrasonicator, targeting 300 bp fragment generation. Library preparation was conducted with the Ovation Ultralow System V2 (NuGEN). After end repair, ligation and amplification, libraries were quantified by qPCR with the KAPA Library Quantification Kit (catalog number KK4835) on the 7900HT Fast Real-time PCR System (Applied Biosystems). Pooled libraries were sequenced on the Illumina HiSeq platform by the Institute for Genomic Medicine at the University of California, San Diego. An average of 13.4 million reads (2.01 million standard deviation) were generated per sample, with 857 million total reads.

Metatranscriptomes were constructed using the RNAseq Annotation Pipeline v0.4 (RAP) as described previously (Bertrand et al., 2015), and 1.71 million *ab initio* open-reading frames were predicted. Taxonomy was assigned to ORFs based on lineage probability index (LPI) (Podell & Gaasterland, 2007), and ORFs were annotated via BLASTP (Altschul et al., 1990) to the phyloDB protein database.

1.3.4 Chlorophyll

Measurements of size fractionated chlorophyll a concentrations were made by filtering seawater collected from the CTD rosette of Niskin bottles, through a series of filters of varying porosity. Using a vacuum filtration manifold, seawater was drawn through 20 μ m Nitex filters and also through polycarbonate filters of 8, 3 and 1 μ m pore size. Additional seawater passed through a GF/F filter, and all filters were extracted in 90% acetone at -20°C for 24 hours. After extraction, fluorescence was measured using a calibrated Turner 10-AU fluorometer, acidified with 1N HCl, and measured again (Holm-Hansen et al., 1965). Chlorophyll a concentrations and size class percentages were then calculated from pre and post acidification fluorescence measurements.

1.3.5 Pigments

Phytoplankton pigments were measured using high performance liquid chromatography in samples collected from Niskin bottles. Samples were filtered onto 25 mm GF/F filters, flash frozen in liquid nitrogen and kept at -80°C until analysis. Filters were then extracted using a canthaxanthin acetone mixture, ground with a pestle, and left to extract further. Particulates were removed via centrifugation and supernatant was injected into a Agilent 1100 series HPLC with a Waters Symmetry reverse phase C8 column (Wright et al., 1991; Zapata et al., 2000). Pigment data were used to reconstruct phytoplankton diversity as described by Goericke and Montoya (1998).

1.3.6 Flow cytometry

Samples for flow cytometry analysis were collected from Niskin bottles were collected and preserved with paraformaldehyde, flash frozen in liquid nitrogen and stored at -80°C until analysis. Thawed samples were stained with Hoechst 33342, and calibration beads were added to each sample. A beckman-Coulter EPICS Altra flow cytometer was used to enumerate cells belonging to *Prochlorococcus*, *Synechococcus*, picoeukaryote and heterotrophic bacteria populations. Cells were excited using both a 488 and UV argon lasers, and a Harvard Apparatus syringe pump was used for sample injection. Biomass estimates for *Prochlorococcus* and *Synechococcus* are made from the assumption of 32 and 101 fg C cell⁻¹, respectively (S. L. Brown et al., 2008; Garrison et al., 2000).

1.3.7 Dissolved iron measurements

Seawater dissolved iron concentrations were determine from samples collected from trace metal clean Niskin-X bottles. All samples for total dissolved iron were filtered through pre-cleaned 0.2 µm Acropak 200 capsule filters (VWR International) into acid-washed bottles (trace metal grade nitric and hydrochloric acid, Fisher Scientific) in a trace metal clean shipboard portable laboratory. Samples for total dissolved iron analysis were filtered into low-density polyethylene bottles (Nalgene) and acidified to pH 1.7 to 1.8 using HCl (optima grade). Prior to analysis, dissolved iron in the acidified samples was oxidized to iron(III) for 1 hour using 10 mM Q-H₂O₂, buffered in-

line with ammonium acetate to pH ~3.5, and selectively pre-concentrated on a chelating column. Dissolved iron was eluted from the column using 0.14 M HCl (Optima grade) and measured by chemiluminescence using flow-injection analysis. The methods used were similarly described by King and Barbeau (A. King & Barbeau, 2007; A. L. King & Barbeau, 2011) and adapted from Lohan et al. (Lohan et al., 2006).

1.3.8 Macronutrients

Macronutrients concentrations were analyzed in seawater collected from Niskin bottles and frozen until analysis using a QuAAtro continuous segmented flow autoanalyzer. Nitrate was measured according to a cadmium reduction method followed by colorimetric determination, while phosphate and silicic acid were detected using ammonium molybdate colorimetric methods (Armstrong et al., 1967; Murphy & Riley, 1962).

1.3.9 POC/PON

Vertical profiles of particulate organic carbon and nitrogen were generated from 4 L seawater samples filtered onto 25 mm GF/F filters under vacuum pressure not exceeding 40 mm Hg. All tools and materials used to prepare samples were cleaned with 91% isopropanol or combusted in a muffle furnace to remove contaminants. Filters were stored in aluminum foil packets and frozen at -20°C until analysis when they were dried at 60-70°C overnight, and then acid fumigated in a dessicator containing 12 N HCl overnight to convert bicarbonate to CO₂. Portions of each filter were packed

into tin capsules and combusted at 1000°C in a ECS 4010 CHNSO Analyzer (COSTECH Analytical Technologies, Inc.). CO₂ and N₂ gases resulting from combustion were quantified by thermal conductivity, and filter blanks were analyzed alongside samples.

1.4 RESULTS AND DISCUSSION

1.4.1 Oceanographic setting

In August of 2014, the California Current Ecosystem Long Term Ecological Research (CCE LTER) site conducted an oceanographic research expedition with the goal of investigating ecosystem transitions in the CCE. This research is ongoing and includes characterization of mechanisms which result in ecosystem state changes, as well as description of distinct pelagic ecosystems. The 2014 cruise occurred during an anomalous period of reduced coastal upwelling which resulted in a significant decrease in the supply of inorganic nutrients to CCE surface waters. Disruption of the typical upwelling regime undoubtedly impacted the microbial communities observed during this cruise, and this is most evident from a regional-scale perspective. Surface chlorophyll concentrations were dramatically lower than typical years, and concentrations above 1 mg/m³ were confined to narrow coastal bands around weak upwelling centers (Figure 1.2). Regional sea surface temperatures were above normal (Figure 1.2), stratification was intensified, and vertical transport was therefore suppressed (Lilly et al., 2019). Despite these departures from mean conditions, the large-scale structure of

distinct biogeochemical provinces within the CCE remained intact. Coastal upwelling regions, transitional mixing zones, and offshore oligotrophic waters were all observed. This study investigates phytoplankton dynamics at three contrasting stations which occur within 200 km of each other. Our coastal station was roughly 75 km south west of the Point Conception upwelling center. Surface temperatures were around 18° C and surface salinity was above 33.4 PSU (Figure 1.3). Fluorescence-derived chlorophyll exceeded 1 mg/m³ at the surface and 1.5 mg/m³ at the deep chlorophyll maximum (DCM). Surface nutrients were largely depleted, although significant nitrate remained at the DCM (Table 1.1). Fucoxanthin was present at one third of chlorophyll a concentrations in the surface (Figure 1.4) which indicates a significant diatom presence (Figure 1.5), and size-fractionated chlorophyll a measurements support this finding with a large proportion of DCM chlorophyll present in the >20 µm size class (Figure 1.6). Flow cytometry measurements indicated that both at the surface and DCM *Prochlorococcus* was outnumbered by *Synechococcus*, and picoeukaryotes were numerous (Figure 1.7). Particulate organic carbon and nitrogen (POC & PON) were highest in the coastal station, and the C:N molar ratio of particulate material was slightly above the canonical Redfield value (Redfield, 1934) in the surface, exhibited a slight maximum at the DCM, and trended negative below the DCM (Figure 1.8). Both POC and PON were greatest at the surface and decreased with depth (Figure 1.8). Although euphotic zone nutrients

were lower than during active upwelling, these measurements are characteristic of a diatom-dominated coastal CCE bloom which is aging, warming, and advecting offshore.

Our transition zone station was warmer and lower salinity than the coastal station (Figure 1.3), despite being in close geographic proximity (Figure 1.2). Surface chlorophyll was lower, but the DCM was more pronounced and reached chlorophyll a concentrations of greater than 2 mg/m³ as measured by fluorescence (Figure 1.3). Extracted chlorophyll measurements showed the transition station to contain less chlorophyll at both surface and DCM depths (Table 1.1). Nutrient patterns were largely the same as the coastal station, though at the DCM a slight increase in nitrate and decrease in dissolved iron resulted in the highest NO₃:Fe out of all stations (Table 1.1). Fucoxanthin concentrations were lower, and cyanobacterial pigments higher than the coastal station (Figure 1.4). 19'-butanoyloxyfucoxanthin, a diagnostic pelagophyte pigment, was present at the highest concentration here out of all three stations (Figure 1.4). The >20 μm size class was all but absent from chlorophyll a measurements, and no other station had a higher percentage of chlorophyll a present in the 3-8 μm class (Figure 1.6). Picoeukaryotes were most abundant at the transition station DCM out of all stations, and here *Synechococcus* outnumbered *Prochlorococcus* (Figure 1.7). POC and PON above about 45 m in this transition station were roughly half the concentration of the coastal station

and about double that of the offshore station (Figure 1.8). At this station, the DCM represented a maximum in both POC and PON concentrations, and the particulate C:N ratio here was consistently below Redfield (Figure 1.8). This station was in some ways a midpoint between the others with the surface possessing offshore characteristics and the DCM similar to the coastal station, but also contained attributes not found in either of the other stations. Additionally, biogeochemical indications of iron limited phytoplankton were strongest at the transition station DCM with $\text{Si:NO}_3 = 0.858$ and $\text{NO}_3:\text{Fe} = 11.8$ (Table 1.1). These values are near the threshold values signifying iron limitation of CCE phytoplankton communities (Brzezinski et al. 2015; Hogle et al., 2018; King & Barbeau, 2007), and it is likely that many phytoplankton are transitioning towards iron stress and adapting physiologically to mitigate growth limitation, while other groups with low iron use efficiency could be truly iron limited.

Less than 200 km to the southwest of the previous stations, our offshore station occurred in an arm of California Current water extending into the transition zone (Figure 1.2). The offshore station was the warmest, lowest salinity and least fluorescent station, with the deepest DCM at around 70 m (Figure 1.3). Both surface and DCM depths had high Si:NO_3 values due to very low NO_3 and over $2 \mu\text{M}$ residual silicic acid (Table 1.1). Cyanobacterial pigments were in abundance while fucoxanthin was not detected (Figure 1.4). Divinyl chlorophyll a was present at over 50% of the total chlorophyll a

concentration indicative of *Prochlorococcus* cyanobacteria (Figures 1.4 and 1.5). Most of the chlorophyll a was present in the <1 μm size class, and 85% was <3 μm (Figure 1.6). Flow cytometry counts for *Prochlorococcus* were high in both the surface and DCM (Figure 1.7). *Synechococcus* counts were low at this station, and picoeukaryote counts exceeded *Synechococcus* at the DCM (Figure 1.7). POC and PON both peaked at 40 m in the offshore station, though overall variation with depth was not substantial (Figure 1.8). In the offshore station, particulate C:N was elevated above Redfield at the majority of depths, with only slightly lower values detected at 5 and 90 m (Figure 1.8). The offshore station was the most oligotrophic with warm temperatures, low surface chlorophyll and the deepest DCM, but further offshore these trends continued. Our offshore station not so far removed as to be outside the CCE and still very much subject to influence from coastal processes.

1.4.2 Coastal DCM diatoms

In all coastal DCM samples, 67% of centric diatom mRNA was annotated as *Thalassiosira* (Figure 1.9). The next highest percentage genus was *Chaetoceros* with 16%, followed by *Skeletonema* with 7.7% (Figure 1.9). Upon DFOB addition, ISIP3, some flavodoxins, and a class I FBA increased in expression (Figure 1.10). Plastocyanin and two bacterial rhodopsin genes were also induced. One plastid localized iron transporter was upregulated under low iron, while at least 3 others turned on when iron was added. Iron

addition stimulated expression of some class II FBAs, ferredoxin, cytochrome b and fructose biphosphatase. Most photosystem I and II genes were preferentially expressed under iron replete conditions, as were light harvesting associated genes. Multiple pTF, flavodoxin and FBA genes showed no sensitivity to iron treatment.

Pennate diatom transcripts represented 36% of all diatom mRNA, and *Pseudo-nitzschia fraudulenta* accounted for 42% of pennate mRNA (Figure 1.9). *P. fraudulenta* is a globally distributed and potentially toxic species known to produce domoic acid (Hasle, 2002). Pennates in the coastal DCM responded to iron limitation in a similar fashion to centrics with upregulation of plastocyanin, ISIP3, some flavodoxins, and class I FBA (Figure 1.11). pTF again showed a muted response, and after release from iron stress, ferredoxins, plastid iron transporters and some class II FBAs were expressed. PSI and PSII generally increased expression in iron replete conditions, as did nitrogen metabolism genes such as urea and nitrate/nitrite transporters, ammonium transporters, nitrite reductase, glutamate synthases, and carbamoyl phosphate synthetases. Several ferric reductases from *P. fraudulenta* were upregulated only when iron was added.

Taken together, results from our coastal DCM incubations reveal a degree of resistance of diatoms to short periods of iron stress. The response we observed included a quick induction of iron sparing mechanisms such as iron protein substitutions by iron-free flavodoxin and plastocyanin. The

function of ISIP3 is unknown, but Δ ISIP3 knockout cell lines created in the model pennate *Phaeodactylum tricornutum* retained normal iron uptake capabilities and RFP labeled ISIP3 localized to internal compartments and not the cell surface (J. McQuaid, personal communication). Additionally, ISIP3 contains a ferritin-like domain which implicates it in a storage or intracellular trafficking role rather than uptake (Behnke & Laroche, 2020).

1.4.3 Transition DCM *Pelagomonas calceolata*

Picoeukaryotic phytoplankton represented a large fraction of total phytoplankton mRNA in the transition station DCM. *Pelagomonas*, *Phaeocystis* and *Bathycoccus* genera accounted for more mRNA than all diatoms and cyanobacteria combined (Figure 1.12). The most abundant ORF detected at this station was from the RuBisCO gene of *P. calceolata*. Measuring approximately $1.5 \times 3 \mu\text{m}$ (Andersen et al., 1993), *P. calceolata* is likely contributing to the two smallest chlorophyll size classes (Figure 1.6), and also produces 19'-butanoyloxyfucoxanthin (Figure 1.4). Pigment-based taxonomy indicates prymnesiophytes may be more abundant at the transition station surface (Figure 1.5), but at the DCM *P. calceolata* might be the most abundant eukaryote by abundance as well as biomass. Interestingly, the C:N ratio of POM at the transition station was well below the Redfield value (Redfield, 1934), and also below C:N measured other picoeukaryote-dominated communities (Martiny et al., 2013), but consistent

with measurements of iron starved *P. calceolata* cultures C:N made in Chapter 2.

The low iron response of *P. calceolata* included the upregulation of flavodoxin and pTF, but class I FBAs were not detected (Figure 1.13). Notably, pelagophytes contain a many dynein genes (Carradec et al., 2018), and 863 *P. calceolata* dynein ORFs were detected at the transition DCM and 760 (88%) of these were overexpressed in low iron (Figure 1.13). One *ycf16* Fe-S assembly plastid iron transporters was expressed at low iron, as were transmembrane amino acid transporters (Figure 1.13). Dyneins and amino acid transporters hint at roles of motility and mixotrophy in the low iron response of *P. calceolata*. One ZIP transporter was upregulated in the DFOB treatment. Most nitrogen metabolism genes were down-regulated in the DFOB treatment, but notably nitrite reductase showed the opposite trend and increased in expression.

In response to iron addition, *P. calceolata* overexpressed ferredoxins and ferredoxin-NADP⁺ reductases (Figure 1.13). Ribulose phosphate epimerase (RPE1), a Calvin-Benson cycle enzyme, was one of the most strongly upregulated genes in response to high iron. Light harvesting genes mostly increased in expression, but a subset were expressed in the DFOB treatment. One β -carbonic anhydrase was expressed after iron addition, and so were a pair of iron-manganese superoxide dismutases. Photosystem I and II genes were upregulated at high iron alongside RuBisCO. One

selenocysteine-specific translation elongation factor was upregulated with iron indicating that selenoproteins may be important to *P. calceolata* as they are to other picoeukaryotic phytoplankton (Gobler et al., 2011; Palenik et al., 2007).

1.4.4 Transition DCM *Bathycoccus prasinos*

Bathycoccus prasinos is a picoplanktonic member of the chlorophyta (Mamiellophyceae) which is critically understudied. The related green algal genera *Ostreococcus* and *Micromonas* have received significantly more scientific attention. *B. prasinos* cells are difficult to identify via microscopy or flow cytometry as they are extremely small (1-2 μm) (Eikrem & Throndsen, 1990), but after the genome of a Mediterranean strain was sequenced in 2012 (Moreau et al., 2012), *B. prasinos* has been increasingly recognized as an important globally distributed picoeukaryote (Vannier et al., 2016).

Metagenomic analysis of *Bathycoccus* populations from a South American upwelling zone (Vaulot et al., 2012) and from a tropical Atlantic DCM (Monier et al., 2012) have been investigated and at least two clades of phylogenetically distinct *Bathycoccus* are characterized, likely representing differentially adapted ecotypes (Limardo, 2016; Simmons et al., 2016).

The *B. prasinos* expression response to changing iron availability was markedly different than other picoeukaryotes. All of the more than 20 pTF ORFs from *B. prasinos* were upregulated at low iron (Figure 1.14). No other species accounted for more pTF gene expression or had more homologs

(Figure 1.15). In addition, all 20 flavodoxin ORFs were highly upregulated at low iron. Four RuBisCO related ORFs were also up in low iron, as was one ZIP and curiously four ferredoxin transcripts. The CobW metal dependent cobalamin biosynthesis gene was upregulated in low iron. At low iron, a serine carboxypeptidase was overexpressed which may have a role in catabolic processes or post translational modification, and either function could indicate increased protein turnover resulting from oxidative damage or iron sparing mechanisms.

B. prasinos likely has the capability to utilize siderophore bound iron. When the FBP1 protein from *Phaeodactylum tricornutum* was used as a target in a blast query of the entire set of de novo assembled peptides, two hits without annotation were assigned to *B. prasinos* based on LPI taxonomy. Both were upregulated in the DFOB treatment, and when analyzed using the protein prediction engine PHYRE2 (Kelly et al., 2015), one of these was modeled with high confidence as a ferric-siderophore receptor protein (contig_575079_998_1818_-). Our DFOB treatment was so far in excess of the dissolved iron concentration (100 nM DFOB to 0.292 nM Fe) that iron limitation was probably still induced even though some siderophore bound iron is bioavailable.

Upon addition of FeCl₃, *B. prasinos* upregulated four plastocyanin transcripts which allows for electron transport to PSI. The constitutive use of plastocyanin over cytochrome c6 is a known adaptation to low iron

conditions adopted by oceanic phytoplankton (Peers & Price, 2006), and if *B. prasinos* operates in this manner then this upregulation is consistent with upregulation of PSI as a whole. Porphyrin synthesis was initiated with iron addition, as evidenced by upregulation of protoporphyrinogen oxidase (PPOX). Serine hydroxymethyltransferase (SHMT) produces 5,10-methylenetetrahydrofolate, an intermediate in one-carbon metabolism (Rao et al., 2003), and was upregulated with iron. The glycolysis gene triose phosphate isomerase (TPI) and a L18ae/LX ribosomal protein were strongly upregulated at high iron. Nitrogen metabolism and light harvesting genes also increased expression.

1.4.5 Transition DCM Phaeocystis

Phaeocystis species were responsible for about 8.1% of eukaryotic mRNA annotated from the transition station (Figure 1.9), and 6% of phytoplankton mRNA (Figure 1.12). This represented the most abundant haptophyte genus; *Chrysochromulina* was second with about 3.3% eukaryotic mRNA and *Emiliania* was third with about 2% (Figure 1.9). Our pigment data attributed about 24.6% of phytoplankton biomass to the *Prymnesiophyceae* (Figure 1.5), and the bulk of this was likely *Phaeocystis*. *P. antarctica* (CCMP1374) was by far the most abundant species, but others were also detected (*P. cordata*, CCMP2710, and CCMP2000). In response to our iron deprivation treatments *Phaeocystis* upregulated ISIP3s and SufB chloroplast localized iron ABC transporters in an apparent effort to mobilize internal iron

stores similar to coastal diatoms (Figure 1.16). Flavodoxins and a bacteriorhodopsin were also expressed at low iron. Class I and II FBAs responded only weakly to our iron treatments and *Phaeocystis* pTF was not differentially expressed which might be an indication that these populations were only in the initial stages of iron stress. The *Phaeocystis* transcriptome contained a large number of ATP synthase genes (1146 ORFs), and a number of these were expressed at low iron. *Phaeocystis* is known to form colonies within an extracellular polysaccharide matrix (Guillard & Hellebust, 1971) which can form extensive blooms and contribute significantly to carbon export (DiTullio et al., 2000). Cells can also persist as individual free-living cells, which is typical during oligotrophic conditions (Schoemann et al., 2005). Our size fractionated chlorophyll data suggest *Phaeocystis* was free-living. A recent culture study of *P. antarctica* in changing iron concentrations found a low iron response including pTF and the motor proteins dynein and myosin (Rizkallah et al., 2020).

1.4.6 Offshore Prochlorococcus

Cyanobacteria of the genus *Prochlorococcus* dominated the phytoplankton community of the offshore station. This was evident at both the surface and DCM depths in pigment (Figures 1.4 and 1.5) and flow cytometry data (Figure 1.7). Metatranscriptomic data allows us to better understand the differences between these vertically separated populations. In our T24 surface samples, around 75% of *Prochlorococcus* transcripts were

attributed to high light adapted *Prochlorococcus* strains MIT 9515, CCMP 1986, and AS9601 (Figure 1.17). In the DCM T24 samples, low light ecotypes NATL1A and NATL2A accounted for over 90% of *Prochlorococcus* transcripts (Figure 1.17). These different microbial populations responded to our incubations in different ways.

In the low light of the DCM, DFOB treated *Prochlorococcus* populations showed signs of iron limitation relative to the Fe treatment. Typical iron-stress biomarkers including flavodoxin, plastocyanin, and class I FBAs were upregulated (Figure 1.18). Impacts on photosynthesis were evident as many photosystem II related transcripts were more highly expressed in the DFOB treatment, while those attributed to photosystem I were upregulated in the Fe treatment (Figure 1.18). Transcripts annotated as related to light harvesting were generally upregulated in the DFOB treatment alongside bacteriochlorophyll a synthase and protochlorophyllide reductase (Figure 1.18). Additionally, carboxysome proteins were upregulated under iron-stress. Many porins were strongly expressed under low iron conditions, as were some CRP and LuxR transcriptional regulators (Figure 1.18). One cuprin-like transcript was observed to be upregulated at low iron (Figure 1.18). Iron trafficking and metabolism was impacted as DFOB samples upregulated ferric iron ABC transporters and heme transporters. Attempts to mitigate iron deprivation related stress were evident in DFOB samples by the upregulation of heat shock proteins, and a nickel-containing superoxide dismutase

precursor. Multiple poorly annotated reductases upregulated under low iron could be related to balancing cellular redox.

Two genes relevant to the pentose phosphate pathway, transketolase and ribulose-phosphate 3-epimerase were expressed under low iron, though other copies of both these genes were expressed at high iron.

Certain components of nitrogen metabolism including a urea transporter, a urease subunit, a nitrogen regulatory protein and a cyanate hydratase were upregulated in the low iron treatments. Thompson et al. (2011) hypothesized changes in N substrate preference in response to iron stress might favor cyanate utilization, and our data support this possibility. Upon iron addition, nitrogen uptake and metabolism related transcripts such as ammonium transporters, nitrite transporters and reductases, glutamine synthetase were expressed, along with a glnB nitrogen regulatory protein and a CRP nitrogen related transcriptional regulator.

Release from iron limitation resulted in the upregulation of Fur family iron/zinc related transcriptional regulators which repress iron acquisition gene expression (Figure 1.18). Magnesium, cobalt/nickel and zinc metal transporters, however, turned on. Ferritin was strongly expressed in high iron samples, as were some poorly annotated flavin reductase-like flavoproteins. Ferredoxin and multiple ferredoxin-dependent proteins increased expression after iron addition.

Surface *Prochlorococcus* populations experiencing low iron conditions upregulated similar genes to DCM populations including CRP regulators, carboxysome proteins, flavodoxins, light harvesting, porins, and class I FBAs (Figure 1.19). The response of flavodoxin, light harvesting genes, and FBAs in surface *Prochlorococcus* was more dramatic than in DCM populations. Photosystem II did not appear to be preferentially expressed at low iron, but photosystem I expression increased with iron (Figure 1.19).

Iron addition dramatically stimulated expression of class II FBAs in surface *Prochlorococcus* populations, which was not observed in DCM populations (Figure 1.19). Plastocyanin also increased in expression with iron contrary to expectation and the DCM populations.

High light adapted *Prochlorococcus* ecotypes have previously been shown to have a higher iron requirement than low light ecotypes (Thompson et al., 2011), and this is consistent with our observation of a more dramatic response to iron bioavailability in the surface populations of *Prochlorococcus*.

1.4.7 pTF expression

In addition to surveying the response of specific taxa to iron bioavailability, we have evaluated the contribution of different groups to total phytotransferrin (pTF) expression. pTF is a recently characterized iron uptake protein which is phylogenetically distributed across algal lineages including green algae, dinoflagellates, cryptophytes, stramenopiles, rhodophytes, haptophytes and chlorarachniophytes (McQuaid et al., 2018). The pTF

protein was first characterized in a model diatom organism, taking advantage of molecular tools which cannot be easily applied to other phytoplankton (McQuaid et al., 2018). This has led phytoplankton ecologists to question the environmental significance of pTF and its carbonate dependence, especially as the model diatom *P. tricornutum* is rarely dominant in marine communities. The susceptibility of this protein to disruption by decreasing ocean pH could result in exacerbation of iron stress for phytoplankton that rely on this uptake strategy over others. Cell surface area normalized uptake rates of heterogeneous natural iron substrates are relatively similar between oceanic phytoplankton taxa (Hudson & Morel, 1993; Shaked et al., 2020; Sunda & Huntsman, 1995), which could indicate other uptake strategies can effectively substitute for pTF at low iron concentrations.

In order to search for pTF homologs, we developed a hidden Markov model (HMM) based on blast hits recovered from the Marine Microbial Eukaryote Transcriptome Sequencing Project (MMETSP) using *P. tricornutum* pTF as input. We then used this HMM to query the list of peptides translated from all ORFs assembled in our p1408 dataset. During the p1408 cruise, pTF homologs were detected from dinoflagellates, stramenopiles, chlorophytes and haptophytes (Figure 1.15). Our HMM search also recovered homologs from Archaea, Bacteria, and Metazoa which are likely phosphonate-binding periplasmic proteins (Archaea and Bacteria) and transferrins (Metazoa) (McQuaid et al., 2018). Phytoplankton pTFs were consistently upregulated in

our DFOB treatment over the FeCl₃ addition (Figure 1.15). In our study, which is one of the first to investigate pTF in natural communities, we observed pTF transcripts coming overwhelmingly from chlorophytes. Chlorophyta accounted for over 74% of all pTF expression at all stations. This is despite Chlorophyta representing only 3-6% of phytoplankton mRNA (Figure 1.12). Diatoms on the other hand, made up over 28% of phytoplankton mRNA at the coastal station yet were only responsible for about 12% of pTF expression. In the transition station DCM, *P. calceolata* made up 10% of phytoplankton mRNA, but only accounted for 1.2% of pTF transcripts. *B. prasinus* at the same station was 3.8% in phytoplankton mRNA and 30% of pTF. Offshore, 85% of pTF reads were from chlorophytes which made up less than 4% of total phytoplankton mRNA. These findings suggest that despite being discovered in diatoms, the utilization of pTF by other phytoplankton groups is at times more significant. Additionally, the pattern of pTF expression is highly variable among taxa. Our incubation experiments occurred during an anomalous year, yet the conditions we encountered are not atypical for many subtropical marine environments and in these regions chlorophyte populations may rely on pTF for iron acquisition more so than other phytoplankton groups. The chlorophyte lineage is known to have a high iron requirement relative to red algal groups (Ho et al., 2003; Quigg et al., 2003), and pTF appears to be the main protein responsible for iron acquisition. This reliance on a carbonate-dependent iron supply could render this clade

especially vulnerable to iron limitation by ocean acidification. In contrast, *Phaeocystis* species produced few detectable pTF transcripts which could indicate that their iron acquisition in these incubations was carbonate independent which could constitute a competitive advantage in acidifying oceans. This agrees with Koch et al. (2018) who reported no negative impacts of increased pCO₂ on iron limited *P. Antarctica* cultures.

1.4.8 Phytoplankton diversity in an anomalous year

In late 2013 a positive temperature anomaly was first detected in the northeastern Pacific offshore of the North American continent. Spring of 2014 saw sea surface temperatures over 2°C above long term means from Alaska to California (Bond et al., 2015). By summer of 2014, this feature had expanded to over 3200 km of coastline and entered popular culture where it was referred to as “The Blob” (Bond et al., 2015). The anomaly was caused by warm weather patterns resulting in record high sea level pressure across the region. This reduced normal surface heat loss which typically occurs due to evaporation, conduction, radiation, and wind-forced currents and mixing (Bond et al., 2015). The Blob’s influence on the northeast Pacific was evident at least until 2016 (Di Lorenzo & Mantua, 2016). Wind strength was diminished in our study region where equatorward winds typically drive spring and summer upwelling which delivers cold water to the euphotic zone (Zaba & Rudnick, 2016). Warm surface waters tend to persist due to positive feedbacks as they inhibit cloud formation which increases radiative warming,

and deepen the thermocline which mitigates inputs of cold water by upwelling (Zaba & Rudnick, 2016). Warm sea surface temperature, increased stratification and decreased nutrient concentrations in the euphotic zone impacted phytoplankton communities as evidenced by low chlorophyll concentrations and primary production (Morrow et al., 2018). The p1408 study region was centered the Point Conception which during typical years is an upwelling center and represents the coastal end member of a macronutrient concentration gradient that extends offshore. This gradient in macronutrients is largely responsible for the diversity of CCE phytoplankton. During August 2014, this concentration gradient was still present even with reduced upwelling and shoreward propagation of oligotrophic conditions. In spite of low biomass in nearshore regions, typical diversity of coastal phytoplankton persisted in their characteristic geographic range. This diversity was characterized using flow cytometry (Figure 1.7), pigment composition (Figures 1.4 and 1.5), metatranscriptomics (Figures 1.9, 1.20A, and 1.22) and ribosomal RNA amplicon sequencing (Figures 1.20B, 1.20C and 1.21). There is reasonable agreement between these in eukaryotic taxonomic categories. In the coastal surface, diatoms accounted for 21.6% of phytoplankton mRNA, while pigment data assigned 39.0% of chlorophyll biomass to diatoms. The transition surface station phytoplankton mRNA was 6.4% pelagophytes, 3.3% chlorophytes and 6.7% prymnesiophytes. Pigments determined these groups to contribute 7.3%, 8.0% and 24.6% to

phytoplankton biomass, respectively. Some of the discrepancy can be explained by relatively large diatom and prymnesiophyte cell size, small pelagophytes and chlorophytes, and very small cyanobacteria. Results from our 18S amplicon approach to eukaryotic phytoplankton diversity were similar to mRNA, but certain groups significantly changed in relative abundance (Figure 1.20). 18Sv4 and 18Sv9 both showed a higher abundance of Ciliophora and Dinophyta (Figure 1.20 and Table 1.2). Ciliophora were more dramatically inflated in 18Sv9, while Dinophyta more so in 18Sv4 (Figure 1.20 and Table 1.2). The considerable increase in Dinophyta is unsupported by the pigment data (Figure 1.5), and likely due to increased 18S copy number in dinoflagellate genomes (Guo et al., 2016). *P. calceolata* relative abundance was very stable across molecular techniques (Figure 1.20 and Table 1.2), but the variation in other taxa makes this result questionable.

Prochlorococcus and *Synechococcus* cyanobacteria made up 5.9%, 14.8% and 20.4% of coastal, transition and offshore surface phytoplankton mRNA and yet the corresponding pigment percentages are significantly higher at 30.0%, 55.3% and 76.9%. Furthermore, the ratio of *Synechococcus* to *Prochlorococcus* obtained via different methodologies varied considerably (Table 1.3). Pigment data appears biased towards *Synechococcus* in the transition and offshore stations when compared with flow cytometry, the typical method used to characterize these organisms (Table 1.3). Transcript abundance show the opposite bias in all samples with *Synechococcus*

consistently low at less than 2% of phytoplankton mRNA, even in the coastal surface where it significantly outnumbers *Prochlorococcus* which comprises 4.7% of phytoplankton mRNA (Table 1.3). 16S amplicon sequencing results show a similar underrepresentation of *Synechococcus* (Figure 1.21 and Table 1.3). While inconsistencies in the eukaryotic results may be explained by gene copy number, the explanation here likely resides in the RNA extraction process. Both mRNA and 16S show the same trend which could be result from inefficient recovery of *Synechococcus* RNA either due to poor retention on the filter, ineffective cell lysis, or preferential degradation of *Synechococcus* RNA.

1.5 CONCLUSIONS

Across the CCE phytoplankton experience the gamut from eutrophy to oligotrophy with the potential for iron limitation at any stage (Figure 1.22). Coastal iron limitation results in the conspicuous symptoms of low chlorophyll biomass and unutilized sea surface nitrate, but throughout the region metabolic processes are modified by varying degrees of iron stress. This is evident on the molecular level in all our incubation experiments, as many iron responsive genes induced by our DFOB treatment are also expressed in the controls (Figures 1.10B, 1.11B, 1.13B, 1.14B, 1.16B, 1.17B and 1.18B). This indicates that even when $\text{NO}_3\text{:Fe}$ suggests iron limitation is improbable, phytoplankton are utilizing their iron sparing and uptake strategies to maintain

growth in a low iron environment, and cellular processes in truly iron replete conditions are drastically different. Coastal diatom communities leverage cell size, luxury uptake and iron storage capacity to exploit iron input. The transition zone favors a differentiated community of small eukaryotic phytoplankton. Small cell size is leveraged to maximize iron use efficiency, while potentially sacrificing iron storage. Motile *P. calceolata* cells express transporters capable of directly acquiring organic compounds from seawater. This may circumvent indirect iron costs of protein synthesis, but it also hints at the function of motility in this organism. Chemotaxis towards organic particles rich in labile iron could be a behavior which benefits this organism when dissolved iron concentrations are low. These findings parallel reports of *P. antarctica* which suggest motility and mixotrophy as low iron adaptations (Rizkallah et al., 2020), and might constitute common adaptations which underlie the low iron requirement of red algal groups (Ho et al., 2003; Quigg et al., 2003). Chlorophyta such as *B. prasinos* are considerably smaller than *P. calceolata* but as members of a green lineage likely operate at higher Fe:C (Ho et al., 2003; Quigg et al., 2003). This iron demand is met with prolific pTF expression upon cells with high surface area to volume. The success of *Phaeocystis* species in the Southern Ocean and the CCE DCM is supported by its low iron tolerance, which was evident in our incubation experiments which failed to elicit the most severe iron stress response.

Prochlorococcus populations in the oligotrophic CCE are sensitive to both iron and DFOB additions. A major feature of their response is the upregulation of porin proteins at low iron which could be involved in iron uptake. Porins have been noted in low iron *Prochlorococcus* transcriptomes (Thompson et al., 2011), and have been implicated in iron uptake strategies of bacteria (Catel-Ferreira et al., 2016; Craig et al., 2011; Meyer, 1992; Sandrini et al., 2013). A subset of pcb chlorophyll a/b binding light harvesting proteins were employed at low iron, which has been previously observed as a low iron strategy (Bibby et al., 2001, 2003; Garczarek et al., 2000). Increased light harvesting proteins may compensate for reduced numbers of photosynthetic reaction centers, but likely also protects against redox stress which is intensified at high light and low iron (Ryan-Keogh et al., 2012). Offshore surface *Prochlorococcus* populations responded more strongly to DFOB and Fe treatments, indicating perhaps an interaction between low iron, high light and redox stress.

Further investigation is required to test hypotheses generated from these incubation experiments. Culture experiments examining the low iron strategies of CCE *B. prasinos* and *Phaeocystis* isolates with a multiomic approach are needed to better understand their particular adaptations to low iron. Additionally, work with model marine phytoplankton species is crucial for studying the function of specific proteins observed in environmental datasets. Finally, more field studies such as this are necessary

to understand the temporal variability in iron stress within the CCE. As of the writing of this chapter, the experimental design conceived of here has been repeated on two additional CCE cruises, and the forthcoming results will bolster our understanding of iron's influence on the CCE.

1.6 FIGURES AND TABLES




Table 1.1. Nitrate, phosphate, silicic acid and dissolved iron measured in surface (SFC) and deep chlorophyll maximum (DCM) seawater used to initiate incubation experiments.

	Offshore		Transition		Coastal	
	SFC	DCM	SFC	DCM	SFC	DCM
Nitrate ($\mu\text{mol/L}$)	0.04	0.1	0.05	3.46	0.05	2.62
Phosphate ($\mu\text{mol/L}$)	0.34	0.34	0.29	0.6	0.22	0.49
Silicic acid ($\mu\text{mol/L}$)	2.35	2.52	1.17	2.97	0.24	2.39
dFe (nmol/L)	0.288	0.152	0.265	0.292	0.317	0.358
Si:NO ₃	58.8	25.2	23.4	0.858	4.8	0.912
NO ₃ :Fe	0.139	0.659	0.189	11.8	0.140	8.26
Chlorophyll a (mg/m^3)	0.1	0.35	0.21	0.68	0.88	1.05

Table 1.2. Comparison of average percentages of mRNA (eukaryotes only), 18Sv4 and 18Sv9 taxonomy estimates given to major eukaryotic groups in all samples from all DCM stations. Within each row, red values are significantly larger than black values (P<0.05).

	mRNA	18Sv4	18Sv9
Coastal			
Centric diatoms	23.2	3.1	3.6
Pennate diatoms	12.9	22.4	12.2
Ciliophora	1.9	5.2	7.0
Dinophyta	4.5	11.4	4.4
Transition			
<i>P. calceolata</i>	13.2	16.1	15.4
<i>B. prasinos</i>	5.1	0.19	2.1
<i>Phaeocystis</i> spp.	8.1	3.6	2.1
Ciliophora	4.3	8.2	16.8
Dinophyta	5.5	31.2	11.6
Offshore			
<i>P. calceolata</i>	11.8	11.7	12.1
Ciliophora	4.3	13.4	18.6
Dinophyta	6.5	28.7	9.8

Table 1.3. Comparison of estimates of *Prochlorococcus* and *Synechococcus* contributions to community composition in surface samples from coastal (yellow), transition, (green) and offshore (red) stations. Flow cytometry (FCM) and pigment (HPLC) data obtained from conventional CTD cast closest to samples collected for RNA. Pigment data represented as percentage of total chlorophyll biomass. mRNA % refers to percent contribution to total mRNA reads assigned to phytoplankton taxonomic groups. 16S % indicates percentage of all 16S amplicon data after removal of eukaryotic plastid sequences.

	FCM cells/mL	FCM µg/L	HPLC %	mRNA %	16S %
 <i>Prochlorococcus</i>	66,841	2.14	12.5	4.7	36.0
<i>Synechococcus</i>	106,216	10.62	17.3	1.2	9.1
 <i>Prochlorococcus</i>	273,666	8.76	19.8	13.1	57.6
<i>Synechococcus</i>	75,472	7.55	35.5	1.7	5.6
 <i>Prochlorococcus</i>	176,349	5.64	30.9	18.7	66.7
<i>Synechococcus</i>	6,300	0.63	46.1	1.6	1.2

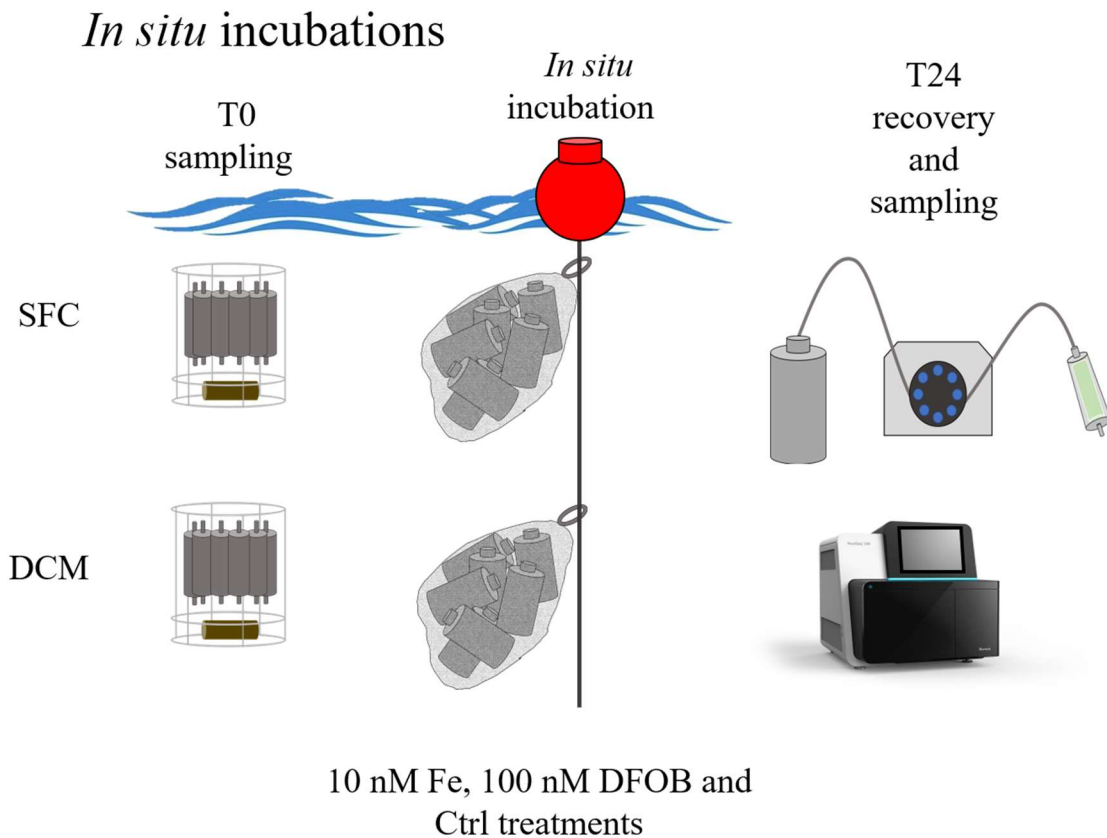


Figure 1.1. Experimental design of *in situ* array incubation experiments. Sampling via trace metal clean rosette was followed by treatments (10 nM FeCl₃, 100 nM DFOB and no addition control) made in a trace metal clean portable laboratory. Incubation bottles were returned to collection depth aboard the floating drifter array, and then collected after 24 hours. Bottles were filtered and material was frozen, brought to the shore lab, extracted and prepared for sequencing.

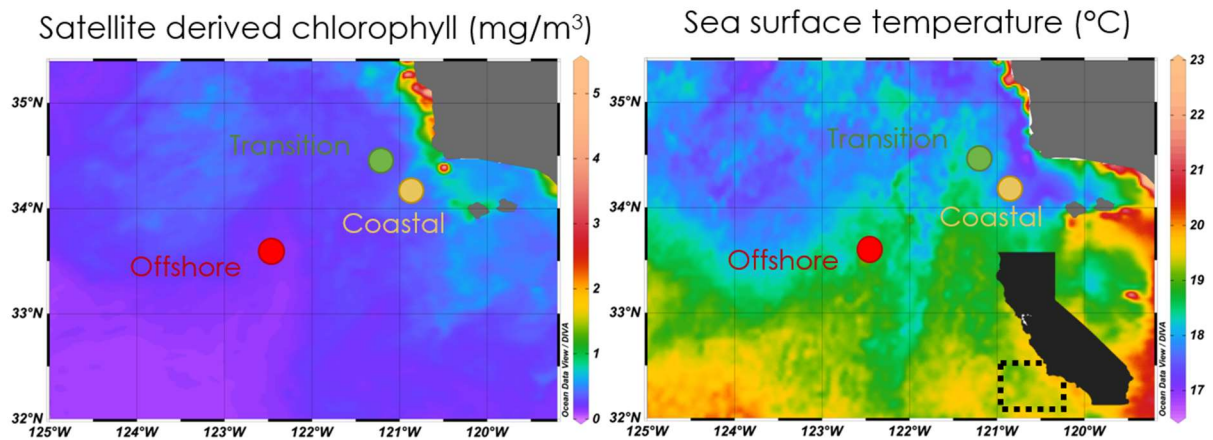


Figure 1.2. Average satellite derived sea surface chlorophyll and temperature measurements from August 2014 obtained from the NASA MODIS spectroradiometer.

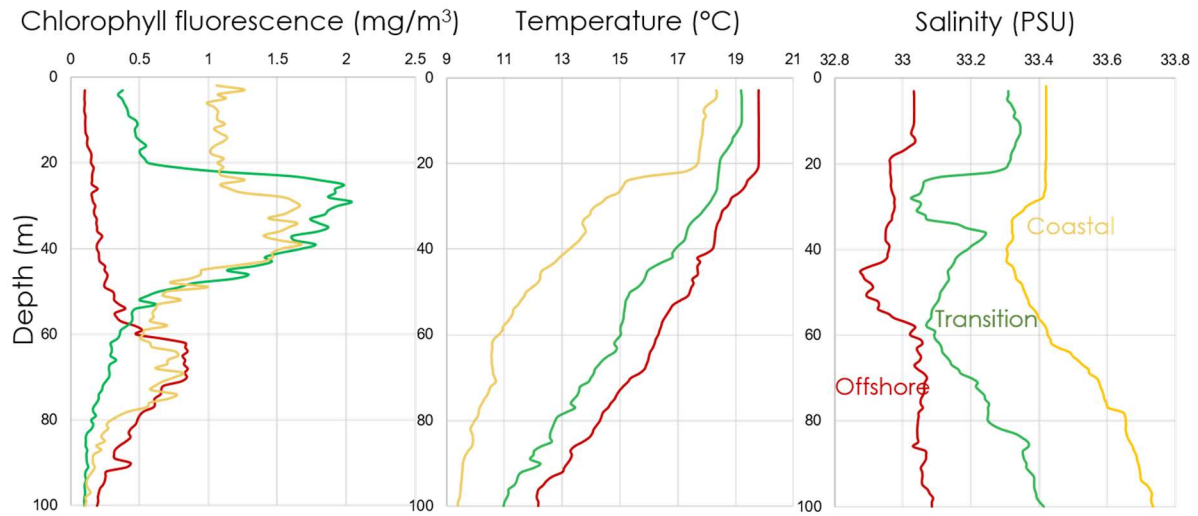


Figure 1.3. Vertical profiles of fluorescence derived chlorophyll, temperature and salinity measured aboard the conventional CTD deployment closest to the trace metal clean sampling event used to initiate incubation experiments.

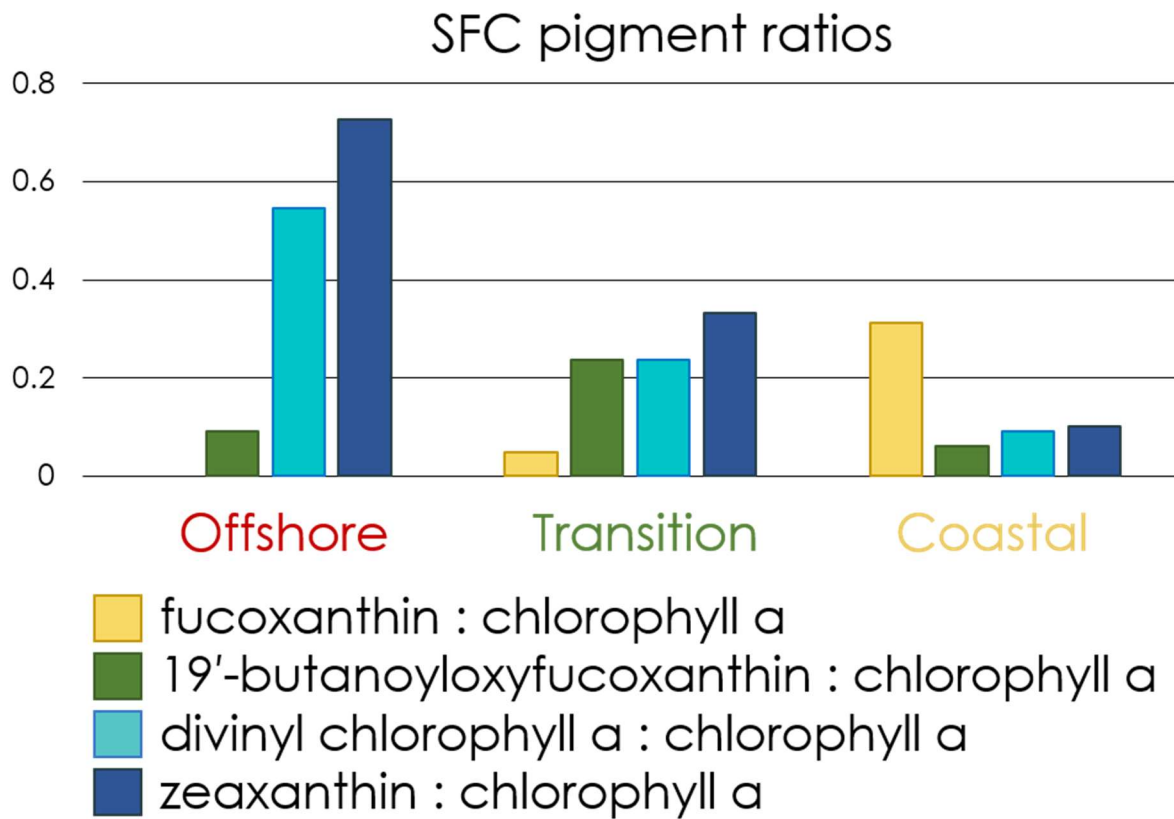


Figure 1.4. Ratios of pigments to chlorophyll a in surface seawater at each station. Collected from the conventional CTD deployment closest to the trace metal clean sampling event used to initiate incubation experiments.

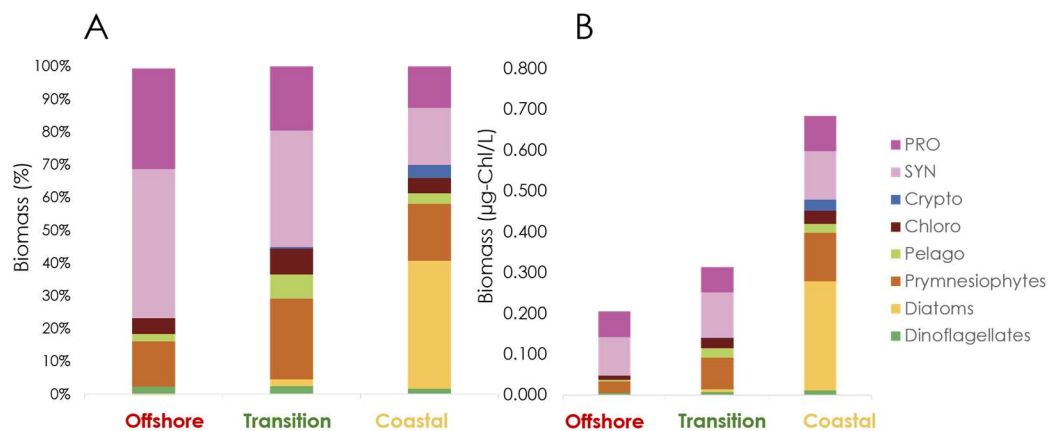


Figure 1.5. Pigment-based taxonomy based on HPLC pigment data for surface samples from all stations. *Prochlorococcus* (PRO), *Synechococcus* (SYN), cryptophytes (Crypto), chlorophytes (Chloro), pelagophytes (Pelago), prymnesiophytes, diatoms and dinoflagellates are shown. **A.** By percent of total chlorophyll biomass. **B.** By μg chlorophyll equivalents.

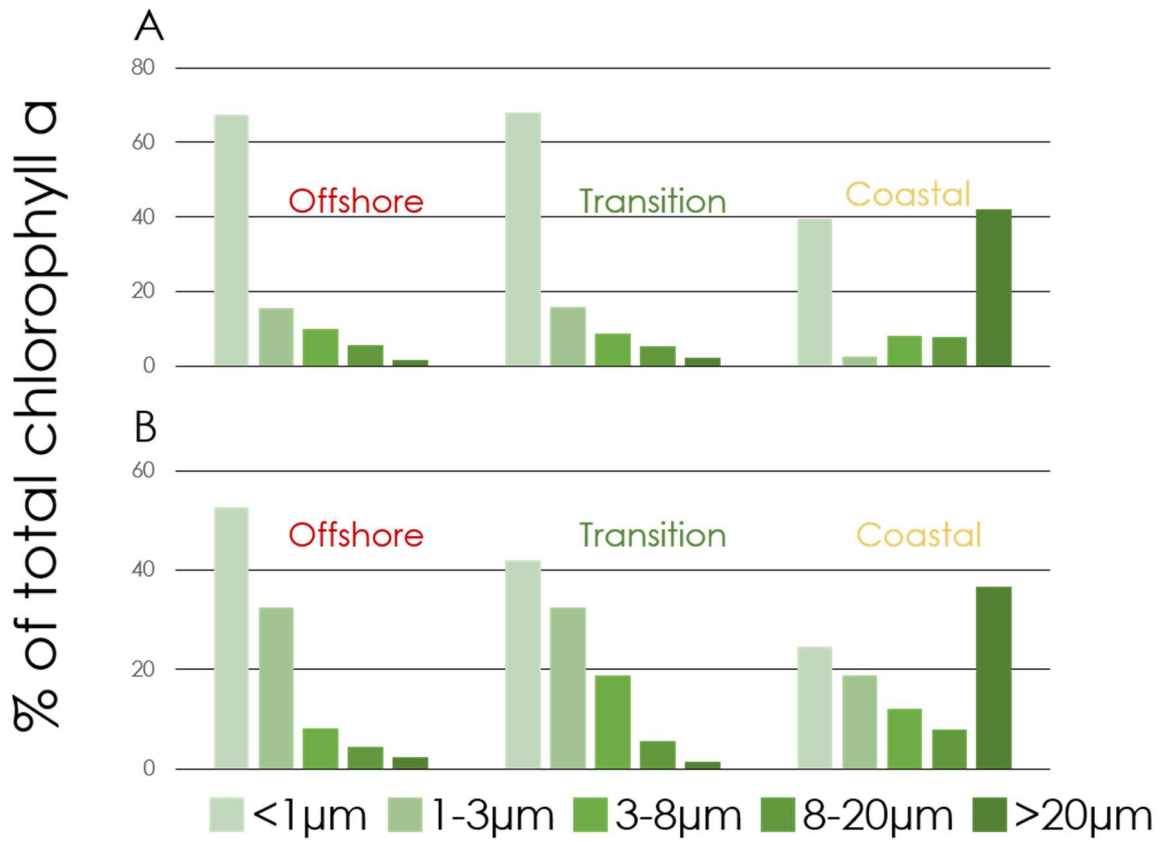


Figure 1.6. Size-fractionated chlorophyll measurements made from conventional water column sample collected closest to incubation initiation samples. **A.** Surface samples. **B.** Deep chlorophyll maximum samples.

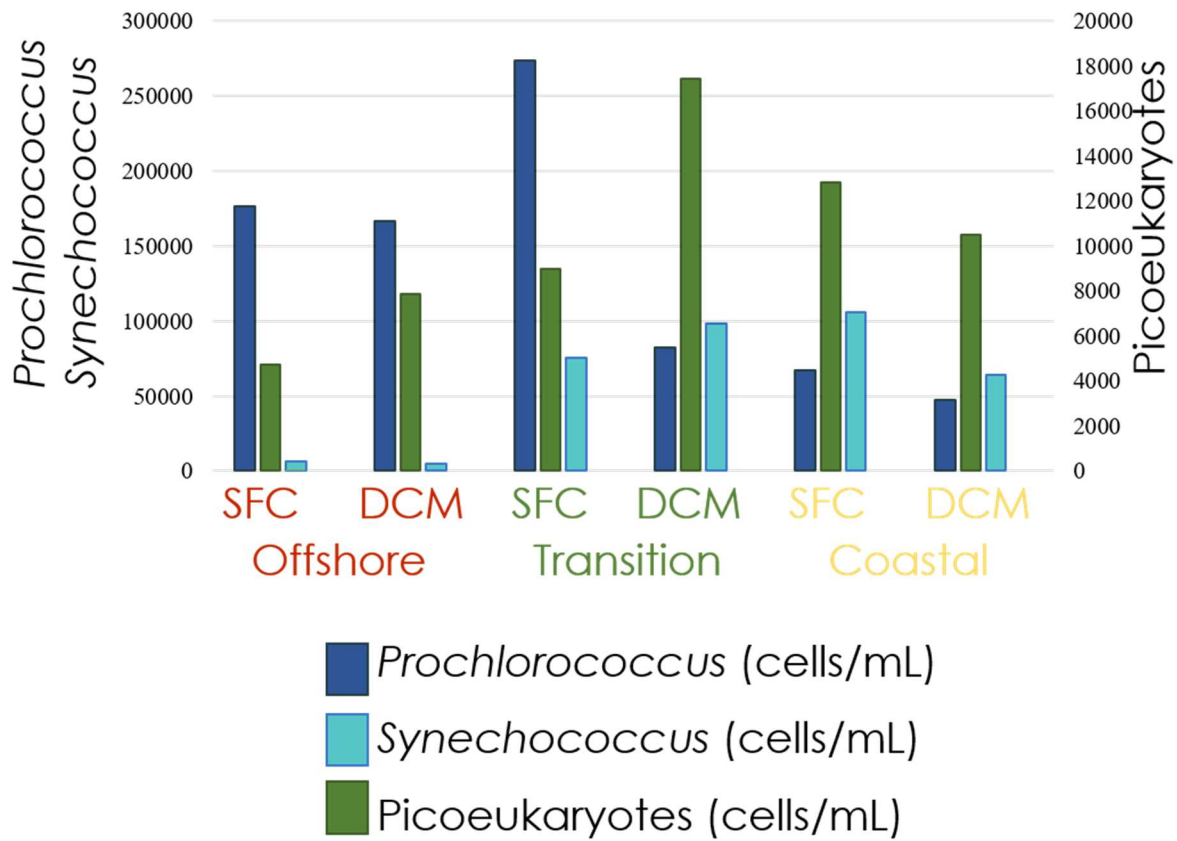


Figure 1.7. Abundances of *Prochlorococcus*, *Synechococcus*, and picoeukaryotes measured by flow cytometry at surface (SFC) and deep chlorophyll maximum (DCM) depths from all stations. Taken from conventional water column sample collected closest to incubation initiation samples.

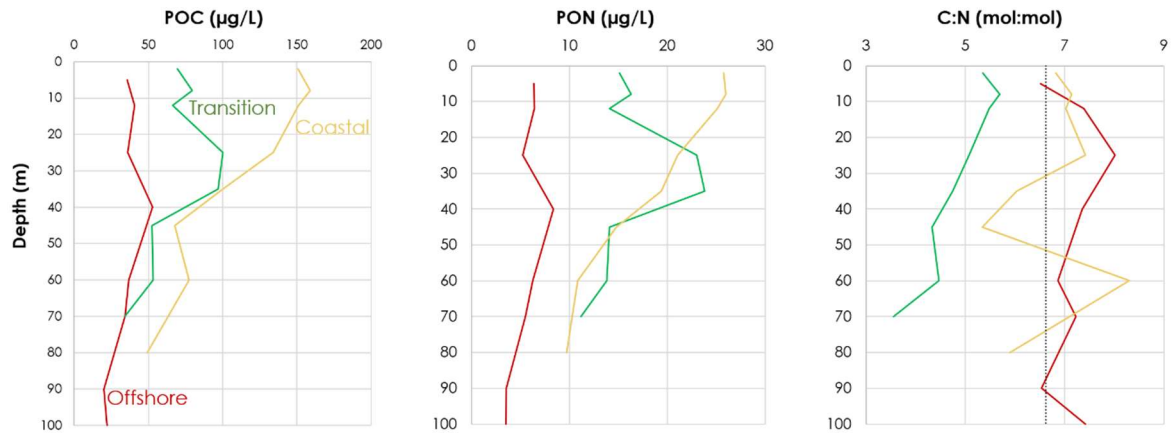


Figure 1.8. Particulate organic carbon (POC), particulate organic nitrogen (PON), and particulate C:N ratios for each station measured in samples collected via the conventional CTD deployment closest to the trace metal clean sampling event used to initiate incubation experiments. Dotted line indicates Redfield value of 106:16 (6.625).

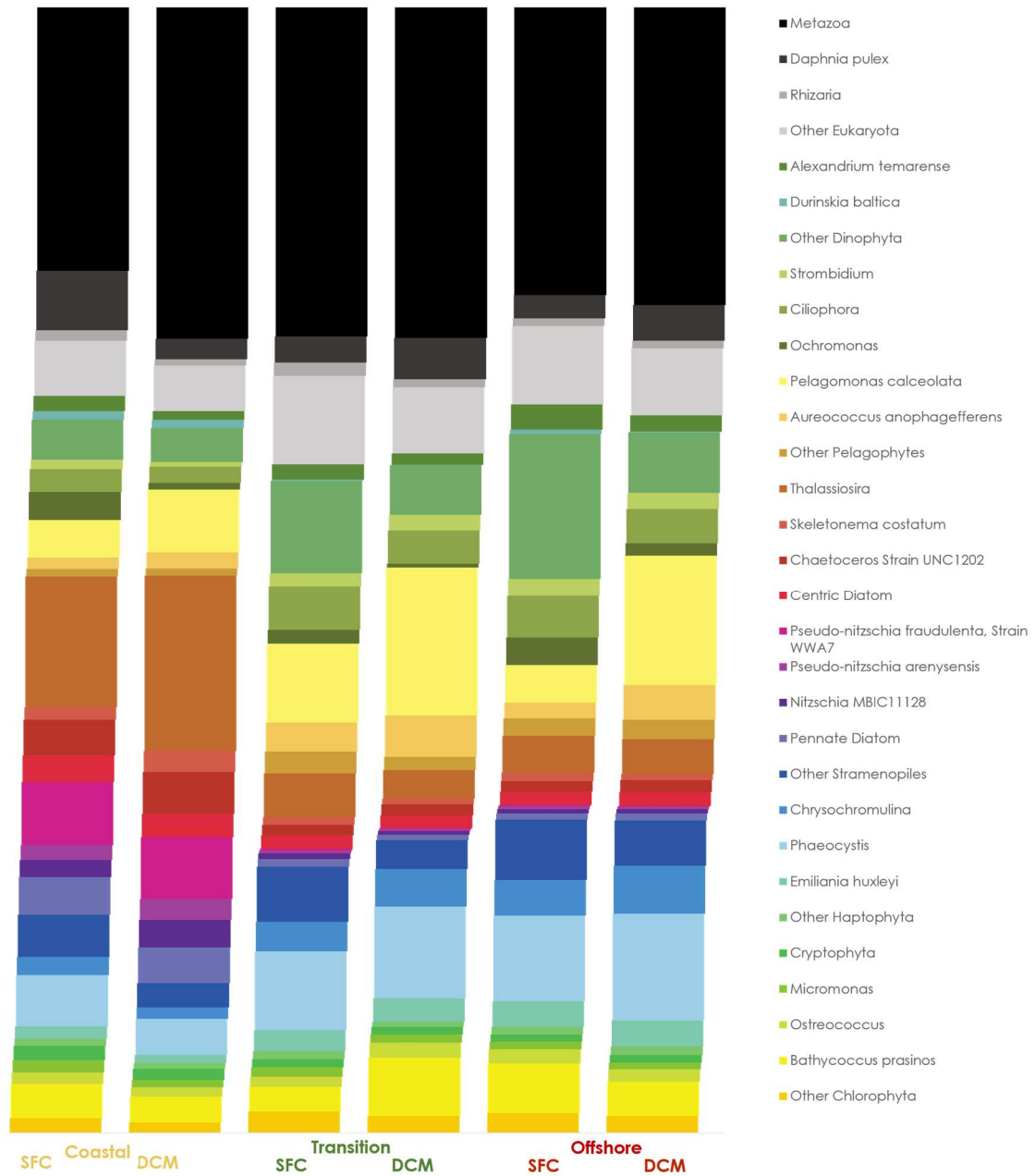


Figure 1.9. Average proportions of mRNA reads attributed to different eukaryotic groups from all incubation samples collected from each station.

Figure 1.10. Transcriptional response of centric diatoms in the coastal DCM. **A.** Manta plots showing differential expression of all ORFs annotated as centric diatoms between T24 Fe and DFOB treatments. X-axes show logCPM. Y-axes show log₂ fold change, with positive values indicating overexpression in the Fe treatment. Dot size shows -log₁₀ of false discovery rate, and significantly differentially expressed (FDR < 0.05) are indicated with red dots, while black dots indicate FDR > 0.05. Each panel shows different functional annotations with abbreviations given in text. **B.** Heatmaps showing log₂ fold change between T0 and T24 for the three treatments (Control, DFOB and Fe). ORFs are hierarchically clustered by expression pattern. **C.** Scatter plot shows log₂ fold change between T24 DFOB and Fe treatments. Positive values indicate overexpression in the Fe treatment. X-axis shows average RPKM in T24 samples.

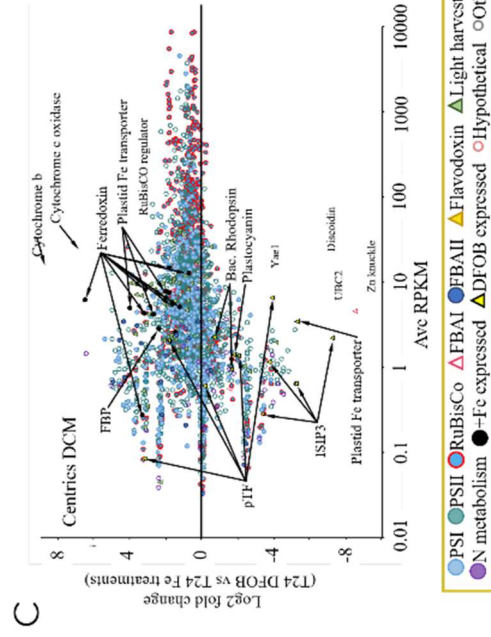
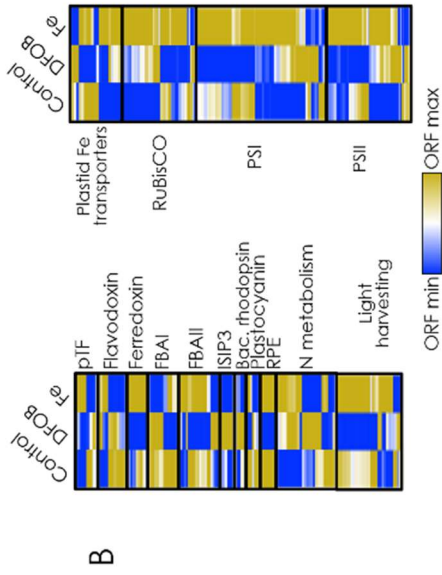
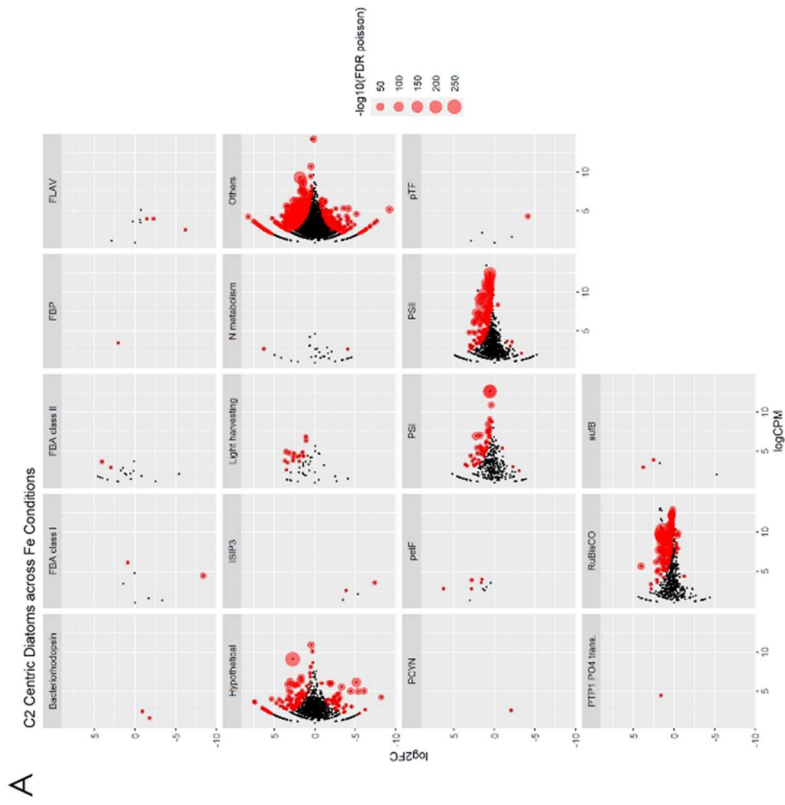
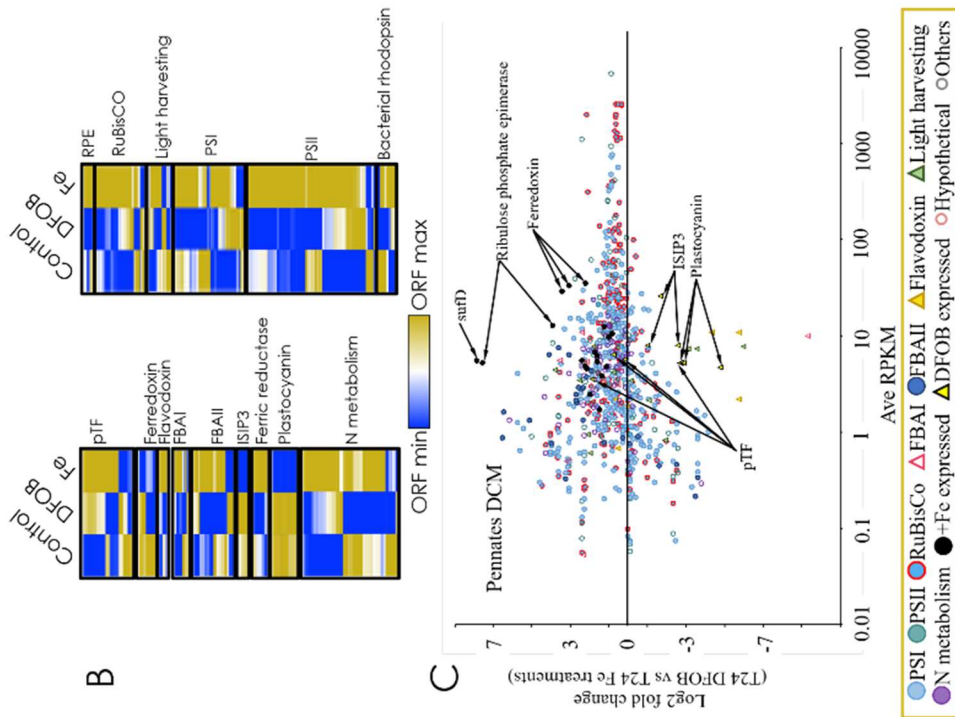
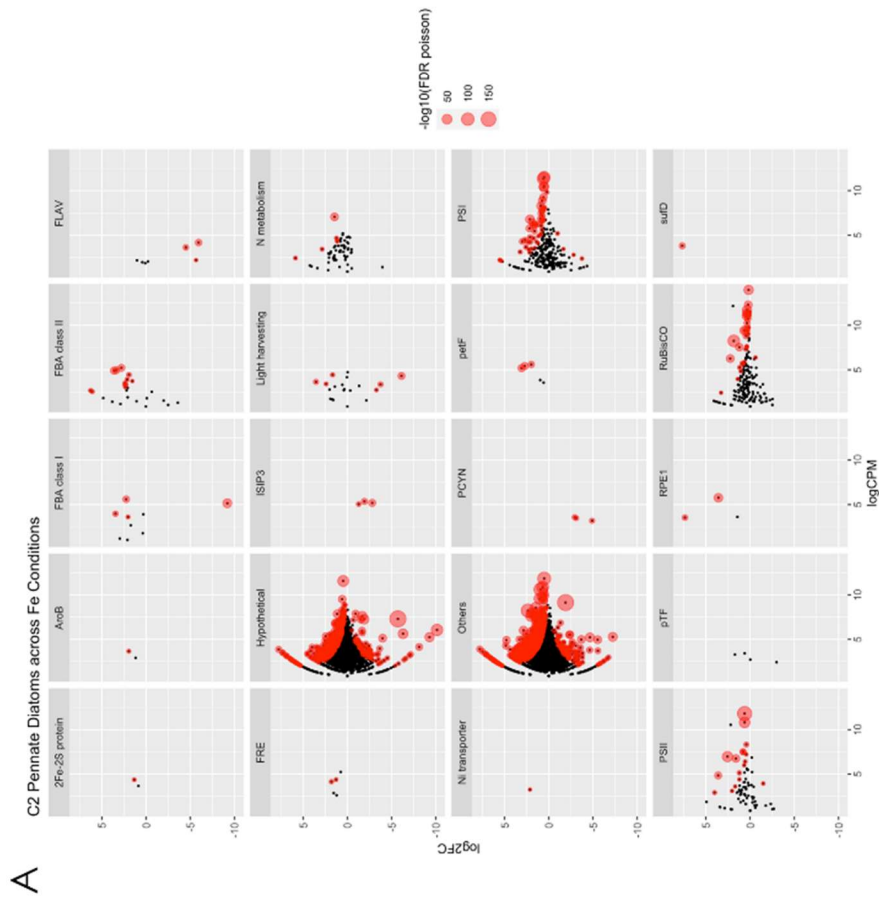


Figure 1.11. Transcriptional response of pennate diatoms in the coastal DCM. **A.** Manta plots showing differential expression of all ORFs annotated as pennate diatoms between T24 Fe and DFOB treatments. X-axes show logCPM. Y-axes show log₂ fold change, with positive values indicating overexpression in the Fe treatment. Dot size shows -log₁₀ of false discovery rate, and significantly differentially expressed (FDR < 0.05) are indicated with red dots, while black dots indicate FDR > 0.05. Each panel shows different functional annotations with abbreviations given in text. **B.** Heatmaps showing log₂ fold change between T0 and T24 for the three treatments (Control, DFOB and Fe). ORFs are hierarchically clustered by expression pattern. **C.** Scatter plot shows log₂ fold change between T24 DFOB and Fe treatments. Positive values indicate overexpression in the Fe treatment. X-axis shows average RPKM in T24 samples.



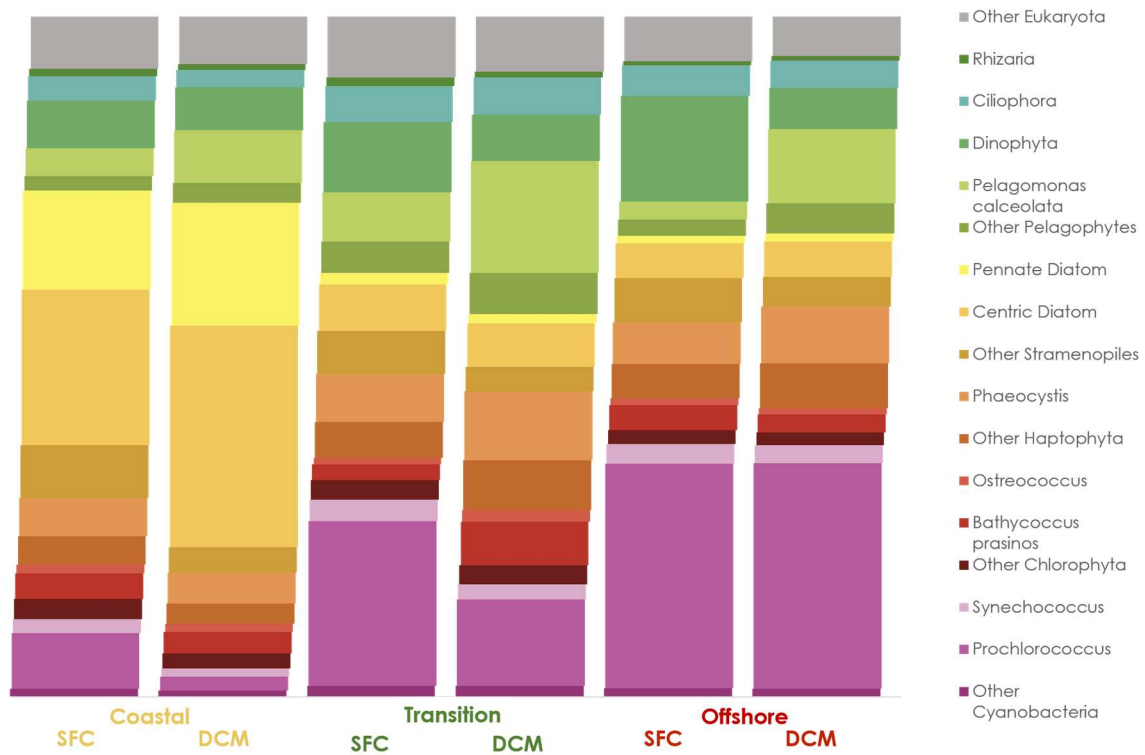
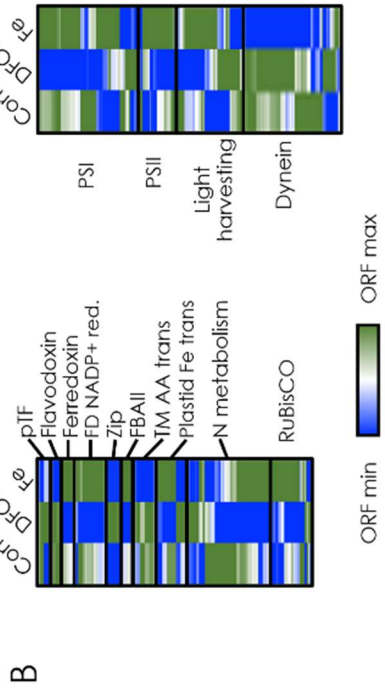
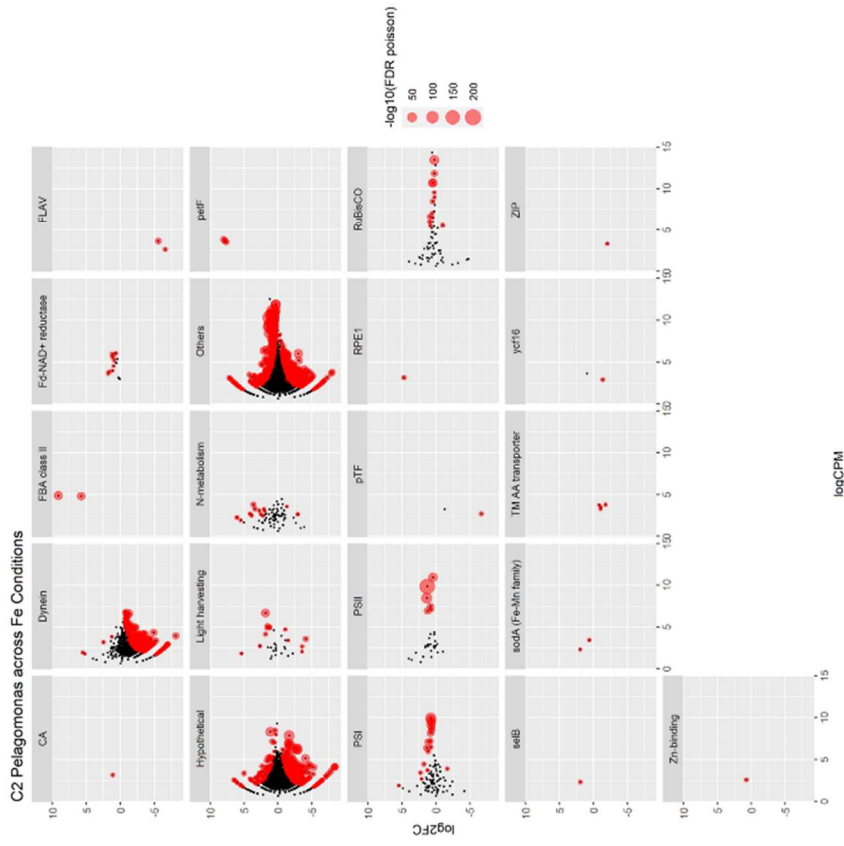


Figure 1.12. Average proportion of mRNA assigned to phytoplankton taxonomic groups for each station and depth. Includes data from all samples (T0 and T24).

Figure 1.13. Transcriptional response of *P. calceolata* in the transition DCM. **A.** Manta plots showing differential expression of all ORFs annotated as *P. calceolata* between T24 Fe and DFOB treatments. X-axes show logCPM. Y-axes show log₂ fold change, with positive values indicating overexpression in the Fe treatment. Dot size shows -log₁₀ of false discovery rate, and significantly differentially expressed (FDR < 0.05) are indicated with red dots, while black dots indicate FDR > 0.05. Each panel shows different functional annotations with abbreviations given in text. **B.** Heatmaps showing log₂ fold change between T0 and T24 for the three treatments (Control, DFOB and Fe). ORFs are hierarchically clustered by expression pattern. **C.** Scatter plot shows log₂ fold change between T24 DFOB and Fe treatments. Positive values indicate overexpression in the Fe treatment. X-axis shows average RPKM in T24 samples.

A



C

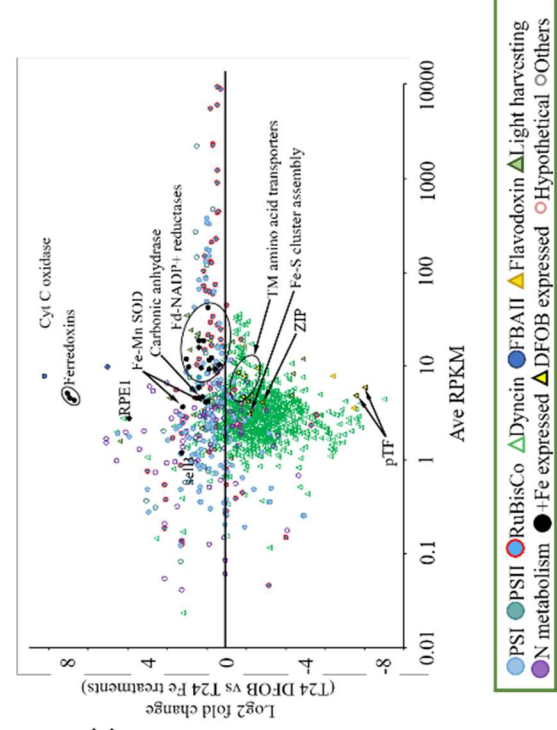


Figure 1.14. Transcriptional response of *B. prasinos* in the transition DCM. **A.** Manta plots showing differential expression of all ORFs annotated as *B. prasinos* between T24 Fe and DFOB treatments. X-axes show logCPM. Y-axes show log₂ fold change, with positive values indicating overexpression in the Fe treatment. Dot size shows -log₁₀ of false discovery rate, and significantly differentially expressed (FDR < 0.05) are indicated with red dots, while black dots indicate FDR > 0.05. Each panel shows different functional annotations with abbreviations given in text. **B.** Heatmaps showing log₂ fold change between T0 and T24 for the three treatments (Control, DFOB and Fe). ORFs are hierarchically clustered by expression pattern. **C.** Scatter plot shows log₂ fold change between T24 DFOB and Fe treatments. Positive values indicate overexpression in the Fe treatment. X-axis shows average RPKM in T24 samples.

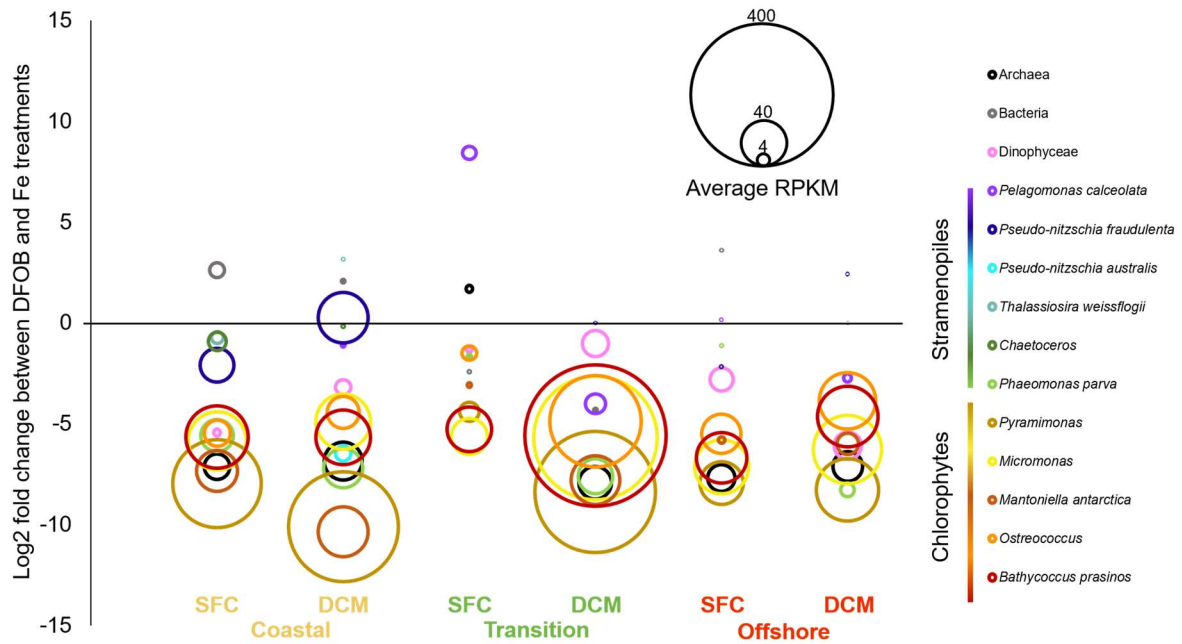
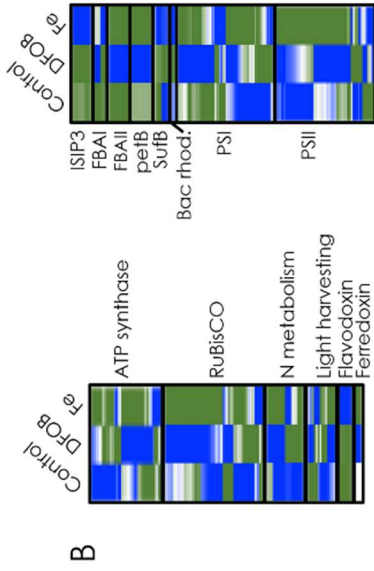
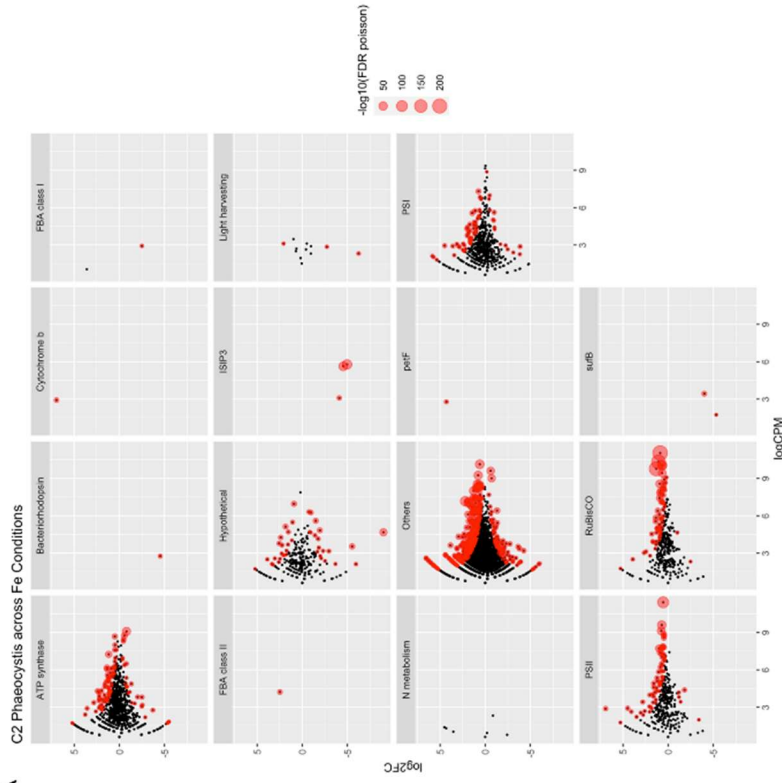


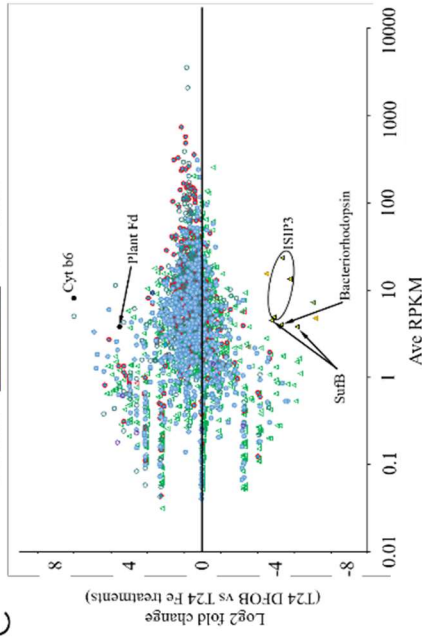
Figure 1.15. Phytotransferrin (pTF) expression at CCE stations. Y-axis shows log₂ fold change between DFOB and Fe treatments, with negative values indicating overexpression in the DFOB treatment. All pTF homologs attributed to each taxonomic group are included, and circle size indicates average transcript abundance of all homologs in all samples (T0 and T24) from each station and depth.

Figure 1.16. Transcriptional response of *Phaeocystis* in the transition DCM. **A.** Manta plots showing differential expression of all ORFs annotated as *Phaeocystis* between T24 Fe and DFOB treatments. X-axes show logCPM. Y-axes show log₂ fold change, with positive values indicating overexpression in the Fe treatment. Dot size shows -log₁₀ of false discovery rate, and significantly differentially expressed (FDR < 0.05) are indicated with red dots, while black dots indicate FDR > 0.05. Each panel shows different functional annotations with abbreviations given in text. **B.** Heatmaps showing log₂ fold change between T0 and T24 for the three treatments (Control, DFOB and Fe). ORFs are hierarchically clustered by expression pattern. **C.** Scatter plot shows log₂ fold change between T24 DFOB and Fe treatments. Positive values indicate overexpression in the Fe treatment. X-axis shows average RPKM in T24 samples.

A



C



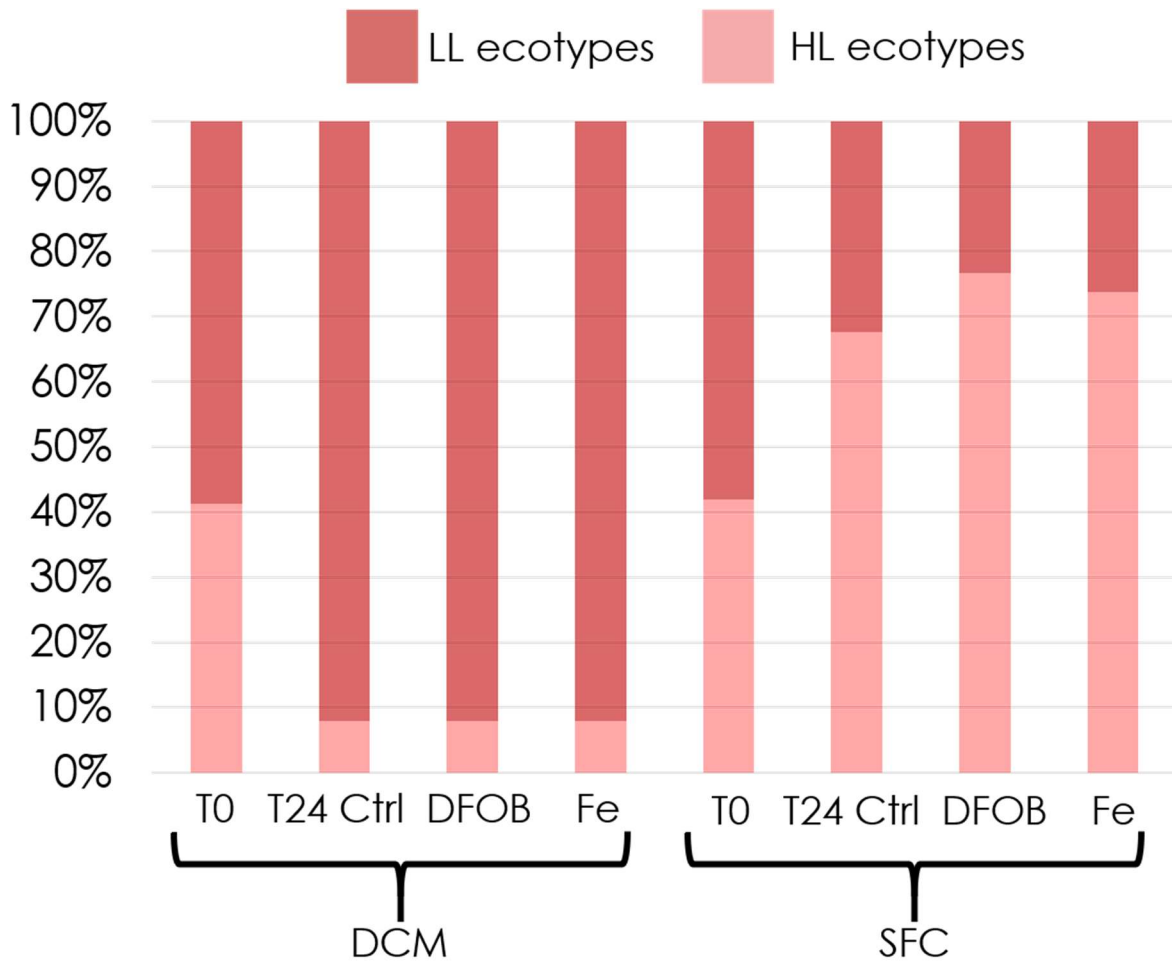


Figure 1.17. Average percentage of *Prochlorococcus* counts attributed to high light (HL) or low light (LL) adapted ecotypes in all samples from the offshore station.

Figure 1.18. Transcriptional response of low light adapted *Prochlorococcus* ecotypes in the offshore DCM. **A.** Manta plots showing differential expression of all ORFs annotated as low light adapted *Prochlorococcus* ecotypes between T24 Fe and DFOB treatments. X-axes show logCPM. Y-axes show log₂ fold change, with positive values indicating overexpression in the Fe treatment. Dot size shows -log₁₀ of false discovery rate, and significantly differentially expressed (FDR < 0.05) are indicated with red dots, while black dots indicate FDR > 0.05. Each panel shows different functional annotations with abbreviations given in text. **B.** Heatmaps showing log₂ fold change between T0 and T24 for the three treatments (Control, DFOB and Fe). ORFs are hierarchically clustered by expression pattern. **C.** Scatter plot shows log₂ fold change between T24 DFOB and Fe treatments. Positive values indicate overexpression in the Fe treatment. X-axis shows average RPKM in T24 samples.

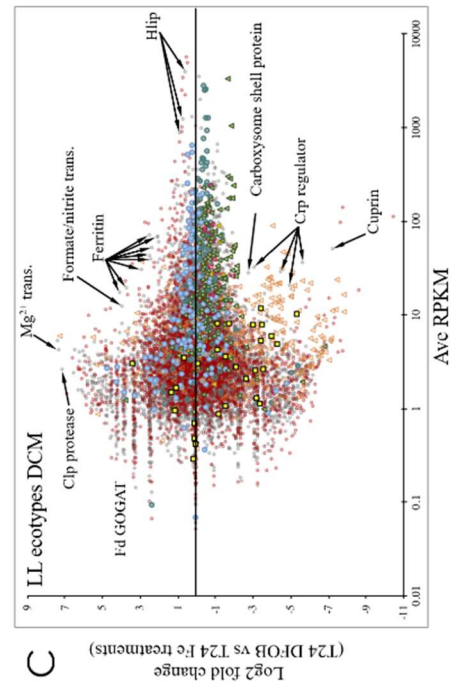
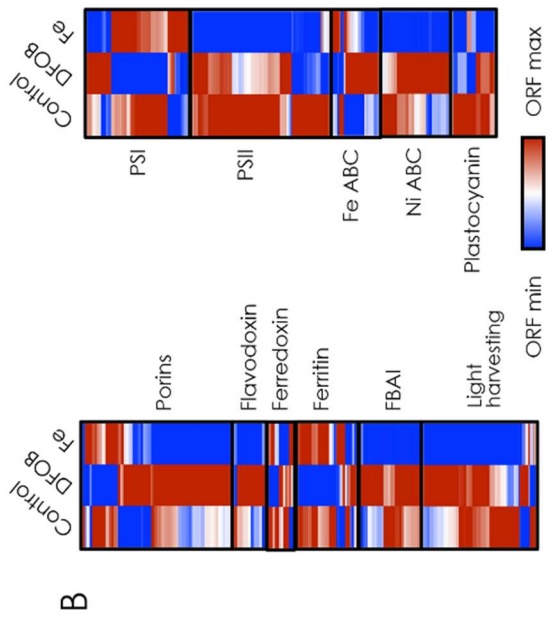
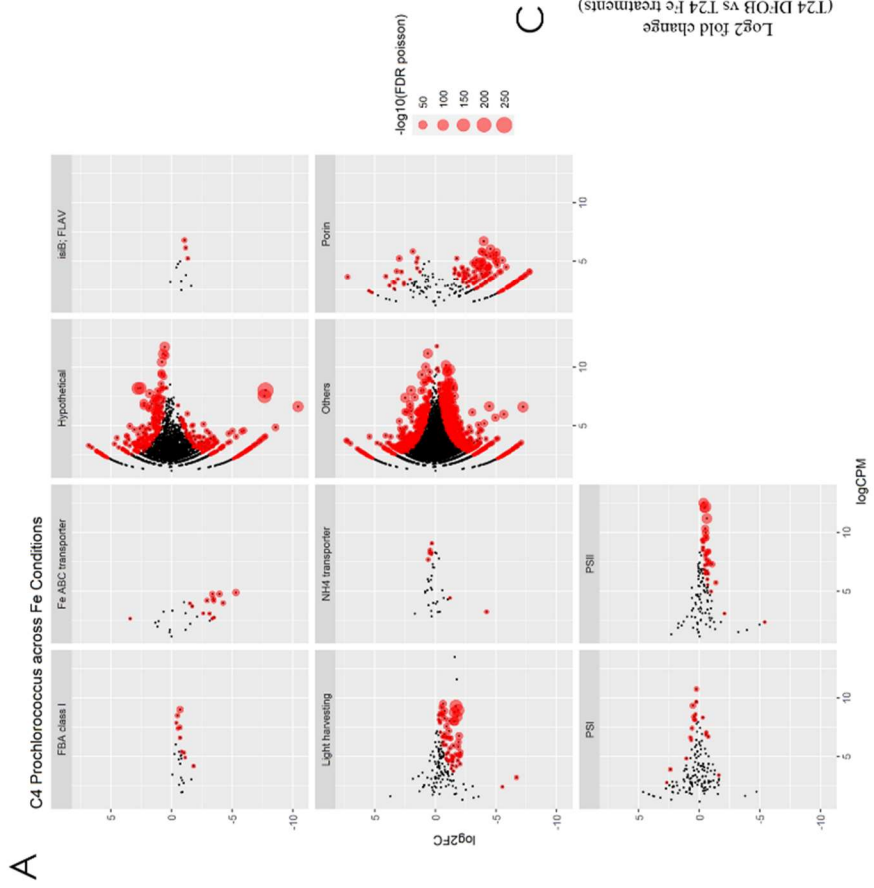


Figure 1.19. Transcriptional response of high light adapted *Prochlorococcus* ecotypes in the offshore surface. **A.** Manta plots showing differential expression of all ORFs annotated as high light adapted *Prochlorococcus* ecotypes between T24 Fe and DFOB treatments. X-axes show logCPM. Y-axes show log₂ fold change, with positive values indicating overexpression in the Fe treatment. Dot size shows -log₁₀ of false discovery rate, and significantly differentially expressed (FDR < 0.05) are indicated with red dots, while black dots indicate FDR > 0.05. Each panel shows different functional annotations with abbreviations given in text. **B.** Heatmaps showing log₂ fold change between T0 and T24 for the three treatments (Control, DFOB and Fe). ORFs are hierarchically clustered by expression pattern. **C.** Scatter plot shows log₂ fold change between T24 DFOB and Fe treatments. Positive values indicate overexpression in the Fe treatment. X-axis shows average RPKM in T24 samples.

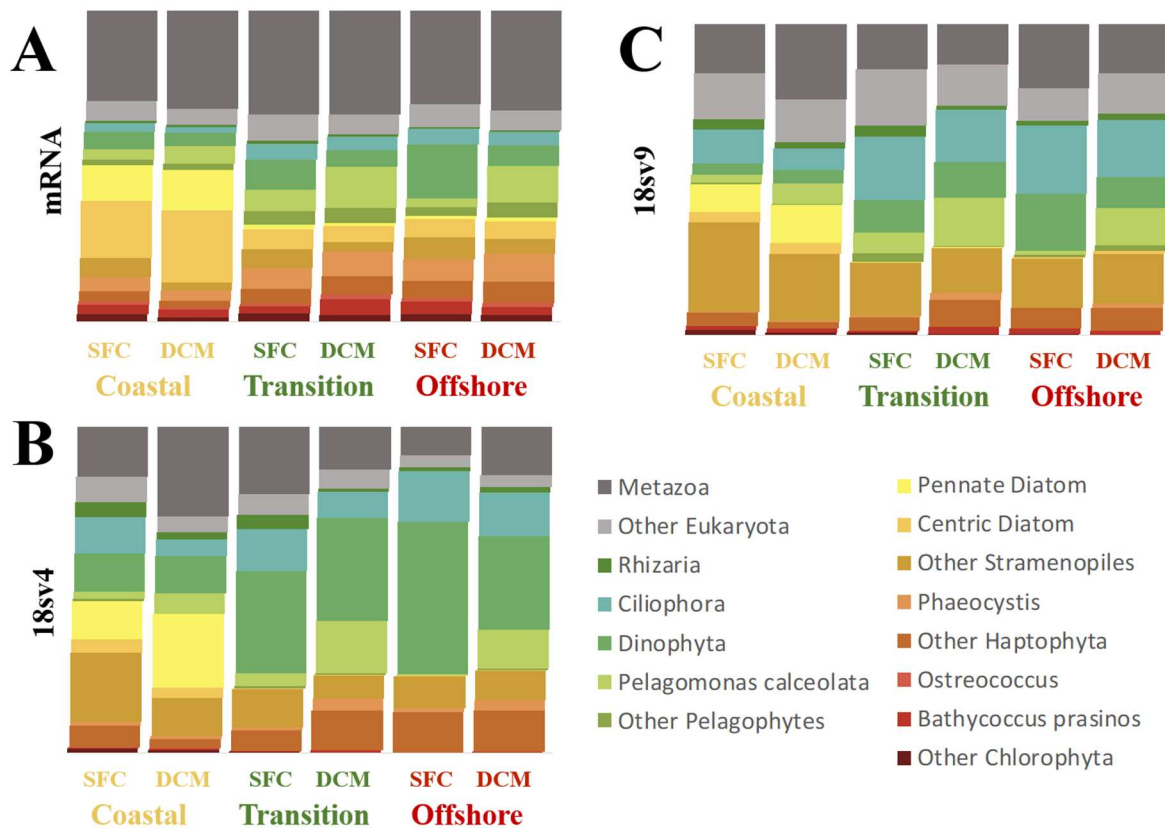


Figure 1.20. Comparison of molecular based diversity metrics. **A.** Proportion of mRNA reads attributed to eukaryotic taxonomic groups by best LPI. **B.** Composition of 18Sv4 amplicon sequencing. **C.** 18Sv9.

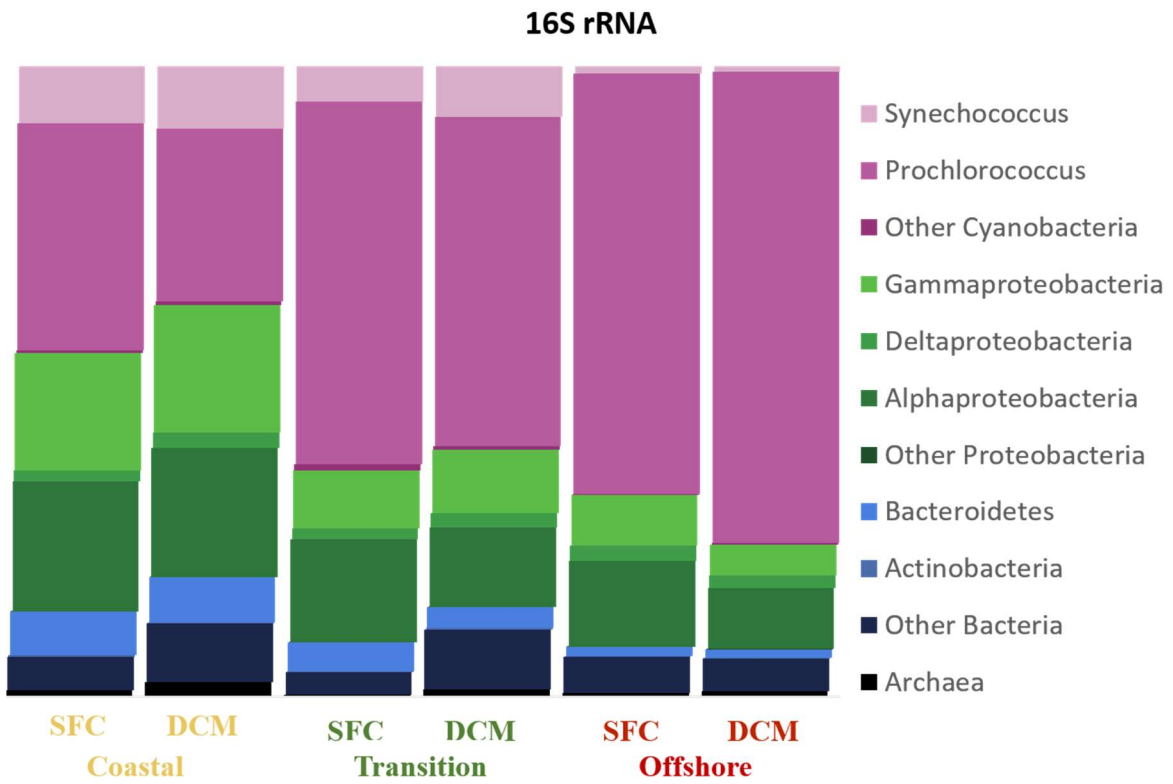


Figure 1.21. Average relative 16S amplicon abundance in all samples from all depths and stations.

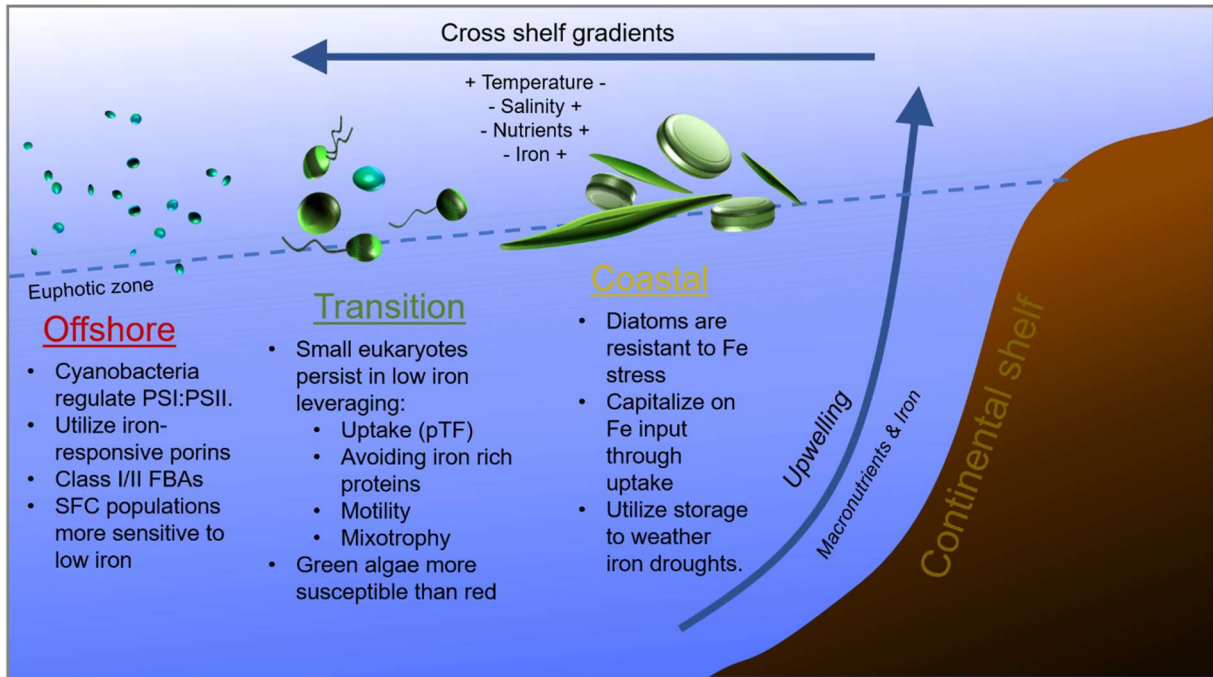


Figure 1.22. Conceptual diagram showing partitioning of phytoplankton ecotypes across the cross shelf gradients of the CCE.

1.7 ACKNOWLEDGEMENTS

Chapter one is currently being prepared for submission for publication of the material. Coale, T., Ruacho, A., Manck, L., Forsch, K., Barbeau, K., and Allen, A. A diversity of responses to iron availability by phytoplankton of the California Current ecosystem. The dissertation author was the primary investigator and author of this paper.

Funding for this work was provided by the National Science Foundation, United States Department of Energy, The Gordon and Betty Moore Foundation. Thanks to the California Current Ecosystem Long Term Ecological Research site and the California Cooperative Oceanic Fisheries Investigation. Special thanks to the captain and crew of the *R/V Melville* and chief scientist Michael Landry. Thanks to Angel Ruacho and Lauren Manck for assistance with sampling, and Michael Stukel for array deployments. Many thanks to Bethany Kolody for programming expertise and Ariel Rabines for amplicon data analysis. Ralf Goericke provided pigment-based taxonomy estimates. Finally, thanks to Hong Zheng for her magic touch in preparing cDNA libraries.

1.8 REFERENCES

Alderkamp, A., Kulk, G., Buma, A. G. J., Visser, R. J. W., Van Dijken, G. L., Mills, M. M., & Arrigo, K. R. (2012). The Effect Of Iron Limitation On The Photophysiology Of *Phaeocystis Antarctica* (Prymnesiophyceae) And *Fragilariopsis Cylindrus* (Bacillariophyceae) Under Dynamic Irradiance 1.

Journal of Phycology, 48(1), 45–59.

- Allen, A. E., Laroche, J., Maheswari, U., Lommer, M., Schauer, N., Lopez, P. J., Finazzi, G., Fernie, A. R., Bowler, C., & Karl, D. M. (2008). Whole-cell response of the pennate diatom *Phaeodactylum tricornutum* to iron starvation. *Proceedings of the National Academy of Sciences of the United States of America*, 105(30), 10438–10443. <https://doi.org/10.1073/pnas.0711370105>
- Allen, A. E., Moustafa, A., Montsant, A., Eckert, A., Kroth, P. G., & Bowler, C. (2012). Evolution and functional diversification of fructose bisphosphate aldolase genes in photosynthetic marine diatoms. *Molecular Biology and Evolution*, 29(1), 367–379. <https://doi.org/10.1093/molbev/msr223>
- Altschul, S. F., Gish, W., Miller, W., Myers, E. W., & Lipman, D. J. (1990). Basic local alignment search tool. *Journal of Molecular Biology*, 215(3), 403–410.
- Andersen, R. A., Saunders, G. W., Paskind, M. P., & Sexton, J. P. (1993). Ultrastructure and 18S Rrna Gene Sequence for *Pelagomonas Calceolata* Gen. Et Sp. Nov. and the Description of a New Algal Class, the Pelagophyceae Classis Nov. *Journal of Phycology*, 29(5), 701–715. <https://doi.org/10.1111/j.0022-3646.1993.00701.x>
- Anderson, M. A., & Morel, F. M. M. (1982). The influence of aqueous iron chemistry on the uptake of iron by the coastal diatom *Thalassiosira weissflogii* 1. *Limnology and Oceanography*, 27(5), 789–813.
- Armstrong, F. A. J., Stearns, C. R., & Strickland, J. D. H. (1967). The measurement of upwelling and subsequent biological process by means of the Technicon Autoanalyzer® and associated equipment. *Deep Sea Research and Oceanographic Abstracts*, 14(3), 381–389.
- Behnke, J., & Laroche, J. (2020). *Iron uptake proteins in algae and the role of Iron Starvation-Induced Proteins (ISIPs)*. <https://doi.org/10.1080/09670262.2020.1744039>
- Behrenfeld, M. J., & Milligan, A. J. (2011). Photophysiological Expressions of Iron Stress in Phytoplankton. *Annual Review of Marine Science*, 5, 120717164858000. <https://doi.org/10.1146/annurev-marine-121211-172356>
- Béja, O., Aravind, L., Koonin, E. V, Suzuki, M. T., Hadd, A., Nguyen, L. P., Jovanovich, S. B., Gates, C. M., Feldman, R. A., & Spudich, J. L. (2000). Bacterial rhodopsin: evidence for a new type of phototrophy in the sea. *Science*, 289(5486), 1902–1906.
- Bertrand, E. M., McCrow, J. P., Moustafa, A., Zheng, H., McQuaid, J. B., Delmont, T. O., Post, A. F., Sipler, R. E., Spackeen, J. L., Xu, K., Bronk, D. A.,

- Hutchins, D. A., & Allen, A. E. (2015). Phytoplankton–bacterial interactions mediate micronutrient colimitation at the coastal Antarctic sea ice edge. *Proceedings of the National Academy of Sciences*, *112*(32). <https://doi.org/10.1073/pnas.1501615112>
- Bibby, T. S., Mary, I., Nield, J., Partensky, F., & Barber, J. (2003). Low-light-adapted *Prochlorococcus* species possess specific antennae for each photosystem. *Nature*, *424*(6952), 1051–1054. <https://doi.org/10.1038/nature01933>
- Bibby, T. S., Nield, J., Partensky, F., & Barber, J. (2001). Antenna ring around photosystem I. *Nature*, *413*(6856), 590.
- Biller, D. V., & Bruland, K. W. (2014). The central California Current transition zone: A broad region exhibiting evidence for iron limitation. *Progress in Oceanography*, *120*, 370–382. <https://doi.org/10.1016/j.pocean.2013.11.002>
- Biller, D. V., Coale, T. H., Till, R. C., Smith, G. J., & Bruland, K. W. (2013). Coastal iron and nitrate distributions during the spring and summer upwelling season in the central California Current upwelling regime. *Continental Shelf Research*, *66*, 58–72. <https://doi.org/10.1016/j.csr.2013.07.003>
- Blaby-Haas, C. E., & Merchant, S. S. (2012). The ins and outs of algal metal transport ☆. *BBA - Molecular Cell Research*, *1823*, 1531–1552. <https://doi.org/10.1016/j.bbamcr.2012.04.010>
- Bograd, S. J., & Lynn, R. J. (2003). Long-term variability in the Southern California Current System. *Deep-Sea Research Part II: Topical Studies in Oceanography*, *50*(14–16), 2355–2370. [https://doi.org/10.1016/S0967-0645\(03\)00131-0](https://doi.org/10.1016/S0967-0645(03)00131-0)
- Boiteau, R. M., & Repeta, D. J. (2015). An extended siderophore suite from *Synechococcus* sp. PCC 7002 revealed by LC-ICPMS-ESIMS. *Metallomics*, *7*(5). <https://doi.org/10.1039/c5mt00005j>
- Bond, N. A., Cronin, M. F., Freeland, H., & Mantua, N. (2015). Causes and impacts of the 2014 warm anomaly in the NE Pacific. *Geophysical Research Letters*, *42*(9), 3414–3420. <https://doi.org/10.1002/2015GL063306>
- Botebol, H., Lelandais, G., Six, C., Lesuisse, E., Meng, A., Bittner, L., Lecrom, S., Sutak, R., Lozano, J.-C., & Schatt, P. (2017). Acclimation of a low iron adapted *Ostreococcus* strain to iron limitation through cell biomass lowering. *Scientific Reports*, *7*(1), 1–11.
- Botebol, H., Lesuisse, E., Šuták, R., Six, C., Lozano, J.-C., Schatt, P., Vergé, V., Kirilovsky, A., Morrissey, J., Léger, T., Camadro, J.-M., Gueneugues, A.,

- Bowler, C., Blain, S., & Bouget, F.-Y. (2015). Central role for ferritin in the day/night regulation of iron homeostasis in marine phytoplankton. *Proceedings of the National Academy of Sciences of the United States of America*, 112(47), 14652–14657. <https://doi.org/10.1073/pnas.1506074112>
- Brown, S. L., Landry, M. R., Selph, K. E., Yang, E. J., Rii, Y. M., & Bidigare, R. R. (2008). Diatoms in the desert: Plankton community response to a mesoscale eddy in the subtropical North Pacific. *Deep Sea Research Part II: Topical Studies in Oceanography*, 55(10–13), 1321–1333.
- Brown, M. V., & Fuhrman, J. A. (2005). Marine bacterial microdiversity as revealed by internal transcribed spacer analysis. *Aquatic Microbial Ecology*, 41(1), 15–23.
- Bruland, K. W., Rue, E. L., & Smith, G. J. (2001). Iron and macronutrients in California coastal upwelling regimes: Implications for diatom blooms. *Limnology and Oceanography*, 46(7), 1661–1674. <https://doi.org/10.4319/lo.2001.46.7.1661>
- Brzezinski M.A., Krause J.W., Bundy R.M., Barbeau K.A., Franks P., Goericke R., L. M. R. and S. M. R. (2015). Enhanced silica ballasting from iron stress sustains carbon export in a frontal zone within the California Current. *Journal of Geophysical Research: Oceans*, 120, 4654–4669. <https://doi.org/10.1002/2015JC010829>.Received
- Busch, A., Rimbauld, B., Naumann, B., Rensch, S., & Hippler, M. (2008). Ferritin is required for rapid remodeling of the photosynthetic apparatus and minimizes photo-oxidative stress in response to iron availability in *Chlamydomonas reinhardtii*. *The Plant Journal*, 55(2), 201–211.
- Carr, M.-E., & Kearns, E. J. (2003). Production regimes in four Eastern Boundary Current systems. *Deep Sea Research Part II: Topical Studies in Oceanography*, 50(22–26), 3199–3221. <https://doi.org/10.1016/j.dsr2.2003.07.015>
- Carradec, Q., Pelletier, E., Da Silva, C., Alberti, A., Seeleuthner, Y., Blanc-Mathieu, R., Lima-Mendez, G., Rocha, F., Tirichine, L., & Labadie, K. (2018). A global ocean atlas of eukaryotic genes. *Nature Communications*, 9(1), 373.
- Catel-Ferreira, M., Marti, S., Guillon, L., Jara, L., Coadou, G., Molle, V., Bouffartigues, E., Bou, G., Shalk, I., & Jouenne, T. (2016). The outer membrane porin OmpW of *Acinetobacter baumannii* is involved in iron uptake and colistin binding. *FEBS Letters*, 590(2), 224–231.
- Chappell, P. D., Whitney, L. P., Wallace, J. R., Darer, A. I., Jean-Charles, S., & Jenkins, B. D. (2014). Genetic indicators of iron limitation in wild

- populations of *Thalassiosira oceanica* from the northeast Pacific Ocean. *The ISME Journal*, 9(3), 1–11. <https://doi.org/10.1038/ismej.2014.171>
- Chase, Z., Johnson, K. S., Elrod, V. A., Plant, J. N., Fitzwater, S. E., Pickell, L., & Sakamoto, C. M. (2005). Manganese and iron distributions off central California influenced by upwelling and shelf width. *Marine Chemistry*, 95(3–4), 235–254. <https://doi.org/10.1016/j.marchem.2004.09.006>
- Chase, Z., Strutton, P. G., & Hales, B. (2007). Iron links river runoff and shelf width to phytoplankton biomass along the U.S. West Coast. *Geophysical Research Letters*, 34(4), 10–13. <https://doi.org/10.1029/2006GL028069>
- Chasteen, N. D., & Harrison, P. M. (1999). Mineralization in ferritin: an efficient means of iron storage. *Journal of Structural Biology*, 126(3), 182–194.
- Checkley, D. M., Barth, J. a., Checkley Jr, D. M., & Barth, J. a. (2009). Patterns and processes in the California Current System. *Progress in Oceanography*, 83(1–4), 49–64. <https://doi.org/10.1016/j.pocean.2009.07.028>
- Cheng, D., & He, Q. (2020). Iron Deficiency in Cyanobacteria. In *Microbial Photosynthesis* (pp. 181–196). Springer.
- Coale, T. H., Moosburner, M., Horák, A. A., Oborník, M., Barbeau, K. A., & Allen, A. E. (2019). Reduction-dependent siderophore assimilation in a model pennate diatom. *Proceedings of the National Academy of Sciences*, 116(47), 23609–23617. <https://doi.org/10.1073/pnas.1907234116>
- Cohen, N. R., Ellis, K. A., Lampe, R. H., McNair, H., Twining, B. S., Maldonado, M. T., Brzezinski, M. A., Kuzminov, F. I., Thamatrakoln, K., Till, C. P., Bruland, K. W., Sunda, W. G., Bargu, S., & Marchetti, A. (2017). Diatom transcriptional and physiological responses to changes in iron bioavailability across ocean provinces. *Frontiers in Marine Science*, 4, 360. <https://doi.org/10.3389/fmars.2018.00115>
- Cohen, N. R., Mann, E., Stemple, B., Moreno, C. M., Rauschenberg, S., Jacquot, J. E., Sunda, W. G., Twining, B. S., & Marchetti, A. (2018). Iron storage capacities and associated ferritin gene expression among marine diatoms. *Limnology and Oceanography*, 63(4). <https://doi.org/10.1002/lno.10800>
- Craig, S. A., Carpenter, C. D., Mey, A. R., Wyckoff, E. E., & Payne, S. M. (2011). Positive regulation of the *Vibrio cholerae* porin OmpT by iron and Fur. *Journal of Bacteriology*, 193(23), 6505–6511.
- De la Rosa, M. A., Navarro, J. A., Díaz-Quintana, A., De La Cerda, B., Molina-Heredia, F. P., Balme, A., del S Murdoch, P., Díaz-Moreno, I., Durán, R. V.,

- Hervás, M., Díaz-Quintana, A., De La Cerda, B., Molina-Heredia, F. P., Balme, A., Murdoch, P. D. S., Díaz-Moreno, I., Durán, R. V., & Hervás, M. (2002). An evolutionary analysis of the reaction mechanisms of photosystem I reduction by cytochrome c6 and plastocyanin. *Bioelectrochemistry*, 55(1–2), 41–45. [https://doi.org/10.1016/S1567-5394\(01\)00136-0](https://doi.org/10.1016/S1567-5394(01)00136-0)
- Di Lorenzo, E., & Mantua, N. (2016). Multi-year persistence of the 2014/15 North Pacific marine heatwave. *Nature Climate Change*, 6(11), 1042–1047. <https://doi.org/10.1038/nclimate3082>
- DiTullio, G. R., Garcia, N., Riseman, S. F., & Sedwick, P. N. (2007). Effects of iron concentration on pigment composition in *Phaeocystis antarctica* grown at low irradiance. In *Phaeocystis, major link in the biogeochemical cycling of climate-relevant elements* (pp. 71–81). Springer.
- DiTullio, G. R., Grebmeier, J. M., Arrigo, K. R., Lizotte, M. P., Robinson, D. H., Leventer, A., Barry, J. P., VanWoert, M. L., & Dunbar, R. B. (2000). Rapid and early export of *Phaeocystis antarctica* blooms in the Ross Sea, Antarctica. *Nature*, 404(6778), 595–598. <https://doi.org/10.1038/35007061>
- Doucette, G. J., Erdner, D. L., Peleato, M. L., Hartman, J. J., & Anderson, D. M. (1996). Quantitative analysis of iron-stress related proteins in *Thalassiosira weissflogii*: Measurement of flavodoxin and ferredoxin using HPLC. *Marine Ecology Progress Series*, 130(1–3), 269–276. <https://doi.org/10.3354/meps130269>
- Dupont, C. L., Mccrow, J. P., Valas, R., Moustafa, A., Walworth, N., Goodenough, U., Roth, R., Hogle, S. L., Bai, J., Johnson, Z. I., Mann, E., Palenik, B., Barbeau, K. A., Venter, J. C., Allen, A. E., Craig Venter, J., Allen, A. E., Venter, J. C., & Allen, A. E. (2014). Genomes and gene expression across light and productivity gradients in eastern subtropical Pacific microbial communities. *The ISME Journal*, 9(5), 1076–1092. <https://doi.org/10.1038/ismej.2014.198>
- Eikrem, W., & Throndsen, J. (1990). The ultrastructure of *Bathycoccus* gen. nov. and *B. prasinos* sp. nov., a non-motile picoplanktonic alga (Chlorophyta, Prasinophyceae) from the Mediterranean and Atlantic. *Phycologia*, 29(3), 344–350.
- Elrod, V. a., Johnson, K. S., Fitzwater, S. E., & Plant, J. N. (2008). A long-term, high-resolution record of surface water iron concentrations in the upwelling-driven central California region. *Journal of Geophysical Research*, 113(C11), C11021. <https://doi.org/10.1029/2007JC004610>
- Firme, G. F., Rue, E. L., Weeks, D. A., Bruland, K. W., & Hutchins, D. A. (2003).

- Spatial and temporal variability in phytoplankton iron limitation along the California coast and consequences for Si, N, and C biogeochemistry. *Global Biogeochemical Cycles*, 17(1), n/a-n/a.
<https://doi.org/10.1029/2001GB001824>
- Fuhrman, J. A., Schwalbach, M. S., & Stingl, U. (2008). Proteorhodopsins: an array of physiological roles? *Nature Reviews Microbiology*, 6(6), 488–494.
- Garcia, N. S., Sedwick, P. N., & DiTullio, G. R. (2009). Influence of irradiance and iron on the growth of colonial *Phaeocystis antarctica*: implications for seasonal bloom dynamics in the Ross Sea, Antarctica. *Aquatic Microbial Ecology*, 57(2), 203–220.
- Garczarek, L., Hess, W. R., Holtzendorff, J., van der Staay, G. W. M., & Partensky, F. (2000). Multiplication of antenna genes as a major adaptation to low light in a marine prokaryote. *Proceedings of the National Academy of Sciences*, 97(8), 4098–4101.
- Garrison, D. L., Gowing, M. M., Hughes, M. P., Campbell, L., Caron, D. A., Dennett, M. R., Shalapyonok, A., Olson, R. J., Landry, M. R., & Brown, S. L. (2000). Microbial food web structure in the Arabian Sea: a US JGOFS study. *Deep Sea Research Part II: Topical Studies in Oceanography*, 47(7–8), 1387–1422.
- Geider, R. J., La Roche, J., Greene, R. M., & Olaizola, M. (1993). RESPONSE OF THE PHOTOSYNTHETIC APPARATUS OF PHAEODACTYLUM TRICORNUTUM (BACILLARIOPHYCEAE) TO NITRATE, PHOSPHATE, OR IRON STARVATION 1. *Journal of Phycology*, 29(6), 755–766.
- Glaesener, A. G., Merchant, S. S., & Blaby-Haas, C. E. (2013). Iron economy in *Chlamydomonas reinhardtii*. *Frontiers in Plant Science*, 4(SEP), 337.
<https://doi.org/10.3389/fpls.2013.00337>
- Gledhill, M., & Buck, K. N. (2012). The organic complexation of iron in the marine environment: a review. *Frontiers in Microbiology*, 3(February), 69.
<https://doi.org/10.3389/fmicb.2012.00069>
- Glover, H. (1977). EFFECTS OF IRON DEFICIENCY ON ISOCHRYSIS GALBANA (CHRYSOPHYCEAE) AND PHAEODACTYLUM TRICORNUTUM (BACILLARIOPHYCEAE) 1. *Journal of Phycology*, 13(3), 208–212.
- Gobler, C. J., Berry, D. L., Dyhrman, S. T., Wilhelm, S. W., Salamov, A., Lobanov, A. V., Zhang, Y., Collier, J. L., Wurch, L. L., Kustka, A. B., Dill, B. D., Shah, M., VerBerkmoes, N. C., Kuo, A., Terry, A., Pangilinan, J., Lindquist, E. A., Lucas, S., Paulsen, I. T., ... Grigoriev, I. V. (2011). Niche of harmful alga *Aureococcus anophagefferens* revealed through ecogenomics. *Proceedings of the National Academy of Sciences*, 108(11), 4352–4357.

<https://doi.org/10.1073/pnas.1016106108>

- Goericke, R., & Montoya, J. P. (1998). Estimating the contribution of microalgal taxa to chlorophyll a in the field--variations of pigment ratios under nutrient-and light-limited growth. *Marine Ecology Progress Series*, 169, 97–112.
- Goldman, J. A. L., Schatz, M. J., Berthiaume, C. T., Coesel, S. N., Orellana, M. V., & Armbrust, E. V. (2019). Fe limitation decreases transcriptional regulation over the diel cycle in the model diatom *Thalassiosira pseudonana*. *Plos One*, 14(9), e0222325. <https://doi.org/10.1371/journal.pone.0222325>
- Greene, R. M., Geider, R. J., Falkowski, P. G., York, N., Geider, R. J., & Falkowski, P. G. (1991). Effect of iron limitation on photosynthesis in a marine diatom. *Limnology and Oceanography*, 36(8), 1772–1782.
- Groussman, R. D., Parker, M. S., & Armbrust, E. V. (2015). Diversity and Evolutionary History of Iron Metabolism Genes in Diatoms. *PLOS ONE*, 10(6), e0129081. <https://doi.org/10.1371/journal.pone.0129081>
- Gueneau, P., Morel, F., Laroche, J., & Erdner, D. (1998). The *petF* region of the chloroplast genome from the diatom *Thalassiosira weissflogii*: sequence, organization and phylogeny. *European Journal of Phycology*, 33(3), 203–211.
- Guillard, R. R. L., & Hellebust, J. A. (1971). GROWTH AND THE PRODUCTION OF EXTRACELLULAR SUBSTANCES BY TWO STRAINS OF PHAEOCYSTIS POUCHETI 1, 2. *Journal of Phycology*, 7(4), 330–338.
- Guo, L., Sui, Z., & Liu, Y. (2016). Quantitative analysis of dinoflagellates and diatoms community via Miseq sequencing of actin gene and v9 region of 18S rDNA. *Scientific Reports*, 6, 34709.
- Halliwell, B. (1989). Protection against oxidants in biological systems. The superoxide theory of oxygen toxicity. *Free Radicals in Biology and Medicine*.
- Harrison, P. M., & Arosio, P. (1996). The ferritins: molecular properties, iron storage function and cellular regulation. *Biochimica et Biophysica Acta (BBA)-Bioenergetics*, 1275(3), 161–203.
- Hasle, G. R. (2002). Are most of the domoic acid-producing species of the diatom genus *Pseudo-nitzschia cosmopolites*? *Harmful Algae*, 1(2), 137–146.
- Hayward, J. (1968). Studies on the growth of *Phaeodactylum tricornutum* Ill. The effect of iron on growth. *Journal of the Marine Biological Association*

- of the United Kingdom, 48(2), 295–302.
- Hider, R. C., & Kong, X. (2010). Chemistry and biology of siderophores. *Natural Product Reports*, 27(5), 637–657.
- Ho, T.-Y. T. Y., Quigg, A., Finkel, Z. V., Milligan, A. J., Wyman, K., Falkowski, P. G., & Morel, F. M. M. (2003). THE ELEMENTAL COMPOSITION OF SOME MARINE PHYTOPLANKTON1. *Journal of Phycology*, 39(6), 1145–1159. <https://doi.org/10.1111/j.0022-3646.2003.03-090.x>
- Hogle, S. L., Dupont, C. L., Hopkinson, B. M., King, A. L., Buck, K. N., Roe, K. L., Stuart, R. K., Allen, A. E., Mann, E. L., Johnson, Z. I., & Barbeau, K. A. (2018). Pervasive iron limitation at subsurface chlorophyll maxima of the California Current. *Proceedings of the National Academy of Sciences*, 115(52), 13300–13305. <https://doi.org/10.17605/OSF.IO/S37TE>
- Holm-Hansen, O., Lorenzen, C. J., Holmes, R. W., & Strickland, J. D. H. (1965). Fluorometric determination of chlorophyll. *ICES Journal of Marine Science*, 30(1), 3–15.
- Horstmann, U., & Soria-Dengg, S. (1995). Ferrioxamines B and E as iron sources for the marine diatom *Phaeodactylum tricornutum*. *Marine Ecology Progress Series*, 127, 269–277. <http://www.int-res.com/articles/meps/127/m127p269.pdf>
- Hudson, R. J. M., & Morel, F. M. M. (1993). Trace metal transport by marine microorganisms: implications of metal coordination kinetics. *Deep Sea Research Part I: Oceanographic Research Papers*, 40(1), 129–150.
- Hunter, K. A., & Boyd, P. W. (2007). Iron-binding ligands and their role in the ocean biogeochemistry of iron. *Environmental Chemistry*, 4(4), 221–232.
- Hutchins, D. A., DiTullio, G. R., Zhang, Y., & Bruland, K. W. (1998). An iron limitation mosaic in the California upwelling regime. *Limnology and Oceanography*, 43(6), 1037–1054. <https://doi.org/10.4319/lo.1998.43.6.1037>
- Hutchins, David A., & Bruland, K. W. K. W. (1998). Iron-limited diatom growth and Si: N uptake ratios in a coastal upwelling regime. *Nature*, 393(June), 65–68. <https://doi.org/Doi 10.1038/31203>
- Ito, Y., & Butler, A. (2005). Structure of synechobactins, new siderophores of the marine cyanobacterium *Synechococcus* sp. PCC 7002. *Limnology and Oceanography*, 50(6), 1918–1923.
- Johnson, K. S., Chavez, F. P., & Friederich, G. E. (1999). Continental-shelf sediment as a primary source of iron for coastal phytoplankton. *Nature*, 398(6729), 697–700. <https://doi.org/10.1038/19511>

- Kazamia, E., Sutak, R., Paz-Yepes, J., Dorrell, R. G., Vieira, F. R. J., Mach, J., Morrissey, J., Leon, S., Lam, F., Pelletier, E., Camadro, J., Bowler, C., & Lesuisse, E. (2018). Endocytosis-mediated siderophore uptake as a strategy for Fe acquisition in diatoms. *Science Advances*, 4(5), eaar4536. <https://doi.org/10.1126/sciadv.aar4536>
- Kelly, L. A., Mezulis, S., Yates, C., Wass, M., & Sternberg, M. (2015). The Phyre2 web portal for protein modelling, prediction, and analysis. *Nature Protocols*, 10(6), 845–858. <https://doi.org/10.1038/nprot.2015-053>
- King, A., & Barbeau, K. (2007). Evidence for phytoplankton iron limitation in the southern California Current System. *Marine Ecology Progress Series*, 342, 91–103. <https://doi.org/10.3354/meps342091>
- King, A. L., & Barbeau, K. A. (2011). Dissolved iron and macronutrient distributions in the southern California Current System. *Journal of Geophysical Research: Oceans*, 116(3), 1–18. <https://doi.org/10.1029/2010JC006324>
- Koch, F., Beszteri, S., Harms, L., & Trimborn, S. (2018). The impacts of iron limitation and ocean acidification on the cellular stoichiometry, photophysiology, and transcriptome of *Phaeocystis antarctica*. *Limnology and Oceanography*, 1–19. <https://doi.org/10.1002/lno.11045>
- Kolody, B. C., McCrow, J. P., Allen, L. Z., Aylward, F. O., Fontanez, K. M., Moustafa, A., Moniruzzaman, M., Chavez, F. P., Scholin, C. A., Allen, E. E., Worden, A. Z., Delong, E. F., & Allen, A. E. (2019). Diel transcriptional response of a California Current plankton microbiome to light, low iron, and enduring viral infection. *The ISME Journal*, 13(11), 2817–2833. <https://doi.org/10.1038/s41396-019-0472-2>
- Kustka, A. B., Allen, A. E., & Morel, F. M. M. (2007). Sequence Analysis and Transcriptional Regulation of Iron Acquisition Genes in Two Marine Diatoms. *Journal of Phycology*, 43(4), 715–729. <https://doi.org/10.1111/j.1529-8817.2007.00359.x>
- Lampe, R. H., Mann, E. L., Cohen, N. R., Till, C. P., Thamatrakoln, K., Brzezinski, M. A., Bruland, K. W., Twining, B. S., & Marchetti, A. (2018). Different iron storage strategies among bloom-forming diatoms. *Proceedings of the National Academy of Sciences of the United States of America*, 115(52), E12275–E12284. <https://doi.org/10.1073/pnas.1805243115>
- Landry, M. R., Ohman, M. D., Goericke, R., Stukel, M. R., & Tsyrklevich, K. (2009). Lagrangian studies of phytoplankton growth and grazing relationships in a coastal upwelling ecosystem off Southern California. *Progress in Oceanography*, 83(1–4), 208–216.

<https://doi.org/10.1016/j.pocean.2009.07.026>

- Lelandais, G., Scheiber, I., Paz-Yepes, J., Lozano, J.-C. C., Botbol, H., Pilátová, J., Žárský, V., Léger, T., Blaiseau, P.-L. L., Bowler, C., Bouget, F. Y., Camadro, J. M., Sutak, R., & Lesuisse, E. (2016). *Ostreococcus tauri* is a new model green alga for studying iron metabolism in eukaryotic phytoplankton. *BMC Genomics*, *17*(1), 319. <https://doi.org/10.1186/s12864-016-2666-6>
- Lesuisse, E., Blaiseau, P. L., Dancis, A., & Camadro, J.-M. M. (2001). Siderophore uptake and use by the yeast *Saccharomyces cerevisiae*. *Microbiology*, *147*(2), 289–298. <https://doi.org/10.1099/00221287-147-2-289>
- Lesuisse, E., & Labbe, P. (1994). *Saccharomyces cerevisiae*. *Metal Ions in Fungi*, *11*, 149.
- Lilly, L. E., Send, U., Lankhorst, M., Martz, T. R., Feely, R. A., Sutton, A. J., & Ohman, M. D. (2019). Biogeochemical Anomalies at Two Southern California Current System Moorings During the 2014–2016 Warm Anomaly-El Niño Sequence. *Journal of Geophysical Research: Oceans*.
- Limardo, A. J. (2016). *Quantitative biogeography of distinct clades of picoplanktonic marine green algae establishes that Bathycoccus ecotypes coexist more frequently than Ostreococcus ecotypes*. UC Santa Cruz.
- Lis, H., Shaked, Y., Kranzler, C., Keren, N., & Morel, F. M. M. (2014). Iron bioavailability to phytoplankton: an empirical approach. *The ISME Journal*, 1–11. <https://doi.org/10.1038/ismej.2014.199>
- Liu, X., & Millero, F. J. (2002). The solubility of iron in seawater. *Marine Chemistry*, *77*(1), 43–54.
- Lohan, M. C., Aguilar-Islas, A. M., & Bruland, K. W. (2006). Direct determination of iron in acidified (pH 1.7) seawater samples by flow injection analysis with catalytic spectrophotometric detection: Application and intercomparison. *Limnology and Oceanography: Methods*, *4*(6), 164–171.
- Lommer, M., Roy, A.-S. S., Schilhabel, M., Schreiber, S., Rosenstiel, P., & LaRoche, J. (2010). Recent transfer of an iron-regulated gene from the plastid to the nuclear genome in an oceanic diatom adapted to chronic iron limitation. *BMC Genomics*, *11*(1), 718. <https://doi.org/10.1186/1471-2164-11-718>
- Lommer, M., Specht, M., Roy, A.-S., Kraemer, L., Andreson, R., Gutowska, M. a, Wolf, J., Bergner, S. V, Schilhabel, M. B., Klostermeier, U. C., Beiko, R. G., Rosenstiel, P., Hippler, M., & LaRoche, J. (2012). Genome and low-iron

- response of an oceanic diatom adapted to chronic iron limitation. *Genome Biology*, 13(7), R66. <https://doi.org/10.1186/gb-2012-13-7-r66>
- Lucas, A. J., Dupont, C. L., Tai, V., Largier, J. L., Palenik, B., & Franks, P. J. S. (2011). The green ribbon: Multiscale physical control of phytoplankton productivity and community structure over a narrow continental shelf. *Limnology and Oceanography*, 56(2), 611–626. <https://doi.org/10.4319/lo.2011.56.2.0611>
- Ludwig, M., & Bryant, D. A. (2012). Acclimation of the global transcriptome of the cyanobacterium *Synechococcus* sp. strain PCC 7002 to nutrient limitations and different nitrogen sources. *Frontiers in Microbiology*, 3, 145.
- Mackey, K. R. M., Post, A. F., Mcilvin, M. R., Cutter, G. A., & John, S. G. (2015). Divergent responses of Atlantic coastal and oceanic *Synechococcus* to iron limitation. 112(32), 9944–9949. <https://doi.org/10.1073/pnas.1509448112>
- Maldonado, M. T., & Price, N. M. (2001). Reduction and transport of organically bound iron by *Thalassiosira oceanica* (Bacillariophyceae). *Journal of Phycology*, 37(2), 298–309. <https://doi.org/10.1046/j.1529-8817.2001.037002298.x>
- Maldonado, Maria T., & Price, N. M. (1999). Utilization of iron bound to strong organic ligands by plankton communities in the subarctic Pacific Ocean. *Deep-Sea Research Part II: Topical Studies in Oceanography*, 46(11–12), 2447–2473. [https://doi.org/10.1016/S0967-0645\(99\)00071-5](https://doi.org/10.1016/S0967-0645(99)00071-5)
- Mann, E. L., & Chisholm, S. W. (2000). Iron limits the cell division rate of *Prochlorococcus* in the eastern equatorial Pacific. *Limnology and Oceanography*, 45(5), 1067–1076. <https://doi.org/10.4319/lo.2000.45.5.1067>
- Marañón, E. (2015). Cell size as a key determinant of phytoplankton metabolism and community structure. *Annual Review of Marine Science*, 7(1), 241–264. <https://doi.org/10.1146/annurev-marine-010814-015955>
- Marchetti, A., Catlett, D., Hopkinson, B. M., Ellis, K., & Cassar, N. (2015). Marine diatom proteorhodopsins and their potential role in coping with low iron availability. *The ISME Journal*, 9(12), 1–4. <https://doi.org/10.1038/ismej.2015.74>
- Marchetti, A., Parker, M. S., Moccia, L. P., Lin, E. O., Arrieta, A. L., Ribalet, F., Murphy, M. E. P., Maldonado, M. T., & Armbrust, E. V. (2009). Ferritin is used for iron storage in bloom-forming marine pennate diatoms. *Nature*, 457(7228), 467–470. <https://doi.org/10.1038/nature07539>

- Marchetti, A., Schruth, D. M., Durkin, C. A., Parker, M. S., Kodner, R. B., Berthiaume, C. T., Morales, R., Allen, A. E., Armbrusta, E. V., & Armbrust, E. V. (2012). Comparative metatranscriptomics identifies molecular bases for the physiological responses of phytoplankton to varying iron availability. *Proceedings of the National Academy of Sciences*, *109*(6), E317–E325. <https://doi.org/10.1073/pnas.1118408109>
- Marsh, J. J., & Lebherz, H. G. (1992). Fructose-bisphosphate aldolases: an evolutionary history. *Trends in Biochemical Sciences*, *17*(3), 110–113.
- Martin, J. (1990). Glacial-interglacial CO₂ change: The iron hypothesis. *Paleoceanography*, *5*(1), 1–13. <http://www.agu.org/pubs/crossref/1990/PA005i001p00001.shtml>
- Martiny, A. C., Vrugt, J. A., Primeau, F. W., & Lomas, M. W. (2013). Regional variation in the particulate organic carbon to nitrogen ratio in the surface ocean. *Global Biogeochemical Cycles*, *27*(3), 723–731. <https://doi.org/10.1002/gbc.20061>
- McQuaid, J. B., Kustka, A. B., Oborník, M., Horák, A., McCrow, J. P., Karas, B. J., Zheng, H., Kindeberg, T., Andersson, A. J., Barbeau, K. A., & Allen, A. E. (2018). Carbonate-sensitive phytoferritin controls high-affinity iron uptake in diatoms. *Nature*, *555*(7697), 534–537. <https://doi.org/10.1038/nature25982>
- Meyer, J.-M. (1992). Exogenous siderophore-mediated iron uptake in *Pseudomonas aeruginosa*: possible involvement of porin OprF in iron translocation. *Microbiology*, *138*(5), 951–958.
- Monier, A., Welsh, R. M., Gentemann, C., Weinstock, G., Sodergren, E., Armbrust, E. V., Eisen, J. A., & Worden, A. Z. (2012). Phosphate transporters in marine phytoplankton and their viruses: Cross-domain commonalities in viral-host gene exchanges. *Environmental Microbiology*, *14*(1), 162–176. <https://doi.org/10.1111/j.1462-2920.2011.02576.x>
- Moore, L. R., Rocap, G., & Chisholm, S. W. (1998). Physiology and molecular phylogeny of coexisting *Prochlorococcus* ecotypes. *Nature*, *393*(6684), 464–467.
- Moreau, H., Verhelst, B., Couloux, A., Derelle, E., Rombauts, S., Grimsley, N., Van Bel, M., Poulain, J., Katinka, M., Hohmann-Marriott, M. F., Piganeau, G., Rouzé, P., Da Silva, C., Wincker, P., Van de Peer, Y., & Vandepoele, K. (2012). Gene functionalities and genome structure in *Bathycoccus prasinos* reflect cellular specializations at the base of the green lineage. *Genome Biology*, *13*(8), R74. <https://doi.org/10.1186/gb-2012-13-8-r74>
- Morrissey, J., & Bowler, C. (2012). Iron utilization in marine cyanobacteria and

eukaryotic algae. In *Environmental Bioinorganic Chemistry of Aquatic Microbial Organisms* (p. 90).

Morrissey, J., Sutak, R., Paz-Yepes, J., Tanaka, A., Moustafa, A., Veluchamy, A., Thomas, Y., Botebol, H., Bouget, F. Y., McQuaid, J. B., Tirichine, L., Allen, A. E., Lesuisse, E., & Bowler, C. (2015). A novel protein, ubiquitous in marine phytoplankton, concentrates iron at the cell surface and facilitates uptake. *Current Biology*, *25*(3), 364–371. <https://doi.org/10.1016/j.cub.2014.12.004>

Morrow, R. M., Ohman, M. D., Goericke, R., Kelly, T. B., Stephens, B. M., & Stukel, M. R. (2018). CCE V: Primary production, mesozooplankton grazing, and the biological pump in the California Current Ecosystem: Variability and response to El Niño. *Deep-Sea Research Part I: Oceanographic Research Papers*, *140*(June), 52–62. <https://doi.org/10.1016/j.dsr.2018.07.012>

Murphy, J., & Riley, J. P. (1962). A modified single solution method for the determination of phosphate in natural waters. *Analytica Chimica Acta*, *27*, 31–36.

Narayan, O. P., Kumari, N., & Rai, L. C. (2011). Iron starvation-induced proteomic changes in *Anabaena* (Nostoc) sp. PCC 7120: exploring survival strategy. *J Microbiol Biotechnol*, *21*(2), 136–146.

Niyogi, K. K. (1999). PHOTOPROTECTION REVISITED: Genetic and Molecular Approaches. *Annual Review of Plant Physiology and Plant Molecular Biology*, *50*(1), 333–359. <https://doi.org/10.1146/annurev.arplant.50.1.333>

Nuester, J., Vogt, S., & Twining, B. S. (2012). Localization of iron within centric diatoms of the genus *Thalassiosira*. *Journal of Phycology*, *48*(3), 626–634.

Oudot-Le Secq, M.-P. P., Grimwood, J., Shapiro, H., Armbrust, E. V., Bowler, C., & Green, B. R. (2007). Chloroplast genomes of the diatoms *Phaeodactylum tricorutum* and *Thalassiosira pseudonana*: comparison with other plastid genomes of the red lineage. *Molecular Genetics and Genomics*, *277*(4), 427–439. <https://doi.org/10.1007/s00438-006-0199-4>

Palenik, B., Grimwood, J., Aerts, A., Rouzé, P., Salamov, A., Putnam, N., Dupont, C., Jorgensen, R., Derelle, E., Rombauts, S., Zhou, K., Otilar, R., Merchant, S. S., Podell, S., Gaasterland, T., Napoli, C., Gendler, K., Manuell, A., Tai, V., ... Haselkorn, R. (2007). The tiny eukaryote *Ostreococcus* provides genomic insights into the paradox of plankton speciation. *Proceedings of the National Academy of Sciences*, *104*(18), 7705–7710. <https://doi.org/10.1073/pnas.0611046104>

Pankowski, A., & McMinn, A. (2009a). DEVELOPMENT OF IMMUNOASSAYS FOR

THE IRON-REGULATED PROTEINS FERREDOXIN AND FLAVODOXIN IN POLAR MICROALGAE 1. *Journal of Phycology*, 45(3), 771–783.

- Pankowski, A., & McMinn, A. (2009b). Iron availability regulates growth, photosynthesis, and production of ferredoxin and flavodoxin in Antarctic sea ice diatoms. *Aquatic Biology*, 4(3), 273–288. <https://doi.org/10.3354/ab00116>
- Peers, G., & Price, N. M. (2004). A role for manganese in superoxide dismutases and growth of iron-deficient diatoms. *Limnology and Oceanography*, 49(5), 1774–1783.
- Peers, G., & Price, N. M. N. (2006). Copper-containing plastocyanin used for electron transport by an oceanic diatom. *Nature*, 441(7091), 341–344. <https://doi.org/10.1038/nature04630>
- Pfaffen, S., Abdulqadir, R., Le Brun, N. E., & Murphy, M. E. P. (2013). Mechanism of ferrous iron binding and oxidation by ferritin from a pennate diatom. *The Journal of Biological Chemistry*, 288(21), 14917–14925. <https://doi.org/10.1074/jbc.M113.454496>
- Pfaffen, S., Bradley, J. M., Abdulqadir, R., Firme, M. R., Moore, G. R., Le Brun, N. E., & Murphy, M. E. P. (2015). A diatom ferritin optimized for iron oxidation but not iron storage. *Journal of Biological Chemistry*, 290(47), 28416–28427.
- Podell, S., & Gaasterland, T. (2007). DarkHorse: A method for genome-wide prediction of horizontal gene transfer. *Genome Biology*, 8(2). <https://doi.org/10.1186/gb-2007-8-2-r16>
- Price, N. M., & Morel, F. M. M. (1998). Biological cycling of iron in the ocean. *Metal Ions in Biological Systems*, 35, 1–36.
- Quigg, A., Finkel, Z. V., Irwin, A. J., Rosenthal, Y., Ho, T.-Y., Reinfelder, J. R., Schofield, O., Morel, F. M. M., & Falkowski, P. G. (2003). The evolutionary inheritance of elemental stoichiometry in marine phytoplankton. *Nature*, 425(6955), 291–294. <https://doi.org/10.1038/nature01953>
- Rao, N. A., Ambili, M., Jala, V. R., Subramanya, H. S., & Savithri, H. S. (2003). Structure – function relationship in serine hydroxymethyltransferase. 1647, 24–29. [https://doi.org/10.1016/S1570-9639\(03\)00043-8](https://doi.org/10.1016/S1570-9639(03)00043-8)
- Redfield, A. C. (1934). On the proportions of organic derivatives in sea water and their relation to the composition of plankton. *James Johnstone Memorial Volume*, 176–192.
- Rizkallah, M. R., Frickenhaus, S., Trimborn, S., Harms, L., Moustafa, A., Benes, V., Gäbler-Schwarz, S., & Beszteri, S. (2020). Deciphering Patterns of

Adaptation and Acclimation in the Transcriptome of *Phaeocystis antarctica* to Changing Iron Conditions¹. *Journal of Phycology*.
<https://doi.org/10.1111/jpy.12979>

- Rocap, G., Larimer, F. W., Lamerdin, J., Malfatti, S., Chain, P., Ahlgren, N. A., Arellano, A., Coleman, M., Hauser, L., & Hess, W. R. (2003). Genome divergence in two *Prochlorococcus* ecotypes reflects oceanic niche differentiation. *Nature*, *424*(6952), 1042–1047.
- Roche, J. La, Murray, H., Orellana, M. M. M., Newton, J., La Roche, J., Murray, H., Orellana, M. M. M., Newton, J., Roche, J. La, Murray, H., Orellana, M. M. M., & Newton, J. (1995). Flavodoxin Expression as an Indicator of Iron Limitation in Marine Diatoms¹. *Journal of Phycology*, *31*(4), 520–530.
<https://doi.org/10.1111/j.1529-8817.1995.tb02545.x>
- Roncel, M., González-Rodríguez, A. A., Naranjo, B., Bernal-Bayard, P., Lindahl, A. M., Hervás, M., Navarro, J. A., Ortega, J. M., Lindahl, M., Hervás, M., Navarro, J. A., & Ortega, J. M. (2016). Iron deficiency induces a partial inhibition of the photosynthetic electron transport and a high sensitivity to light in the diatom *Phaeodactylum tricornutum*. *Frontiers in Plant Science*, *7*(AUG2016), 1050. <https://doi.org/10.3389/fpls.2016.01050>
- Rose, A. L., & Waite, T. D. (2002). Kinetic model for Fe (II) oxidation in seawater in the absence and presence of natural organic matter. *Environmental Science & Technology*, *36*(3), 433–444.
- Ryan-Keogh, T. J., Macey, A. I., Cockshutt, A. M., Moore, C. M., & Bibby, T. S. (2012). The cyanobacterial chlorophyll-binding-protein *isia* acts to increase the in vivo effective absorption cross-section of *psi* under iron limitation. *Journal of Phycology*, *48*(1), 145–154.
<https://doi.org/10.1111/j.1529-8817.2011.01092.x>
- Sandrini, S., Masania, R., Zia, F., Haigh, R., & Freestone, P. (2013). Role of porin proteins in acquisition of transferrin iron by enteropathogens. *Microbiology*, *159*(Pt_12), 2639–2650.
- Schoemann, V., Becquevort, S., Stefels, J., Rousseau, V., & Lancelot, C. (2005). *Phaeocystis* blooms in the global ocean and their controlling mechanisms: a review. *Journal of Sea Research*, *53*(1–2), 43–66.
- Schoepp, B., Brugna, M., Lebrun, E., & Nitschke, W. (1999). Iron-sulfur centers involved in photosynthetic light reactions. *Adv Inorg Chem*, *47*, 335–360.
- Sétif, P. (2001). Ferredoxin and flavodoxin reduction by photosystem I. *Biochimica et Biophysica Acta - Bioenergetics*, *1507*(1–3), 161–179.
[https://doi.org/10.1016/S0005-2728\(01\)00205-5](https://doi.org/10.1016/S0005-2728(01)00205-5)

- Shaked, Y., Buck, K. N., Mellett, T., & Maldonado, M. T. (2020). Insights into the bioavailability of oceanic dissolved Fe from phytoplankton uptake kinetics. *The ISME Journal*, 1–12. <https://doi.org/10.1038/s41396-020-0597-3>
- Simmons, M. P., Sudek, S., Monier, A., Limardo, A. J., Jimenez, V., Perle, C. R., Elrod, V. A., Pennington, J. T., & Worden, A. Z. (2016). Abundance and biogeography of picoprasinophyte ecotypes and other phytoplankton in the eastern North Pacific Ocean. *Applied and Environmental Microbiology*, 82(6), 1693–1705. <https://doi.org/10.1128/AEM.02730-15>
- Smayda, T. J. (1997). Harmful algal blooms: Their ecophysiology and general relevance to phytoplankton blooms in the sea. *Limnology and Oceanography*, 42(5 II), 1137–1153. https://doi.org/10.4319/lo.1997.42.5_part_2.1137
- Smith, S. R., Gillard, J. T. F., Kustka, A. B., McCrow, J. P., Badger, J. H., Zheng, H., New, A. M., Dupont, C. L., Obata, T., Fernie, A. R., Allen, A. E., Martin, J., Fitzwater, S., Kolber, Z., Barber, K., Coale, S., Fitzwater, S., Greene, R., Johnson, K., ... Allen, A. A. E. (2016). Transcriptional Orchestration of the Global Cellular Response of a Model Pennate Diatom to Diel Light Cycling under Iron Limitation. *PLoS Genetics*, 12(12), e1006490. <https://doi.org/10.1371/journal.pgen.1006490>
- Soria-Dengg, S., Reissbrodt, R., & Horstmann, U. (2001). Siderophores in marine coastal waters and their relevance for iron uptake by phytoplankton: experiments with the diatom *Phaeodactylum tricornutum*. *Marine Ecology Progress Series*, 220, 73–82. <https://doi.org/10.3354/meps220073>
- Stefels, J., van Leeuwe, M. A., & Stefels, J. (1998). Effects of iron and light stress on the biochemical composition of Antarctic *Phaeocystis* sp. (Prymnesiophyceae). II. Pigment composition. *Journal of Phycology*, 34(3), 496–503.
- Strzepek, R. F., & Harrison, P. J. (2004). Photosynthetic architecture differs in coastal and oceanic diatoms. *Nature*, 431(7009), 689–692. <https://doi.org/10.1038/nature02954>
- Sunda, W. G., & Huntsman, S. a. (1995). Iron uptake and growth limitation in oceanic and coastal phytoplankton. *Marine Chemistry*, 50(1–4), 189–206. [https://doi.org/10.1016/0304-4203\(95\)00035-P](https://doi.org/10.1016/0304-4203(95)00035-P)
- Taylor, A. G., Goericke, R., Landry, M. R., Selph, K. E., Wick, D. A., & Roadman, M. J. (2012). Sharp gradients in phytoplankton community structure across a frontal zone in the California Current Ecosystem. *Journal of Plankton Research*, 34(9), 778–789. <https://doi.org/10.1093/plankt/fbs036>
- Thompson, A. W., Huang, K., Saito, M. A., & Chisholm, S. W. (2011).

- Transcriptome response of high- and low-light-adapted *Prochlorococcus* strains to changing iron availability. *ISME Journal*, 5(10), 1580–1594. <https://doi.org/10.1038/ismej.2011.49>
- Till, C. P., Solomon, J. R., Cohen, N. R., Lampe, R. H., Marchetti, A., Coale, T. H., & Bruland, K. W. (2019). The iron limitation mosaic in the California Current System: Factors governing Fe availability in the shelf/near-shelf region. *Limnology and Oceanography*, 64(1). <https://doi.org/10.1002/lno.11022>
- Trick, C. G., & Kerry, A. (1992). Isolation and purification of siderophores produced by cyanobacteria, *Synechococcus* sp. PCC 7942 and *Anabaena variabilis* ATCC 29413. *Current Microbiology*, 24(5), 241–245.
- Turnšek, J., Brunson, J. K., Deerinck, T. J., Horák, A., Bielinski, V. A., & Allen, A. E. (2019). Phytotransferrin endocytosis mediates a direct cell surface-to-chloroplast iron trafficking axis in marine diatoms. *BioRxiv*, 1–93.
- Van Leeuwe, M. A., & Stefels, J. (2007). Photosynthetic responses in *Phaeocystis antarctica* towards varying light and iron conditions. In *Phaeocystis, major link in the biogeochemical cycling of climate-relevant elements* (pp. 61–70). Springer.
- Vannier, T., Leconte, J., Seeleuthner, Y., Mondy, S., Pelletier, E., Aury, J. M., De Vargas, C., Sieracki, M., Iudicone, D., Vaulot, D., Wincker, P., & Jaillon, O. (2016). Survey of the green picoalga *Bathycoccus* genomes in the global ocean. *Scientific Reports*, 6(November), 1–11. <https://doi.org/10.1038/srep37900>
- Vaulot, D., Lepère, C., Toulza, E., de la Iglesia, R., Poulain, J., Gaboyer, F., Moreau, H., Vandepoele, K., Ulloa, O., Gavory, F., & Piganeau, G. (2012). Metagenomes of the Picoalga *Bathycoccus* from the Chile coastal upwelling. *PLoS ONE*, 7(6). <https://doi.org/10.1371/journal.pone.0039648>
- Venrick, E. L. (2012). Phytoplankton in the California Current system off southern California: Changes in a changing environment. *Progress in Oceanography*, 104, 46–58. <https://doi.org/10.1016/j.pocean.2012.05.005>
- Vraspir, J. M., & Butler, A. (2009). Chemistry of marine ligands and siderophores. *Annual Review of Marine Science*, 1, 43–63.
- Webb, E. A., Moffett, J. W., & Waterbury, J. B. (2001). Iron stress in open-ocean cyanobacteria (*synechococcus*, *trichodesmium*, and *crocospaera* spp.): Identification of the idia protein. *Appl. Environ. Microbiol.*, 67(12), 5444–5452. <https://doi.org/10.1128/AEM.67.12.5444>
- Wheatcroft, R. A., Sommerfield, C. K., Drake, D. E., Borgeld, J. C., & Nittrouer,

- C. A. (1997). *Rapid and widespread dispersal of flood sediment on the northern California margin*. [https://doi.org/10.1130/0091-7613\(1997\)025<0163](https://doi.org/10.1130/0091-7613(1997)025<0163)
- Whitney, L. P., Lins, J. J., Hughes, M. P., Wells, M. L., Chappell, P. D., & Jenkins, B. D. (2011). Characterization of putative iron responsive genes as species-specific indicators of iron stress in thalassiosiroid diatoms. *Frontiers in Microbiology*, *2*, 234.
- Wilhelm, S. W., Maxwell, D. P., & Trick, C. G. (1996). Growth, iron requirements, and siderophore production in iron-limited *Synechococcus* PCC 72. *Limnology and Oceanography*, *41*(1), 89–97.
- Wolfe-Simon, F., Grzebyk, D., Schofield, O., Falkowski, P. G., Wolfe-Simon, F., Grzebyk, D., Schofield, O., & Falkowski, P. G. (2005). THE ROLE AND EVOLUTION OF SUPEROXIDE DISMUTASES IN ALGAE1. *Journal of Phycology*, *41*(3), 453–465. <https://doi.org/10.1111/j.1529-8817.2005.00086.x>
- Worden, A. Z., & Not, F. (2008). Ecology and diversity of picoeukaryotes. *Microbial Ecology of the Oceans*, *2*, 159–205.
- Wright, S. W., Jeffrey, S. W., Mantoura, R. F. C., Llewellyn, C. A., Bjørnland, T., Repeta, D., & Welschmeyer, N. (1991). Improved HPLC method for the analysis of chlorophylls and carotenoids from marine phytoplankton. *Marine Ecology Progress Series*, 183–196.
- Xu, J. P., Noble, M., & Eittrheim, S. L. (2002). Suspended sediment transport on the continental shelf near Davenport, California. *Marine Geology*, *181*(1–3), 171–193. [https://doi.org/10.1016/S0025-3227\(01\)00266-3](https://doi.org/10.1016/S0025-3227(01)00266-3)
- Yoshinaga, R., Niwa-Kubota, M., Matsui, H., & Matsuda, Y. (2014). Characterization of iron-responsive promoters in the marine diatom *Phaeodactylum tricornutum*. *Marine Genomics*, *16*(1), 1–8. <https://doi.org/10.1016/j.margen.2014.01.005>
- Zaba, K. D., & Rudnick, D. L. (2016). The 2014–2015 warming anomaly in the Southern California Current System observed by underwater gliders. *Geophysical Research Letters*, *43*(3), 1241–1248. <https://doi.org/10.1002/2015GL067550>
- Zapata, M., Rodríguez, F., & Garrido, J. L. (2000). Separation of chlorophylls and carotenoids from marine phytoplankton: a new HPLC method using a reversed phase C8 column and pyridine-containing mobile phases. *Marine Ecology Progress Series*, *195*, 29–45.
- Zeigler Allen, L., Allen, E. E., Badger, J. H., McCrow, J. P., Paulsen, I. T., Elbourne, L. D. H., Thiagarajan, M., Rusch, D. B., Nealson, K. H., Williamson, S. J.,

Venter, J. C., Allen, A. E., Allen, L. Z., Allen, E. E., Badger, J. H., McCrow, J. P., Paulsen, I. T., Elbourne, L. D. H., Thiagarajan, M., ... Allen, A. E. (2012). Influence of nutrients and currents on the genomic composition of microbes across an upwelling mosaic. *The ISME Journal*, 6(7), 1403–1414. <https://doi.org/10.1038/ismej.2011.201>

Zinser, E. R., Lindell, D., Johnson, Z. I., Futschik, M. E., Steglich, C., Coleman, M. L., Wright, M. A., Rector, T., Steen, R., & McNulty, N. (2009). Choreography of the transcriptome, photophysiology, and cell cycle of a minimal photoautotroph, *Prochlorococcus*. *PLoS One*, 4(4), e5135.

CHAPTER 2: Iron/light co-limitation in an globally significant pelagophyte

2.1 ABSTRACT

Pelagomonas calceolata is a globally distributed pelagophyte with ecological significance and remarkable low iron tolerance. It is abundant in the deep chlorophyll maximum (DCM) communities of the Eastern subtropical Pacific where in some cases it is responsible for a majority of nitrate assimilation (Dupont et al., 2014). These communities are frequently characterized by iron limitation (Hogle et al., 2018), and early work on the low iron physiology of this organism has shown it to have the lowest iron requirement for growth of any eukaryotic phytoplankton (Sunda & Huntsman, 1995). DCM communities are also light limited, resulting in an increased need for iron-rich photosynthetic machinery. Consequently, to survive and compete in these DCM environments calls for an iron/light co-limitation specialist. In order to understand the strategies behind *P. calceolata*'s success, we have profiled this organism's physiology and gene expression. Iron replete and deplete cultures were grown under high and low light conditions and sampled over the diel cycle. Additional treatments included an iron resupply and a chelator spike. Physiological parameters measured include fluorescence, Fv/Fm, and cellular quotas for C, N, P, Fe, Cu, and chlorophyll. Our results show perturbations of cellular stoichiometry under iron limitation, which in some cases quickly revert to normal following iron resupply.

Iron limited cells contained less carbon than replete cells and exhibited higher rates of iron uptake following resupply. Co-limited cells contained less nitrogen than any other cells, and iron limitation alone did not alter this parameter. The molecular basis for these physiological differences between treatments was investigated in transcriptomic samples taken over the 24 period. Day and night proteomic profiling provided insight on the coupling of gene expression and protein abundance. Our study describes the changes in cellular function which accompany iron limitation and replenishment, and reveal novel adaptation to the challenge posed by low iron concentrations in marine environments.

2.2 INTRODUCTION

The rapid attenuation of sunlight in seawater restricts the vertical distribution of photoautotrophs to surface waters where their nutrients are quickly depleted. This results in the formation of subsurface or deep chlorophyll maximum (DCM) phytoplankton communities which straddle light and nutrient limitations. DCM communities are ubiquitous features of aquatic environments which sometimes also represent biomass and primary production maxima (Cullen, 1982; Cullen, 2014; Revelante & Gilmarin, 1973; Venrick, 1973). Oceanic ferriclines are typically deeper than nitriclines even in regions without HNLC surface water (Bowie et al., 2005; Johnson et al., 1997, 2003), and this produces low subsurface Fe:N and the potential for iron limitation as nutrient drawdown occurs. Iron limitation of natural DCM

communities is understudied, but recent evidence indicates it could be widespread and intensifying (Hogle et al., 2018; Holm-Hansen et al., 2005; Hopkinson & Barbeau, 2008; Johnson et al., 2010). Phytoplankton which successfully inhabit these environments are adapted to endure despite scarcity of two essential components of photosynthesis.

After the Pelagophyte class was established in 1993 (Andersen et al., 1993), environmental surveys of the diagnostic pigment 19'-butanoyloxyfucoxanthin were used to confirm the presence of this stramenopile lineage in the Atlantic and Pacific oceans (Andersen et al., 1996; Suzuki et al., 1997). Following the emergence of marine metagenomics, *Pelagomonas calceolata* was observed worldwide in the global ocean sampling (GOS) datasets (Rusch et al., 2007; Worden et al., 2011). Subsequently, studies have identified *P. calceolata* as a significant member of DCM phytoplankton communities found in the Eastern subtropical Pacific (Dupont et al., 2014; Hogle et al., 2018). Southern Pacific DCM phytoplankton communities are frequently dominated by *P. calceolata* (Shi et al., 2011). Additionally, the TARA Oceans expedition found pelagophytes to be one of the principal photosynthetic groups in the world's oceans, with *Pelagomonas* being among the most common oceanic genera (Carradec et al., 2018).

The pioneering work of Bill Sunda and Susan Huntsman in the 1990s provided phytoplankton biologists with the first detailed physiological assessments of iron limited algal cells (Sunda & Huntsman, 1995, 1997). Their

findings revealed large disparities in the iron requirements of different phytoplankton which might underlie community composition in iron limited regions. In particular, their measurements of growth rates demonstrated that at the lowest levels of bioavailable iron examined, *P. calceolata* was the fastest growing phytoplankton in their study (growing at 75% of the iron replete growth rate) ahead of diatoms, a coccolithophore and a dinoflagellate (Sunda & Huntsman, 1995). Again in 2005, *P. calceolata* defended its title as low iron champion (by the same growth metric) against a prasinophyte and a species of cyanobacteria (Timmermans et al., 2005). These studies underscore the ultimate consequences of *P. calceolata*'s specialization but provide few insights into the biological mechanisms at play. Hypotheses about the proteins involved have had to rely extensively on investigations of iron limited model organisms and natural microbial communities.

A handful of modern studies have investigated the impact of iron limitation on marine phytoplankton (e.g. Allen et al., 2008; Cohen et al., 2018; Koch et al., 2018; Lelandais et al., 2016; Lommer et al., 2012; Marchetti et al., 2012; Smith et al., 2016). Many of these studies have focused on diatoms as they represent the group which responds most dramatically to iron addition in the marine environment (de Baar et al., 2005). This research has identified a set of genes which are iron sensitive across taxa, such as the iron-starvation-induced proteins (ISIPs), as well as iron permeases, multi-copper oxidases,

rhodopsins, plastocyanin, flavodoxin and phytoferritin. The model pennate diatom *Phaeodactylum tricornutum* has been investigated in 2008 and 2016, and the latter study monitored changes in gene expression around the clock. Many iron related genes exhibited a diel pattern, and iron-stress related changes to central metabolic processes were differentially expressed across the day/night cycle. One study has investigated the low iron response of a picoeukaryotic phytoplankton species throughout the diel cycle, but the organism studied (*Ostreococcus tauri*) is not a close relative of *P. calceolata* (Lelandais et al., 2016). Nevertheless, they found a low iron response which was largely coordinated with the day/night cycle, and involved some of the components of the diatom low iron response. These studies highlight the influence of diel cycling on gene expression and physiology, and greatly influenced the experimental design of our study (Ashworth et al., 2013; Dimier et al., 2009; Monnier et al., 2010; Smith et al., 2016). Phototrophic organisms modify their transcriptomes in tight synchrony with light availability (Ashworth et al., 2013; Poliner et al., 2015; Zinser et al., 2009; Zones et al., 2015) and when photosynthesis is impacted by iron stress the timing and orchestration of these changes likely becomes more important. Many iron-containing photosynthetic proteins are not required at night, therefore efficient use of iron requires protein and/or cofactor recycling on a diel timescale (Blaby-Haas & Merchant, 2013). In order to faithfully characterize the physiological strategies employed by this organism in the marine environment we decided

high resolution diel sampling through light/dark transitions was essential. Single transcriptomes from cultures grown in constant illumination would fail to resolve tradeoffs between day and night metabolism, and single time points from the light or dark period could miss genes with narrow expression windows.

The stoichiometry of phytoplankton biomass can vary wildly between cells experiencing different physicochemical environments, and iron availability can be a major factor. Cellular iron quotas can fluctuate due to luxury uptake and storage, or substitution of low iron alternative proteins. Iron requirements also vary by algal lineage, with the red plastid containing superfamily generally needing less iron than the green superfamily (Ho et al., 2003; Quigg et al., 2003). Given that iron quotas are already low (in relation to carbon, nitrogen, or phosphorous), the ratios of these macronutrients to iron are highly variable. Iron also exerts influence on the stoichiometry of other elements through its role in carbon and nitrogen metabolism. Iron limitation has been shown to alter nutrient uptake, as well as carbon fixation rates in diatoms (Price, 2005; Takeda, 1998). Iron stressed communities typically have lower carbon and nitrogen relative to phosphorous, and more silicon (Brzezinski et al. 2015; Hutchins & Bruland, 1998). In light of this, measuring the changes in stoichiometry which accompany iron starvation was designed to be a central component of this study.

The iron demand of photosynthesis has the potential to result in a type of biochemically mediated colimitation (Saito et al., 2008). Phytoplankton experience light limitation frequently in subsurface chlorophyll maxima, deep mixed layers and high latitude winters; environments which can also be low iron. The typical physiological reaction to low light is to increase their cellular inventories of photosynthetic proteins in order to capitalize on limited light resources. This entails an increased iron requirement and therefore low light has the potential to exacerbate iron limitation (Raven, 1990).

Laboratory studies of marine phytoplankton have demonstrated increased iron quotas at low light intensities (R F Strzepek & Price, 2000; Sunda & Huntsman, 1997) and short photoperiods (Sunda & Huntsman, 2011). However, certain species adapted to iron and light colimitation behave differently. A laboratory study of *Fragilariopsis kerguelensis*, a diatom native to the Southern Ocean, was able to detect the antagonistic effects of iron-light colimitation at the transcript level as iron stress biomarker expression increased when low light accompanied low iron (Moreno et al., 2020). Still, this did not result in a slower growth rate of colimited cultures (Moreno et al., 2020). Further physiological investigation revealed Fe:C ratios in Southern Ocean diatoms remain low, even at low irradiance (Strzepek et al., 2012). Maintenance of growth in these conditions is attributed to large light harvesting antennae, which benefit from low temperatures (Strzepek et al., 2019). In contrast to oceanic phytoplankton from temperate regions which

substantially increase PSII:PSI during iron light colimitation, certain Southern Ocean diatoms decrease inventories of both photosystems more evenly and PSII:PSI fluctuates less. High PSII:PSI results in an imbalance of NADPH and ATP production. Supplemental ATP can be generated independently of PSI through the water-water cycle (Asada, 1999; Behrenfeld & Milligan, 2011) or via proteorhoopsins (Marchetti et al., 2015). The latter strategy uses less iron, and may be favored by phytoplankton adapted to low iron conditions (Moreno et al., 2018; Strzepek et al., 2019). It remains to be determined how broadly the physiology of iron-starved diatoms mirrors that of other stramenopiles.

2.3 METHODS

2.3.1 Low iron culturing

P. calceolata (CCMP 1756) was obtained from the National Center for Marine Algae and Microbiota (NCMA). Cultures were grown in Aquil (Morel et al., 1979; Price et al., 1989) synthetic seawater which was treated with Chelex 100 resin (Bio-Rad Laboratories) to remove contaminating iron, and then microwave sterilized. Macronutrients (nitrate and phosphate) were also treated with Chelex 100, filtered through an acid-cleaned 0.2 μm PVDF filter, and added to sterile media at f/2 concentrations (Guillard, 1975). Vitamins stocks of B1 (thiamine), B7 (biotin) and B12 (cobalamin) were filter sterilized and added to f/2 concentrations in final media. Trace metals without iron were prepared according to Sunda and Huntsman (1995), and final media

contained 100 μM EDTA. Iron replete cultures were amended with 100 nM FeCl_3 and iron deplete cultures contained no added iron but background iron contamination in the media was measured at 0.360 ± 0.039 nM using a sulfite reduction luminol chemiluminescence flow injection method (King & Barbeau, 2011). Cultures were grown at 23°C and exposed to a 14:10 light:dark regime with either 165 or 20 $\mu\text{mol quanta m}^{-2} \text{s}^{-1}$ in high light and low light treatments, respectively. Iron replete and deplete cultures were acclimated to their conditions (iron and light) for at least two weeks before experimental cultures were inoculated. All cultures were maintained in polycarbonate bottles which cleaned by a 24 hour detergent (Citranox®) soak followed by a two week treatment in 1 N trace metal grade HCl. All media preparation, manipulations and sampling were performed in a class-100 HEPA filtered laminar flow workbench.

Acclimated pre-cultures were used to inoculate 2 L of Aquil media in 2.7 L polycarbonate bottles for the diel experiment. Biological triplicate bottles were inoculated for each treatment. Iron replete pre-cultures were used for the iron replete diel cultures while iron deplete cultures were used for iron deplete, resupply and DFOB diel cultures. Diel cultures were grown under experimental conditions until early exponential phase ($\sim 1 \times 10^6$ cells mL^{-1}) when the sampling program was commenced.

2.3.2 Transcriptomics

Cells were harvested over the diel cycle for transcriptomic analysis. Cells were pelleted via centrifugation, flash frozen in liquid nitrogen, and stored at -80°C. RNA extraction was performed using the TRIzol™ Reagent (Thermo Fisher Scientific) and DNA excluded with DNase I (TURBO DNA-free™ kit, Thermo Fisher Scientific). RNA was purified using Agencourt RNAClean XP beads (Beckman Coulter) and ribosomal RNA was depleted using a Ribo-Zero rRNA Removal Kit (Illumina). cDNA libraries were prepared with a ScriptSeq v2 RNA-seq kit (Illumina) and quality evaluated on an Agilent 220 TapeStation instrument. Sequencing of 120 cDNA libraries was performed on the Illumina MiSeq platform. Transcripts were assembled using the RNAseq Annotation Pipeline v0.4 (RAP) as described previously (Bertrand et al., 2015). MAKER software was used to deduce gene models by mapping RAP-annotated transcripts to the *P. calceolata* genomic sequence, inference by homology to proteins from *P. calceolata* RAP assembly (translated transcripts) and proteins from multiple taxonomically related proteins, SNAP² ab initio prediction (Hecht et al., 2015) and ab initio prediction by Augustus (Stanke & Morgenstern, 2005) using proteins from closely related well-annotated species.

2.3.3 Proteomics

Cells for proteomic analysis were pelleted by centrifugation, flash frozen in liquid nitrogen and stored at -80°C until extraction. Cell pellets were resuspended in methanol with a ribitol internal standard and lysis performed by freeze-thaw. After centrifugation, supernatant was removed and pellets

were resuspended in SDS extraction buffer, heated to 95°C, sonicated and debris removed, and proteins precipitated and washed with acetone. These pellets were then dissolved in 100 µl, 8M urea, 50 mM Tris HCl, pH 8.5 at room temperature and reduced with 10 mM DTT at 54°C in a thermomixer with 400 rpm shaking for 20 minutes. Samples were alkylated with 15 mM iodoacetamide at room temperature in the dark for 30 minutes then quenched with a second addition of DTT. Samples were made up to 200 µl with 10 mM TrisHCl, pH 8.5 and protein concentrations determined by micro BCA assay (Thermo Scientific). 120 µg aliquots of each sample were diluted with 4M urea, 10 mM TrisHCl to give equal volumes and then further diluted with 10mM TrisHCl to give a final concentration of 0.8M Urea. Samples were digested with 1.2 µg trypsin at 37°C for 5hr, followed by a second trypsin addition and incubation at 37°C for 12 hr. Following digestion samples were acidified with 3.5 µl formic acid on ice and desalted using 50 mg Strata C18-E (55 µm, 70 Å) SPE columns (Phenomenex) to remove any primary amines and then brought to dryness in a vacuum centrifuge (Eppendorf).

Peptides were suspended in 120 µl of 50mM HEPES pH 8.5 to give 1 µg/µl total protein and 70 µg aliquots of each sample were transferred to 2 mL tubes. Two internal reference standards were prepared by mixing 5 µl of each sample to give pool 1 (210 µl) or 8.3 µl of each sample to give pool 2 (350 µl). Each TMT reagent (1.6 µg per channel – two kits combined) was dissolved in 82 µl anhydrous acetonitrile. 16 µl (0.31 mg) of TMT labelling reagent was

added to each sample; 48 μ l and 80 μ l was added to pool 1 and pool 2 respectively. Samples were vortexed briefly, centrifuged and incubated at r.t. for 1 hr. The labelling reaction was quenched with 2 μ l 5% NH_4OH . The 42 labeled samples were mixed to give five independent TMT 10-plex sets, each containing at least one internal reference channel (channel 9 or 10). Samples were then diluted with 1% formic acid to acidify and reduce the acetonitrile concentration to <5%. Each TMT set was desalted as described above. Please note that TMT set E contains 70% of the desired protein amount for pool 2 (channel 10) due to insufficient volume.

Each TMT set was fractionated by high pH C18 chromatography using an Onyx C18 100 x 4.6 mm column (Phenomenex) with a 30 minute linear gradient from 5% to 30% solvent B at flow rate of 1 mL/min (solvent A, 95% water, 5% acetonitrile, 10 mM ammonium formate pH 9; solvent B, 95% acetonitrile, 5% water, 10 mM ammonium formate pH 9). 60 x 0.6 mL fractions were collected and concatenated (e.g. 1, 11, 21, 31, 41, 51) to give 10 fractions for each TMT set. Fractions were brought to dryness by vacuum centrifuge and re-suspended in 50 μ l 0.5% formic acid, 3% acetonitrile.

Nanoflow LC-MS/MS was conducted using a Dionex Ultimate 3000 UHPLC (Thermo-Scientific, San Jose, CA) interfaced to the Thermo nanosource of an Orbitrap Velos Pro (Thermo Scientific). The ten fractions from each TMT set were analyzed in duplicate. 1 μ l (1.4 μ g) of each sample was injected directly onto 30 cm x 0.075 mm ID, Proteo C18, 4 μ m, 90 \AA column, self-

packed in a Picofrit fused silica nanospray emitter (New Objective, Woburn, MA). Two hour runs were performed with a flow rate of 0.3 $\mu\text{L}/\text{min}$ during sample loading and equilibration and 0.25 $\mu\text{L}/\text{min}$ during sample elution. The gradient was 5% to 25% acetonitrile (0.1% formic acid) over 46 min then 25% to 55% acetonitrile over 25 min followed by 7 min at 95% acetonitrile.

Mass spectrometry was performed in data-dependent mode using a lock mass of 445.12003 m/z for internal mass calibration. The ion spray voltage was 1.6 kV and the heated capillary temperature was 275°C. Advanced gain control (AGC) targets were 1e6 and 5e4 for Orbitrap full MS and MS_n scans respectively, 1e4 for ion trap MS_n scans. A single microscan was performed for each MS event with maximum injection times of 250 ms for Orbitrap scans and 150 ms for ion trap MS_n scans.

Orbitrap survey scans (MS₁) were performed over a scan range of 300-2000 m/z at 30,000 resolution. Ion trap MS₂ scans were performed for the top 10 most intense precursor ions (MS₁) using collision induced dissociation (CID) with 35% normalized collision energy and a precursor isolation window of 2 m/z . MS₂ scans were only collected on peptides with charge states of 2+, 3+, 4+ and 5+ with a minimum MS₁ intensity threshold of 3e4 counts. Relative reporter ion abundances were determined from MS₃ scans. The most intense fragment ion from each MS₂ scan was selected for high-energy collision dissociation HCD with 65% normalized collision energy, and scanned in the Orbitrap at 15,000 resolution.

Proteome Discoverer version 2.2.0.338 was used to conduct database searches and to quantify reporter ions across samples. A single database search was performed for all samples (50 samples times 2 replicate injections) against a transcriptome assembly from *Pelagomonas* (denovo.orfs.pep.fa) concatenated with common protein contaminants (cRAP) using SequestHT. Precursor and fragment ion mass tolerances were 15 ppm and 0.8 Da respectively. Enzyme specificity was full trypsin with two missed cleavages allowed. Fixed modifications were peptide N-terminus and Lys TMT10plex (+229.163 Da) and carbamidomethyl cysteine (+57.021 Da). Variable modification were oxidation Met, N-Terminal Gln to pyro-Glu, N-terminal protein Met-loss and or Acetylation. A false discovery rate (FDR) of 1% was estimated using decoy database searches and validated using Percolator with a delta Cn of 0.05 (Käll and MacCoss 2007 Nature Methods). Only peptides below a co-isolation threshold of 40% were used for peptide quantification. The reporter ion integration mass tolerance was 0.003 Da. Reporter abundances were reported as signal to noise values. To calculate protein abundance across a given TMT set, all peptides from the 10 LC fractions and two replicate injections were considered. For protein quantification all unique peptides matching to a given protein plus the shared peptides allocated according to occam's razor were averaged.

TMT based protein abundances were exported from Proteome Discoverer, processed and normalized using R according to Plubell et al.

(2017). Briefly, we first normalized for sample loading and labelling reaction efficiency, second to compare across the two TMT experiments, and third to scale using the weighted trimmed means as recommended by Mills et al. (2010) and described by Robinson and Oshlack (2010). Only proteins observed in all experimental TMT channels can be normalized by this procedure and rows (proteins) containing missing values must be removed. Certain samples in our dataset gave overall lower protein abundances and contained many more missing values than other samples. Collection of these samples differed from others (filters were used instead of centrifugation) and in one case a separate protein digest was performed after spilling some of the original digest. Including these proteins in the analysis gives a limited number of quantifiable proteins. Therefore we removed/filtered seven low abundance samples from the whole to yield a significantly larger list of quantified proteins. Lastly, using the un-normalized, filtered data set mentioned above, we imputed missing values with $\frac{1}{2}$ of the row minimum for that protein (with the exception of the internal reference standards that were not imputed) as reported by Webb-Robertson et al. (2015). Final normalized values (TMM) were used for determining differential expression, conducting principle component analyses, and calculating standard scores.

2.3.4 Photophysiology

Fv/Fm of cultures was measured over the course of the diel experiment using a WATER-ED PAM (Heinz Walz GmbH). 2 mL aliquots from all cultures were dark adapted for 20 minutes before Fv/Fm measurements.

2.3.5 Cell counts

P. calceolata cells were quantified using a Quanta bench top flow cytometer (Beckman-Coulter) which was validated by comparison to manual cell counts conducted with a hemocytometer.

2.3.6 Carbon and nitrogen cellular quotas

Cellular inventories of carbon and nitrogen were quantified using an ECS 4010 CHNSO Analyzer (COSTECH Analytical Technologies, Inc.). Cultures were filtered onto combusted 25 mm GF/F filters which were then acid fumigated using concentrated HCl and then dried for 48 hours at 60°C. Portions of each filter were packed into tin capsules and combusted at 1000°C. CO₂ and N₂ gases resulting from combustion were quantified by thermal conductivity, and filter blanks were analyzed alongside samples.

2.3.7 Chlorophyll measurements

Chlorophyll a content of cells was determined using standard fluorometric techniques (Osmund Holm-Hansen et al., 1965). Cultures were filtered onto 25 mm GF/F filters, extracted overnight in 90% acetone, and fluorescence was measured using a Turner 10-AU fluorometer before and after acidification alongside quantitative standards and blanks.

2.3.8 Inductively coupled plasma mass spectrometry

Cells for elemental analysis were filtered onto acid cleaned 47mm polycarbonate filters using a Teflon filter rig inside a laminar flow hood. After filtration, cells were rinsed using an oxalate-EDTA solution to remove extracellular metals (Tovar-Sanchez et al., 2003), and filters placed in acid-cleaned 1.5 mL polypropylene vials. Filters were digested in 20 mL quartz beakers using 2 mL 7.9 N Optima™ grade nitric acid (Fisher Chemical) heated to 80°C for 4 hours. Filters were then removed using clean Teflon forceps, placed in their original 1.5 vial and rinsed three times with trace metal clean 18.2 MΩ·cm Milli-Q water. Rinses were collected in the quartz beakers which were brought to dryness overnight and resuspended in 6 mL 1 N nitric acid with a 10 ppb Rh internal standard. Unused acid-cleaned filters were digested as blanks, and certain sample filters were re-digested to confirm all detectable metals were recovered. Sample digests were analyzed on the ThermoElement XR magnetic sector ICP-MS at the Institute of Marine Sciences, University of California, Santa Cruz.

2.4 RESULTS AND DISCUSSION

2.4.1 Low iron physiology of P. calceolata

Iron availability has major consequences for *P. calceolata* cells at either light level. Iron starved *P. calceolata* is photosynthetically impaired as indicated by low Fv/Fm ratios; <0.45 for low light cultures and <0.35 for high light cultures (Figure 2.1B and 2.1C). Photosynthetic competency was highest in the iron replete cultures, and the iron resupply cultures showed a steady

increase in Fv/Fm over the experiment. By the final time point 23 hours after the iron addition, both resupply treatments had recovered to an Fv/Fm of 0.55.

Iron starved cells had a much lower carbon content than iron replete cells at both high and low light (Figure 2.2A and 2.2B). Co-limited cells had the lowest carbon quotas. Nitrogen quotas showed the same trend in the low light cultures, but high light iron limited cells had about as much nitrogen per cell as high light iron replete (Figure 2.2C and 2.2D). This results in the high light iron limited cells having the largest departure from a Redfield-like C:N (Redfield, 1934), presumably due to a lack of carbon (Figure 2.3A).

Interestingly, even resource replete cells had lower C:N than has been reported for other groups of phytoplankton (Martiny et al., 2013; Quigg et al., 2003). Co-limited cells had the lowest nitrogen content, although this recovered following iron resupply (Figure 2.2B). Collectively these findings indicate that iron limitation alone reduces carbon fixation, whereas co-limitation significantly hinders both carbon fixation and nitrate assimilation. Differences between iron deplete and chelator treated cells were not evident in any of these physiological measurements.

Chlorophyll quotas were higher in all the dark-adapted cells than in any of the high light cultures (Figure 2.2E and 2.2F). Iron had a major effect of chlorophyll per cell, and the duration of the experiment was insufficient to capture the complete recovery of chlorophyll quotas in the resupply cultures.

Chlorophyll to iron ratios were lower in the high light cultures, which is consistent with previous findings (W G Sunda & Huntsman, 1997). In both light treatments the iron resupply cultures had the lowest Chl a : Fe (Figure 2.4A and 2.4B), which stems from the temporal offset between iron uptake and chlorophyll biosynthesis.

Iron quotas were highest in the iron replete cultures and very similar in the resupply cultures (Figure 2.2G 2.2H). In spite of the high carbon quota of iron replete cells, the Fe:C ratio was still higher in these relative to the iron limited cells, especially at high light (Figure 2.3E and 2.3F). Iron resupply cultures at the 3 hour time point had the highest Fe:C due to low initial carbon quotas, and likely high iron uptake rates subsequent to the resupply spike (Figure 2.3E and 2.3F).

Quotas of copper followed a trend opposite of the that of iron quotas (Figure 2.4). Iron limited cells had higher quotas for Cu (Figure 2.4C and 2.4D). This was also the case for Cu:C ratios, which were higher in the iron limited cultures (Figure 2.4E and 2.4F). Copper (both Cu/cell and Cu:C) in resupply cultures at both light levels began high but returned to values seen in the iron replete cultures by the end of the experiment (Figure 2.4). High copper quotas could be explained by transport mechanisms which poorly discriminate between metal cations. Upregulation of transport mechanisms at low iron could result in accumulation of other metals especially in media replete with nutrient metals. Additionally, if detoxification is likewise unspecific

iron limited cells may repress export mechanisms to avoid losing valuable iron resources. Iron limited diatoms have been shown to be more susceptible to copper toxicity (Stauber & Florence, 1985), and detoxifying phytochelatins are known to chelate a variety of transition metals (Clemens, 2006).

2.4.2 Transcriptomic analysis

Transcriptomes of three biological replicates of each treatment were sequenced at five time points after spiking the resupply and DFOB cultures (15 minutes, 3 hours, 11 hours, 15 hours and 23 hours). The impact of our culturing conditions was evident at a global transcriptomic scale. There was clear differentiation between day and night samples, and also by iron treatment (Figure 2.5). Iron deplete and DFOB treatments were closely clustered, and separated from iron replete samples (Figure 2.5). Iron resupply samples began associated with the low iron treatments, but later time points were associated with iron replete (Figure 2.5). In the low light treatment this shift occurred by the 15 hour time point while in the high light treatment all resupply points after 15 minutes appeared similar to iron replete samples (Figure 2.5).

RuBisCO expression was coordinated with daylight, and highest in the iron replete cultures (Figure 2.6). Iron resupply only marginally increased RuBisCO expression, and mostly in the low light cultures (Figure 2.6). Other Calvin-Benson cycle genes responded to iron. Class I fructose bisphosphate aldolase (FBA) was preferentially expressed in low iron day samples, while

multiple class II FBAs (FBAC1 and FBAC2) were expressed at high light during the day (Figure 2.6). Resupply cultures largely made the switch in expression from class I to class II within 3 hours. Certain fructose 1,6-bisphosphatase (FBP) ORFs expressed during the night were also mostly expressed at high iron (FBP1, Figure 2.6). Other versions of this gene expressed during the day were only expressed at low iron and quickly turned off following iron resupply. Similarly with ribose 5-phosphate 3-epimerase, different copies were expressed at replete and deplete iron levels, though both mostly during the day (Figure 2.6). Most other ORFs associated with the Calvin-Benson cycle were primarily expressed in iron replete and resupply treatments at both light levels. All subunits of plastid localized ATPases showed a daytime expression pattern which was unimpacted by iron concentration at low light, and slightly downregulated at high iron in high light cultures (Figure 2.6).

Photosystem I (PSI) reaction center proteins had different expression patterns. Most psa proteins were slightly upregulated after the iron spike, but expression did not change much with light levels or iron replete versus deplete. The psaA/psaB protein was expressed at night, and more so in the iron resupply cultures, and the high light replete culture (Figure 2.6). The PsaD protein was also expressed at night, and least of all in the iron replete cultures (Figure 2.6). Other Psa proteins (C, M, E, and F) were expressed in the day, and mostly in the resupply cultures after 15 minutes (Figure 2.6). PsaJ was upregulated in low iron cultures in the day at high light and night at low light,

and turned off with high iron (Figure 2.6). The *petB* gene which encodes cytochrome b_6 , was expressed at low iron at the dark time points and expression was repressed after resupply and at high iron (Figure 2.6).

Many photosystem II (PSII) reaction center proteins in low light cultures responded strongly to iron addition, being upregulated within 15 minutes of the iron spike (Figure 2.6). This upregulation was present in high light cultures to a lesser degree (Figure 2.6). In iron replete cultures, *psb* proteins were expressed during the day, but a few (B, C, and D) were upregulated in the night following iron resupply (Figure 2.6).

Light harvesting complex proteins (Lhc) fell broadly into two expression categories. Fucoxanthin binding Lhcf and red algal Lhcr proteins (Koziol et al., 2007) were expressed in iron replete and resupply cultures, while photoprotective Lhcx proteins (Bailleul et al., 2010; Buck et al., 2019) are upregulated at low iron and mostly in low light cultures (Figure 2.6). This mirrors the response of diatom Lhc proteins to iron availability (Smith et al., 2016).

Nitrogen metabolism was also impacted by iron concentration, and this was most evident at high light where high iron and resupply cultures upregulated many components of the nitrogen assimilation pathway (Figure 2.7). Iron resupply triggered expression of both ferredoxin and NADPH-dependent nitrite reductases, nitrite and nitrate transporters, urea and ammonia transporters and urease (Figure 2.7). Multiple glutamine synthetase (GS) ORFs were induced by iron addition, as were carbamoyl phosphate

synthetases (CPSase) and glutamine oxoglutarate aminotransferases (GOGAT). Most nitrogen compound transporters were expressed primarily at night, while assimilation genes (CPSase, GS, and GOGAT) were expressed in the day or constitutively (Figure 2.7). These findings suggest low iron induced impairment of nitrogen uptake and assimilation, and potentially the urea cycle.

Mitochondrial proteins were impacted by iron limitation and light limitation, and slow to respond to iron resupply. Respiratory complex I proteins NADH dehydrogenases and NADH-ubiquinone oxidoreductases were all most highly expressed in the high light iron replete condition and showed virtually no recovery in iron resupply treatments (Figure 2.7). The same was true of cytochrome c oxidases predicted to be localized to the mitochondrion (Figure 2.7). Mitochondrial ATPases were downregulated in low iron cultures and upregulated in the night following iron resupply (Figure 2.7).

Expression of ribosomal subunits was highly coordinated and occurred in the night time points (Figure 2.7), which contrasts with *P. tricornutum* which expresses these proteins during the day (Smith et al., 2016). Low iron treatments generally repressed ribosome expression, and the highest expression was seen in the resupply cultures reflecting a release from iron stress. Ribosomes are required for remodeling the cell's proteome to capitalize on new environmental conditions, and are known to be downregulated in response to stressors (Brauer et al., 2008; Warner, 1999).

Many of the iron stress biomarkers known from field studies of phytoplankton were present in our *P. calceolata* transcriptomes. Transcript abundance for flavodoxin shows the predicted pattern of up-regulation in all low iron cultures (Figure 2.7), and this provides evidence that iron concentrations were low enough to force iron sparing. Flavodoxin expression shows a diel pattern, and is only highly expressed in the day time points of low iron cultures (Figure 2.7). Expression down-regulated within 15 minutes of iron addition, and reaches iron replete levels by 3 hours (Figure 2.7). Ferredoxin transcripts achieved maximum abundance in high iron cultures, did not display a diel pattern, and were upregulated by 3 hours after the iron spike at both light levels. This could indicate that flavodoxin is used primarily to free up iron resources during the day when the iron demand of photosynthetic electron transport is high and at night, devoting iron to ferredoxin is more favorable. Another well characterized low iron substitution is the copper-containing plastocyanin for iron containing cytochrome c_6 (Peers & Price, 2006). In *P. calceolata*, this substitution was not detected, despite abundant copper (40 nM) in the culture media and identification of transcripts of both proteins. Both plastocyanin and cytochrome c_6 were upregulated in iron replete cultures at both light levels without a diel pattern (Figure 2.7).

Under iron limitation at both light levels, transcripts for cullin proteins were expressed during night time points (Figure 2.7). These proteins facilitate

protein degradation (Bosu & Kipreos, 2008), and could be involved in recycling of iron containing photosynthetic proteins not required in the dark.

Many transporters in the *P. calceolata* genome are iron sensitive. Notably, phytoferritin (pTF) is strongly expressed across the diel cycle only in iron-limited cultures (Figure 2.7), representing a strategy for acquisition of dissolved inorganic iron (McQuaid et al., 2018). Zinc responsive transporter/iron responsive transporter-like proteins (ZIP) and natural resistance-associated macrophage protein (NRAMP) divalent metal cation transporters were expressed in all cultures during the night, potentially indicating a role in intracellular trafficking of iron acquired from nighttime protein degradation, but not specific to low iron conditions (Figure 2.7). SufB proteins are ABC transporters involved in assembly of Fe-S clusters, particularly under iron stress (Bandyopadhyay et al., 2008; Layer et al., 2007). In *P. calceolata*, these proteins are expressed preferentially under low iron conditions, likely supporting iron mobilization to photosynthetic proteins in the chloroplast. Additionally, on NCS2 uracil/xanthine permease and transmembrane amino acid transporters are upregulated at low iron, especially in the low light cultures, which is evidence for the utilization of exogenous organic compounds as carbon and/or nitrogen sources under conditions where photosynthesis is impaired and nitrate assimilation may be too great an iron cost. Finally, a few transporters of the resistance-nodulation-division (RND) family were upregulated in low iron cultures (Figure 2.7). RND

transporters are large proteins which pump a variety substrates across the outer membrane (Division et al., 1999; Saier et al., 1994). HAE family RND proteins are involved in the export of amphiphilic and hydrophobic organic compounds including lipids and siderophores (Poole et al., 1993; Yang et al., 2014). We can only speculate as to the substrate of these, but related proteins are also involved in efflux of heavy metals (Nikaido, 2018). It could be that these transporters are involved in efflux of excess non-iron metal ions acquired as a result of non-specific metal uptake in media with replete other nutrient metals.

Previously, pelagophyte transcriptomes have been characterized as “dynein heavy” (Carradec et al., 2018), and our *P. calceolata* transcriptomes fit this description with 440 ORFs were annotated as dyneins. All dynein ORFs were preferentially expressed in the night time points in all treatments (Figure 2.8). At high light, low iron cultures had the greatest dynein expression, and resupply reduced expression to the levels seen in iron replete cultures (Figure 2.8). At low light, all cultures showed a similar degree of dynein expression, except iron resupply which downregulated these ORFs (Figure 2.8). The function of these iron-sensitive dyneins, whether involving motility, intracellular trafficking or cell division, is highly coordinated with the light dark cycle. A small subset of dynein ORFs were expressed at high iron in high light, probably indicating a separate function (Figure 2.8). The other major groups of motor proteins, kinesin and myosin, were similarly expressed at night but

preferentially under iron replete conditions at high light (Figure 2.8). Both kinesin and myosin ORFs were downregulated with iron resupply. These results indicate that dynein serves a distinct role at low light and/or low iron that is not shared with other motor proteins.

ORFs annotated as glycolysis by KEGG Orthology (KO) pathway (Kanehisa & Goto, 2000) were strongly upregulated in iron replete and resupply cultures (Figure 2.9). Most of these ORFs were nocturnally expressed, though about 24% were expressed primarily during the day (Figure 2.9). This list of ORFs likely includes proteins participating in other central metabolic processes including the pentose phosphate pathway, gluconeogenesis and the citrate cycle (TCA). The impact of iron limitation restricting the flow of photosynthetically fixed carbon to fundamental energetic reactions is apparent in the expression of these genes.

2.4.3 Proteomic analysis

Protein samples were analyzed from day (0 or 23 hours) and night (11 hours) time points for replete, deplete and resupply cultures at both light levels, in triplicate. Resupply cultures were sampled 11 and 23 hours after the spike therefore the night sample was closest to the iron addition and iron deplete conditions. PCA analysis of these proteomes show little discernable separation by time of day; the major differences were between iron levels (Figure 2.10). Nighttime samples from the low light resupply were more similar to iron deplete samples, while high light resupply had recovered to near iron

replete by 11 hours post spike (Figure 2.10). High light and low light transcriptomes showed the greatest similarity at low iron (Figure 2.10). Overall, our proteomes appear less dynamic than our transcriptomes and show much less variation by time of day.

Major photosynthetic proteins showed clear patterns relating to iron and light availability. RuBisCO is expressed at similar levels in both high light and low light cultures (Figure 2.11). No variation in RuBisCO abundance was observed between day and night samples, and recovery of RuBisCO protein quotas by the 11 hour time point was achieved at both high and low light, although the high light culture at 23 hours was not significantly different from iron deplete (Figure 2.11). Reaction center subunits from PSI and PSII were much more abundant in low light cultures when iron was present (Figure 2.11). At 11 hours, significantly more reaction center proteins were detected (Figure 2.11). Low light cultures were enriched in fucoxanthin type light harvesting proteins and little variation was observed with iron treatment (Figure 2.11).

The influence of iron availability was apparent in quotas of proteins related to nitrogen uptake and assimilation (Figure 2.12). Nitrite reductases were expressed primarily in high iron cultures, and this pattern was significant for proteins requiring either NADPH or ferredoxin as a reductant (Figure 2.12). Both nitrite reductases were more abundant during the day at both light levels and returned to iron replete levels by the 11 hour time point (Figure 2.12). Nitrate transport proteins increased after iron addition in high light

cultures, but no significant trends were observed in low light cultures or with respect to time of day (Figure 2.12). Ammonia transport was significantly overexpressed in low light iron deplete cultures and decreased after iron was added (Figure 2.12). The same expression pattern was observed in urea transport (Figure 2.12). Urease showed the same pattern, contrary to transcriptomic results, but the differences in protein abundance were not significant (Figure 2.12). Nitrogen assimilation proteins GSIII and GOGAT were repressed in low iron cultures at both light levels and iron replenishment resulted in partial recovery of these proteins by the end of the experiment (Figure 2.12).

Some of the predominant genes of the iron stress transcriptome were identified in our proteomic dataset. At both light levels, ferredoxin expression in high iron cultures was replaced by flavodoxin in low iron, and the reversal was observed following resupply (Figure 2.13). A similar relationship was detected between class I and II FBAs, and in both cases the surplus of the low iron protein took longer to degrade than the new high iron protein took to synthesize (Figure 2.12). Cytochrome c_6 was detected in our dataset and like its transcript was expressed at high iron but unlike mRNA, the protein was more abundant in low light cultures (Figure 2.13). Dyneins were also quantified and showed upregulation at low iron in high light, and little sensitivity to iron concentration at low light (Figure 2.13). The two copies of RPE in our proteomes behaved similarly to their transcripts with one expressed

at high iron and one at low iron (Figure 2.13). All RPE transcripts were preferentially expressed at mid-day time points, but despite this diel pattern quantities of RPE proteins measured during the day and night were indistinguishable (Figure 2.13). FBP1 was one of the most iron sensitive proteins in our dataset and was highly expressed in low iron at both light levels (Figure 2.13). Also, a glutamate semialdehyde aminotransferase (GSA) likely involved in chlorophyll biosynthesis (Grimm, 1990) was expressed most dramatically in resupply cultures at both light levels (Figure 2.13), correlating with the recovery of chlorophyll inventories (Figures 2.2 and 2.3).

Transcriptional regulation is a fundamental process which controls how cells remodel their physiology in response to changing environmental conditions and stramenopiles are believed to possess transcription factors which initiate specific stress responses (Rayko et al., 2010). In our proteomes, two transcription related proteins were identified which appear to be involved in the response to iron availability. One mRNA export factor (ELF1) was upregulated in iron replete conditions especially during the day (Figure 2.13 and 2.15A). At low iron, a transcription elongation factor homologous to SPT5 from *Saccharomyces cerevisiae* (Lindstrom et al., 2003) was among the most upregulated proteins (Figures 2.13 and 2.15). These proteins apparently help orchestrate changes in transcription related to iron nutritional status.

Proteins potentially participating in iron uptake and storage responded to iron availability. pTF was strongly expressed in all low iron cultures (Figure

2.14), suggesting an essential role in high affinity iron uptake. ISIP3 was also overexpressed at low iron (Figure 2.14). One other poorly annotated protein containing a ferritin-like oxidoreductase domain was expressed at low iron but primarily at low light (Figure 2.14). The only ferric reductase and ZIP proteins quantified were upregulated at high iron, implying functions other than iron uptake (Figure 2.14). Iron sensitive RND transporters identified in transcriptomes were not detected in proteomic data, however a different efflux transporters of the multidrug resistance protein family was significantly upregulated at low iron in high light cultures, and in all low light cultures (Figure 2.14). Proteins involved in intracellular iron trafficking in stramenopiles are largely unknown (Turnšek et al., 2019), but two proteins from our dataset may be candidates. *sufC* is predicted to be a chloroplast localized Fe-S cluster assembly ABC transporter. Suf proteins are involved in the biosynthesis and trafficking of Fe-S clusters (Kaplan et al., 2006; Layer et al., 2007; Outten et al., 2004), and therefore this protein probably facilitates delivery of Fe-S cofactors to photosynthetic proteins. In *P. calceolata*, *sufC* is expressed in response to high iron. Another protein upregulated at low iron is a vacuolar proton pump (VAT2, Figure 2.14). These ATP-dependent proteins are involved in various cellular processes notably endosome acidification, acid-base homeostasis and vesicle trafficking (Finbow & Harrison, 1997; Maxson & Grinstein, 2014; Merkulova et al., 2015). Turnšek et al. (2019) detected these proteins associated with pTF endosomes in the diatom *P. tricornutum* and

hypothesized their involvement in the release of iron from pTF. Their role in *P. calceolata* could be similar, but this hypothesis needs to be tested.

2.5 CONCLUSIONS

During iron replete conditions, *P. calceolata* expresses some pathways and processes which are common to a related stramenopiles lineage: the diatoms. Diatom nitrogen metabolism is largely nitrate fueled (Cermeño et al., 2011; McCarthy et al., 2017; Villareal et al., 1993), which also appears to be the case for *P. calceolata* when iron is available. Nitrate transport and assimilation in the chloroplast is upregulated regardless of light availability when bioavailable iron is present. Diatoms also possess an ornithine-urea cycle which is considered a central carbon and nitrogen hub that links catabolic and anabolic metabolism by efficiently recycling ammonium and bicarbonate derived from protein turnover (Allen et al., 2011). *P. calceolata* contains urea cycle enzymes (Figure 2.16) affording it the same metabolic flexibility which is thought to confer a competitive advantage during episodic nutrient input (Allen et al., 2011). Diatoms maintain expression of urea cycle proteins at low iron (Cohen, Gong, et al., 2018; Smith et al., 2016), while in *P. calceolata* the urea cycle is preferentially expressed at high iron alongside nitrate assimilation (Figure 2.16). *P. calceolata* utilizes other strategies to minimize iron costs, including exploitation of reduced and/or organic nitrogen sources. Reduction of nitrate to ammonia requires two iron containing enzymes (Raven et al., 1992), and significant ATP and NAD(P)H (Pate &

Layzell, 1990). This investment of iron could be circumvented via acquisition of ammonium, urea, amino acids, and purines. *P. calceolata* contains transporters for all these substrates, all of which are upregulated in iron deplete conditions (Figure 2.16). Diatoms require more iron when grown on nitrate than when grown on ammonium, presumably due to iron containing nitrate and nitrite reductases (Maldonado & Price, 1996). Additionally, as *P. calceolata* is motile, it presumably has the capability to navigate towards hotspots of organic matter rich in fixed carbon and nitrogen (Azam & Ammerman, 1984). If any such chemotaxis occurs, it could effectively give *P. calceolata* preferential access the labile particulate iron pool which typically far exceeds dissolved iron concentrations (Berger et al., 2008; Biller et al., 2013; Lippitt et al., 2010, 2011). Dynein proteins, which contribute to motility in other phytoplankton (Mitchell & Rosenbaum, 1985), are upregulated at low iron or light when photosynthesis is impaired (Figure 2.8).

When experiencing light limitation, *P. calceolata* upregulates photosynthetic reaction center proteins in a manner consistent with observations of other phytoplankton (Friedman & Alberte, 1986). Photosynthetic reaction centers are upregulated with high iron (Figure 2.16), and low iron cultures are impaired in their cellular inventories of these proteins especially at low light (Figure 2.11). Chlorophyll binding proteins are insensitive to iron levels, but light harvesting is likely impaired in low iron cultures as chlorophyll quotas are low and chlorophyll biosynthesis is

downregulated (Figure 2.13). Low ferredoxin quotas in iron limited cultures (Figure 2.13) impacts photosynthetic electron transport, and a host of other ferredoxin-dependent processes. Photosynthetic proteins which are upregulated at low iron include three components of the regenerative phase of the Calvin-Benson cycle (Figure 2.16). Class I FBA proteins are expressed in many iron limited phytoplankton species, including cyanobacteria (Allen et al., 2008; Cohen et al., 2017; Cohen et al., 2018; Narayan et al., 2011; Smith et al., 2016), but the rationale behind this is still unknown. It may be a substitution for class II FBAs which are upregulated at high iron and require a metal cofactor, but this is thought to be zinc (Marsh & Leberherz, 1992). FBP is not known to be overexpressed in iron starved diatoms yet is one of the most iron sensitive proteins in *P. calceolata* (Figure 2.13 and 2.15). Transcripts for the low iron expressed FBP (FBP2) peak during the day (Figure 2.6), which contrasts with the night-expressed FBP in *P. tricornutum* (Smith et al., 2016). At night in *P. calceolata*, a second FBP (FBP1) peaks in expression as it does in *P. tricornutum* (Figure 2.6). Finally, two copies of the Calvin-Benson cycle enzyme RPE exist in *P. calceolata*. RPE is a metalloenzyme which binds two divalent metal cofactors and is a component of both the Calvin-Benson cycle and the pentose phosphate metabolic pathway (Akana et al., 2006). Both homologs are expressed during the day, but RPE1 at low iron and RPE2 at high iron (Figure 2.6). The transcription of low iron FBA, FBP, and RPE is temporally coordinated, which might be taken as evidence they are working

together regenerating ribulose 1,5-bisphosphate for RuBisCO. Alternatively, these three proteins could function in new roles during iron limitation and further investigation is needed to characterize their significance.

Other characteristics of *P. calceolata* help it persist in low iron. Many highly upregulated proteins used by *P. calceolata* in low iron conditions have been observed in diatoms. Flavodoxin and pTF and ISIP3 are prime examples of this (Allen et al., 2008; Smith et al., 2016). Flavodoxin decreases iron requirements, pTF acquires iron from the environment, and ISIP3 presumably stores and transports iron intracellularly. These are the general categories of protein adaptations adopted by photoautotrophic microbes experiencing iron limitation. In addition, small size can benefit phytoplankton by decreasing iron quotas and increasing surface area to volume ratios during nutrient stress (Chisholm, 1992; Hudson & Morel, 1990). This lead to the prediction that small phytoplankton cells would be especially favored under iron/light co-limitation (Sunda & Huntsman, 1997). *P. calceolata* is among the smallest of eukaryotes and its biomass decreases substantially under iron limitation (Figure 2.2) which probably allows it to more easily satisfy iron requirements.

A collection of known low iron strategies enable *P. calceolata* to grow at iron concentrations which would be lethal to diatoms. These involve enzymes with well characterized functions, and novel proteins with unknown roles. Motility and mixotrophic capabilities likely contribute to its success in

low iron marine environments. Resolving the details of protein function in this non-model organism is a monumental challenge for future studies, but well justified considering the ecological significance of this picoeukaryote.

2.6 FIGURES

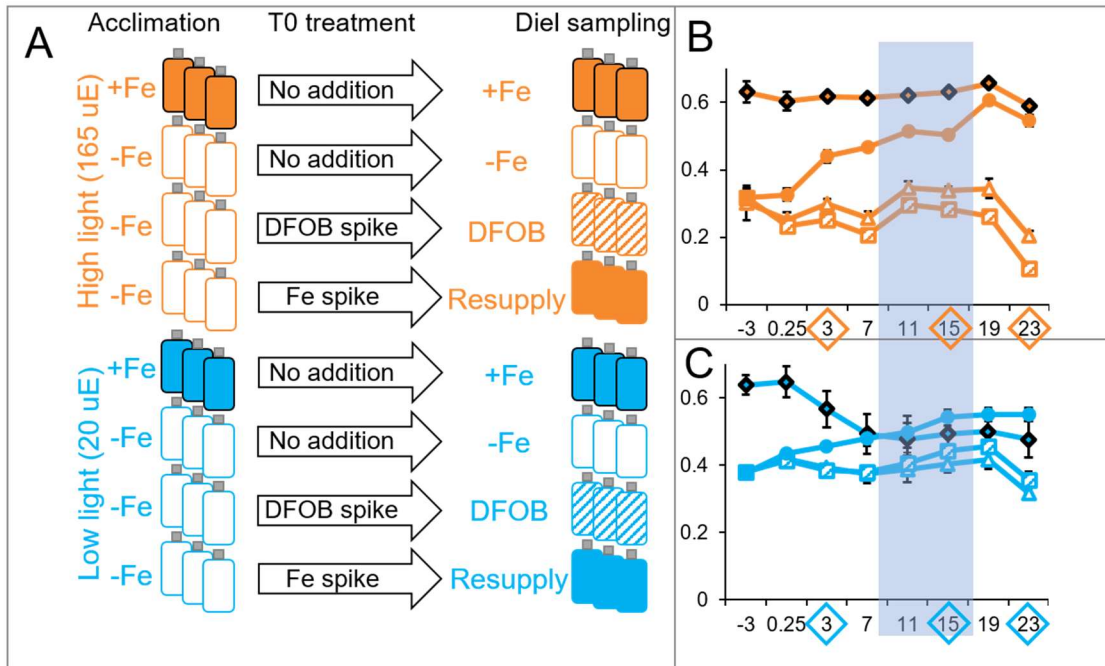


Figure 2.1. (A) Experimental design of Fe/light co-limitation experiment. Triplicate cultures were acclimated initial conditions, and experiment was initiated at T0 with chelator (DFOB) and Fe additions to certain cultures. Sampling then occurred over the ensuing 23 hours. F_v/F_m of *P. calceolata* cultures over the diel cycle are shown for high light (B) and low light (C) experiments. Hours since spike given on x-axes. Fe resupply and DFOB spike occurred at 0 hrs. Shaded area indicates night (lights off). Major time points for physiological characterization are indicated with diamonds.

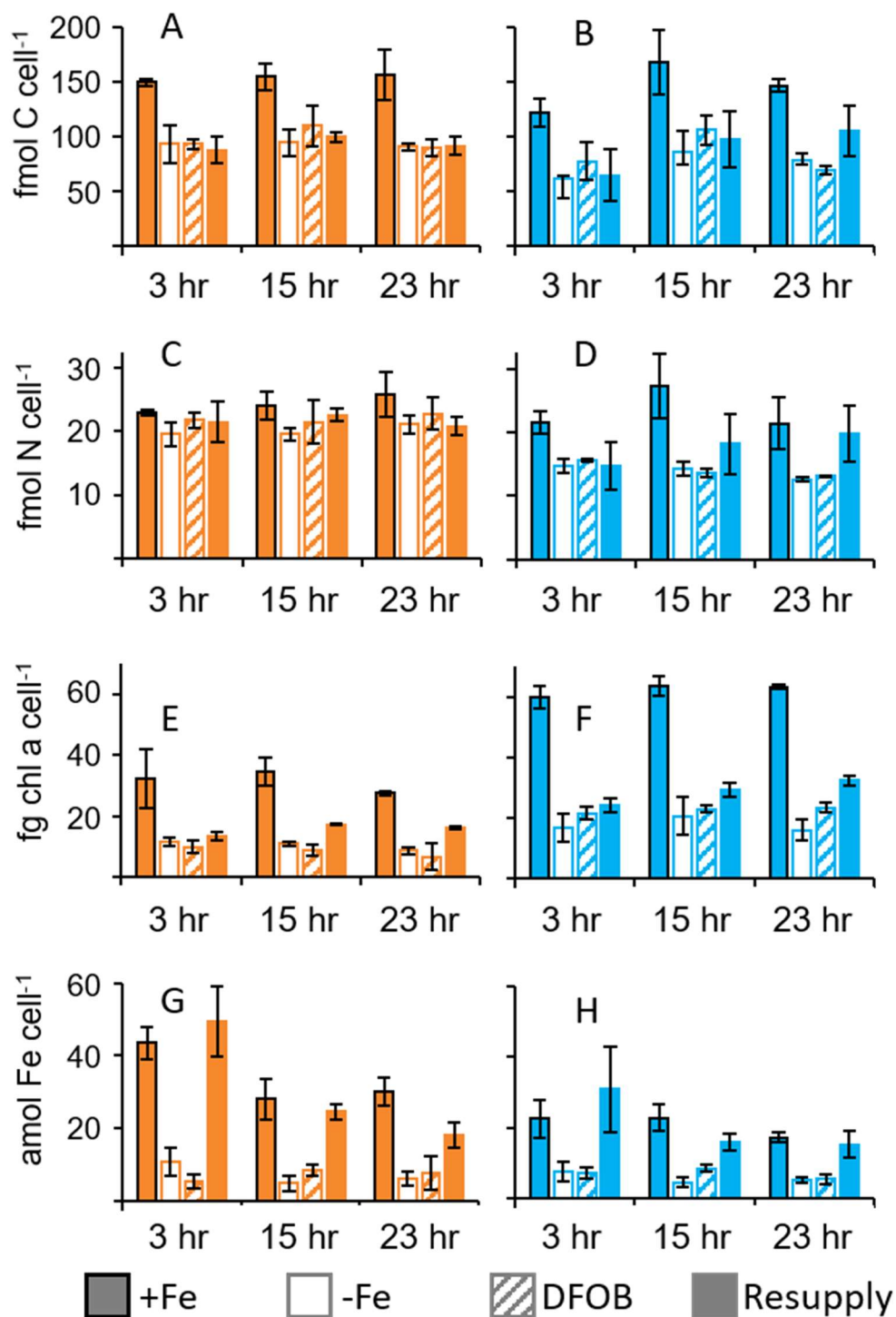


Figure 2.2. Cellular quotas at the three major time points for (A, B) carbon, (C, D) nitrogen, (E, F) chlorophyll a, (G, H) and Fe. High light treatments are in orange, low light in blue. Bars show mean of biological triplicate cultures and error bars represent ± 1 SD.

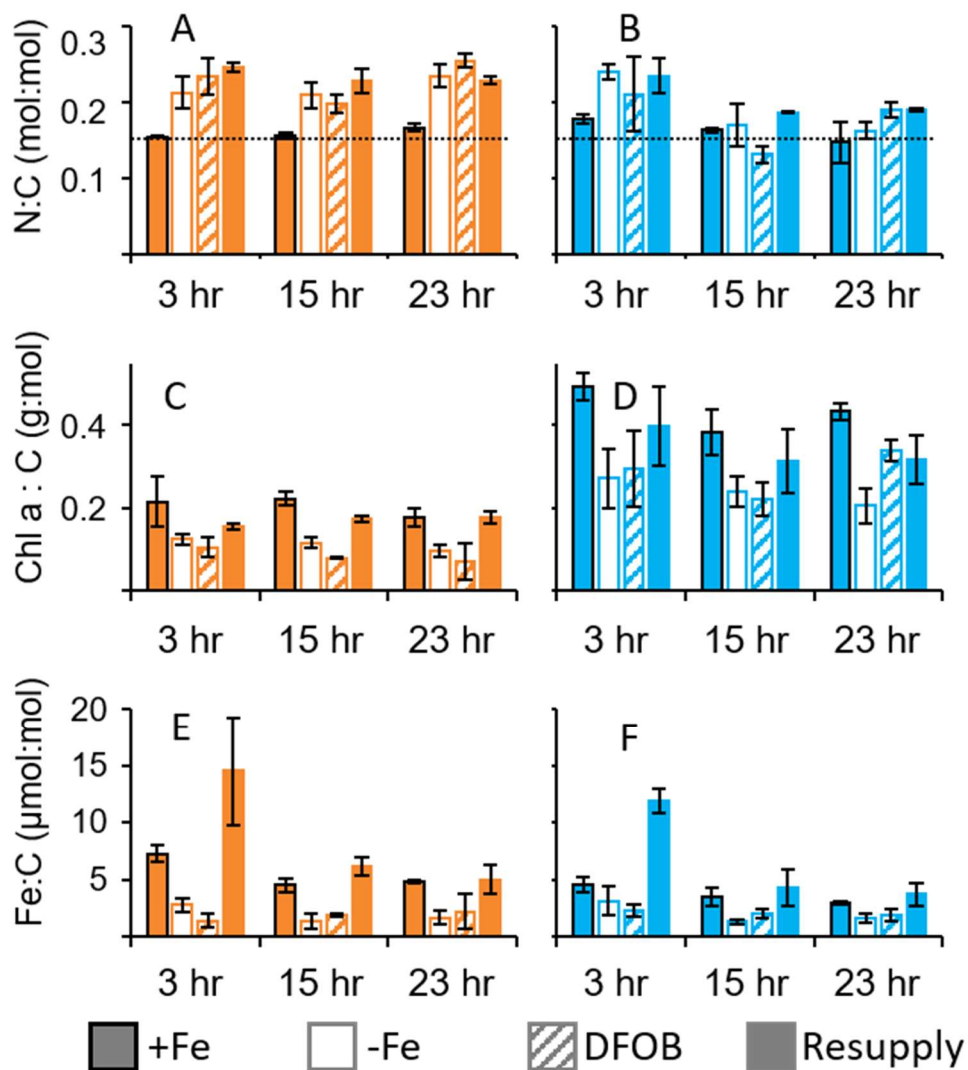


Figure 2.3. Ratios of nitrogen (A,B), chlorophyll a (C,D), and Fe (E,F) to carbon at the three major time points. High light treatments are in orange, low light in blue. Bars show mean of biological triplicate cultures and error bars represent ± 1 SD. Dotted line in A and B indicates the Redfield (1934) value of 0.151.

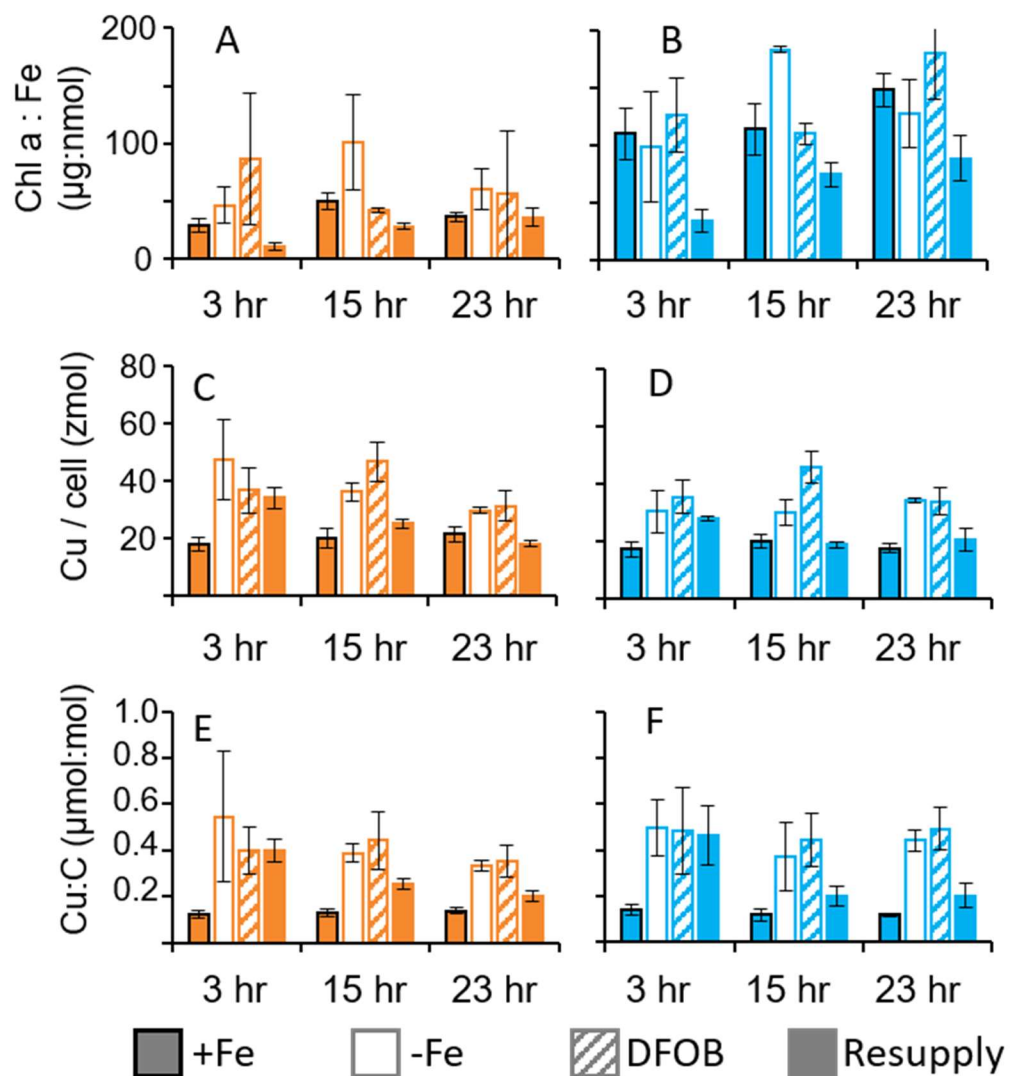


Figure 2.4. Ratios of chlorophyll a to iron (A,B), cellular copper quotas (C,D), and ratios of copper to carbon (E,F) at the three major time points. High light treatments are in orange, low light in blue. Bars show mean of biological triplicate cultures and error bars represent ± 1 SD.

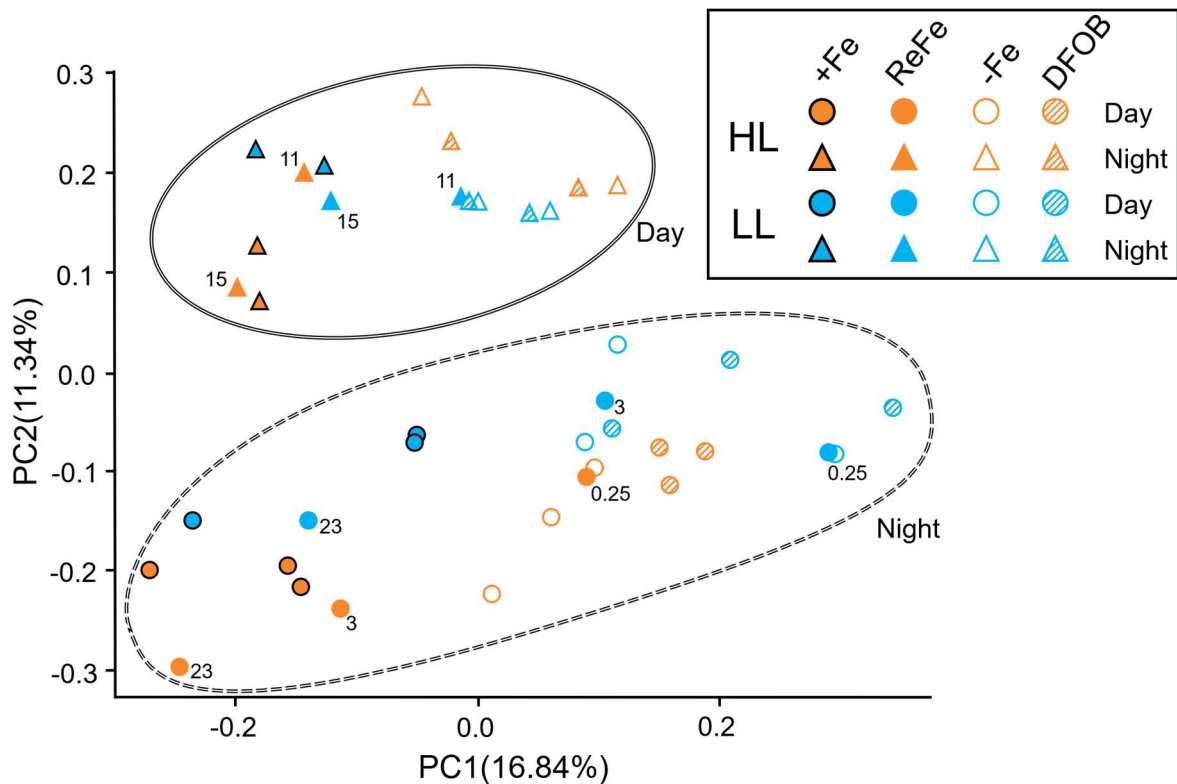


Figure 2.5. Principal component analysis plot of *P. calceolata* transcriptomes. Each symbol represents biological triplicates at a single time point. Orange and blue indicate high light (HL) and low light (LL) respectively. Triangles indicate day time points and circles show night time points. Black outlines indicate iron replete (+Fe), solid fill with no outline indicates iron resupply (ReFe), no fill indicates iron deplete (-Fe), and diagonal stripes indicate DFOB. ReFe points are labeled with hours since iron spike.

Figure 2.6. Heatmap showing average standardized transcript abundance (standardized RPKM to standard deviation across samples) of photosynthesis related genes across the diel cycle. Orange brackets indicate high light treatments and blue brackets show low light. Orange arrows show day time points and blue arrows show night time points. RuBisCO = ribulose 1,5 biphosphate carboxylase large subunit, FBA = fructose-bisphosphate aldolase, FBP = fructose 1,6-bisphosphatase, RPE = ribulose 5-phosphate 3-epimerase, RPI = ribose-5-phosphate isomerase, GAPDH = glyceraldehyde 3-phosphate dehydrogenase, PRK = phosphoribulokinase, TKT = transketolase, PGK = phosphoglycerate kinase, TPI = triosephosphate isomerase, psa = photosystem I reaction center proteins, petB = cytochrome b₆, psb = photosystem II reaction center proteins, Lhc = light harvesting complex protein.

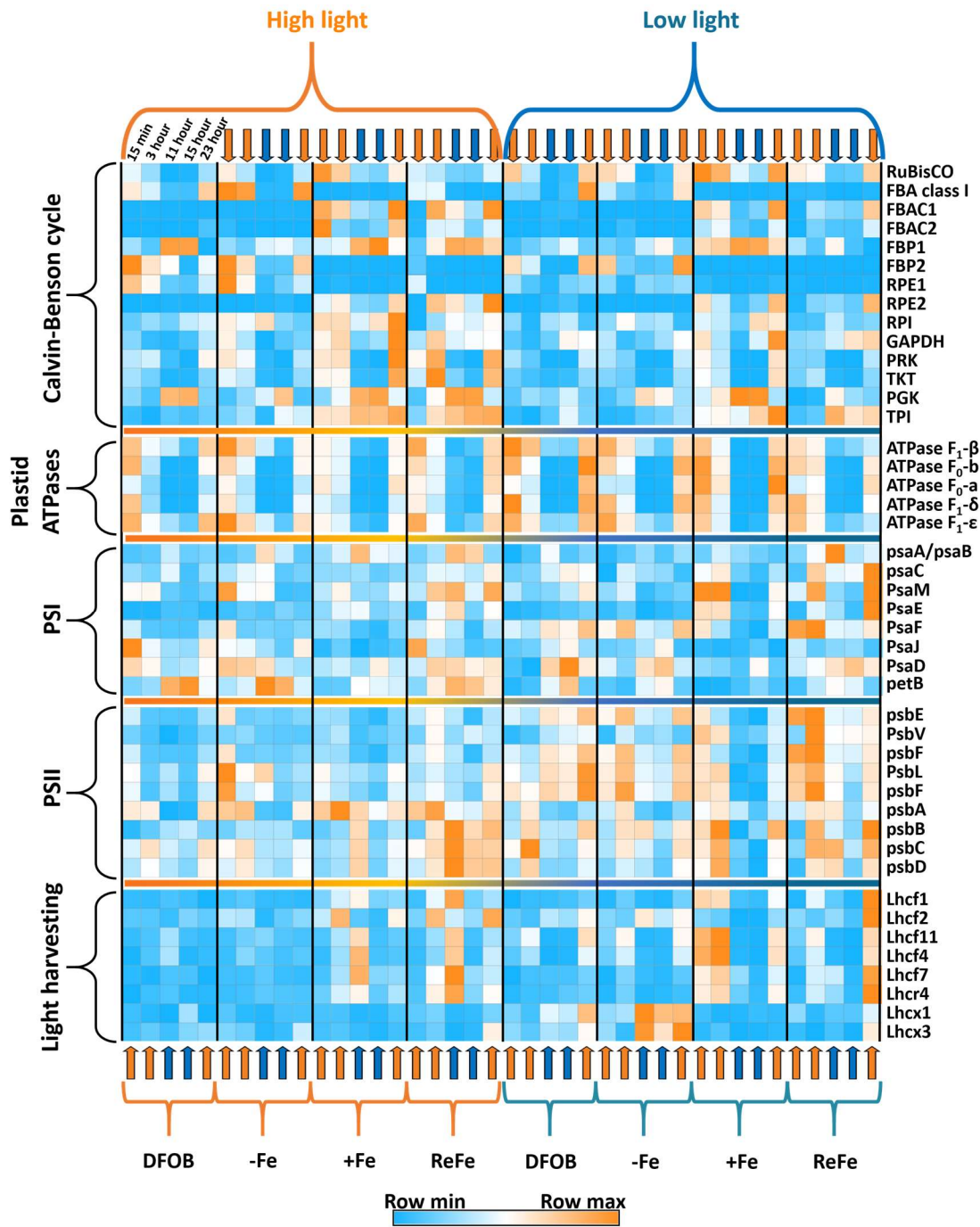


Figure 2.7. Heatmap showing average standardized transcript abundance (standardized RPKM to standard deviation across samples) of nitrogen metabolism, respiration, ribosome and iron-related related genes across the diel cycle. Orange brackets indicate high light treatments and blue brackets show low light. Orange arrows show day time points and blue arrows show night time points. NIR = NADPH nitrite reductase, Fd-NIR = ferredoxin nitrite reductase, FNT = formate/nitrite transporter, NRT1 = nitrate transporter, AMT = ammonia transporter, NOD = nitric oxide dioxygenase, GS II = glutamine synthetase II, GS III = glutamine synthetase III, CPSase = chloroplast carbamoyl phosphate synthetase, CPS III = carbamoyl phosphate synthetase III, cGOGAT = chloroplast glutamine oxoglutarate aminotransferase, mGOGAT = mitochondrial glutamine oxoglutarate aminotransferase, NADH dehydr. = mitochondrial NADH dehydrogenase, NDUFS = NADH-ubiquinone oxidoreductase, Cyt = cytochrome, rps = small subunit ribosomal protein, rpm = large subunit ribosomal protein, rpl = large subunit ribosomal protein, PCYN = plastocyanin, FDX = [2Fe-2S] plant ferredoxin, FLAV = flavodoxin, pTF = phytotransferrin, ISIP3 = iron starvation induced protein 3, MCO = multicopper oxidase, NRAMP = natural resistance-associated macrophage protein, ZIP = zinc responsive transporter/iron responsive transporter-like protein, SufB = Fe-S cluster assembly protein, NCS2 = uracil-xanthine permease, TM AA = transmembrane amino acid, RND = resistance-nodulation-division family transporters, EST = eukaryotic sterol transporter, HAE = hydrophobe/amphiphile efflux.

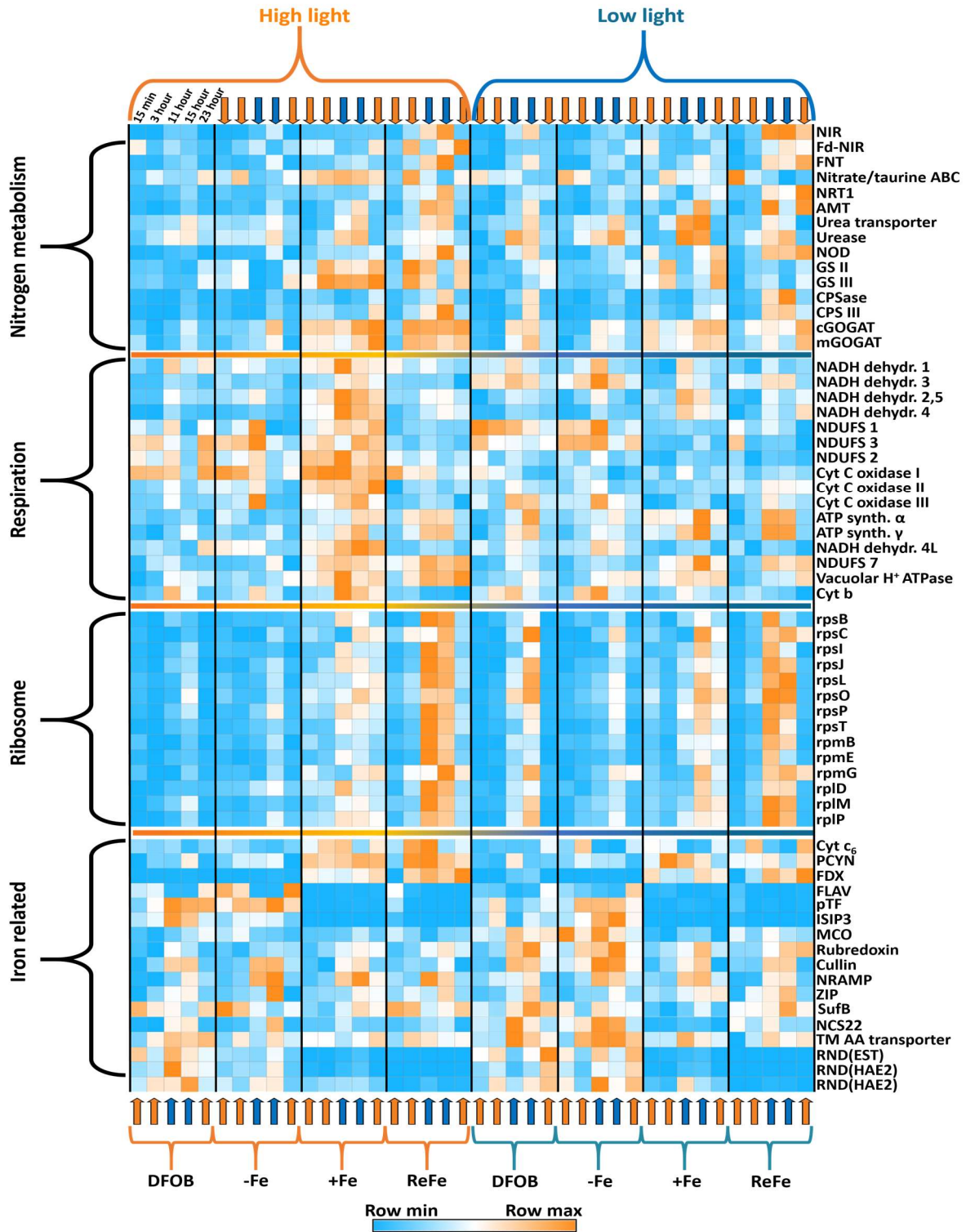
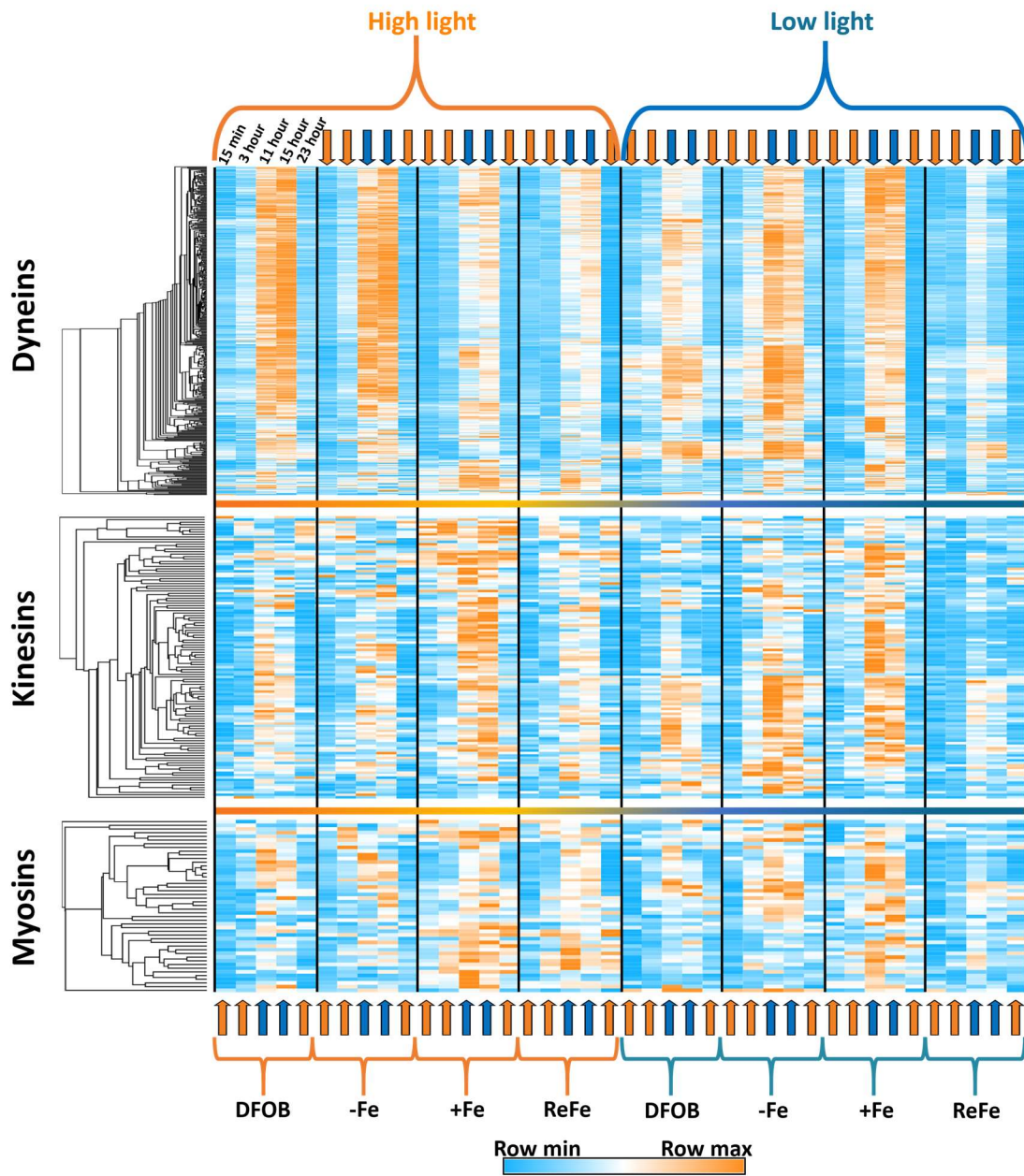


Figure 2.8. Dynein, kinesin and myosin motor protein gene expression across all conditions and time points. Heatmap showing average standardized transcript abundance (standardized RPKM to standard deviation across samples) of ORFs annotated as dyneins or kinesin across the diel cycle. 440 dynein, 115 kinesin and 47 myosin ORFs are shown, hierarchically clustered by expression pattern (Pearson correlation).



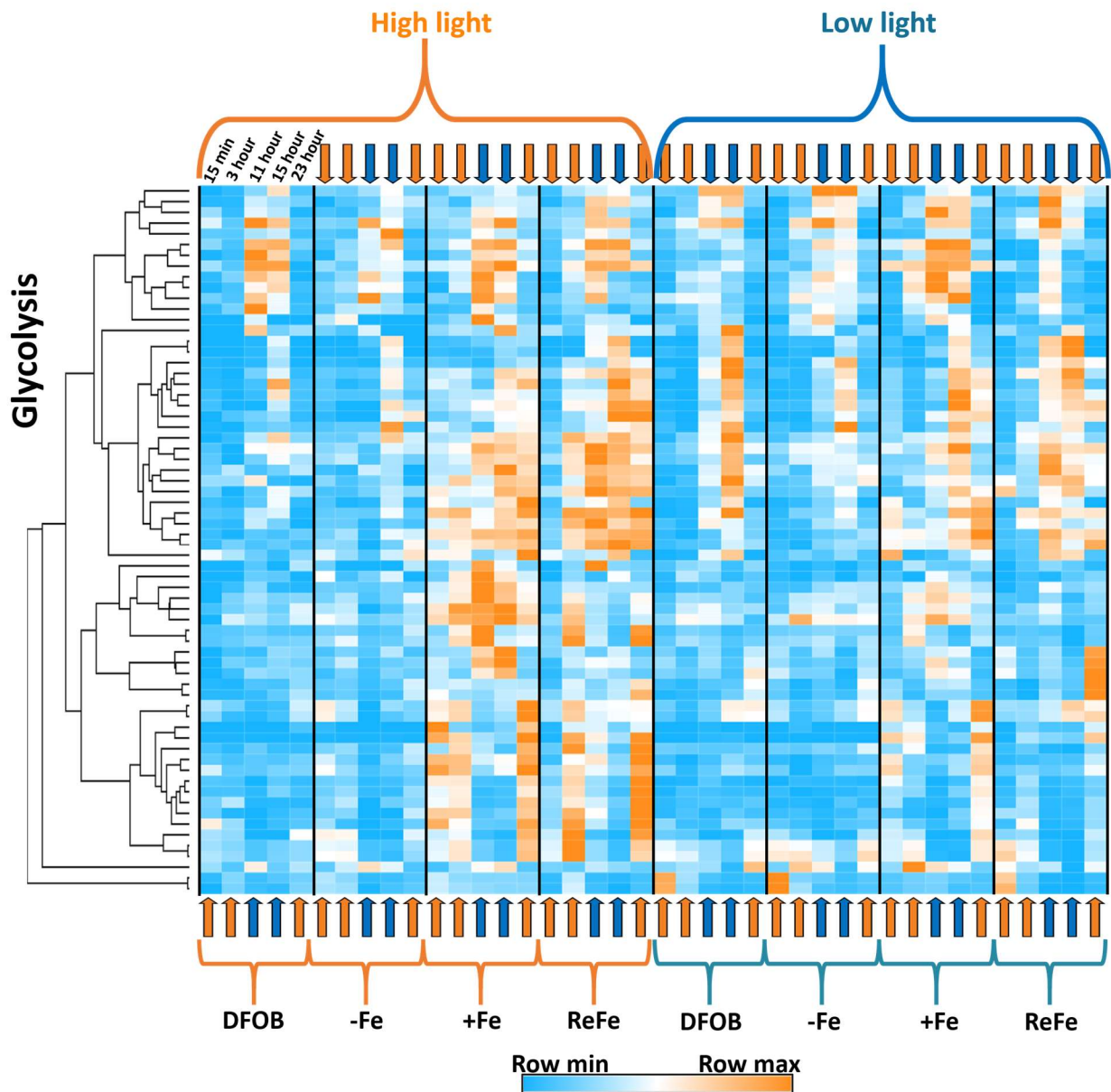


Figure 2.9. Glycolysis gene expression across all conditions and time points. Heatmap showing average standardized transcript abundance (standardized RPKM to standard deviation across samples) of ORFs annotated as glycolysis by KO pathway, across the diel cycle. 66 ORFs are shown, hierarchically clustered by expression pattern (Pearson correlation).

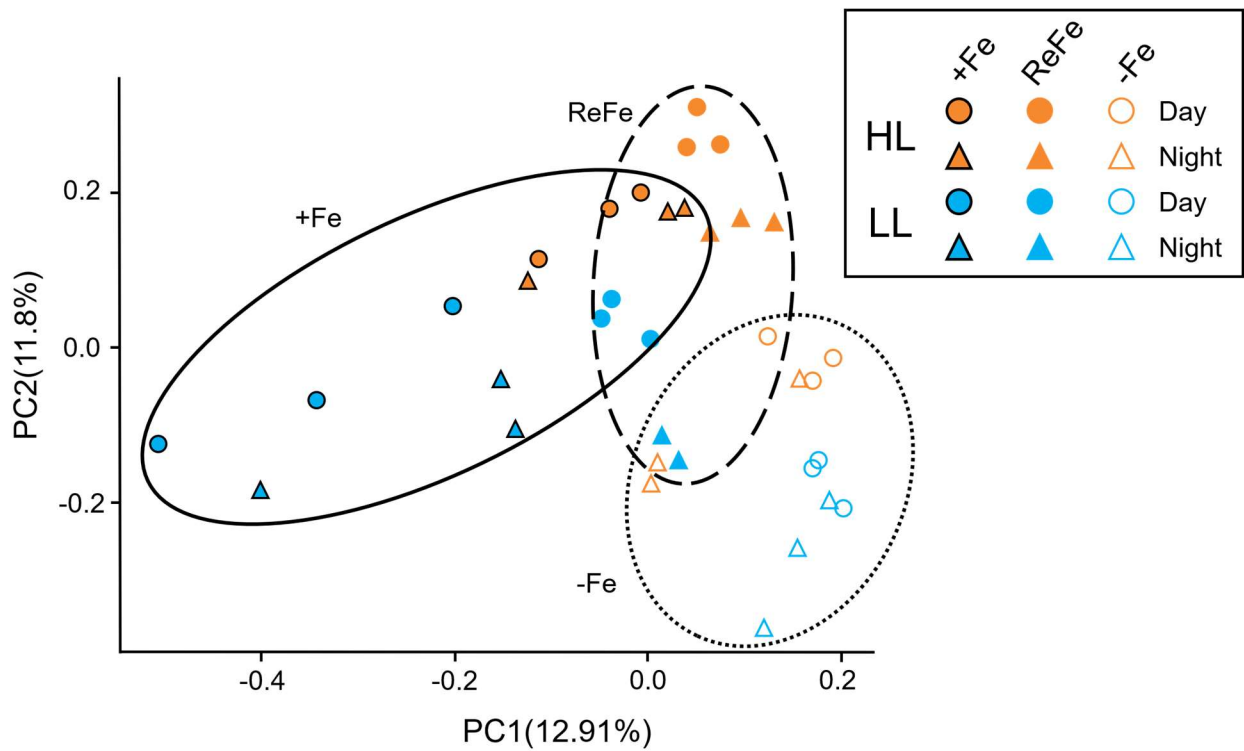
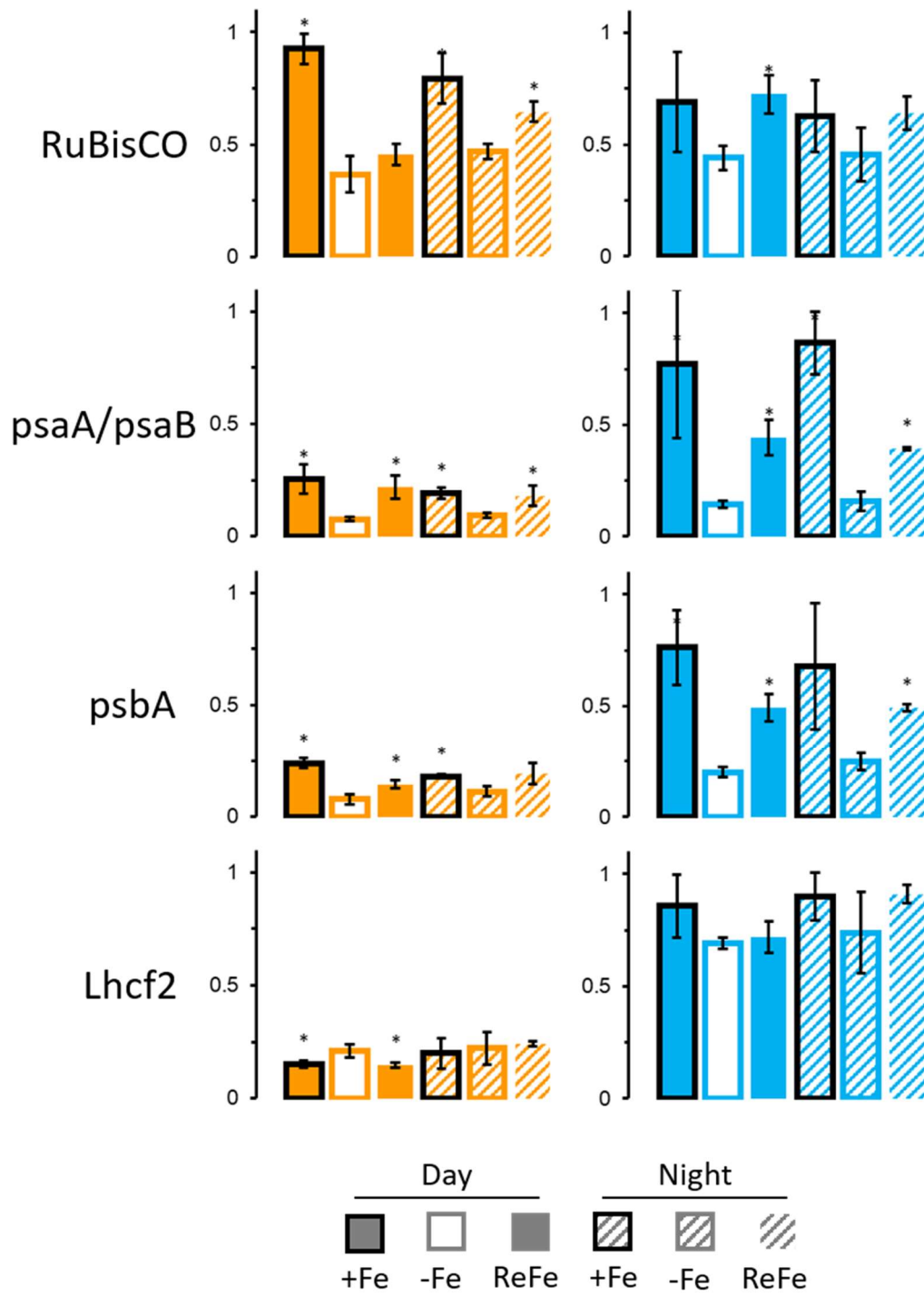


Figure 2.10. Principal component analysis plot of *P. calceolata* proteomes (TMM of 2924 quantified proteins). Each symbol represents a single sample. Orange and blue indicate high light (HL) and low light (LL) respectively. Triangles indicate day time points and circles show night time points. Black outlines indicate iron replete (+Fe), solid fill with no outline indicates iron resupply (ReFe), no fill indicates iron deplete (-Fe).

Figure 2.11. Scaled abundance of photosynthetic proteins. Protein expression values (TMM) normalized per cell, averaged across biological triplicates, and scaled from 0-1. Orange indicated high light cultures; blue shows low light cultures. Error bars show +/- 1 SD and asterisk indicates $p < 0.05$ (Student unpaired two-tailed t test) difference from -Fe value at same time of day. RuBisCO = ribulose 1,5 biphosphate carboxylase large subunit, psaA/psaB = photosystem I reaction center proteins A/B, psbA = photosystem II reaction center proteins A, Lhcf2 = light harvesting complex protein f2.

Photosynthesis



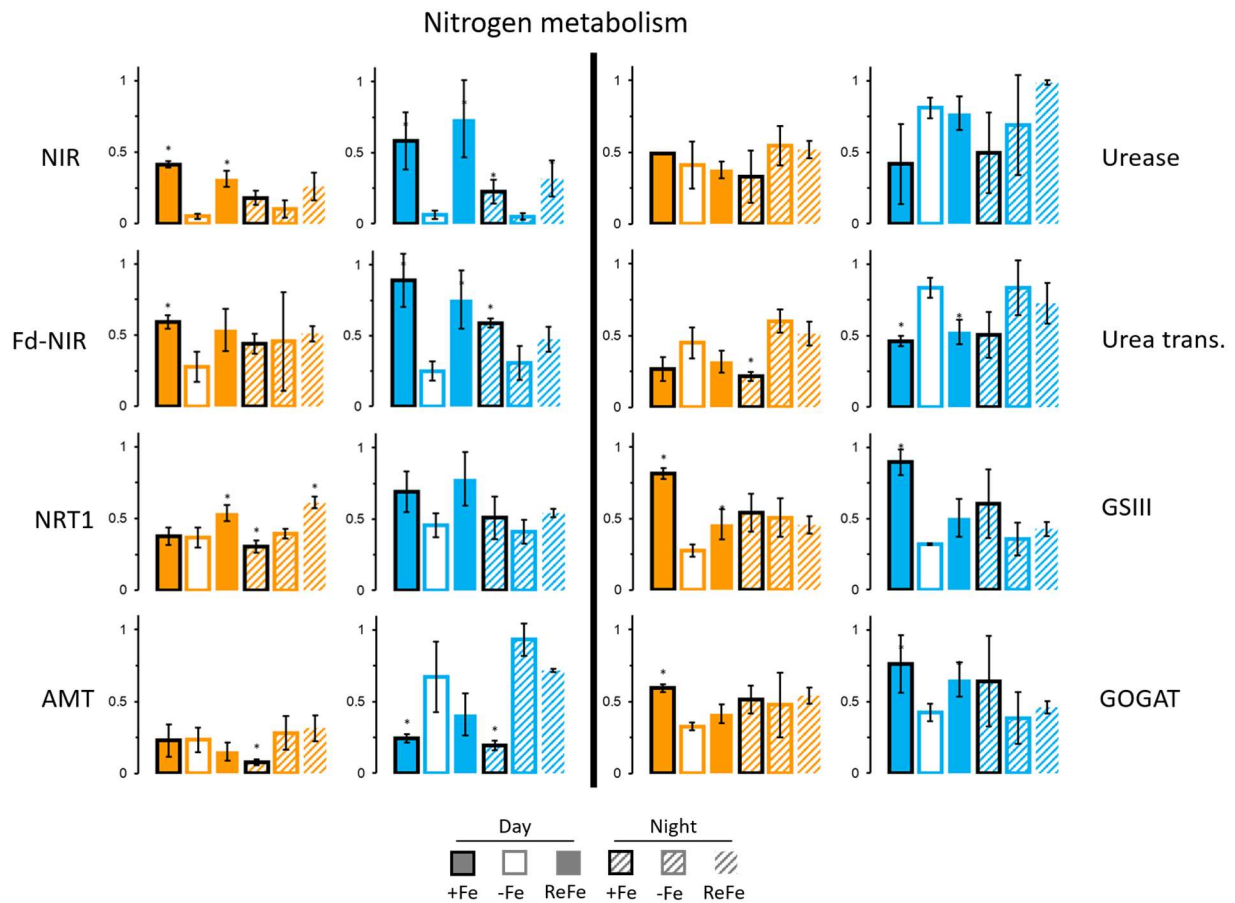
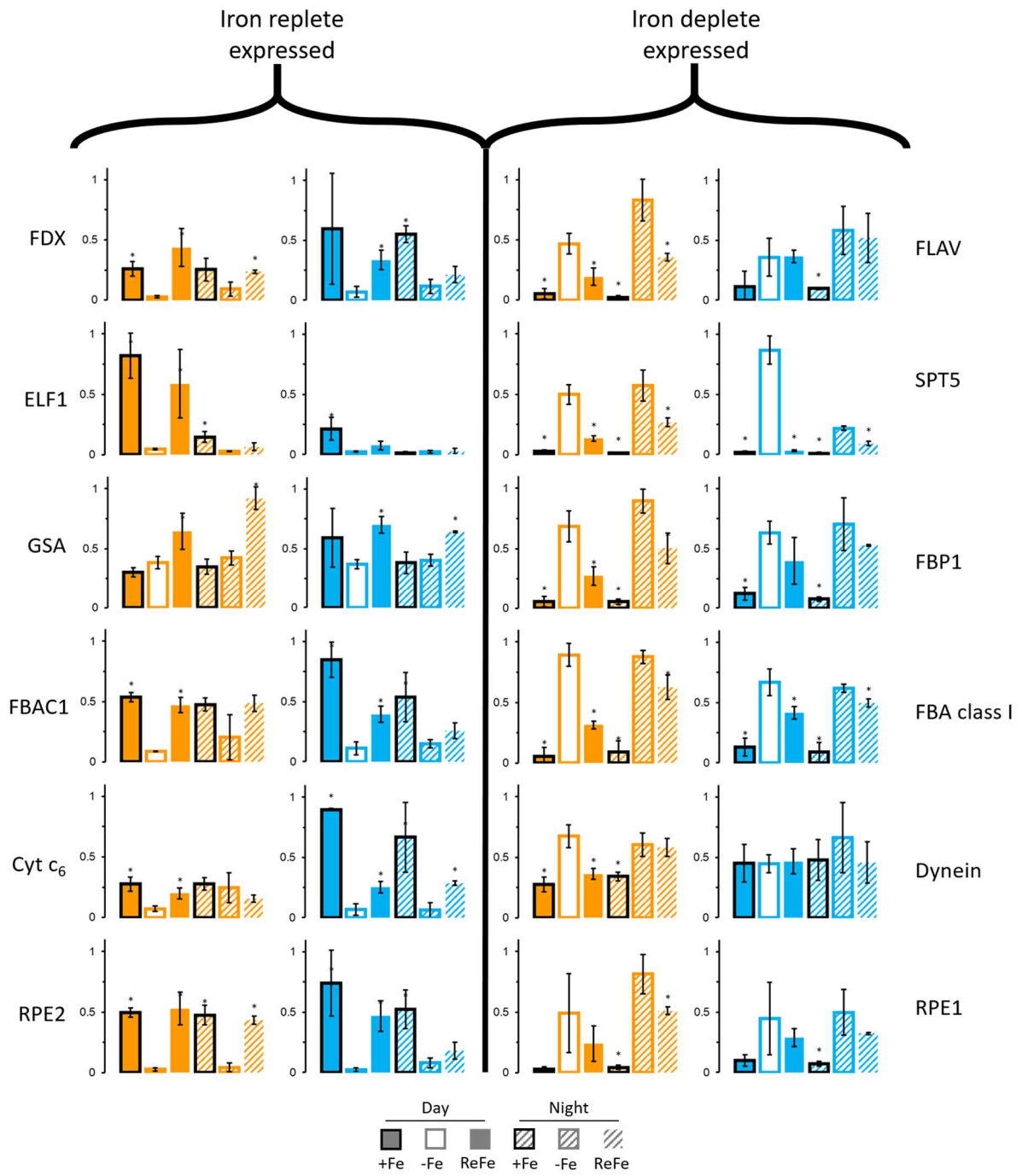


Figure 2.12. Scaled abundance of nitrogen metabolism proteins. Protein expression values (TMM) normalized per cell, averaged across biological triplicates, and scaled from 0-1. Orange indicated high light cultures; blue shows low light cultures. Error bars show +/- 1 SD and asterisk indicates $p < 0.05$ (Student unpaired two-tailed t test) difference from -Fe value at same time of day. NIR = NADPH nitrite reductase, Fd-NIR = ferredoxin nitrite reductase, NRT1 = nitrate transporter, AMT = ammonia transporter, GSIII = glutamine synthetase III, GOGAT = glutamine oxoglutarate aminotransferase.

Figure 2.13. Scaled abundance of iron-sensitive proteins. Protein expression values (TMM) normalized per cell, averaged across biological triplicates, and scaled from 0-1. Orange indicated high light cultures; blue shows low light cultures. Error bars show +/- 1 SD and asterisk indicates $p < 0.05$ (Student unpaired two-tailed t test) difference from -Fe value at same time of day. FDX = ferredoxin, FBP1 = fructose 1,6-bisphosphatase, ELF1 = mRNA export factor elf1, SPT5 = transcription elongation factor, GSA = glutamate-1-semialdehyde aminotransferase, FBAC1 = fructose bisphosphate aldolase class II, Cyt c_6 = cytochrome c_6 , RPE = ribulose 5-phosphate 3-epimerase, FLAV = flavodoxin.



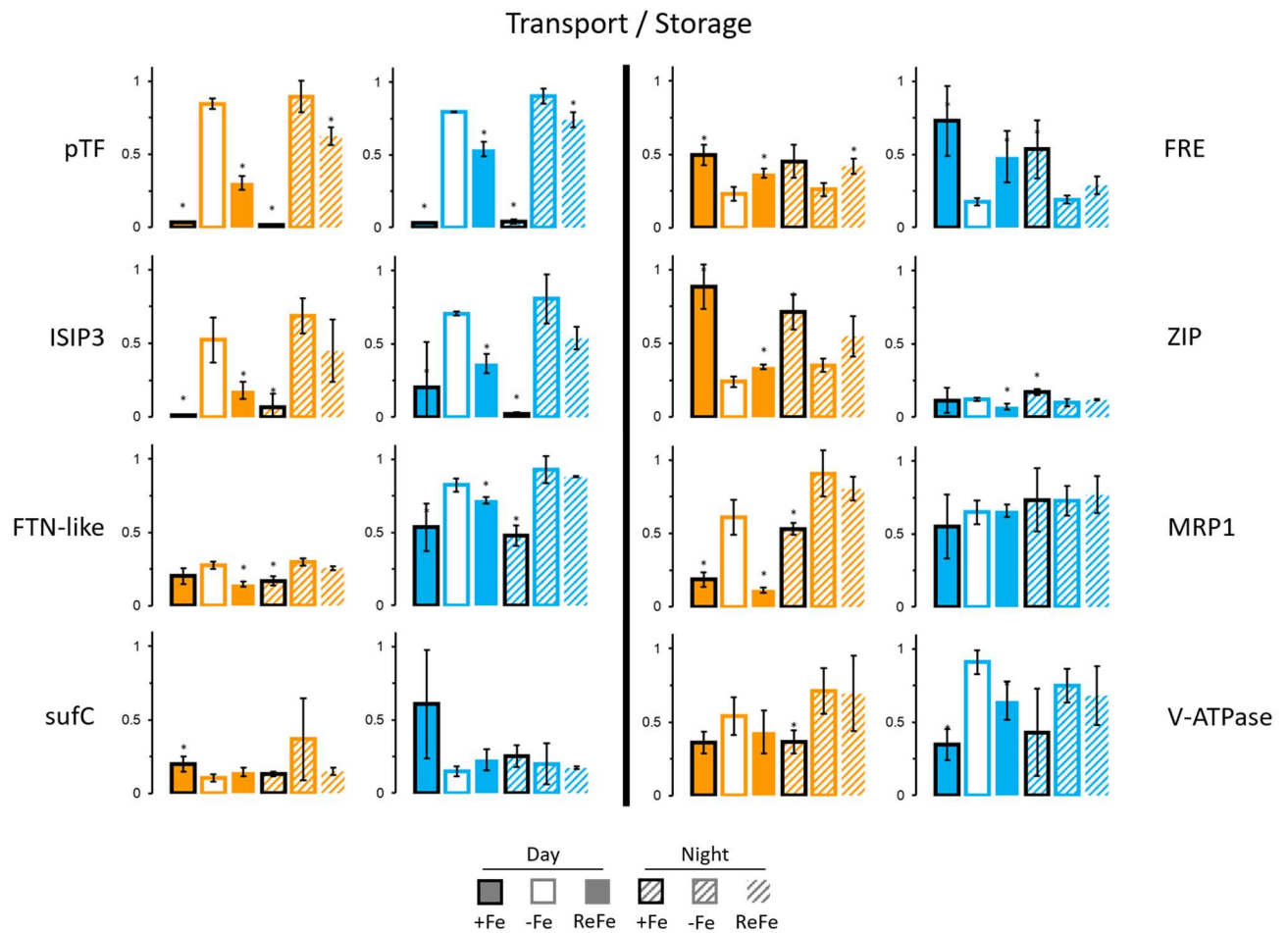
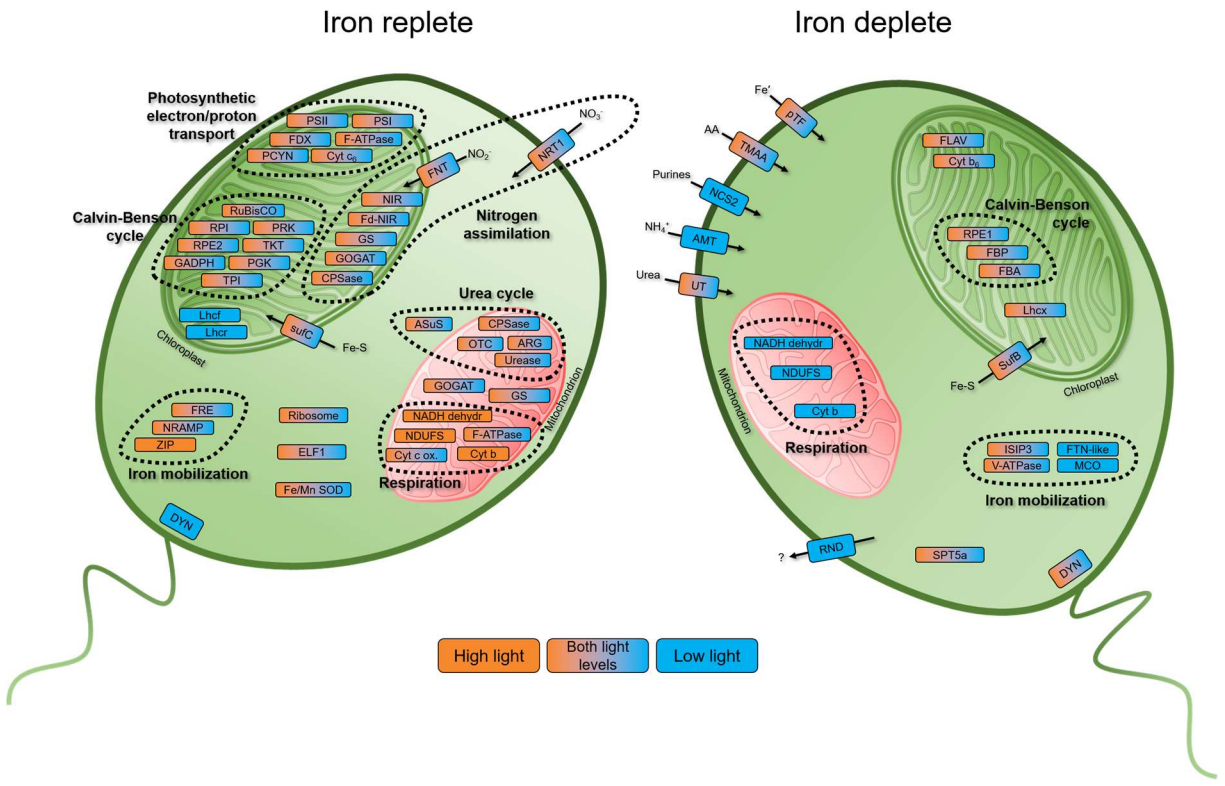


Figure 2.14. Scaled abundance of iron transport and storage related proteins. Protein expression values (TMM) normalized per cell, averaged across biological triplicates, and scaled from 0-1. Orange indicated high light cultures, blue shows low light cultures. Error bars show +/- 1 SD and asterisk indicates $p < 0.05$ (Student unpaired two-tailed t test) difference from -Fe value at same time of day. pTF = phyto transferrin, ISIP3 = iron starvation induced protein 3, FTN-like = ferritin like, FRE = ferric reductase, ZIP = zinc responsive transporter/iron responsive transporter-like protein, MRP1 = multidrug resistance protein, sufC = chloroplast Fe-S cluster assembly ABC transporter, V-ATPase = vacuolar proton pump.

Figure 2.15. Global proteomic response of *P. calceolata* to iron starvation at high light (**A**) and low light (**B**). X-axes show average cell-normalized protein expression (TMM) of triplicate iron replete cultures and Y-axes show iron deplete cultures. The 2924 proteins which were quantified in every sample are plotted at day and night. Orange circles indicate day time points and night time points are indicated with blue triangles. Black line shows a 1:1 line. 14-3-3 = 14-3-3 regulatory protein, ACS3 = long chain fatty acyl-CoA synthetase, ELF1 = mRNA export factor elf1, Fas = fascilin, FBP1 = fructose 1,6-bisphosphatase, FDX = ferredoxin, FTN-like = ferritin like, GAPD1 = glyceraldehyde-3-phosphate dehydrogenase, H2A/B = histone h2a/b, Hsp70 = 70kDa heat shock protein, L13Ae = large ribosomal subunit L13Ae, L5e = large subunit ribosomal protein L5e, Lhc = chlorophyll A-B binding protein, MSP = manganese stabilizing protein, nudel = nudel serine protease, OpdB = prolyl oligopeptidase, P-ATPase = P-ATPase family sodium/potassium transporter, ponA = pontin signaling protein, pTF = phytotransferrin, RBL = RuBisCO large subunit, RBS = RuBisCO small subunit, RPE = ribulose 5-phosphate 3-epimerase, SNARE = SNAP receptor, SPT5 = transcription elongation factor, TFase = transferase, tRNA = prolyl-tRNA synthetase, TUB2 = tubulin.

Figure 2.16. Iron and light induced state changes in the cellular functioning of *P. calceolata*. Cellular diagrams showing impacts of light and iron on key processes. Orange indicates significant upregulation in the indicated iron nutritional status at the protein and/or RNA level only in high light cultures, and blue indicates low light. Student unpaired two-tailed t test ($p < 0.05$) was used for comparisons between RPKM or cell normalized TMM from biological triplicates of iron replete and deplete cultures, collected at the same time point. PSI = photosystem I reaction center proteins, PSII = photosystem II reaction center proteins, FDX = ferredoxin, PCYN = plastocyanin, Cyt c_6 = cytochrome c_6 , RuBisCO = ribulose 1,5 bisphosphate carboxylase, FBA = fructose-bisphosphate aldolase, FBP = fructose 1,6-bisphosphatase, RPE = ribulose 5-phosphate 3-epimerase, RPI = ribose-5-phosphate isomerase, GAPDH = glyceraldehyde 3-phosphate dehydrogenase, PRK = phosphoribulokinase, TKT = transketolase, PGK = phosphoglycerate kinase, TPI = triosephosphate isomerase, Lhc = light harvesting complex protein, FRE = ferric reductase, NRAMP = natural resistance-associated macrophage protein, ZIP = zinc responsive transporter/iron responsive transporter-like protein, sufC = Fe-S cluster assembly protein, DYN = dynein, NIR = NADPH nitrite reductase, Fd-NIR = ferredoxin nitrite reductase, FNT = formate/nitrite transporter, NRT1 = nitrate transporter, GS = glutamine synthetase, GOGAT = glutamine oxoglutarate aminotransferase, CPSase = carbamoyl phosphate synthetase, OTC = ornithine transcarbamylase NADH dehydr. = mitochondrial NADH dehydrogenase, NDUFS = NADH-ubiquinone oxidoreductase, Cyt c ox. = cytochrome c oxidase, Cyt b = cytochrome b, ELF1 = mRNA export factor elf1, Fe/Mn SOD = Fe/Mn superoxide dismutase, pTF = phytostraferrin, TMAA = transmembrane amino acid transporter, AA = amino acid, NCS2 = uracil-xanthine permease, AMT = ammonia transporter, UT = urea transporter, FLAV = flavodoxin, SufB = Fe-S cluster assembly protein, ISIP3 = iron starvation induced protein 3, MCO = multicopper oxidase, FTN-like = ferritin like, V-ATPase = vacuolar proton pump, RND = resistance-nodulation-division family transporter, SPT5 = transcription elongation factor.



2.7 ACKNOWLEDGEMENTS

Chapter 2 is currently being prepared for submission for publication of the material. Coale, T., Tan, M., Venepally, P., Rowland, E., Bertrand, E., and Allen, A. Iron/light co-limitation in a globally significant pelagophyte. The dissertation author was the primary investigator and author of this paper.

Thanks to Hong Zheng for assistance with RNA and protein sample preparation, Maxine Tan for late night sampling heroics and Rob Franks for expert operation of the ICP-MS at the University of California, Santa Cruz Marine Analytical Laboratory. Also to Pratap Venepally for assistance developing gene models, assembling and annotating transcriptomes.

2.8 REFERENCES

- Akana, J., Fedorov, A. A., Fedorov, E., Novak, W. R. P., Babbitt, P. C., Almo, S. C., & Gerlt, J. A. (2006). D-ribulose 5-phosphate 3-epimerase: Functional and structural relationships to members of the ribulose-phosphate binding (??/??) 8-barrel superfamily. *Biochemistry*, 45(8), 2493–2503. <https://doi.org/10.1021/bi052474m>
- Allen, A. E., Dupont, C. L., Oborník, M., Horák, A., Nunes-Nesi, A., McCrow, J. P., Zheng, H., Johnson, D. A., Hu, H., Fernie, A. R., & Bowler, C. (2011). Evolution and metabolic significance of the urea cycle in photosynthetic diatoms. *Nature*, 473(7346), 203–207. <https://doi.org/10.1038/nature10074>
- Allen, A. E., Laroche, J., Maheswari, U., Lommer, M., Schauer, N., Lopez, P. J., Finazzi, G., Fernie, A. R., Bowler, C., & Karl, D. M. (2008). Whole-cell response of the pennate diatom *Phaeodactylum tricornutum* to iron starvation. *Proceedings of the National Academy of Sciences of the United States of America*, 105(30), 10438–10443. <https://doi.org/10.1073/pnas.0711370105>

- Andersen, R. A., Bidigare, R. R., Keller, M. D., & Latasa, M. (1996). A comparison of HPLC pigment signatures and electron microscopic observations for oligotrophic waters of the North Atlantic and Pacific Oceans. *Deep Sea Research Part II: Topical Studies in Oceanography*, 43(2–3), 517–537.
- Andersen, R. A., Saunders, G. W., Paskind, M. P., & Sexton, J. P. (1993). Ultrastructure and 18S Rna Gene Sequence for *Pelagomonas Calceolata* Gen. Et Sp. Nov. and the Description of a New Algal Class, the Pelagophyceae Classis Nov. *Journal of Phycology*, 29(5), 701–715. <https://doi.org/10.1111/j.0022-3646.1993.00701.x>
- Asada, K. (1999). The water-water cycle in chloroplasts: scavenging of active oxygens and dissipation of excess photons. *Annual Review of Plant Biology*, 50(1), 601–639.
- Ashworth, J., Coesel, S., Lee, A., Armbrust, E. V., Orellana, M. V., & Baliga, N. S. (2013). Genome-wide diel growth state transitions in the diatom *Thalassiosira pseudonana*. *Proceedings of the National Academy of Sciences of the United States of America*, 110(18), 7518–7523. <https://doi.org/10.1073/pnas.1300962110>
- Azam, F., & Ammerman, J. W. (1984). Cycling of Organic Matter by Bacterioplankton in Pelagic Marine Ecosystems: Microenvironmental Considerations. *Flows of Energy and Materials in Marine Ecosystems*, 345–360. https://doi.org/10.1007/978-1-4757-0387-0_14
- Bailleul, B., Rogato, A., De Martino, A., Coesel, S., Cardol, P., Bowler, C., Falciatore, A., & Finazzi, G. (2010). An atypical member of the light-harvesting complex stress-related protein family modulates diatom responses to light. *Proceedings of the National Academy of Sciences*, 107(42), 18214–18219.
- Bandyopadhyay, S., Chandramouli, K., & Johnson, M. K. (2008). *Iron–sulfur cluster biosynthesis*. Portland Press Ltd.
- Behrenfeld, M. J., & Milligan, A. J. (2011). Photophysiological Expressions of Iron Stress in Phytoplankton. *Annual Review of Marine Science*, 5, 120717164858000. <https://doi.org/10.1146/annurev-marine-121211-172356>
- Berger, C. J. M., Lippitt, S. M., Lawrence, M. G., & Bruland, K. W. (2008). Application of a chemical leach technique for estimating labile particulate aluminum, iron, and manganese in the Columbia River plume

and coastal waters off Oregon and Washington. *Journal of Geophysical Research*, 113, 1–16. <https://doi.org/10.1029/2007JC004703>

Bertrand, E. M., McCrow, J. P., Moustafa, A., Zheng, H., McQuaid, J. B., Delmont, T. O., Post, A. F., Sipler, R. E., Spackeen, J. L., Xu, K., Bronk, D. A., Hutchins, D. A., & Allen, A. E. (2015). Phytoplankton–bacterial interactions mediate micronutrient colimitation at the coastal Antarctic sea ice edge. *Proceedings of the National Academy of Sciences*, 112(32). <https://doi.org/10.1073/pnas.1501615112>

Biller, D. V., Coale, T. H., Till, R. C., Smith, G. J., & Bruland, K. W. (2013). Coastal iron and nitrate distributions during the spring and summer upwelling season in the central California Current upwelling regime. *Continental Shelf Research*, 66, 58–72. <https://doi.org/10.1016/j.csr.2013.07.003>

Blaby-Haas, C. E., & Merchant, S. S. (2013). Iron sparing and recycling in a compartmentalized cell. *Current Opinion in Microbiology*, 1–9. <https://doi.org/10.1016/j.mib.2013.07.019>

Bosu, D. R., & Kipreos, E. T. (2008). Cullin-RING ubiquitin ligases: Global regulation and activation cycles. *Cell Division*, 3, 1–13. <https://doi.org/10.1186/1747-1028-3-7>

Bowie, A. R., Johnson, R. J., Church, T. M., Achilles, K. M., Lethaby, P. J., McGillicuddy, D. J., Marsay, C. M., Sarin, M. M., Ussher, S. J., Sedwick, P. N., Church, T. M., Bowie, A. R., Marsay, C. M., Ussher, S. J., Achilles, K. M., Lethaby, P. J., Johnson, R. J., Sarin, M. M., McGillicuddy, D. J., ... Sedwick, P. N. (2005). Iron in the Sargasso Sea (Bermuda Atlantic Time-series Study region) during summer: Eolian imprint, spatiotemporal variability, and ecological implications. *Global Biogeochemical Cycles*, 19(4), n/a-n/a. <https://doi.org/10.1029/2004gb002445>

Brauer, M. J., Huttenhower, C., Airoidi, E. M., Rosenstein, R., Matese, J. C., Gresham, D., Boer, V. M., Troyanskaya, O. G., & Botstein, D. (2008). Coordination of growth rate, cell cycle, stress response, and metabolic activity in yeast. *Molecular Biology of the Cell*, 19(1), 352–367.

Brzezinski M.A., Krause J.W., Bundy R.M., Barbeau K.A., Franks P., Goericke R., L. M. R. and S. M. R. (2015). Enhanced silica ballasting from iron stress sustains carbon export in a frontal zone within the California Current. *Journal of Geophysical Research: Oceans*, 120, 4654–4669. <https://doi.org/10.1002/2015JC010829>.Received

- Buck, J. M., Sherman, J., Bártulos, C. R., Serif, M., Halder, M., Henkel, J., Falciatore, A., Lavaud, J., Gorbunov, M. Y., & Kroth, P. G. (2019). Lhcx proteins provide photoprotection via thermal dissipation of absorbed light in the diatom *Phaeodactylum tricornutum*. *Nature Communications*, *10*(1), 1–12.
- Carradec, Q., Pelletier, E., Da Silva, C., Alberti, A., Seeleuthner, Y., Blanc-Mathieu, R., Lima-Mendez, G., Rocha, F., Tirichine, L., & Labadie, K. (2018). A global ocean atlas of eukaryotic genes. *Nature Communications*, *9*(1), 373.
- Cermeño, P., Lee, J.-B., Wyman, K., Schofield, O., & Falkowski, P. G. (2011). Competitive dynamics in two species of marine phytoplankton under non-equilibrium conditions. *Marine Ecology Progress Series*, *429*, 19–28.
- Chisholm, S. W. (1992). Phytoplankton size. In *Primary productivity and biogeochemical cycles in the sea* (pp. 213–237). Springer.
- Clemens, S. (2006). Evolution and function of phytochelatin synthases. *Journal of Plant Physiology*, *163*(3), 319–332.
- Cohen, N. R., Ellis, K. A., Lampe, R. H., McNair, H., Twining, B. S., Maldonado, M. T., Brzezinski, M. A., Kuzminov, F. I., Thammatrakoln, K., Till, C. P., Bruland, K. W., Sunda, W. G., Bargu, S., & Marchetti, A. (2017). Diatom transcriptional and physiological responses to changes in iron bioavailability across ocean provinces. *Frontiers in Marine Science*, *4*, 360. <https://doi.org/10.3389/fmars.2018.00115>
- Cohen, N. R., Gong, W., Moran, D. M., McIlvin, M. R., Saito, M. A., & Marchetti, A. (2018). Transcriptomic and proteomic responses of the oceanic diatom *Pseudo-nitzschia granii* to iron limitation. *Environmental Microbiology*, *20*(8), 3109–3126. <https://doi.org/10.1111/1462-2920.14386>
- Cohen, N. R., Mann, E., Stemple, B., Moreno, C. M., Rauschenberg, S., Jacquot, J. E., Sunda, W. G., Twining, B. S., & Marchetti, A. (2018). Iron storage capacities and associated ferritin gene expression among marine diatoms. *Limnology and Oceanography*, *63*(4). <https://doi.org/10.1002/lno.10800>
- Cullen, J. (1982). Cullen1982CJFAS.pdf. In *Canadian Journal of Fisheries and Aquatic ...*. <http://www.nrcresearchpress.com/doi/abs/10.1139/f82-108>
- Cullen, J. J. (2014). Subsurface Chlorophyll Maximum Layers: Enduring Enigma

or Mystery Solved? *Annual Review of Marine Science*, 7(1), 207–239.
<https://doi.org/10.1146/annurev-marine-010213-135111>

de Baar, H. J. W. W., Boyd, P. W., Coale, K. H., Landry, M. R., Tsuda, A., Assmy, P., Bakker, D. C. E., Bozec, Y., Barber, R. T., Brzezinski, M. A., Buesseler, K. O., Boyé, M., Croot, P. L., Gervais, F., Gorbunov, M. Y., Harrison, P. J., Hiscock, W. T., Laan, P., Lancelot, C., ... Wong, C. S. (2005). Synthesis of iron fertilization experiments: From the Iron Age in the Age of Enlightenment. *Journal of Geophysical Research*, 110(C9), C09S16.
<https://doi.org/10.1029/2004JC002601>

Dimier, C., Brunet, C., Geider, R., & Raven, J. (2009). Growth and photoregulation dynamics of the picoeukaryote *Pelagomonas calceolata* in fluctuating light. *Limnology and Oceanography*, 54(3), 823–836. <https://doi.org/10.4319/lo.2009.54.3.0823>

Division, R., Goldberg, M., Pribyl, T., Nies, D. H., & Juhnke, S. (1999). MEMBRANES AND BIOENERGETICS : Energetics and Topology of CzcA , a Cation / Proton Antiporter of the Protein Family Energetics and Topology of CzcA , a Cation / Proton Antiporter of the Resistance-Nodulation-Cell Division Protein Family *. *Journal of Biological Chemistry*, 274(37), 26065–26070.

Dupont, C. L., Mccrow, J. P., Valas, R., Moustafa, A., Walworth, N., Goodenough, U., Roth, R., Hogle, S. L., Bai, J., Johnson, Z. I., Mann, E., Palenik, B., Barbeau, K. A., Venter, J. C., Allen, A. E., Craig Venter, J., Allen, A. E., Venter, J. C., & Allen, A. E. (2014). Genomes and gene expression across light and productivity gradients in eastern subtropical Pacific microbial communities. *The ISME Journal*, 9(5), 1076–1092.
<https://doi.org/10.1038/ismej.2014.198>

Finbow, M. E., & Harrison, M. A. (1997). The vacuolar H⁺-ATPase: a universal proton pump of eukaryotes. *Biochemical Journal*, 324(3), 697–712.

Friedman, A. L., & Alberte, R. S. (1986). Biogenesis and light regulation of the major light harvesting chlorophyll-protein of diatoms. *Plant Physiology*, 80(1), 43–51.

Grimm, B. (1990). Primary structure of a key enzyme in plant tetrapyrrole synthesis: glutamate 1-semialdehyde aminotransferase. *Proceedings of the National Academy of Sciences*, 87(11), 4169–4173.

Guillard, R. R. L. (1975). Culture of phytoplankton for feeding marine

- invertebrates. In *Culture of marine invertebrate animals* (pp. 29–60). Springer.
- Hecht, M., Bromberg, Y., & Rost, B. (2015). Better prediction of functional effects for sequence variants. *BMC Genomics*, *16*(8), S1.
- Ho, T.-Y. T. Y., Quigg, A., Finkel, Z. V., Milligan, A. J., Wyman, K., Falkowski, P. G., & Morel, F. M. M. F. M. M. (2003). THE ELEMENTAL COMPOSITION OF SOME MARINE PHYTOPLANKTON1. *Journal of Phycology*, *39*(6), 1145–1159. <https://doi.org/10.1111/j.0022-3646.2003.03-090.x>
- Hogle, S. L., Dupont, C. L., Hopkinson, B. M., King, A. L., Buck, K. N., Roe, K. L., Stuart, R. K., Allen, A. E., Mann, E. L., Johnson, Z. I., & Barbeau, K. A. (2018). Pervasive iron limitation at subsurface chlorophyll maxima of the California Current. *Proceedings of the National Academy of Sciences*, *115*(52), 13300–13305. <https://doi.org/10.17605/OSF.IO/S37TE>
- Holm-Hansen, O., Kahru, M., & Hewes, C. D. (2005). Deep chlorophyll a maxima (DCMs) in pelagic Antarctic waters. II. Relation to bathymetric features and dissolved iron concentrations. *Marine Ecology Progress Series*, *297*, 71–81. <https://doi.org/10.3354/meps297071>
- Holm-Hansen, Osmund, Lorenzen, C. J., Holmes, R. W., & Strickland, J. D. H. (1965). Fluorometric determination of chlorophyll. *ICES Journal of Marine Science*, *30*(1), 3–15.
- Hopkinson, B. M., & Barbeau, K. A. (2008). Interactive influences of iron and light limitation on phytoplankton at subsurface chlorophyll maxima in the eastern North Pacific. *Limnology and Oceanography*, *53*(4), 1303–1318.
- Hudson, R. J. M., & Morel, F. M. M. (1990). Iron transport in marine phytoplankton: Kinetics of cellular and medium coordination reactions. *Limnology and Oceanography*, *35*(5), 1002–1020. <https://doi.org/10.4319/lo.1994.39.3.0520>
- Hutchins, D. A., & Bruland, K. W. K. W. (1998). Iron-limited diatom growth and Si: N uptake ratios in a coastal upwelling regime. *Nature*, *393*(June), 65–68. <https://doi.org/Doi 10.1038/31203>
- Johnson, K. S., Elrod, V. A., Fitzwater, S. E., Plant, J. N., Chavez, F. P., Tanner, S. J., Gordon, R. M., Westphal, D. L., Perry, K. D., Wu, J., Karl, D. M., Elrod, V. A., Perry, K. D., Plant, J. N., Gordon, R. M., Johnson, K. S., Westphal, D. L., Tanner, S. J., Fitzwater, S. E., ... Wu, J. (2003). Surface ocean-lower

- atmosphere interactions in the northeast Pacific Ocean gyre: Aerosols, iron, and the ecosystem response. *Global Biogeochemical Cycles*, 17(2), n/a-n/a. <https://doi.org/10.1029/2002gb002004>
- Johnson, K. S., Gordon, R. M., & Coale, K. H. (1997). What controls dissolved iron concentrations in the world ocean? *Marine Chemistry*, 57(3–4), 137–161.
- Johnson, Z. I., Shyam, R., Ritchie, A. E., Mioni, C., Lance, V. P., Murray, J. W., & Zinser, E. R. (2010). The effect of iron-and light-limitation on phytoplankton communities of deep chlorophyll maxima of the western Pacific Ocean. *Journal of Marine Research*, 68(2), 283–308.
- Kanehisa, M., & Goto, S. (2000). KEGG: kyoto encyclopedia of genes and genomes. *Nucleic Acids Research*, 28(1), 27–30.
- Kaplan, J., McVey Ward, D., Crisp, R. J., & Philpott, C. C. (2006). Iron-dependent metabolic remodeling in *S. cerevisiae*. *Biochimica et Biophysica Acta - Molecular Cell Research*, 1763(7), 646–651. <https://doi.org/10.1016/j.bbamcr.2006.03.008>
- King, A. L., & Barbeau, K. A. (2011). Dissolved iron and macronutrient distributions in the southern California Current System. *Journal of Geophysical Research: Oceans*, 116(3), 1–18. <https://doi.org/10.1029/2010JC006324>
- Koch, F., Beszteri, S., Harms, L., & Trimborn, S. (2018). The impacts of iron limitation and ocean acidification on the cellular stoichiometry, photophysiology, and transcriptome of *Phaeocystis antarctica*. *Limnology and Oceanography*, 1–19. <https://doi.org/10.1002/lno.11045>
- Koziol, A. G., Borza, T., Ishida, K.-I., Keeling, P., Lee, R. W., & Durnford, D. G. (2007). Tracing the evolution of the light-harvesting antennae in chlorophyll a/b-containing organisms. *Plant Physiology*, 143(4), 1802–1816. <https://doi.org/10.1104/pp.106.092536>
- Layer, G., Aparna Gaddam, S., Ayala-Castro, C. N., Choudens, S. O. De, Lascoux, D., Fontecave, M., & Outten, F. W. (2007). SufE transfers sulfur from SufS to SufB for iron-sulfur cluster assembly. *Journal of Biological Chemistry*, 282(18), 13342–13350. <https://doi.org/10.1074/jbc.M608555200>
- Lelandais, G., Scheiber, I., Paz-Yepes, J., Lozano, J.-C. C., Botebol, H., Pilátová, J., Žárský, V., Léger, T., Blaiseau, P.-L. L., Bowler, C., Bouget, F. Y.,

- Camadro, J. M., Sutak, R., & Lesuisse, E. (2016). *Ostreococcus tauri* is a new model green alga for studying iron metabolism in eukaryotic phytoplankton. *BMC Genomics*, *17*(1), 319. <https://doi.org/10.1186/s12864-016-2666-6>
- Lindstrom, D. L., Squazzo, S. L., Muster, N., Burckin, T. A., Wachter, K. C., Emigh, C. A., McCleery, J. A., Yates, J. R., & Hartzog, G. A. (2003). Dual Roles for Spt5 in Pre-mRNA Processing and Transcription Elongation Revealed by Identification of Spt5-Associated Proteins. *Molecular and Cellular Biology*, *23*(4), 1368–1378. <https://doi.org/10.1128/mcb.23.4.1368-1378.2003>
- Lippiatt, S. M., Brown, M. T., Lohan, M. C., Berger, C. J. M., & Bruland, K. W. (2010). Leachable particulate iron in the Columbia River, estuary, and near-field plume. *Estuarine, Coastal and Shelf Science*, *87*(1), 33–42. <https://doi.org/10.1016/j.ecss.2009.12.009>
- Lippiatt, S. M., Brown, M. T., Lohan, M. C., & Bruland, K. W. (2011). Reactive iron delivery to the Gulf of Alaska via a Kenai eddy. *Deep Sea Research Part I: Oceanographic Research Papers*, *58*(11), 1091–1102. <https://doi.org/10.1016/j.dsr.2011.08.005>
- Lommer, M., Specht, M., Roy, A.-S., Kraemer, L., Andreson, R., Gutowska, M. a, Wolf, J., Bergner, S. V, Schilhabel, M. B., Klostermeier, U. C., Beiko, R. G., Rosenstiel, P., Hippler, M., & LaRoche, J. (2012). Genome and low-iron response of an oceanic diatom adapted to chronic iron limitation. *Genome Biology*, *13*(7), R66. <https://doi.org/10.1186/gb-2012-13-7-r66>
- Maldonado, M. T., & Price, N. M. (1996). Influence of N substrate on Fe requirements of marine centric diatoms. *Marine Ecology Progress Series*, *141*(1–3), 161–172. <https://doi.org/10.3354/meps141161>
- Marchetti, A., Catlett, D., Hopkinson, B. M., Ellis, K., & Cassar, N. (2015). Marine diatom proteorhodopsins and their potential role in coping with low iron availability. *The ISME Journal*, *9*(12), 1–4. <https://doi.org/10.1038/ismej.2015.74>
- Marchetti, A., Schrueth, D. M., Durkin, C. A., Parker, M. S., Kodner, R. B., Berthiaume, C. T., Morales, R., Allen, A. E., Armbrusta, E. V., & Armbrust, E. V. (2012). Comparative metatranscriptomics identifies molecular bases for the physiological responses of phytoplankton to varying iron availability. *Proceedings of the National Academy of Sciences*, *109*(6), E317–E325. <https://doi.org/10.1073/pnas.1118408109>

- Marsh, J. J., & Lebherz, H. G. (1992). Fructose-bisphosphate aldolases: an evolutionary history. *Trends in Biochemical Sciences*, 17(3), 110–113.
- Martiny, A. C., Vrugt, J. A., Primeau, F. W., & Lomas, M. W. (2013). Regional variation in the particulate organic carbon to nitrogen ratio in the surface ocean. *Global Biogeochemical Cycles*, 27(3), 723–731.
<https://doi.org/10.1002/gbc.20061>
- Maxson, M. E., & Grinstein, S. (2014). *The vacuolar-type H⁺-ATPase at a glance—more than a proton pump*. The Company of Biologists Ltd.
- McCarthy, J. K., Smith, S. R., McCrow, J. P., Tan, M., Zheng, H., Beerli, K., Roth, R., Lichtle, C., Goodenough, U., Bowler, C. P., Dupont, C. L., & Allen, A. E. (2017). Nitrate Reductase Knockout Uncouples Nitrate Transport from Nitrate Assimilation and Drives Repartitioning of Carbon Flux in a Model Pennate Diatom. *The Plant Cell*, 29(8), 2047–2070.
<https://doi.org/10.1105/tpc.16.00910>
- McQuaid, J. B., Kustka, A. B., Oborník, M., Horák, A., McCrow, J. P., Karas, B. J., Zheng, H., Kindeberg, T., Andersson, A. J., Barbeau, K. A., & Allen, A. E. (2018). Carbonate-sensitive phytotransferrin controls high-affinity iron uptake in diatoms. *Nature*, 555(7697), 534–537.
<https://doi.org/10.1038/nature25982>
- Merkulova, M., Păunescu, T. G., Azroyan, A., Marshansky, V., Breton, S., & Brown, D. (2015). Mapping the H⁺(V)-ATPase interactome: identification of proteins involved in trafficking, folding, assembly and phosphorylation. *Scientific Reports*, 5, 14827.
- Mills, M. M., Kropuenske, L. R., Van Dijken, G. L., Alderkamp, A., Berg, G. M., Robinson, D. H., Welschmeyer, N. A., & Arrigo, K. R. (2010). PHOTOPHYSIOLOGY IN TWO SOUTHERN OCEAN PHYTOPLANKTON TAXA: PHOTOSYNTHESIS OF PHAEOCYSTIS ANTARCTICA (PRYMNESIOPHYCEAE) AND FRAGILARIOPSIS CYLINDRUS (BACILLARIOPHYCEAE) UNDER SIMULATED MIXED-LAYER IRRADIANCE 1. *Journal of Phycology*, 46(6), 1114–1127.
- Mitchell, D. R., & Rosenbaum, J. L. (1985). A motile Chlamydomonas flagellar mutant that lacks outer dynein arms. *The Journal of Cell Biology*, 100(4), 1228–1234.
- Monnier, A., Liverani, S., Bouvet, R., Jesson, B., Smith, J. Q., Mosser, J., Corellou, F., & Bouget, F.-Y. (2010). Orchestrated transcription of biological

processes in the marine picoeukaryote *Ostreococcus* exposed to light/dark cycles. *BMC Genomics*, *11*, 192. <https://doi.org/10.1186/1471-2164-11-192>

Morel, F. M. M., Rueter, J. G., Anderson, D. M., & Guillard, R. R. L. (1979). AQUIL: A CHEMICALLY DEFINED PHYTOPLANKTON CULTURE MEDIUM FOR TRACE METAL STUDIES 1 2. *Journal of Phycology*, *15*(2), 135–141.

Moreno, C. M., Gong, W., Cohen, N. R., DeLong, K., & Marchetti, A. (2020). Interactive effects of iron and light limitation on the molecular physiology of the Southern Ocean diatom *Fragilariopsis kerguelensis*. *Limnology and Oceanography*.

Moreno, C. M., Lin, Y., Davies, S., Monbureau, E., Cassar, N., & Marchetti, A. (2018). Examination of gene repertoires and physiological responses to iron and light limitation in Southern Ocean diatoms. *Polar Biology*, *41*(4), 679–696.

Narayan, O. P., Kumari, N., & Rai, L. C. (2011). Iron starvation-induced proteomic changes in *Anabaena* (Nostoc) sp. PCC 7120: exploring survival strategy. *J Microbiol Biotechnol*, *21*(2), 136–146.

Nikaido, H. (2018). RND transporters in the living world. *Research in Microbiology*, *169*(7–8), 363–371.

Outten, F. W., Djaman, O., & Storz, G. (2004). A suf operon requirement for Fe-S cluster assembly during iron starvation in *Escherichia coli*. *Molecular Microbiology*, *52*(3), 861–872. <https://doi.org/10.1111/j.1365-2958.2004.04025.x>

Pate, J. S., & Layzell, D. B. (1990). Energetics and biological costs of nitrogen assimilation. *The Biochemistry of Plants*, *16*, 1–42.

Peers, G., & Price, N. M. N. (2006). Copper-containing plastocyanin used for electron transport by an oceanic diatom. *Nature*, *441*(7091), 341–344. <https://doi.org/10.1038/nature04630>

Plubell, D. L., Wilmarth, P. A., Zhao, Y., Fenton, A. M., Minnier, J., Reddy, A. P., Klimek, J., Yang, X., David, L. L., & Pamir, N. (2017). Extended multiplexing of tandem mass tags (TMT) labeling reveals age and high fat diet specific proteome changes in mouse epididymal adipose tissue. *Molecular & Cellular Proteomics*, *16*(5), 873–890.

- Poliner, E., Panchy, N., Newton, L., Wu, G., Lapinsky, A., Bullard, B., Zienkiewicz, A., Benning, C., Shiu, S., & Farré, E. M. (2015). Transcriptional coordination of physiological responses in *Nannochloropsis oceanica* CCMP 1779 under light/dark cycles. *The Plant Journal*, *83*(6), 1097–1113.
- Poole, K., Heinrichs, D. E., & Neshat, S. (1993). Cloning and sequence analysis of an EnvCD homologue in *Pseudomonas aeruginosa*: regulation by iron and possible involvement in the secretion of the siderophore pyoverdine. *Molecular Microbiology*, *10*(3), 529–544. <https://doi.org/10.1111/j.1365-2958.1993.tb00925.x>
- Price, N. M. (2005). The elemental stoichiometry and composition of an iron-limited diatom. *Limnology and Oceanography*, *50*(4), 1159–1171. <https://doi.org/10.4319/lo.2005.50.4.1159>
- Price, N. M., Harrison, G. I., Hering, J. G., Hudson, R. J., Nirel, P. M. V., Palenik, B., & Morel, F. M. M. (1989). Preparation and chemistry of the artificial algal culture medium Aquil. *Biological Oceanography*, *6*(5–6), 443–461. <https://doi.org/10.1080/01965581.1988.10749544>
- Quigg, A., Finkel, Z. V., Irwin, A. J., Rosenthal, Y., Ho, T.-Y., Reinfelder, J. R., Schofield, O., Morel, F. M. M., & Falkowski, P. G. (2003). The evolutionary inheritance of elemental stoichiometry in marine phytoplankton. *Nature*, *425*(6955), 291–294. <https://doi.org/10.1038/nature01953>
- Raven, John A. (1990). Predictions of Mn and Fe use efficiencies of phototrophic growth as a function of light availability for growth and of C assimilation pathway. *New Phytologist*, *116*(1), 1–18. <https://doi.org/10.1111/j.1469-8137.1990.tb00505.x>
- Raven, John A, Wollenweber, B., & Handley, L. L. (1992). A comparison of ammonium and nitrate as nitrogen sources for photolithotrophs. *New Phytologist*, *121*(1), 19–32.
- Rayko, E., Maumus, F., Maheswari, U., Jabbari, K., & Bowler, C. (2010). Transcription factor families inferred from genome sequences of photosynthetic stramenopiles. *New Phytologist*, *188*(1), 52–66. <https://doi.org/10.1111/j.1469-8137.2010.03371.x>
- Redfield, A. C. (1934). On the proportions of organic derivatives in sea water and their relation to the composition of plankton. *James Johnstone Memorial Volume*, 176–192.

- Revelante, N., & Gilmartin, M. (1973). Some observations on the chlorophyll maximum and primary production in the eastern North Pacific. *Internationale Revue Der Gesamten Hydrobiologie Und Hydrographie*, 58(6), 819–834.
- Robinson, M. D., & Oshlack, A. (2010). A scaling normalization method for differential expression analysis of RNA-seq data. *Genome Biology*, 11(3), R25.
- Rusch, D. B., Halpern, A. L., Sutton, G., Heidelberg, K. B., Williamson, S., Yooseph, S., Wu, D., Eisen, J. a, Hoffman, J. M., Remington, K., Beeson, K., Tran, B., Smith, H., Baden-Tillson, H., Stewart, C., Thorpe, J., Freeman, J., Andrews-Pfannkoch, C., Venter, J. C. E., ... Venter, J. C. E. (2007). The Sorcerer II global ocean sampling expedition: northwest Atlantic through eastern tropical Pacific. *PLoS Biology*, 5(3), e77.
<https://doi.org/10.1371/journal.pbio.0050077>
- Saier, M. H., Tam, R., Reizer, A., & Reizer, J. (1994). Two novel families of bacterial membrane proteins concerned with nodulation, cell division and transport. *Molecular Microbiology*, 11(5), 841–847.
<https://doi.org/10.1111/j.1365-2958.1994.tb00362.x>
- Saito, M. A., Goepfert, T. J., & Ritt, J. T. (2008). *Some thoughts on the concept of colimitation : Three definitions and the importance of bioavailability*. 53(1), 276–290.
- Shi, X. L., Lepère, C., Scanlan, D. J., & Vaultot, D. (2011). Plastid 16S rRNA gene diversity among eukaryotic picophytoplankton sorted by flow cytometry from the South Pacific Ocean. *PloS One*, 6(4), e18979.
<https://doi.org/10.1371/journal.pone.0018979>
- Smith, S. R., Gillard, J. T. F., Kustka, A. B., McCrow, J. P., Badger, J. H., Zheng, H., New, A. M., Dupont, C. L., Obata, T., Fernie, A. R., Allen, A. E., Martin, J., Fitzwater, S., Kolber, Z., Barber, K., Coale, S., Fitzwater, S., Greene, R., Johnson, K., ... Allen, A. A. E. (2016). Transcriptional Orchestration of the Global Cellular Response of a Model Pennate Diatom to Diel Light Cycling under Iron Limitation. *PLOS Genetics*, 12(12), e1006490.
<https://doi.org/10.1371/journal.pgen.1006490>
- Stanke, M., & Morgenstern, B. (2005). AUGUSTUS: a web server for gene prediction in eukaryotes that allows user-defined constraints. *Nucleic Acids Research*, 33(suppl_2), W465–W467.

- Stauber, J. L., & Florence, T. M. (1985). The influence of iron on copper toxicity to the marine diatom, *Nitzschia closterium* (Ehrenberg) W. Smith. *Aquatic Toxicology*, 6(4), 297–305.
- Strzepek, R F, & Price, N. M. (2000). Influence of irradiance and temperature on the iron content of the marine diatom *Thalassiosira weissflogii* (Bacillariophyceae). *Marine Ecology Progress Series*, 206, 107–117.
- Strzepek, Robert F., Hunter, K. A., Frew, R. D., Harrison, P. J., & Boyd, P. W. (2012). Iron-light interactions differ in Southern Ocean phytoplankton. *Limnology and Oceanography*, 57(4), 1182–1200. <https://doi.org/10.4319/lo.2012.57.4.1182>
- Strzepek, Robert F, Boyd, P. W., & Sunda, W. G. (2019). Photosynthetic adaptation to low iron, light, and temperature in Southern Ocean phytoplankton. *Proceedings of the National Academy of Sciences*, 116(10), 4388–4393.
- Sunda, W. G., & Huntsman, S. a. (1995). Iron uptake and growth limitation in oceanic and coastal phytoplankton. *Marine Chemistry*, 50(1–4), 189–206. [https://doi.org/10.1016/0304-4203\(95\)00035-P](https://doi.org/10.1016/0304-4203(95)00035-P)
- Sunda, W. G., & Huntsman, S. A. (1997). Interrelated influence of iron, light and cell size on marine phytoplankton growth. *Nature*, 390(1977), 389–392. <https://doi.org/10.1038/37093>
- Sunda, W. G., & Huntsman, S. A. (2011). Interactive effects of light and temperature on iron limitation in a marine diatom: Implications for marine productivity and carbon cycling. *Limnology and Oceanography*, 56(4), 1475–1488. <https://doi.org/10.4319/lo.2011.56.4.1475>
- Suzuki, K., Handa, N., Kiyosawa, H., & Ishizaka, J. (1997). Temporal and Spatial Distribution of Phytoplankton Pigments in the Central Pacific Ocean along 175°E during the Boreal Summers of 1992 and 1993. *Journal of Oceanography*, 53, 383–396.
- Takeda, S. (1998). Influence of iron availability on nutrient consumption ratio of diatoms in oceanic waters. *Nature*, 393(JUNE), 774–777. <https://doi.org/10.1038/31674>
- Timmermans, K. R., Van Der Wagt, B., Veldhuis, M. J. W., Maatman, a., & De Baar, H. J. W. (2005). Physiological responses of three species of marine pico-phytoplankton to ammonium, phosphate, iron and light limitation.

Journal of Sea Research, 53, 109–120.
<https://doi.org/10.1016/j.seares.2004.05.003>

- Tovar-Sanchez, A., Sañudo-Wilhelmy, S. A., Garcia-Vargas, M., Weaver, R. S., Popels, L. C., & Hutchins, D. A. (2003). A trace metal clean reagent to remove surface-bound iron from marine phytoplankton. *Marine Chemistry*, 82(1–2), 91–99.
- Turnšek, J., Brunson, J. K., Deerinck, T. J., Horák, A., Bielinski, V. A., & Allen, A. E. (2019). Phytotransferrin endocytosis mediates a direct cell surface-to-chloroplast iron trafficking axis in marine diatoms. *BioRxiv*, 1–93.
- Venrick, E. L. (1973). Deep maxima of photosynthetic chlorophyll in the Pacific Ocean. *Fish. Bull. US*, 71, 41–52.
- Villareal, T. A., Altabet, M. A., & Culver-Rymsza, K. (1993). Nitrogen transport by vertically migrating diatom mats in the North Pacific Ocean. *Nature*, 363(6431), 709–712.
- Warner, J. R. (1999). The economics of ribosome biosynthesis in yeast. *Trends in Biochemical Sciences*, 24(11), 437–440.
- Webb-Robertson, B.-J. M., Wiberg, H. K., Matzke, M. M., Brown, J. N., Wang, J., McDermott, J. E., Smith, R. D., Rodland, K. D., Metz, T. O., & Pounds, J. G. (2015). Review, evaluation, and discussion of the challenges of missing value imputation for mass spectrometry-based label-free global proteomics. *Journal of Proteome Research*, 14(5), 1993–2001.
- Worden, A. Z., Janouskovec, J., Mcrose, D., Engman, A., Welsh, R. M., Malfatti, S., Tringe, S. G., & Keeling, P. J. (2011). Global distribution of a wild alga revealed by targeted metagenomics. *CURBIO*, 22(17), R675–R677.
<https://doi.org/10.1016/j.cub.2012.07.054>
- Yang, L., Lu, S., Belardinelli, J., Huc-Claustre, E., Jones, V., Jackson, M., & Zgurskaya, H. I. (2014). RND transporters protect *Corynebacterium glutamicum* from antibiotics by assembling the outer membrane. *MicrobiologyOpen*, 3(4), 484–496. <https://doi.org/10.1002/mbo3.182>
- Zinser, E. R., Lindell, D., Johnson, Z. I., Futschik, M. E., Steglich, C., Coleman, M. L., Wright, M. A., Rector, T., Steen, R., & McNulty, N. (2009). Choreography of the transcriptome, photophysiology, and cell cycle of a minimal photoautotroph, *Prochlorococcus*. *PloS One*, 4(4), e5135.

Zones, J. M., Blaby, I. K., Merchant, S. S., & Umen, J. G. (2015). High-resolution profiling of a synchronized diurnal transcriptome from *Chlamydomonas reinhardtii* reveals continuous cell and metabolic differentiation. *The Plant Cell*, 27(10), 2743–2769.

**CHAPTER 3: Reduction-dependent siderophore assimilation in a model
pennate diatom**

3.1 ABSTRACT

Iron uptake by diatoms is a biochemical process with global biogeochemical implications. In large regions of the surface ocean diatoms are both responsible for the majority of primary production and frequently experiencing iron limitation of growth. The strategies used by these phytoplankton to extract iron from seawater constrain carbon flux into higher trophic levels and sequestration into sediments. In this study we use reverse genetic techniques to target putative iron acquisition genes in the model pennate diatom *Phaeodactylum tricornutum*. We describe components of a reduction-dependent siderophore acquisition pathway that relies on a bacterial derived receptor protein and provides a viable alternative to inorganic iron uptake under certain conditions. This form of iron uptake entails a close association between diatoms and siderophore producing organisms during low iron conditions. Homologs of these proteins are found distributed across diatom lineages suggesting the significance of siderophore utilization by diatoms in the marine environment. Evaluation of specific proteins enables us to confirm independent iron acquisition pathways in diatoms and characterize their preferred substrates. These findings refine our mechanistic understanding of the multiple iron uptake systems used by diatoms and help

us better predict the influence of iron speciation on taxa-specific iron bioavailability.

3.2 SIGNIFICANCE

Diatoms can access inorganic iron with remarkable efficiency, but this process is contingent on carbonate ion concentration. As ocean acidification reduces carbonate concentration, inorganic iron uptake may be discouraged in favor of carbonate-independent uptake. We report details of an iron assimilation process that needs no carbonate but requires exogenous compounds produced by co-occurring organisms. We show this process to be critical for diatom growth at high siderophore concentrations, but ineffective at acquiring iron from low affinity organic chelators or lithogenic particulates. Understanding the caveats associated with iron source preference in diatoms will help predict the impacts of climate change on microbial community structure in high nitrate low chlorophyll ecosystems.

3.3 INTRODUCTION

Chronic iron limitation of primary production shapes the ecology of large regions of the world's sunlit ocean and the physiology of its microbial inhabitants (Moore et al., 2004). Photoautotrophs are additionally burdened by the abundance of iron containing proteins present in the photosynthetic electron transport chain which increase the cellular iron requirement (Behrenfeld & Milligan, 2011). Among phytoplankton clades, diatoms are

disproportionally impacted by iron stress as they consist of large cells with larger iron quotas and relatively small surface area to volume ratios which can exacerbate diffusion limitation of nutrient uptake (Raven & Kübler, 2002). Still, diatoms frequently inhabit iron-depleted high nutrient low chlorophyll (HNLC) regions and respond strongly to iron addition (de Baar et al., 2005; David A. Hutchins & Bruland, 1998). Diatoms, like many eukaryotic phytoplankton, rely on phytoferritin (ISIP2a) proteins for the acquisition of uncomplexed iron (Fe') which is considered the most readily bioavailable iron species in seawater (Lis et al., 2014; McQuaid et al., 2018). Yet the vast majority of iron present in seawater is complexed by organic ligands originating from a variety of sources (Gledhill & Buck, 2012). Certain compounds common in dissolved organic matter such as humic/fulvic acids or extracellular polysaccharides function as iron chelating substances and are characterized by relatively low stability (Laglera & van den Berg, 2009). This results in sufficient dissociation to maintain iron concentrations at suitable levels for phytoferritin to operate. Other ligands (e.g. L1 type ligands, siderophores) have such high affinities for iron that very little Fe' exists at equilibrium (Rue & Bruland, 1995). In a situation where iron speciation is dominated by such ligands, organisms which have the tools to access this iron source directly are at a competitive advantage. Recent basin-scale spatial surveys of iron-binding ligand stability and concentration in seawater have revealed unexpected heterogeneity in ligand distributions, and iron

concentration itself is variable in time and space (Fitzsimmons et al., 2015; Mawji et al., 2015). Overall variation in the factors determining iron speciation results in different iron sources becoming more lucrative at different times, and thus diatoms have evolved multiple iron uptake strategies to capitalize on the heterogeneity of available iron substrates.

Siderophores are low molecular weight iron chelators with high affinity for Fe(III). Octahedral coordination of the metal ion is typically achieved by hydroxamate, catecholate, or α -hydroxy acid moieties (Butler & Theisen, 2010). Siderophores are produced by many types of bacteria and archaea, but production by eukaryotes is known only in fungi and higher plants (Hider & Kong, 2010). Marine siderophore production is attributed primarily to bacteria, and many different types of siderophores are produced (Vraspir & Butler, 2009). Amphiphilic siderophores such as marinobactins and aquachelins possess a hydrophobic fatty acid tail (J S Martinez et al., 2000) which could limit diffusion from the cell membrane and loss of these nitrogen-rich compounds to the environment (Xu et al., 2002). Some siderophores such as enterobactin are hydrophobic without tails (Braun & Braun, 2002). Many siderophores are tail-less and hydrophilic, and therefore more likely to diffuse into the milieu and interact with non-producing organisms.

Desferrioxamine b (DFOB) is a model trihydroxamate siderophore which has been used extensively in studies of marine iron limitation. It has been used

primarily for two purposes. FOB (iron-containing DFOB) can be used as a model iron source to study acquisition of organically complexed iron (e.g. Horstmann & Soria-Dengg, 1995; Maldonado & Price, 1999). Speciation of dissolved iron in marine environments is frequently dominated by strong iron binding ligands of unknown chemical identity but well characterized stability constants ($K_{FeL_1,Fe'}^{cond} > 10^{12}$), termed L₁ ligands (Gledhill & Buck, 2012). DFOB and L₁ exhibit a similar affinity for free Fe(III) (Maria T. Maldonado et al., 2005). DFOB is also known to be produced by marine bacteria (J. S. Martinez et al., 2001) and in recent studies which have conducted direct measurements of siderophores in seawater, DFOB has been detected in coastal eutrophic and offshore oligotrophic environments (Boiteau et al., 2016, 2018). Therefore, DFOB appears to be a reasonable option in assays or experimentation where an L₁ analog is needed. While results from these research efforts have generally characterized DFOB as a relatively low value iron source, with uptake rates roughly 1000 times slower than those for inorganic iron (Lis et al., 2014), it is rare for phytoplankton cultures or communities to be shown not to use DFOB at all as an iron source.

The second common use for DFOB is to artificially induce an iron limitation response in phytoplankton cultures or natural communities (e.g. Hutchins et al., 1999; Timmermans et al., 2005; Wells, 1999; Wells & Trick, 2004). This technique is effective as the high seawater conditional stability constant

of DFOB drives inorganic iron concentrations down to exceedingly low levels with only nanomolar additions of DFOB. EDTA in contrast has been used for similar purposes but requires micromolar additions to achieve similar Fe' concentrations. Even in seawater with an abundance of siderophore production, L1 concentrations rarely exceed 5 nM, therefore small (<10 nM) DFOB additions to natural seawater dramatically increase the L1 concentration and sequester iron in the refractory side of the dissolved iron bioavailability spectrum. Moreover, a large excess of siderophore beyond the dissolved iron concentration can competitively inhibit iron acquisition by uptake strategies that cannot differentiate between iron-containing and deferrated siderophores (Hoegy et al., 2005; Schalk et al., 2004). It can be the case in certain situations that iron bound to DFOB represents a more accessible iron source than in situ dissolved ligands to certain phytoplankton taxa, or that added DFOB could scavenge iron from particles or colloids and bolster the soluble iron pool (Kraemer, 2004; Leventhal et al., 2019). Additionally, DFOB may enter cells during the iron uptake process and disrupt intracellular iron binding kinetics. The potential for unexpected effects which may even have the opposite of the intended result means that DFOB must be used with caution in culture experiments.

Siderophore utilization can be defined as the process of using siderophore-bound iron to satisfy cellular iron requirements. This requires that

the organism facilitates dissociation of the siderophore-iron complex and internalizes the iron. These steps can happen in either order, and both types of mechanistic sequences have been characterized. Bacteria utilize siderophore binding proteins to facilitate transport of iron-siderophore complexes to the cytoplasm. These proteins are dissolved in the periplasm of Gram-negative bacteria (Krewulak & Vogel, 2008), and in Gram-positive bacteria they are tethered to the cytoplasmic membrane by a posttranslationally lipidated N-terminus (Sutcliffe & Russell, 1995). These siderophore binding proteins deliver siderophore-iron complexes to ABC transporters which internalize the complex. Once inside the cell, siderophore interacting proteins (SIPs) reduce the siderophore complex leading to the release of Fe(II) (M. Miethke & Marahiel, 2007). Eukaryotes, on the other hand, can utilize outer membrane ferric reductases which perform the reduction step extracellularly. The generated Fe(II) is then transported into the cell via specific ferrous iron transporters (e.g. ZIP or NRAMP proteins) or reoxidized by a copper-dependent ferroxidase and transported as Fe(III) through an iron permease (Blaby-Haas & Merchant, 2012b; E. Lesuisse & Labbe, 1989). Ferric reductase proteins were first extensively studied in yeast and higher plants and some have been characterized as iron uptake proteins (Zhang et al., 2013). These genes were then observed to be widespread across eukaryotic phytoplankton (Blaby-Haas & Merchant, 2012b), though limited genetic tractability of most marine phytoplankton has prevented the definitive

classification of these reductases as assimilatory. Closely related ferric reductases could mediate different functions such as generation of superoxide (Diaz et al., 2019; Suzuki et al., 2011; Zhang et al., 2013) or facilitation of intracellular metal trafficking (Jeong et al., 2008; Singh et al., 2007). Extracellular iron reduction has been examined in diatoms growing on organically complexed iron, and is thought to be an important strategy for converting refractory ferric chelates into inorganic iron species of higher bioavailability (M. T. Maldonado & Price, 2001; M T Maldonado & Price, 1999; Maria T. Maldonado et al., 2006). Few of the proteins involved in diatom iron acquisition have been identified, and several studies have suggested that diatoms possess multiple independent iron uptake mechanisms (Kazamia et al., 2018; Kustka et al., 2007; McQuaid et al., 2018).

No diatom species has been subjected to as intensive transcriptomic profiling under low iron conditions as *Phaeodactylum tricornutum*. Previous work includes an initial comparison of high and low iron transcriptomes in 2008, and an exhaustive timecourse of transcriptomes over the light/dark cycles at multiple iron concentrations published in 2016 (Allen et al., 2008; Smith et al., 2016). More recently, the function of ISIP2a as a carbonate-dependent phytotransferrin which is responsible for high affinity ferric iron uptake in diatoms was confirmed in the *P. tricornutum* model system (McQuaid et al., 2018). Studies of other diatoms have revealed a common

core of low iron expressed genes in diatoms including flavodoxin, ISIPs, class I fructose-bisphosphate aldolases, copper dependent oxidases, ferric reductases and permeases (Cohen et al., 2018; Lommer et al., 2012; Mock et al., 2008). Many iron sensitive genes identified in *P. tricornutum* cultures have been also observed in metatranscriptomes of naturally occurring iron-limited diatom communities (Chappell et al., 2014; Marchetti et al., 2012). While some variation exists in the iron metabolism genes present in available diatom genomes, the subset found in *P. tricornutum* is typical of many members of the Bacillariophyceae (Groussman et al., 2015). *P. tricornutum* was chosen for these studies because of its low iron tolerance which is similar to the native diatom inhabitants of HNLC regions (Kustka et al., 2007). Additionally, *P. tricornutum* has a high-quality published genome which facilitates robust transcriptome annotation (Bowler et al., 2008). *P. tricornutum* is genetically tractable which allows gene targets identified in transcriptomic datasets to be efficiently investigated in their native organism using modern biological techniques such as gene knockouts and fusion proteins (Karas et al., 2015; Nymark et al., 2016). After a long history of culturing and experimentation, *P. tricornutum* has emerged as the principal diatom model organism, especially when investigating iron limitation of marine primary production.

One intriguing observation noted from previous low iron *P. tricornutum* culture experiments was the upregulation of a cluster of putative iron uptake

genes, FRE2 and FBP1 (Allen et al., 2008; Kustka et al., 2007). FRE2 is well annotated as a NADPH oxidase type ferric reductase, which in yeast are responsible for siderophore iron acquisition (Yun et al., 2001). This protein contains a ferric reductase transmembrane domain with FAD and NADPH binding domains on the cytosolic side which is typical of the ferric reductase domain superfamily (Zhang et al., 2013). FBP1 shows structural homology to receptor proteins such as FhuD and DesE found in bacteria which bind hydroxamate siderophores (Coulton et al., 1987; Roberts et al., 2012). FRE2 and FBP1 occur in a divergent orientation with ~1.5 kb between them and although their transcript abundance is consistently lower than canonical diatom iron stress biomarkers (e.g. flavodoxin and ISIP genes), expression of both are correlated and significantly sensitive to iron concentration (Allen et al., 2008; Yoshinaga et al., 2014). FBP1 was the first putative siderophore receptor identified in a diatom, and after its discovery the FRE2/FBP1 gene cluster was hypothesized to be involved in siderophore utilization (Allen et al., 2008).

In this study we characterize components of a diatom ferri-siderophore acquisition system using a reverse genetics approach in *P. tricornutum*. This iron uptake strategy relies on a eukaryotic ferric reductase protein which is coupled to a siderophore binding protein of possible bacterial origin and represents a convergence of two characterized uptake paradigms. We

examined the subcellular location of these proteins with fluorescent fusion proteins and used CRISPR/Cas9 technology to create knockout cell lines for genes of interest. FBP1 knockouts were complemented by reintroduction of the native FBP1 gene and also with a homolog from the marine actinomycete *Salinispora tropica*. Both proteins are required for growth in the presence of as little as 2 nM DFOB. Homologs of both proteins are also present in the genomes of other diatoms. We characterized the specificity of this uptake system using purified siderophore standards and challenged diatom cell lines with a panel of iron sources typical of marine environments. We demonstrate this mode of iron uptake to be distinct from phytoferritin-mediated Fe' uptake and contrast these two systems in scenarios designed to shed light on their roles in the marine biogeochemical cycling of iron.

3.4 MATERIALS AND METHODS

3.4.1 Gene knockouts, fusion proteins, and complementation

All cell lines used in this study were created from *P. tricornutum* strain CCMP 632 (Bowler et al., 2008). FBP1, FRE1 and FRE2 were disrupted in the *P. tricornutum* genome using CRISPR/Cas9 technology (Moosburner et al., 2020). Constructs containing the Cas9 endonuclease gene, guide RNAs for the target gene, and the ShBle marker for phleomycin resistance were introduced into *P. tricornutum* cells via bacterial conjugation (Karas et al., 2015) or particle bombardment (Falciatore et al., 1999). Cells were spread on selective

plates (phleomycin 100 ug/mL) until colonies appeared, then picked and screened by PCR to verify ShBle insertion or Sanger sequencing of the endonuclease cut site to detect small insertions or deletions. ISIP2a was disrupted as described previously (McQuaid et al., 2018) using TALEN technology (Weyman et al., 2015), but with a ShBle marker instead of nourseothricin resistance. Details of each cell line are described in Table 3.1.

FBP1-mCherry and FRE2-YFP fusions were placed under control of promoter/terminator pairs derived from *P. tricornutum* flavodoxin and phytotransferrin, respectively. Native promoters yielded insufficient fluorescence for localization and prompted the need for strong iron-sensitive promoters (Yoshinaga et al., 2014), and different promoter/terminator pairs were used to facilitate plasmid construction. All components were assembled using Gibson cloning into a pPTPBR11 cargo plasmid containing the ShBle marker (Diner et al., 2016), and transferred into *P. tricornutum* cells from EPI300 *E. coli* cells containing the pTA-MOB conjugation vector (Karas et al., 2015). After selection, cells were grown in low iron Aquil to induce expression and imaged using a Leica SP5 confocal microscope with a 100x oil immersion objective. YFP emission was collected from 520-550 nm, mCherry from 580-620, and chlorophyll from 675-720, all excited with a 514 nm laser.

Δ FBP1 cells were complemented with native the FBP1 gene including flanking upstream and downstream regions and a NAT resistance cassette

conferring nourseothricin resistance. Δ FBP1 cells were also complemented with the DesE gene which was amplified from *Salinispora tropica* CNB-440, fused to the FBP1 N' signal peptide and C' transmembrane anchor, and placed under control of the FBP1 promoter and terminator. Both constructs were delivered to Δ FBP1 cells via particle bombardment and selected on antibiotic plates containing 200 ug/mL nourseothricin and 100 ug/mL phleomycin. Complemented cell lines were grown alongside WT and Δ FBP1 cultures in Aquil media with 100 nM DFOB, 10 nM Fe and 100 μ M EDTA at 150 μ mol quanta $m^{-2} s^{-1}$ on a 12:12 light/dark cycle and maintained at 18° C.

3.4.2 Low iron culturing

All labware used in growth or uptake assays consisted of polycarbonate bottles which were treated first with an acidic detergent (Citranox®) for one day. Subsequently, bottles were acid cleaned with 1N trace metal grade HCl for one week minimum. All media preparation and culturing was conducted using sterile trace metal clean techniques. Aquil synthetic seawater media was prepared using trace metal grade salts and passed through a column containing Chelex 100 beads (Bio-Rad Laboratories) to remove contaminating iron. Background iron concentration in media prior to the Chelex treatment was measured at greater than 20 nM using a sulfite reduction luminol chemiluminescence flow injection method (A. L. King & Barbeau, 2011). After Chelex, media iron concentration was 0.26 nM.

Aquil media was microwave sterilized. Nutrient stocks (nitrate, phosphate and silicic acid) were prepared using trace metal grade salts, passed over Chelex resin, and filter sterilized. Trace metals other than iron were added to media in an EDTA solution prepared using only trace metal grade reagents. Media pH was adjusted to 8.2 using trace metal grade NaOH. Final media contained 880 μM NO_3 , 36 μM PO_4 , 100 nM Zn, 48 nM Mn, 40 nM Co, 40 nM Cu, 10 nM Se, 100 nM Ni with 100 μM EDTA.

Natural low-iron seawater media was prepared using seawater collected from Station ALOHA during a November 2015 cruise. Surface water was pumped through a 0.2 μm cartridge filter into LDPE carboys using a PTFE diaphragm pump. All sampling gear was acid cleaned and rinsed with clean seawater. ALOHA media was microwave sterilized, amended with Chelex-treated nutrients (NO_3 , PO_4), vitamins, and trace metals (without EDTA). Iron concentrations in this seawater was measured at 0.858 ± 0.039 nM before additions.

3.4.3 Iron speciation calculations

Average free iron (Fe') was calculated in Aquil media with EDTA according to Sunda et al. 2005 (W. G. Sunda et al., 2005) based on media pH, total iron concentration, temperature, light intensity, photoperiod and EDTA concentration. In media containing both EDTA and desferrioxamine b, Fe'

was estimated using $K_{FOB,Fe'}^{cond} = 10^{11.8}$ (Maria T. Maldonado et al., 2005) by the equation:

$$Fe' = \frac{[Fe_{total}]}{K_{FOB,Fe'}^{cond}[DFOB] + K_{FeEDTA,Fe'}^{cond}[EDTA]}$$

3.4.4 Growth rates

Growth rates for *P. tricornutum* cultures grown on a variety of iron sources were determined using *in vivo* fluorescence measured with a Turner 10-AU fluorometer. Cultures were pre-cultured for 2 weeks in low-iron ALOHA seawater with 0.5 nM added Fe, after which triplicate cultures were inoculated in 30 mL polycarbonate vials containing ALOHA seawater with various iron sources. Cultures were grown under constant illumination at 150 $\mu\text{mol quanta m}^{-2} \text{s}^{-1}$ and maintained at 18° C. RFU was monitored daily and growth rates calculated when cells entered exponential phase by linear regression of $\ln(\text{RFU})$ over time.

3.4.5 Benthic boundary layer

Seawater from the particle rich nepheloid layer was collected during a 2018 cruise to a central California upwelling zone aboard the *R/V Sally Ride*. The BBL above the continental shelf offshore of Morro Bay was identified via a beam transmissometer deployed on a CTD. Trace metal clean GO-Flo™ (General Oceanics) bottles were subsequently deployed to collect this seawater which was frozen whole and transported to the shore lab for

experimentation. Portions of BBL water were filtered through acid cleaned 0.4 μm polycarbonate track etched filters using a Teflon filter rig. Filters with associated particles were then added to an equivalent volume of low iron Stn ALOHA seawater. In growth rate experiments, whole BBL water, filtered BBL water, and particle enriched ALOHA water were added to low iron Stn ALOHA water to a final concentration of 10%. Antibiotics gentamycin, tetracyclin and ampicillin were added at a concentration of 1 mg/L each to all BBL media to control bacteria growth. 2 nM FeCl_3 , 2 nM DFOB, and no iron added controls were included. A humic acid reference material (Suwannee River Humic Acid, SRHA) was also tested at a final media concentration of 0.12 mg/L which corresponds to ~ 2 nM Fe (Laglera & van den Berg, 2009).

3.4.6 *Iron uptake assays*

Iron uptake was assayed in short term uptake experiments lasting no more than 2.5 hours. ^{59}Fe was loaded into various iron chelating substances, and then equilibrated in Aquil media at 10x final assay concentration overnight. At the onset of the experiment, 10% ^{59}Fe containing media was added to cell cultures. Cell concentrations were limited to less than 2×10^5 cells/mL, and cells were assayed during the early exponential phase of growth. Uptake cultures were kept in low light for the duration of the assay.

3.4.7 *Ga siderophore analogs*

Gallium siderophores can be prepared in the same manner as iron siderophores (Muller & Raymond, 1984). GaCl_3 was equilibrated with a 25% excess of DFOB or EDTA for 8 hours in 0.001 N HCl, which was then diluted into pH 8 Aquil seawater to 100 nM gallium and left to equilibrate overnight. Uptake experiments were conducted in a fashion similar to ^{59}Fe uptake assays, not exceeding 2 hours. At the beginning of uptake experiments, gallium containing media was added to diatom cultures to a final gallium concentration of 10 nM. Cells were harvested via filtration onto acid cleaned polycarbonate track etched filters and rinsed with an oxalate EDTA solution to remove extracellular metals (Tovar-Sanchez et al., 2003). Filters were transferred to acid cleaned polypropylene vials and digested using 1N Optima grade nitric acid with a 10 ppb Rh internal standard for 1 month at room temperature, similar to Hawco and Saito 2018 (Hawco & Saito, 2018). Gallium was detected in cell digests using a magnetic sector inductively coupled plasma mass spectrometer at the UC Santa Cruz Institute of Marine Sciences. Gallium uptake rates and standard deviations from 10 nM GaEDTA substrates were 0.0132 ± 0.0012 , 0.0110 ± 0.0019 and 0.0068 ± 0.0014 amol cell⁻¹ hr⁻¹ for WT, ΔFBP1 and ΔFRE2 cell lines, respectively.

3.4.8 Ferric reductase activity

Ferric reductase activity was measured in cells grown in Aquil medium with either 30 pM or 400 pM total added Fe. Cells were concentrated by

centrifugation, rinsed and resuspended in Aquil without EDTA or added metals, and then incubated with 600 μ M bathophenanthrolinedisulphonic acid (BPDS) and 200 μ M Fe chelated with N-hydroxyethyl ethylenediamine triacetic acid (Eckhardt & Buckhout, 1998). After 10 minutes, samples were centrifuged again and absorbance of the supernatant was measured at 535 nm using a Beckman Coulter DU 800 spectrophotometer.

3.4.9 Phylogenetics

Homologs of FRE2 and FBP1 were identified using blast search using NCBI nr and MMETSP databases (Keeling et al., 2014; Pruitt et al., 2006). Sequences were aligned using local-pair algorithm as implemented in MAFFT (Kato & Standley, 2013). For FBP1, this preliminary alignment was used to create HMM profile and we then used HMMER3 (Eddy, 2011) on both datasets for more sensitive search of FBP1 homologs. Finalized datasets were aligned using MAFFT under the conditions described above. Hyper variable and poorly aligned region were identified by eye and manually removed in SeaView 4 (Gouy et al., 2009). Bayesian trees with posterior probabilities were constructed using Phylobayes 4 (Lartillot et al., 2009) under the LG+C40 model for both datasets with two independent MCMC chains run until reaching convergence (i.e. the maximum observed discrepancy was lower than 0.1 and effective sample size of model parameters was at least 100). Alternatively, the highest scoring maximum likelihood topology for both genes

was inferred using IQTree (Nguyen et al., 2015) under the best-fitting model selected using built-in model finder. Branching support was assessed using thorough non-parametric analysis from 500 replicates. Siderophore binding annotations were derived from publicly available databases including National Center for Biotechnology Information (<https://www.ncbi.nlm.nih.gov/>) and Ensembl Genomes (Kersey et al., 2018), unannotated sequences were analyzed using PANNZER2 (Törönen et al., 2018), and peptide sequences were modeled using Phyre2 normal mode and top three templates were considered (Kelly et al., 2015).

3.5 RESULTS

3.5.1 Knockout growth curves

Aquil synthetic seawater enables careful and reproducible manipulation of iron speciation at the low concentrations typical of open ocean environments (Price et al., 1989). Wild type and knockout (Δ FBP1 and Δ FRE2) *P. tricornutum* cells were grown in low iron Aquil medium with either Fe' or FOB as an iron source. Aquil medium at pH 8.2, 18°C and with 100 μ M EDTA and 10 nM total Fe has at equilibrium \sim 16 pM Fe', and the remaining iron bound to EDTA is not bioavailable (W. Sunda & Huntsman, 2003). In this medium WT and knockout cell lines all grow indicating sufficient Fe' to sustain growth and no obvious role of either protein (Figure 3.1A). Addition of 100 nM

DFOB to this same medium results in a decrease in Fe' to ~0.174 pM which is negligible in terms of supporting phytoplankton growth (see 3.4.3 for Fe' calculations). Importantly, when DFOB is added to this media a new pool of ligand-bound iron (FOB) far exceeds the concentration of any other iron species in solution at ~10 nM. If cells can utilize FOB at even a small fraction of the efficiency with which they use Fe', growth rates in this medium could exceed rates in identical medium without the DFOB addition. WT cells showed this response, demonstrating the ability to directly use FOB as an iron source though not as efficiently as Fe' (Figure 3.1B). If diatoms could grow at the observed rates in low iron Aquil with 100nM added DFOB by solely utilizing Fe', iron would never limit marine primary productivity and the Iron Hypothesis would need to be reconsidered. Both the Δ FBP1 and Δ FRE2 lines in contrast failed to grow when DFOB was added, indicating that Fe' present could not sustain growth in *P. tricornutum*, and that both these proteins are integral in assimilating FOB as an iron source (Figure 3.1B). This phenotype was replicated in duplicate knockout cell lines for both FBP1 and FRE2 which differed in genotype but all lacked a functional copy of the target gene (Table 3.1). Utilization of FOB was restored in Δ FBP1 by complementation with the native gene, and also with the DesE gene from *Salinispora tropica*, a marine Actinobacteria known to produce and utilize DFOB (Figure 3.2A) (Roberts et al., 2012).

3.5.2 Localizations

P. tricornutum cells expressing FBP1-mCherry and FRE2-YFP fluorescent fusion proteins were imaged under low iron conditions in order to determine the subcellular locations of both proteins simultaneously. While FBP1 showed a clear signal at the periphery of the cell, FRE2 was associated with the outer membrane but less specifically and each differed in their intracellular distribution (Figure 3.2B). FBP1 was observed in a small compartment near the plastid, a location which recent studies have implicated in intracellular iron trafficking and may represent the periplastidal compartment (Kazamia et al., 2018; McQuaid et al., 2018). FRE2 was absent from this location but was weakly present on other internal membranes. Expression at the cell surface further implicates both proteins in uptake processes. In yeast, some siderophore receptors are embedded in the cell wall and facilitate transport to plasma membrane localized reductases (Philpott & Protchenko, 2008), and we cannot rule out a similar configuration here.

3.5.3 Iron uptake rates

Uptake of model iron sources was evaluated using short term ^{59}Fe uptake assays. ISIP2a (phytotransferrin) was confirmed as essential for inorganic Fe' uptake (Figure 3A). Uptake rate data demonstrate that FBP1 and FRE2 are responsible for the majority of uptake from the tri-hydroxamate siderophore iron sources ferrioxamine b and ferrichrome (Figure 3B and 3D).

Aerobactin, a di-hydroxamate siderophore with an α -hydroxy acid, was accessed by FBP1 and FRE2 but overall uptake rates were slow. (Figure 3E). Uptake from the di-hydroxamate siderophore rhodotorulic acid was unaffected by disruption of any of the proteins in question (Figure 3C). Uptake from the catecholate siderophore enterobactin was not detected in any cultures (Figure 3.4). Fe' concentrations in all siderophore uptake assays was negligible due to excess siderophore and EDTA present in the uptake medium.

3.5.4 Growth rates in natural seawater

In natural oligotrophic seawater amended with nutrients but without EDTA or iron, all cell lines struggled to grow (Figure 3.5A). Added inorganic iron restored growth in all but the Δ ISIP2a line (Figure 3.5B), and added DFOB restored growth in WT and Δ ISIP2a while arresting growth in Δ FBP1 and Δ FRE2 (Figure 3.5C). Δ ISIP2a achieved a faster growth rate than WT after DFOB addition possibly due to upregulation of the siderophore acquisition pathway in lieu of phytoferritin.

The benthic boundary layer (BBL) of coastal California constitutes a reservoir of bioavailable iron that fortifies new production in this eastern boundary current upwelling system (Johnson et al., 1999). Iron in the BBL exists primarily in the particulate phase, but dissolved concentrations are also elevated (Biller et al., 2013). This complex mixture of naturally occurring and

environmentally relevant iron sources was used to challenge *P. tricornutum* cells.

Filtered BBL water, unfiltered whole BBL water, and resuspended BBL particles were all able to relieve iron stress experienced by diatoms growing in low iron seawater (Figure 3.5). Results indicate that dissolved iron sources in the BBL are not acquired via the FBP1 receptor or the FRE2 reductase (Figure 3.5e and 4f). Instead, dissolved iron in this seawater appeared to be internalized by the ISIP2a protein as Fe³⁺. Particulate iron was much less bioavailable than dissolved iron, and utilization was not attributable to a single uptake system (Figure 3.5G). A commonly used humic acid reference material (Suwannee River Humic Acid, SRHA) was also tested and appeared to provide iron which was assimilated via ISIP2a (Figure 3.5D).

3.5.5 Gallium uptake rates

When gallium siderophores were supplied to *P. tricornutum* cultures at a concentration of 10 nM, WT cells achieved uptake rates of 0.284 amol Ga cell⁻¹ hr⁻¹ (Figure 3.6A). Similarly, Δ FRE2 cells attained rates of 0.303 amol Ga cell⁻¹ hr⁻¹, while the Δ FBP1 uptake rate was suppressed to 0.077 amol Ga cell⁻¹ hr⁻¹. Gallium complexed to EDTA resulted in very little uptake in all cell lines (<0.014 amol Ga cell⁻¹ hr⁻¹), indicating that the gallium siderophore uptake rates cannot be explained by Ga³⁺ or GaEDTA uptake. When FOB is supplied to cells at this same high concentration, WT uptake rates of 0.992 amol Fe cell⁻¹

$^1 \text{ hr}^{-1}$ exceed the Ga uptake rate by 3-fold (Figure 3.6A). Unlike iron, gallium is inert to reduction and therefore these results demonstrate the effect of removing the reductive step from the siderophore assimilation process, either by editing the reductase gene or by modifying the substrate. Both methodologies achieve the same degree of uptake rate impairment.

3.5.6 Ferric reductase activity

Extracellular ferric reductase activity measured in iron-deplete *P. tricornutum* cells far exceeded activity from replete cells using the BPDS method (Figure 3.6B) as has previously been reported (Allen et al., 2008; Eckhardt & Buckhout, 1998). This result was similar in all cell lines assayed, indicating no role of either FBP1 or FRE2 in this process.

3.5.7 Phylogenetic analysis

Our phylogenetic survey of FBP1 revealed homologs in both centric and pennate diatom lineages, haptophytes and dinoflagellates (Figure 3.7). These proteins share a common ancestor with hydroxamate siderophore lipoprotein receptors found in Gram-positive bacteria. The FBP1 homologs from Actinobacteria recovered in our search are all annotated as iron siderophore ABC transporter solute binding proteins, and 7 out of 9 are further annotated as hydroxamate siderophore binding which gives us confidence that our hidden Markov model (HMM) is specific for this function. 10 of the eukaryotic homologs are annotated as siderophore binding proteins, and the

remaining 37 are hypothetical proteins with no ascribed function. All but 5 of these peptides were predicted to be structurally similar to ferri-siderophore binding receptors. After arriving in eukaryotes this protein passed through at least two duplication events, and some paralogs were lost. *P. tricornutum* retains only a single copy, while the centric diatom *Thalassiosira oceanica* has three paralogs, the Antarctic pennate *Fragilariopsis cylindrus* has four, and *F. kerguelensis* has two (Figure 3.8). *T. oceanica*, *F. kerguelensis*, *Eucampia antarctica*, and *Phaeocystis antarctica* all contain FBP1 homologs and have been confirmed to utilize FOB as an iron source (Strzepek et al., 2011). *Proboscia alata* contains five homologs and a closely related species, *P. inermis*, also uses FOB (Strzepek et al., 2011).

NADPH oxidase type ferric reductases are ubiquitous proteins, again originating from a series of gene duplications, and as such FRE2 homologs are much more widespread across diatoms (Figure 3.9). It is unlikely that all these proteins share the function of FRE2 in *P. tricornutum*, especially if a compatible receptor is absent. Our search for FRE2 homologs returned FRE1 and FRE5 from *P. tricornutum*, which are unable to substitute for FRE2 in our siderophore assimilation experiments and highlights the difficulty in determining the physiological roles of ferric reductase proteins from peptide sequence. FRE2 homologs were also detected in other algal groups and eukaryotes, but again this is probably not evidence of siderophore utilization given the diverse

cellular processes in which these proteins have been implicated (Blaby-Haas & Merchant, 2012a; Jeong et al., 2008; Singh et al., 2007; Suzuki et al., 2011; Zhang et al., 2013). We found homologs also in cyanobacteria which are, however, evolutionarily not directly related to the investigated enzyme from diatoms. The occurrence of ferric reductase genes in cyanobacteria has been previously reported and attributed to lateral transfer from eukaryotes (Zhang et al., 2013). FRE genes in diatoms thus originate from a eukaryotic ancestor and not from cyanobacteria or the plastid.

3.6 DISCUSSION

3.6.1 Advantages of direct siderophore uptake

Iron has long been known as a keystone element exerting pronounced bottom-up influence on marine ecosystems in spite of its low concentration (Cooper, 1935). Yet it took many decades of advancement in analytical technique and sampling methods before reliable measurements of dissolved iron were possible (Bruland & Franks, 1983; Gordon et al., 1982), and even more before these measurements were widespread (Mawji et al., 2015). Our understanding of the speciation of dissolved iron in seawater has been informed primarily by electrochemical measurements of iron ligands (Gledhill & Buck, 2012). These measurements reveal the ubiquitous presence of iron binding substances in seawater which exceed the concentration of inorganic iron. Inorganic dissolved iron (Fe^3+) is the substrate preferred by eukaryotic

phytoplankton to satisfy their demand for this essential nutrient metal (Lis et al., 2014; Shaked & Lis, 2012). Fe' has been shown to be exceedingly bioavailable and represents one extreme in the spectrum of iron sources present in the oceans. Fe' is, however, vanishingly scarce due to low solubility but also as a result of organic ligands. The presence of iron-binding ligands in seawater results in higher overall dissolved iron concentrations by preventing hydrolysis and precipitation but can simultaneously decrease inorganic iron concentrations through complexation. These factors tip the scale towards organic iron serving as a valuable alternative iron source in certain circumstances.

Organic iron is not a single substrate and individual uptake proteins are generally specific only to a limited subset of organic compounds. Therefore, the repertoire of iron acquisition machinery possessed by an organism must be compatible with the local environmental iron speciation for cellular quotas to be fulfilled and nutrient limitation avoided. Weak ligands are a poor target for receptor proteins as they are a heterogeneous pool of substrates and are less likely to be populated by iron ions when iron concentrations are low and strong ligands are present. Non-specific, extracellular reduction may be a better strategy for accessing weakly complexed iron. Siderophores are much better suited to uptake by specific receptors. Certain bacteria utilize high specificity siderophore receptors which bind to the siderophore's iron

coordinating ligands (Patel et al., 2010). Lower affinity generalist siderophore receptors which select for Fe(III) are also known in Gram-negative bacteria (Stintzi et al., 2000).

Given that eukaryotic phytoplankton are not known to synthesize siderophores themselves, compounds which are loosely coupled to the producing organism would likely be more bioavailable. Amphiphilic siderophores contain hydrophobic tails which tether them to cell membranes, mitigate diffusive loss to the environment, and potentially decrease their utility to eukaryotic phytoplankton (Jennifer S Martinez & Butler, 2007). Hydrophilic siderophores such as DFOB are more likely to diffuse away from their bacterial sources and become available to any organism with the appropriate uptake mechanism. In *P. tricornutum*, FBP1 apparently facilitates the initial uptake process but reduction and liberation of the iron ion must follow for assimilation to occur. In bacteria, reduction of DFOB is carried out by a variety of enzymes including SIPs and non-specific reductases. SIPs are unrelated to eukaryotic ferric reductases yet can accomplish the same reductive step likely performed by FRE2 and in certain bacterial genomes the DesF SIP is adjacent to the DesE receptor (Marcus Miethke et al., 2011; Roberts et al., 2012).

3.6.2 Reduction matters

This study investigates the role of specific ferric reductases in the iron uptake and assimilation process of diatoms. Others have measured increased

generation of Fe(II) by iron-limited diatoms and suggested the involvement of reductase proteins (Anderson & Morel, 1980; Jones et al., 1987; M. T. Maldonado & Price, 2001; Shaked et al., 2004). Diatom ferric reductase transcription has also been correlated with low cellular iron quotas (Kustka et al., 2007), but a definitive link between these proteins and iron uptake has remained elusive. Our results indicate FRE2 is critical for uptake and assimilation of iron from siderophore substrates, and our uptake rate data show that FRE2 is also important to the actual uptake step. Trivalent metal cations other than Fe(III) can form useful high stability complexes with siderophores. Cr(III) and Ga(III) have been loaded into siderophores and used to study the processes that bacteria use to facilitate release of iron from siderophores (Stintzi et al., 2000). These analogs have been shown to be taken up at rates comparable to ferric siderophores when no reductive step is involved (Muller & Raymond, 1984). Uptake rates of gallium siderophores plummet if reduction is critical to the uptake process, as gallium has no stable divalent state. Cr(III) can be reduced to Cr(II), but due to a much lower reduction potential than Fe(III), ferric reductase proteins are unable to effect this transition. In addition to being effectively inert to reduction, chromic siderophores do not participate in ligand exchange (Muller & Raymond, 1984). These important differences from ferric siderophores empower these substrates to rule out specific processes. Due to the high affinity of siderophores for Ga(III), this metal has also been used to label siderophores for

detection in seawater (McCormack et al., 2003). Chromium was not used in this study due to the ubiquity of contaminating chromium in polycarbonate filters. Gallium in contrast was detectable via ICP-MS due to low blanks. The gallium uptake experiments further demonstrate that the role of FRE2 is indeed that of a reductase and without reduction, uptake of siderophore-bound metals is inhibited (Figure 3.6A).

Here we confirm the involvement of one diatom cell surface reductase protein in organic iron assimilation, but reduction of inorganic iron and certain organic chelators occurs independently of this protein. Our Δ FRE2 cells exhibited comparable extracellular ferric reductase activity to wild type in BPDS assays which reflects the specificity of FRE proteins in diatoms. Multiple iron-responsive ferric reductase proteins in the *P. tricornutum* genome could account for this finding (Allen et al., 2008; Smith et al., 2016), although none are able to substitute for FRE2 in certain siderophore acquisition processes. Of the five annotated ferric reductases in *P. tricornutum*, expression of FRE1, 2 and 3 are significantly sensitive to iron starvation (Smith et al., 2016) (Table 3.2). FRE1, 2 and 5 are NADPH oxidase type reductases with a ferric reductase transmembrane domain, and NAD and FAD binding motifs. These proteins could be involved in superoxide generation but only FRE1 has all four putative molecular oxygen binding residues found in the human NOX2 protein (Zhang et al., 2013) (Figure 3.10). FRE 3 and 4 are cytochrome b_{561} type ferric

reductases which also could reduce ferric chelates (McKie et al., 2001), but only FRE2 and FRE3 show evidence of outer membrane localization (Table 3.2). FRE1 knockouts tend to grow slower than WT in low iron EDTA or FOB media (Figure 3.11), but normal uptake of both substrates was observed (Figure 3.12). Therefore, we propose that FRE1 is the best candidate for a regulatory ferric reductase involved in coordinating the cell's response to low iron through reactive oxygen species generation or balancing cellular redox by adjusting the oxidation state of the NADP⁺/NADPH pool (Diaz et al., 2019), while FRE3 alongside FRE2 could be participating in reductive iron uptake with a difference in substrate preference. The exact location of reduction is uncertain as endocytosis could internalize membrane proteins prior to the reductive step. If phytoferritin, like transferrin requires a ferric reductase to facilitate iron uptake (Ohgami et al., 2005), FRE3 could serve this role although an iron sensitive CREG protein is also hypothesized to perform this function (Turnšek et al., 2019). Recent studies have confirmed endocytosis to be required for acquisition of both inorganic and organic iron (Kazamia et al., 2018; McQuaid et al., 2018), and binding Fe(III) at the cell surface has no impact on Fe²⁺ or FOB uptake rates (Figure 3.13). It is possible that reduction of ferric chelates occurs in multiple locations depending on the stability or identity of the complex, as has been previously proposed (Horstmann & Soria-Dengg, 1995). Weaker ligands could be reduced at the cell surface by generalist reductases and the resultant inorganic iron transported via

phytotransferrin or ferrous iron importers (Figure 3.14). Refractory complexes such as FOB could be bound by specific receptors and internalized to a specialized iron processing vesicle (ferrosome). If the timescale of vesicle endocytosis and recycling back to the membrane is fast enough, uptake assays may not distinguish this process from conventional transporter mediated uptake. The kinetics of diatom iron acquisition vesicles are unknown, but studies of transferrin kinetics have revealed recycling timescales of around 15 minutes (Ciechanover et al., 1983) which could be too fast to detect with traditional short-term uptake assays. Disruption of the assimilation process by preventing siderophore reduction could result in release of ferric siderophores back into the medium or irreversible blocking of uptake proteins and the net result of either scenario is diminished measured uptake rates. The advantage of performing reduction inside a compartment could be due to the high thermodynamic stability of ferric siderophores in the marine environment. At the high pH of seawater, the redox potential of such complexes can be too negative for reductases alone to overcome, but at the lower pH found inside cells this potential could shift towards the positive (Harrington & Crumbliss, 2009). Yeast and plants roots typically experience lower pH environments than seawater which could explain the prominence of extracellular reduction in these organisms (E. Lesuisse & Labbe, 1989; Marschner et al., 1989). The particular iron-binding moieties present in a siderophore can also determine the redox potential of the complex with

catechols being the most negative (Crumbliss & Harrington, 2009), and this may explain why enterobactin appears inert to the FBP1/FRE2 uptake system. Iron uptake related vesicles have been observed, but the proteins present in these compartments are largely unknown (Kazamia et al., 2018; McQuaid et al., 2018). Possible candidates include proton ATPases and reductases, ISIPs, CREG proteins, and endocytosis related proteins (e.g. clathrin and SNARE proteins). Turnsek et al. (2019) have made a considerable contribution here, but further work is needed to characterize diatom proteins associated with iron assimilation processes.

3.6.3 Roles of uptake proteins in accessing environmentally significant iron sources

Mutant diatom cell lines were used as bioreporters to characterize the bioavailability of size fractionated iron sources found in the BBL directly overlying sediment in a coastal upwelling zone. Along the California coast, BBL water is rich in dissolved and particulate iron and represents the source of iron that alongside upwelled macronutrients fuels phytoplankton blooms (Biller et al., 2013; Johnson et al., 1999). Weak acid leachable particulate iron concentrations typically exceed 50 nM in this seawater, while dissolved iron is usually above 5 nM (Biller et al., 2013). This is in contrast to surface waters in the region which rarely exceed 1 nM dissolved iron (Biller & Bruland, 2013, 2014; A. King & Barbeau, 2007; A. L. King & Barbeau, 2011), and incentivizes

the rapid assimilation of this resource whenever sporadic upwelling events deliver it to the euphotic zone. This water is also characterized by high concentrations of weak iron binding ligands presumably derived from degraded organic matter (Bundy et al., 2014). It is therefore unlikely that siderophore specific uptake proteins would be effective at acquiring this iron source. Instead this iron is most effectively acquired by diatom phytoferritin after dissociation from organic complexes. Particulate iron is markedly refractory to diatom iron uptake proteins, and the chance of a diatom cell encountering a lithogenic particle are low (Leventhal et al., 2019). Siderophores can aid in the solubilization of particulate iron (Kraemer et al., 2005), but this interaction was not investigated here. In natural upwelling events where BBL water is delivered into the euphotic zone, siderophore producing microbes may increase the flux of iron from particulates into diatom cells in a process mediated by uptake proteins such as FBP1 and FRE2. The particle enrichment here failed to explain how diatoms interact with iron containing particles in the absence of microbial companions.

3.6.4 Origin of siderophore acquisition proteins in diatoms

The low concentration of bioavailable iron in certain marine environments presents a common challenge faced by many oceanic microbes from distantly related lineages. As microbes transition from relatively iron rich coastal environments into offshore iron deserts, modifications are

required to their iron uptake or budgeting capabilities. Acquisition of such traits via horizontal gene transfer (HGT) could represent an evolutionary shortcut which renders new expanses of habitat hospitable. Rates of HGT are high in marine environments (McDaniel et al., 2010), and cases of siderophore uptake related HGT have been documented in phytoplankton (Malmstrom et al., 2013). In this case the diatoms already had the required reductase component. FRE2 likely could function without a receptor to dissociate certain ferric chelates, or simply to solubilize mineral iron. Alongside a receptor, however, the system provides high affinity iron uptake in any environment inhabited by compatible siderophore producers. Given that the algal groups with FBP1 homologs arose from secondary endosymbiosis of red algae, it is possible that the gene was first acquired via HGT from Gram-positive bacteria by this rhodophyte ancestor and then inherited by subsequent lineages.

Fungi can access organically complexed iron with multiple uptake strategies. Reductive assimilation involves extracellular reduction of siderophores, followed by active oxidation to Fe(III) and internalization through a Fe(III) permease. This strategy has low substrate specificity but also generally lower affinity and is only used at siderophore concentrations far exceeding those found in marine environments (Emmanuel Lesuisse et al., 2001). Non-reductive uptake of intact ferri-siderophores occurs via a major

facilitator superfamily membrane bound transport protein which is unrelated to the ABC transporters used by bacteria (E. Lesuisse & Labbe, 1989). This non-reductive strategy appears to utilize endocytosis (Kim et al., 2002) and therefore may share some associated proteins with the FBP1/FRE2 system, but the recognition and binding of substrates in these two systems is performed by unrelated proteins.

Directly downstream of FRE2 in the *P. tricornutum* genome is a CoDi5 type long terminal repeat retrotransposon (LTR-RT) which could be relevant to HGT. Endogenous retrotransposons are known to recombine with exogenous DNA and incorporate it into the genome, integrate into foreign genomes, or simply introduce instability into the local genomic region which could favor integration by other means (Egue et al., 2015). CoDi5 LTR-RT elements are known to be upregulated during low iron conditions in diatoms (Maumus et al., 2009), and this may have played a role in genome rearrangement resulting in the colocalization of this gene pair in *P. tricornutum*. Similar microsynteny was not observed in the few other available diatom genomes, but the organization in *P. tricornutum* likely facilitates co-expression (Yoshinaga et al., 2014). Interestingly, this is not the first report of a bacterial siderophore related gene to be commandeered by a eukaryotic cell and combined with a ferric reductase presumably to coordinate expression and improve iron uptake competency (Kominek et al., 2019).

3.7 CONCLUSIONS

Given these and other recent results, our conceptual model of iron uptake and assimilation in *P. tricornutum* and related diatoms continues to develop (Figure 3.14). Phytotransferrin appears to be the workhorse iron uptake protein for a variety of substrates via an Fe⁺ intermediate, though other proteins become important when iron speciation is dominated by strong ligands. ZIP ferrous iron transporters likely play a major role in intracellular iron trafficking and possibly in acquisition of extracellular Fe(II), which may be produced by ferric reductases or simply be transiently present in seawater (Schallenberg et al., 2015). Endocytosis of iron uptake proteins certainly involves many additional proteins which are unknown at this point but likely include additional reductases and proton ATPases which facilitate liberation of iron from various chelators. It is also unclear if ISIPs, FBP1/FRE2, and other uptake systems occur in common iron processing vesicles and share associated vesicle proteins, or if they are segregated into completely separate pathways. Other ferric reductase proteins in the *P. tricornutum* genome may be involved in the reduction of extracellular iron which can then be acquired by ISIP2a or ZIPs, and/or may be present in vesicles. Our measurements of iron uptake from rhodotorulic acid could complicate the situation further. As none of our gene knockouts impacted these rates lines

either this substrate is accessible via both uptake pathways, or a third unknown pathway exists.

Additionally, the specific environmental role of high affinity siderophore uptake remains elusive. Concentrations of FOB where FBP1 becomes an important iron uptake protein are much higher than observed siderophore concentrations in bulk seawater (Boiteau et al., 2016, 2018), though could be comparable to observed L₁ concentrations (Gledhill & Buck, 2012). Consistent microbial associations could result in high local siderophore concentrations in the phycosphere favoring direct siderophore utilization over inorganic iron uptake, thus the study of iron uptake in diatoms needs to move beyond axenic culture experiments in order to determine the actual roles of these proteins in nature. Acquisition of siderophores produced by other organisms is a common strategy in certain environments (e.g. soils) and is typically thought of as a competitive or parasitic interaction (Traxler et al., 2012), but examples of siderophore mediated mutualisms are also known (Amin et al., 2009). The nature of this interaction in the marine HNLC environment might be more mutualistic as iron availability limits the fixed carbon supply of the entire community. Heterotrophs starving for carbon might benefit from sharing iron, especially if they have better access to particulate sources and require fewer iron-rich proteins. The duplication and diversification of siderophore receptors within diatoms could expand the variety of bioavailable iron sources and thus

the number of potential interacting microbial partners. The resulting iron economy could favor synergistic relationships where heterotrophs relieve diatom iron stress in exchange for fixed carbon, especially as ocean acidification reduces the efficacy of the phytotransferrin alternative.

3.8 FIGURES AND TABLES

Table 3.1. *P. tricornutum* knockout cell lines. KO cell lines used in this study. The ShBle cassette containing phleomycin resistance was directed to the cut site by flanking 1kb homology regions in some cell lines. This cassette was co-transformed with the CRISPR/Cas9 or TALEN cassette and homologous recombination (HR) resulted in ShBle insertion at the cut site. FBP1 was inactivated with a single plasmid containing the gRNA, CRISPR/Cas9 components, and ShBle cassette. Colonies were screened via Sanger sequencing of the cut site which revealed small deletions caused by non-homologous end joining (NHEJ) and resulted in frame shifts and introduction of premature stop codons.

Phatr3 PID	Description	Cell line number	KO technology	Transformation method	KO genotype
Phatr3_J54486	FRE1	1	CRISPR/Cas9	particle bombardment	HR directed ShBle insertion
Phatr3_J54486	FRE1	2	CRISPR/Cas9	particle bombardment	HR directed ShBle insertion
Phatr3_J46928	FRE2	1	CRISPR/Cas9	particle bombardment	HR directed ShBle insertion
Phatr3_J46928	FRE2	2	CRISPR/Cas9	particle bombardment	HR directed ShBle insertion
Phatr3_J46929	FBP1	1	CRISPR/Cas9	bacterial conjugation	NHEJ with 5 bp deletion
Phatr3_J46929	FBP1	2	CRISPR/Cas9	bacterial conjugation	NHEJ with 14 bp deletion
Phatr3_J54465	ISIP2a	1	TALEN	particle bombardment	HR directed ShBle insertion

Table 3.2. *P. tricornutum* ferric reductase genes. Genes with ferric reductase related annotations in the Phatr3 genome. Reproduced from Smith *et al.* 2016 S1 dataset.

Phatr3 PID	Phatr3 Alt ID	Description	Iron sensitive	Iron Depl. vs. Iron Repl.	TM domains	Predicted targeting	Pfam ID
Phatr3_J54486	303991	FRE1	yes	4.22617	10	other localisation	PF01794 PF08022 PF08030 PF12678 PF13639
Phatr3_J46928	302263	FRE2	yes	11.109	5	signal peptide	PF01794 PF08030
Phatr3_J54940	300652	FRE3	yes	3.53369	5	signal peptide	PF03188 PF03351
Phatr3_J54409	305978	FRE4	no	0.847652	9	other localisation	PF08022 PF08030
Phatr3_J54982	302959	FRE5	no	1.05249	9	other localisation	PF01794 PF08022 PF08030
Phatr3_J48658	306784	hypothetical protein	yes	1.88189	5	other localisation	PF03188 PF03351
Phatr3_J54818	300445	hypothetical protein	no	1.10291	5	signal peptide	PF03351
Phatr3_J16648	305290	hypothetical protein	no	0.773427	3	signal peptide	PF04178
Phatr3_J16490	305264	hypothetical protein	no	2.15346	1	signal anchor	PF00175 PF00970 PF08030
Phatr3_Jdraft295	310304	hypothetical protein	no	0.790555	3	signal peptide	PF04178

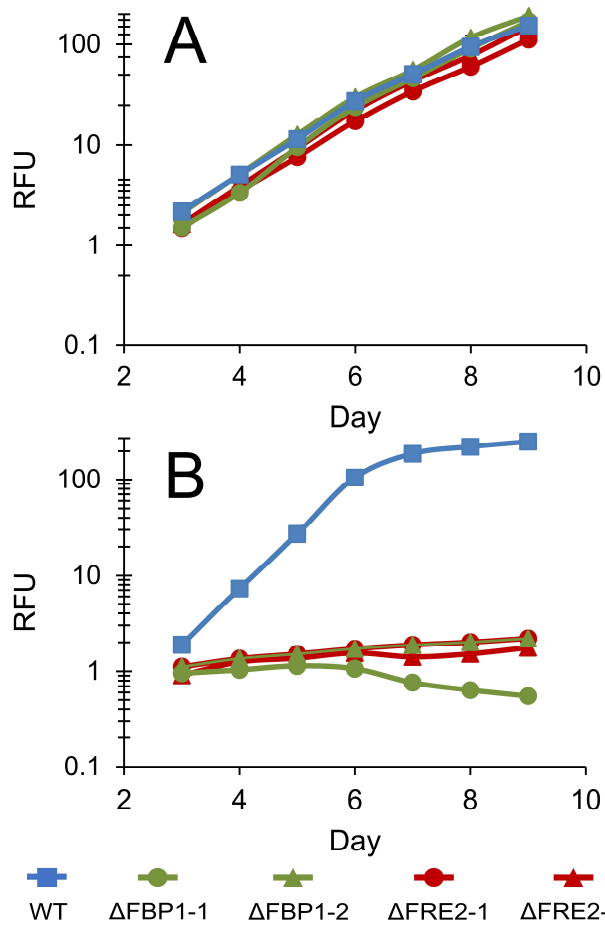


Figure 3.1. Growth of WT, Δ FRE2 and Δ FBP1 *P. tricornutum* cells in low iron Aquil media. RFU of diatom cultures grown under 24 hour illumination in Aquil media with 10 nM total Fe. Error bars represent \pm 1 SD of biological triplicate cultures and are obscured by line markers. **(A)** 100 μ M EDTA **(B)** 100 μ M EDTA and 100 nM DFB. Two cell lines for each knockout are included, and descriptions of these lines are found in Table 3.1.

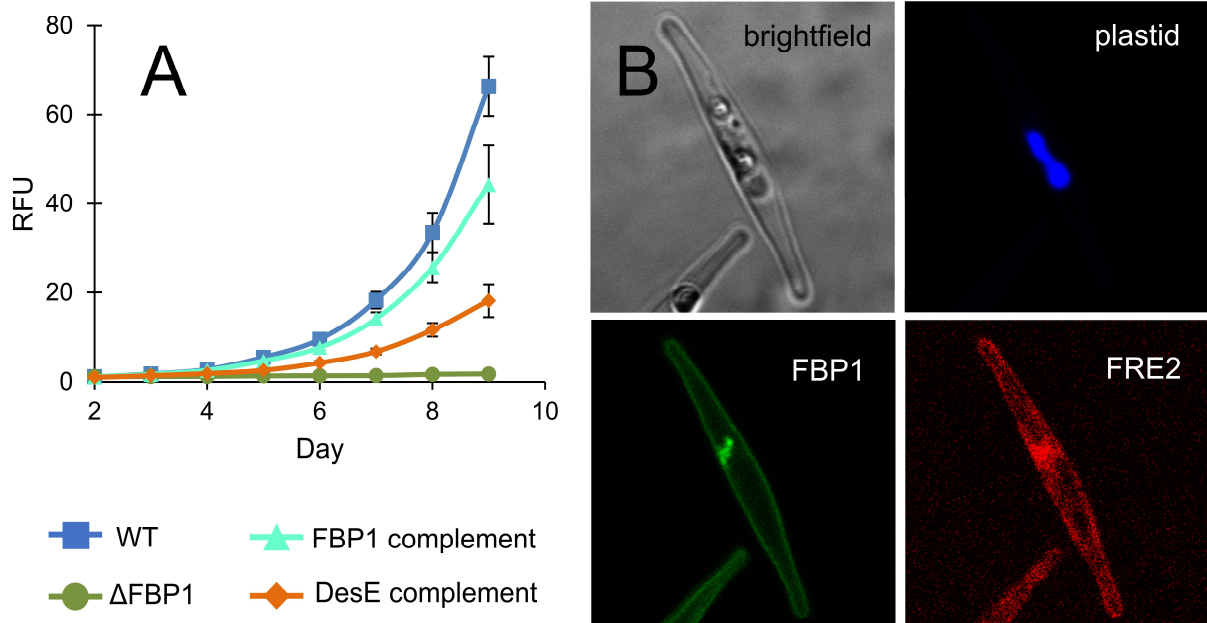


Figure 3.2. Characterization of iron acquisition proteins. **(A)** Growth curves of WT, Δ FBP1, and Δ FBP1 complement cultures grown in Aquil media under 12 hour illumination, 10 nM total Fe, 100 μ M EDTA and 100 nM DFOB. Error bars represent \pm SD of biological triplicate cultures. **(B)** Confocal microscopy of *P. tricornutum* cells expressing FBP1-mCherry and FRE2-YFP. Cells were acclimated to low iron conditions prior to imaging. FBP1 localizes to the outer membrane, and is consistently present in a small compartment near the plastid. FRE2 is present on the outer membrane, but not usually in the same location near the plastid.

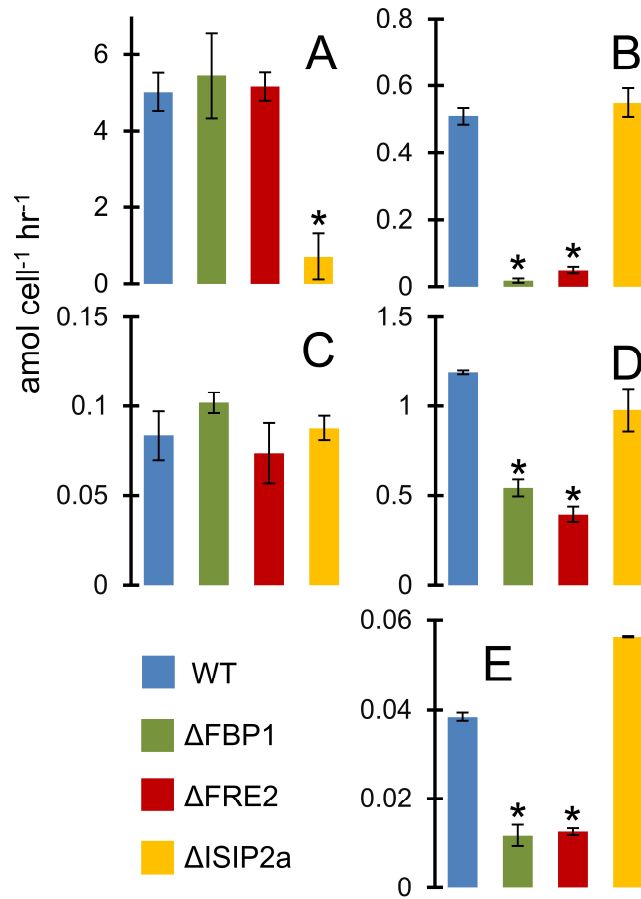


Figure 3.3. Short term iron uptake rates in Aquil media. All rates in amol cell⁻¹ hr⁻¹. Error bars represent ± 1 SD of biological triplicate cultures. * indicates $P < 0.05$ difference from WT (Student's t-test). (A) 15.7 pM Fe' (B) 250 pM FOB (C) 250 pM rhodotorulic acid (D) 4 nM ferrichrome (E) 250 pM aerobactin.

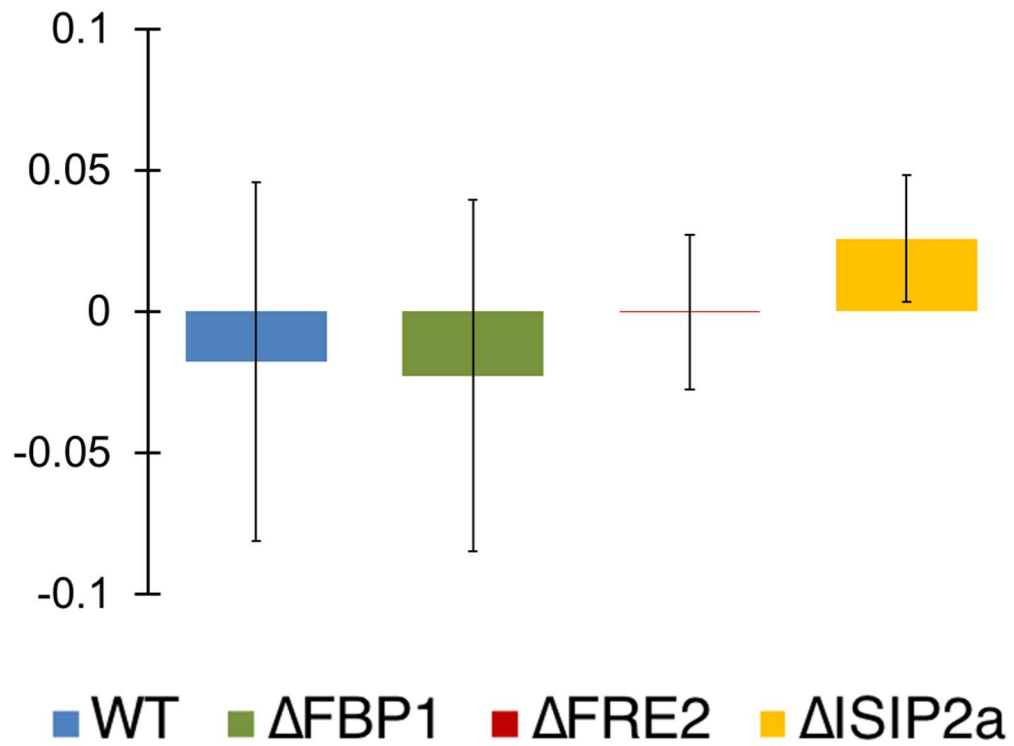


Figure 3.4. Iron uptake rates in Aquil media with 250 pM enterobactin. Results of short term uptake assays. Values are amol cell⁻¹ hr⁻¹. Error bars represent ± 1 SD of biological triplicate cultures.

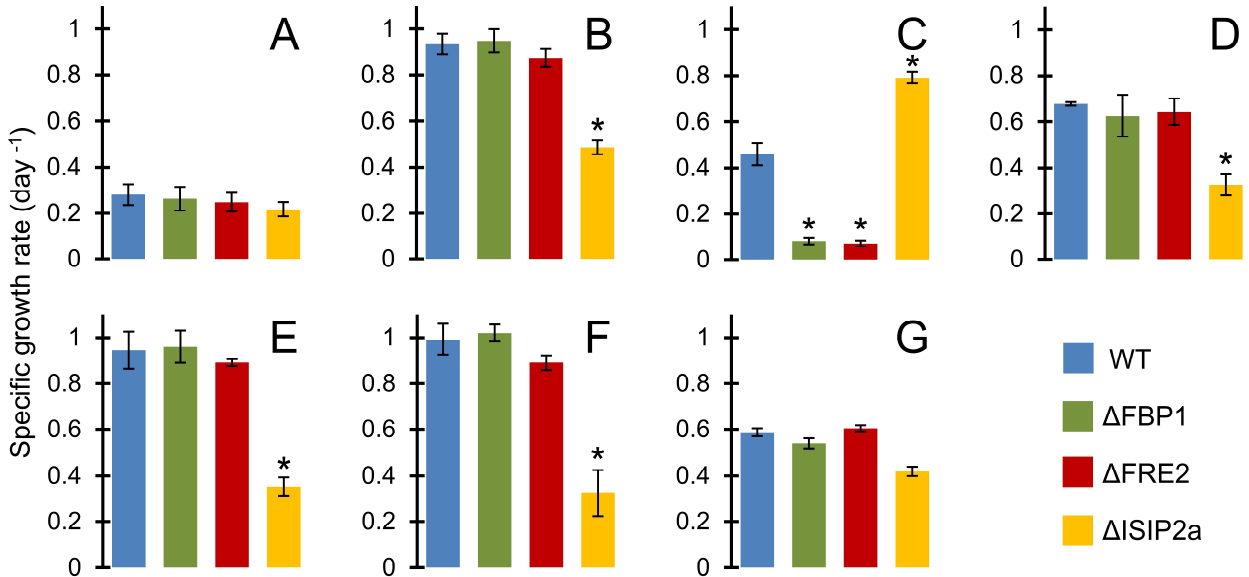


Figure 3.5. Specific growth rates (day⁻¹) of diatom cultures in natural seawater. Error bars represent ± 1 SD of biological triplicate cultures. * indicates P < 0.05 difference from WT (Student's t-test). (A) 0 added Fe (B) 2 nM added FeCl₃ (C) 2 nM added DFOB (D) 0.17 g/L SRHA (E) 10% whole BBL SW (F) 10% filtered BBL SW (G) BBL particles.

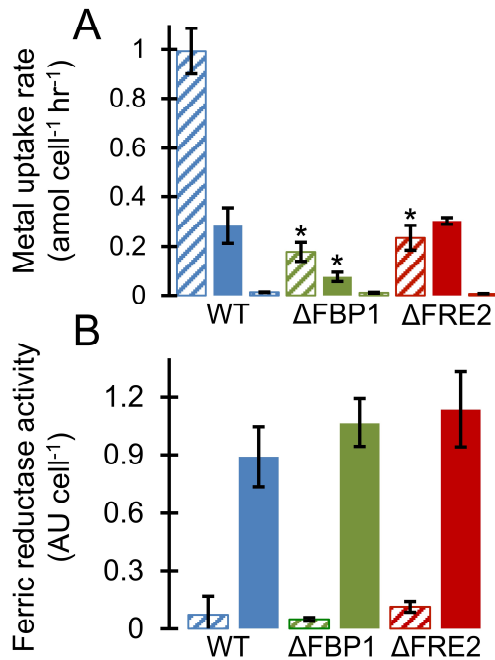


Figure 3.6. (A) Results of short-term uptake experiments. Error bars represent ± 1 SD of biological triplicate cultures. * indicates $P < 0.05$ difference from WT (Student's t-test). Diagonal striped bars show uptake rates from 10 nM FOB. Solid bars show rates from 10 nM Ga-DFOB. Vertical striped bars show uptake rates from 10 nM GaEDTA. (B) Ferric reductase activity measured using the BPDS method in WT and KO cells grown in Aquil media with 100 μ M EDTA. Diagonal bars represent iron-replete cells (157 μ M Fe'), solid bars indicate iron-deplete cells (15.7 μ M Fe'). Error bars represent ± 1 SD of biological triplicate cultures.

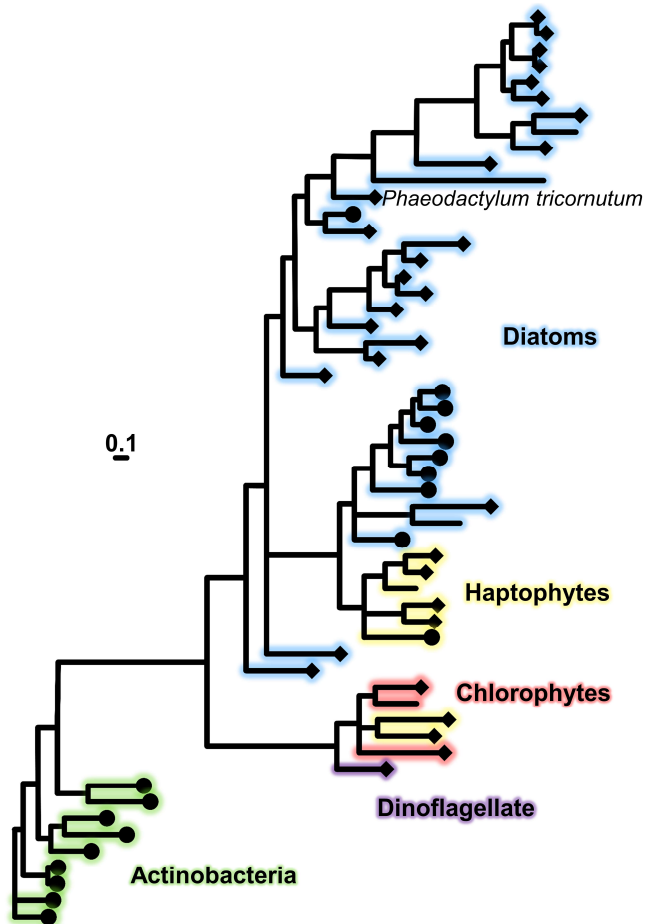


Figure 3.7. Bayesian phylogenetic tree (PhyloBayes 4) as inferred from publicly accessible amino acid sequences of FBP1 and related homologs from diatoms, hatophytes, chlorophytes, dinoflagellate and Actinobacteria. Protein sequences which modeled as ferri-siderophore receptors using Phyre2 are indicated with diamonds, and sequences with additional siderophore binding annotations are indicated by circles. Scale bar indicates 0.1 amino acid substitutions per position. Branch color indicates phylogenetic group. Posterior probabilities indicating the Bayesian support of the tree, Maximum-likelihood (LG) bootstrap support, and species identification are given in Figure 3.8.

Figure 3.9. Bayesian phylogenetic tree (PhyloBayes 4) as inferred from publicly accessible amino acid sequences of FRE2 and homologs from diatoms, other algae with rhodophyte derived plastids, plants, animals, fungi, amoebozoans and cyanobacteria. Posterior probabilities above branches indicating the Bayesian support of the tree are complemented by Maximum-likelihood (LG) bootstrap support. In *P. tricornutum*, XP_002185965 is FRE2, XP_002180058 is FRE1, and XP_002183592.1 is FRE5.



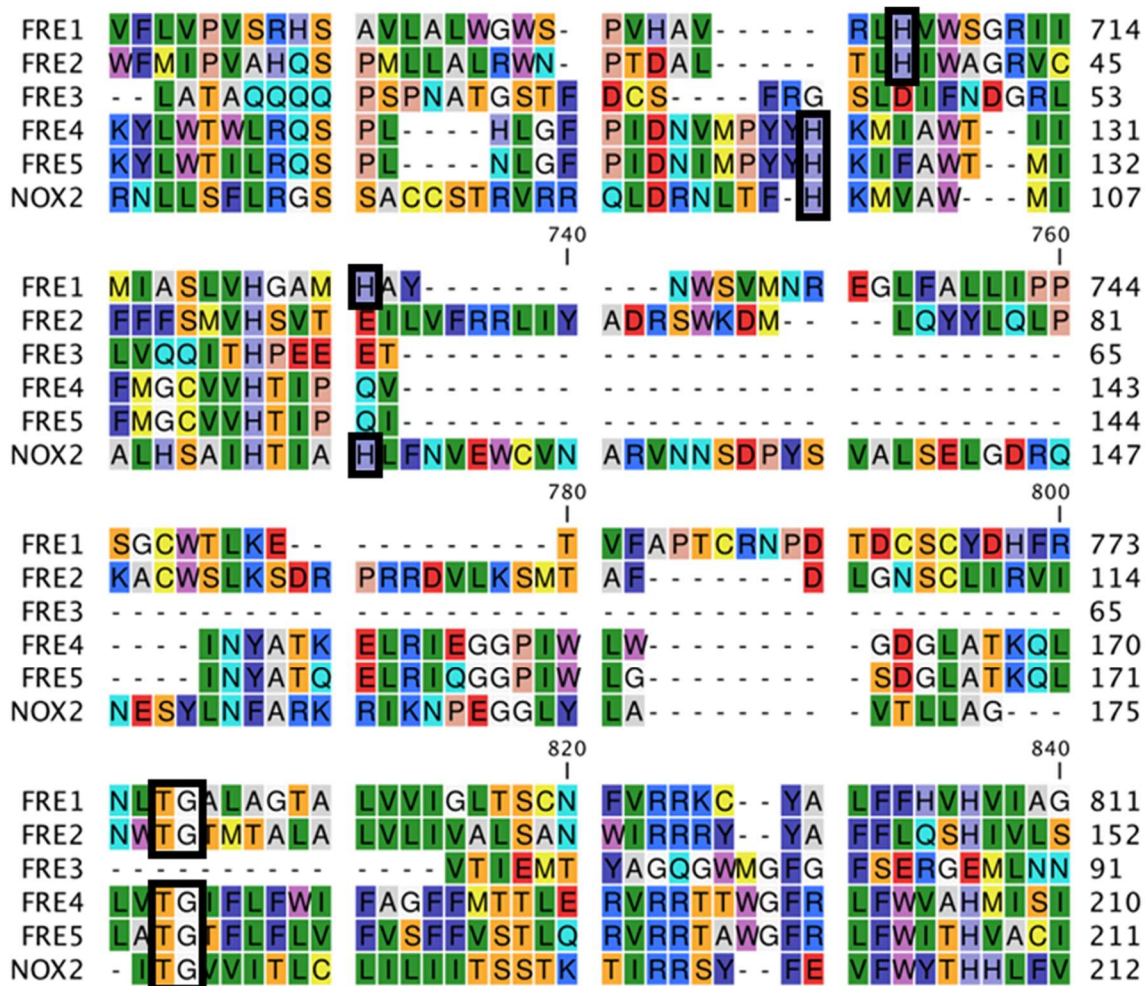


Figure 3.10. Alignment of *P. tricornutum* ferric reductase genes with human NOX2. Putative molecular oxygen binding residues indicated with black outline. Alignment performed in CLC Genomics software using default parameters.

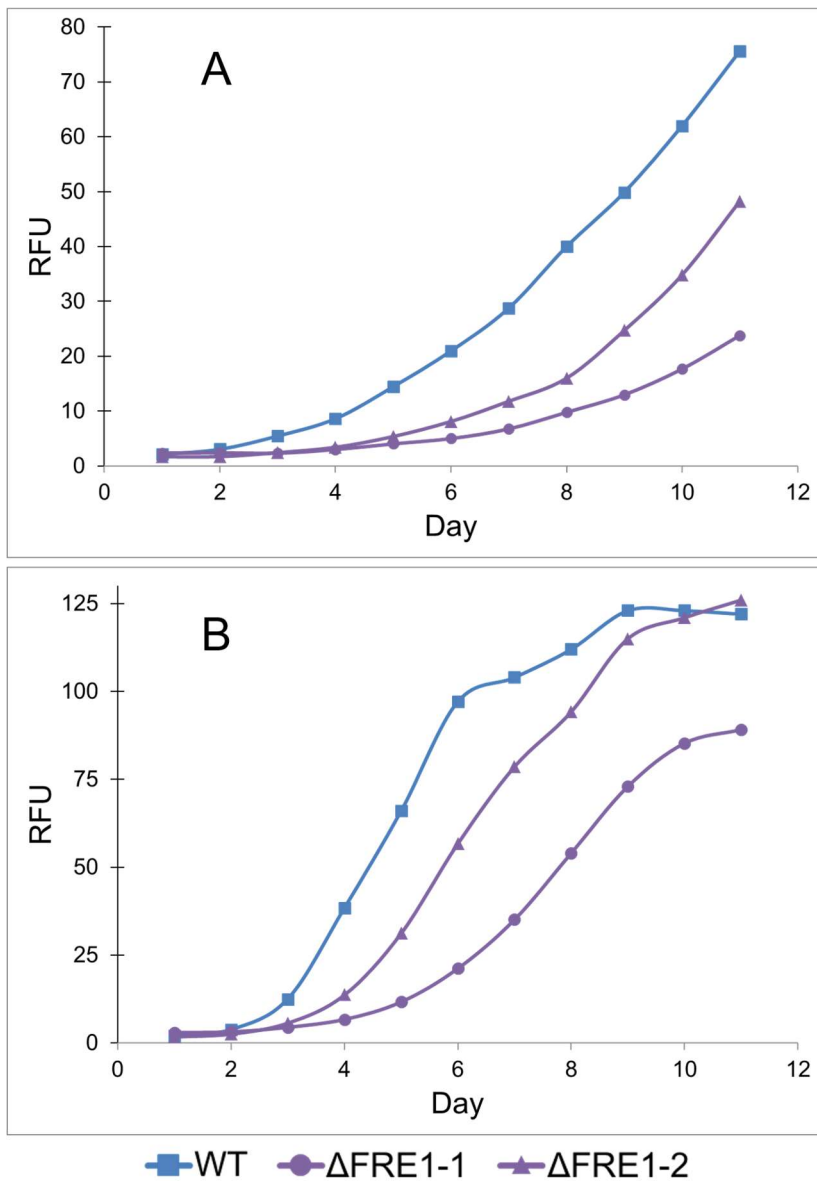


Figure 3.11. Growth of WT and Δ FRE1 *P. tricornutum* cells in low iron Aquil media. RFU of diatom cultures grown under 12 hour illumination in Aquil media with 10 nM total Fe. Error bars represent \pm 1 SD of biological triplicate cultures. **(A)** 100 μ M EDTA. **(B)** 100 μ M EDTA and 100 nM DFOB.

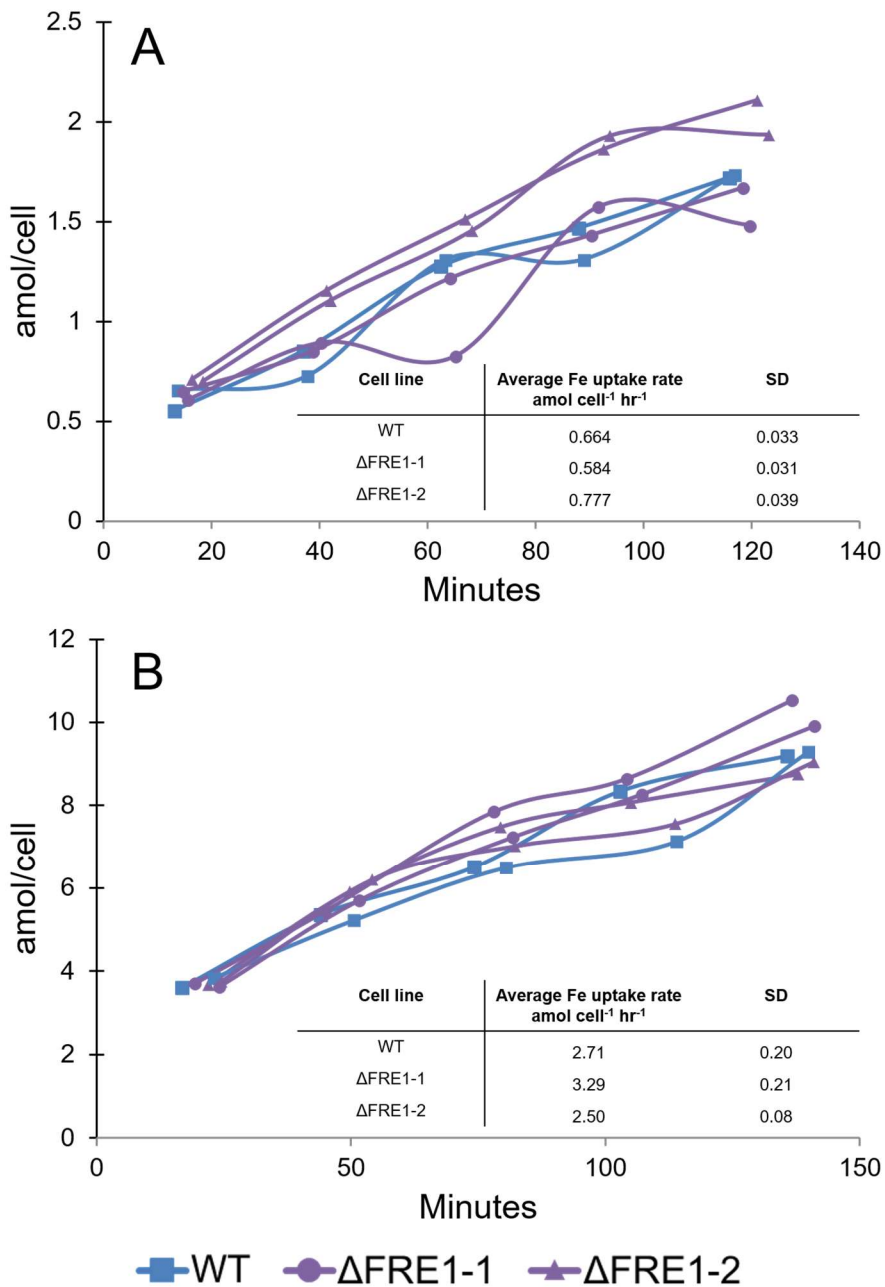


Figure 3.12. Iron uptake of WT and Δ FRE1 *P. tricornutum* cells in low iron Aquil media. Results of short-term uptake assays with (A) 1 nM FOB and (B) 5 pM Fe'. Average rates and standard deviations are given in tables within each panel.

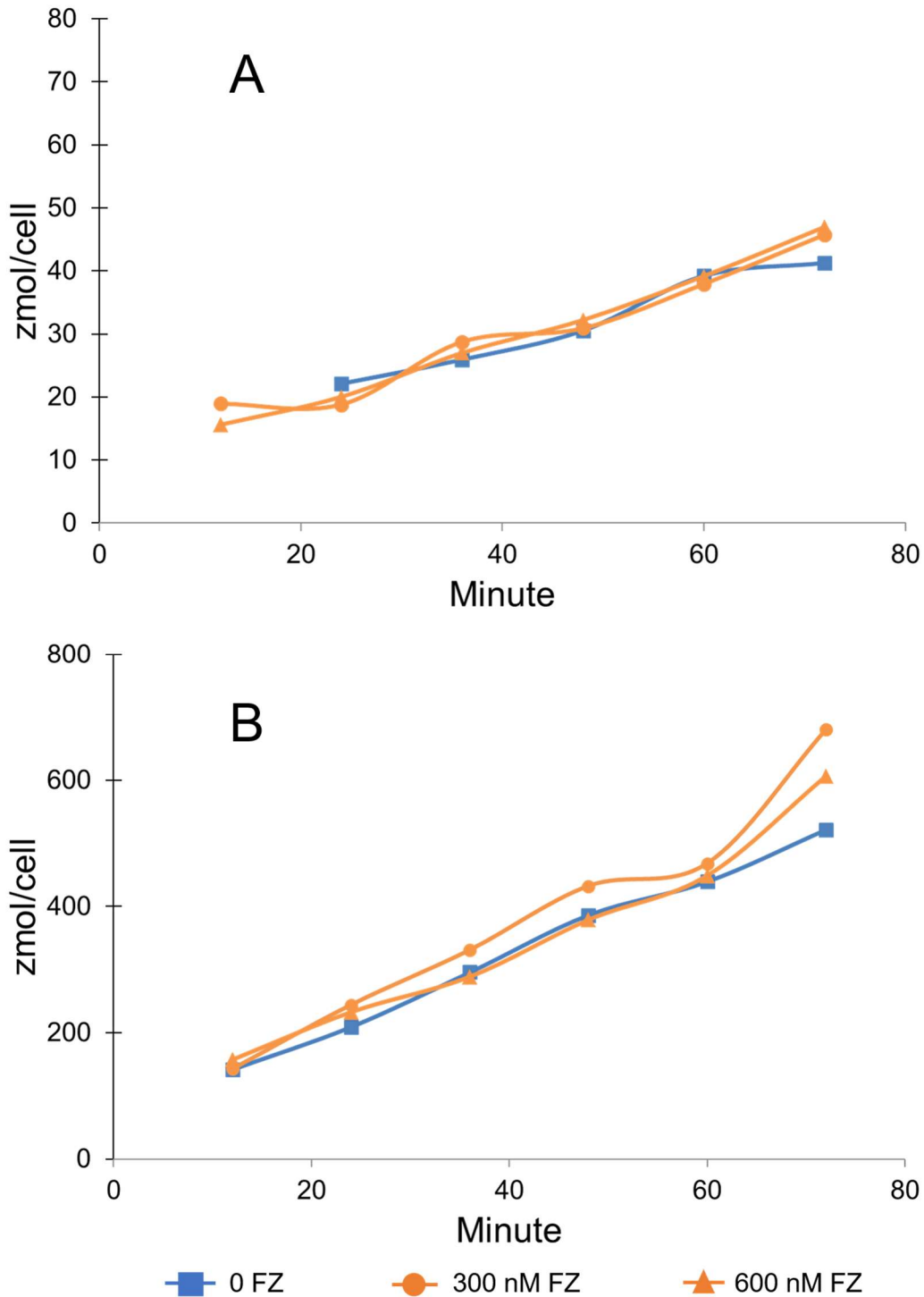


Figure 3.13. Iron uptake experiments with the Fe(II) trapping agent Ferrozine (FZ). Short-term uptake experiments conducted with WT cells in Aquil media with (A) 2 pM Fe²⁺ and (B) 250 pM FeOB. FZ additions (300 or 600 nM) were made 20 minutes before ⁵⁹Fe substrates were added.

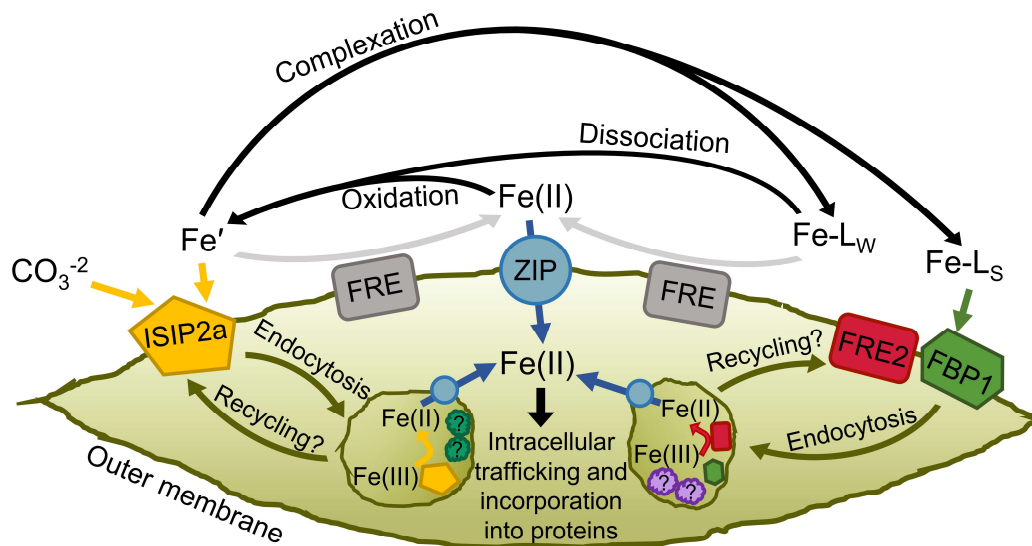


Figure 3.14. Proposed model of iron uptake in *P. tricornutum*. Four main pools of soluble iron exist as substrates in marine environments: Fe' , Fe(II) , iron bound to weak ligands (Fe-L_w), and iron complexed by high affinity chelators (Fe-L_s). Fe' is bound to ISIP2a at the cell surface with a carbonate companion anion. Clathrin mediated endocytosis internalizes the iron-protein complex to vesicles where dissociation occurs, aided by reduction and acidification facilitated by unknown proteins. Certain cell surface reductases transfer some Fe' to the Fe(II) pool. Certain strong iron binding ligands are bound at the cell surface by the FBP1/FRE2 system and endocytosed to iron processing vesicles. Weak ligands may be reduced at the cell surface, bolstering the Fe(II) pool, or may spontaneously dissociate into Fe' . Fe(II) is transported across the membrane by ZIP proteins, or abiotically re-oxidized to Fe(III) which becomes substrate for ISIP2a. ZIP proteins also traffic reduced iron between subcellular compartments.

3.9 ACKNOWLEDGEMENTS

Chapter three, in full, is a reprint of previously published material in Proceedings of the National Academy of Sciences of the United States of America Coale, T. H., Moosburner, M., Horák, A., Oborník, M., Barbeau, K. A., & Allen, A. E. (2019). Reduction-dependent siderophore assimilation in a model pennate diatom. The dissertation author was the primary investigator and author of this paper.

Many thanks to Jeff McQuaid for ISIP2a TALEN plasmids and Maxine Tan for help with plasmid design. Miroslav Oborník and Ales Horák generated phylogenies, and Mark Moosburner designed CRISPR-Cas9 constructs. Kathy Barbeau helped immeasurably with experimental design, interpretation of results and writing. Thanks to UC Ship Funds for supporting BBL field work, the captain and crew of *R/V Sally Ride*, chief scientist Angel Ruacho, Kayleen Fulton for sampling assistance, and Kiefer Forsch for dissolved iron measurements. Additional thanks to Vince Bielinski for conjugation plasmids, Rob Franks for assistance with ICP-MS analyses, Randelle Bundy and *R/V Kilo Moana* personnel for Stn ALOHA water collection, and Jia Jia Zhang for *Salinispora* cultures. This study was supported by National Science Foundation (NSF-OCE-1756884, NSF-OCE-1756860, and NSF-MCB-1818390), United States Department of Energy Genomics Science program (DE-SC0018344), and Gordon and Betty Moore Foundation (GBMF3828 and GBMF5006) grants to

A.E.A., and the Czech Science Foundation, project 15-17643S (M.O. and A.H.).

3.10 REFERENCES

- Allen, A. E., Laroche, J., Maheswari, U., Lommer, M., Schauer, N., Lopez, P. J., Finazzi, G., Fernie, A. R., Bowler, C., & Karl, D. M. (2008). Whole-cell response of the pennate diatom *Phaeodactylum tricornutum* to iron starvation. *Proceedings of the National Academy of Sciences of the United States of America*, *105*(30), 10438–10443. <https://doi.org/10.1073/pnas.0711370105>
- Amin, S. A., Green, D. H., Hart, M. C., Küpper, F. C., Sunda, W. G., & Carrano, C. J. (2009). Photolysis of iron–siderophore chelates promotes bacterial–algal mutualism. *Proceedings of the National Academy of Sciences*, *106*(40), 17071–17076.
- Anderson, M. A., & Morel, F. M. (1980). Uptake of Fe (II) by a diatom in oxic culture medium. *Marine Biology Letters*, *1*(5), 263–268.
- Behrenfeld, M. J., & Milligan, A. J. (2011). Photophysiological Expressions of Iron Stress in Phytoplankton. *Annual Review of Marine Science*, *5*, 120717164858000. <https://doi.org/10.1146/annurev-marine-121211-172356>
- Biller, D. V., & Bruland, K. W. (2013). Sources and distributions of Mn, Fe, Co, Ni, Cu, Zn, and Cd relative to macronutrients along the central California coast during the spring and summer upwelling season. *Marine Chemistry*, *155*, 50–70. <https://doi.org/10.1016/j.marchem.2013.06.003>
- Biller, D. V., & Bruland, K. W. (2014). The central California Current transition zone: A broad region exhibiting evidence for iron limitation. *Progress in Oceanography*, *120*, 370–382. <https://doi.org/10.1016/j.pocean.2013.11.002>
- Biller, D. V., Coale, T. H., Till, R. C., Smith, G. J., & Bruland, K. W. (2013). Coastal iron and nitrate distributions during the spring and summer upwelling season in the central California Current upwelling regime. *Continental Shelf Research*, *66*, 58–72. <https://doi.org/10.1016/j.csr.2013.07.003>

- Blaby-Haas, C. E., & Merchant, S. S. (2012a). The ins and outs of algal metal transport ☆. *BBA - Molecular Cell Research*, 1823, 1531–1552. <https://doi.org/10.1016/j.bbamcr.2012.04.010>
- Blaby-Haas, C. E., & Merchant, S. S. (2012b). The ins and outs of algal metal transport. *Biochimica et Biophysica Acta*, 1823(9), 1531–1552. <https://doi.org/10.1016/j.bbamcr.2012.04.010>
- Boiteau, R. M., Mende, D. R., Hawco, N. J., McIlvin, M. R., Fitzsimmons, J. N., Saito, M. A., Sedwick, P. N., DeLong, E. F., & Repeta, D. J. (2016). Siderophore-based microbial adaptations to iron scarcity across the eastern Pacific Ocean. *Proceedings of the National Academy of Sciences of the United States of America*, 113(50), 14237–14242. <https://doi.org/10.1073/pnas.1608594113>
- Boiteau, R. M., Till, C. P., Coale, T. H., Fitzsimmons, J. N., Bruland, K. W., & Repeta, D. J. (2018). Patterns of iron and siderophore distributions across the California Current System. *Limnology and Oceanography*, 64(1), 376–389.
- Bowler, C., Allen, A. E., Badger, J. H., Grimwood, J., Jabbari, K., Kuo, A., Maheswari, U., Martens, C., Maumus, F., O'illar, R. P., Rayko, E., Salamov, A., Vandepoele, K., Beszteri, B., Gruber, A., Heijde, M., Katinka, M., Mock, T., Valentin, K., ... Grigoriev, I. V. (2008). The *Phaeodactylum* genome reveals the evolutionary history of diatom genomes. *Nature*, 456(7219), 239–244. <https://doi.org/10.1038/nature07410>
- Braun, V., & Braun, M. (2002). Iron transport and signaling in *Escherichia coli*. *FEBS Letters*, 529(1), 78–85. [https://doi.org/10.1016/S0014-5793\(02\)03185-X](https://doi.org/10.1016/S0014-5793(02)03185-X)
- Bruland, K. W., & Franks, R. P. (1983). Trace metals in seawater. *Chemical Oceanography*, 8, 157–220.
- Bundy, R. M., Biller, D. V., Buck, K. N., Bruland, K. W., & Barbeau, K. A. (2014). Distinct pools of dissolved iron-binding ligands in the surface and benthic boundary layer of the California Current. *Limnology and Oceanography*, 59(3), 769–787. <https://doi.org/10.4319/lo.2014.59.3.0769>
- Butler, A., & Theisen, R. M. (2010). Iron (III)–siderophore coordination chemistry: reactivity of marine siderophores. *Coordination Chemistry Reviews*, 254(3–

4), 288–296.

Chappell, P. D., Whitney, L. P., Wallace, J. R., Darer, A. I., Jean-Charles, S., & Jenkins, B. D. (2014). Genetic indicators of iron limitation in wild populations of *Thalassiosira oceanica* from the northeast Pacific Ocean. *The ISME Journal*, 9(3), 1–11. <https://doi.org/10.1038/ismej.2014.171>

Ciechanover, A., Schwartz, A. L., Dautry-Varsat, A., & Lodish, H. F. (1983). Kinetics of internalization and recycling of transferrin and the transferrin receptor in a human hepatoma cell line. Effect of lysosomotropic agents. *Journal of Biological Chemistry*, 258(16), 9681–9689.

Cohen, N. R., Gong, W., Moran, D. M., McIlvin, M. R., Saito, M. A., & Marchetti, A. (2018). Transcriptomic and proteomic responses of the oceanic diatom *Pseudo-nitzschia granii* to iron limitation. *Environmental Microbiology*, 20(8), 3109–3126. <https://doi.org/10.1111/1462-2920.14386>

Cooper, L. H. N. (1935). Iron in the Sea and in Marine Plankton. *Proceedings of the Royal Society of London*, 118(810), 419–438.

Coulton, J., Mason, P., & Allatt, D. (1987). *fhuC* and *fhuD* Genes for Iron(III)-Ferrichrome Transport into *Escherichia coli* K-12. *Journal of Bacteriology*, 169(8), 3844–3849. <http://jb.asm.org/content/169/8/3844.short>

Crumbliss, A. L., & Harrington, J. M. (2009). Iron sequestration by small molecules: thermodynamic and kinetic studies of natural siderophores and synthetic model compounds. *Advances in Inorganic Chemistry*, 61, 179–250.

de Baar, H. J. W. W., Boyd, P. W., Coale, K. H., Landry, M. R., Tsuda, A., Assmy, P., Bakker, D. C. E., Bozec, Y., Barber, R. T., Brzezinski, M. A., Buesseler, K. O., Boyé, M., Croot, P. L., Gervais, F., Gorbunov, M. Y., Harrison, P. J., Hiscock, W. T., Laan, P., Lancelot, C., ... Wong, C. S. (2005). Synthesis of iron fertilization experiments: From the Iron Age in the Age of Enlightenment. *Journal of Geophysical Research*, 110(C9), C09S16. <https://doi.org/10.1029/2004JC002601>

Diaz, J. M., Plummer, S., Hansel, C. M., Andeer, P. F., Saito, M. A., & McIlvin, M. R. (2019). NADPH-dependent extracellular superoxide production is vital to photophysiology in the marine diatom *Thalassiosira oceanica*.

Proceedings of the National Academy of Sciences, 116(33), 16448–16453.
<https://doi.org/10.1073/pnas.1821233116>

Diner, R. E., Bielinski, V. A., Dupont, C. L., Allen, A. E., & Weyman, P. D. (2016). Refinement of the Diatom Episome Maintenance Sequence and Improvement of Conjugation-Based DNA Delivery Methods. *Frontiers in Bioengineering and Biotechnology*, 4(August).
<https://doi.org/10.3389/fbioe.2016.00065>

Eckhardt, U., & Buckhout, T. J. (1998). Iron assimilation in *Chlamydomonas reinhardtii* involves ferric reduction and is similar to Strategy I higher plants. *Journal of Experimental Botany*, 49(324), 1219–1226.
<https://doi.org/10.1093/jxb/49.324.1219>

Eddy, S. R. (2011). Accelerated profile HMM searches. *PLoS Computational Biology*, 7(10), e1002195.

Egue, F., Chenais, B., Tastard, E., Marchand, J., Hiard, S., Gateau, H., Hermann, D., Morant-Manceau, A., Casse, N., & Caruso, A. (2015). Expression of the retrotransposons Surcouf and Blackbeard in the marine diatom *Phaeodactylum tricorutum* under thermal stress. *Phycologia*, 54(6), 617–627.

Falciatore, A., Casotti, R., Leblanc, C., Abrescia, C., & Bowler, C. (1999). Transformation of nonselectable reporter genes in marine diatoms. *Marine Biotechnology*, 1(3), 239–251.

Fitzsimmons, J. N., Hayes, C. T., Al-Subiaï, S. N., Zhang, R., Morton, P. L., Weisend, R. E., Ascani, F., & Boyle, E. A. (2015). Daily to decadal variability of size-fractionated iron and iron-binding ligands at the Hawaii Ocean Time-series Station ALOHA. *Geochimica et Cosmochimica Acta*, 171, 303–324.

Gledhill, M., & Buck, K. N. (2012). The organic complexation of iron in the marine environment: a review. *Frontiers in Microbiology*, 3(February), 69.
<https://doi.org/10.3389/fmicb.2012.00069>

Gordon, R. M., Martin, J. H., & Knauer, G. A. (1982). Iron in north-east Pacific waters. *Nature*, 299, 611. <http://dx.doi.org/10.1038/299611a0>

- Gouy, M., Guindon, S., & Gascuel, O. (2009). SeaView version 4: a multiplatform graphical user interface for sequence alignment and phylogenetic tree building. *Molecular Biology and Evolution*, 27(2), 221–224.
- Groussman, R. D., Parker, M. S., & Armbrust, E. V. (2015). Diversity and Evolutionary History of Iron Metabolism Genes in Diatoms. *PLOS ONE*, 10(6), e0129081. <https://doi.org/10.1371/journal.pone.0129081>
- Harrington, J. M., & Crumbliss, A. L. (2009). The redox hypothesis in siderophore-mediated iron uptake. *Biometals*, 22(4), 679–689.
- Hawco, N. J., & Saito, M. A. (2018). Competitive inhibition of cobalt uptake by zinc and manganese in a pacific *Prochlorococcus* strain: Insights into metal homeostasis in a streamlined oligotrophic cyanobacterium. *Limnology and Oceanography*, 63(5), 2229–2249.
- Hider, R. C., & Kong, X. (2010). Chemistry and biology of siderophores. *Natural Product Reports*, 27(5), 637–657.
- Hoegy, F., Celia, H., Mislin, G. L., Vincent, M., Gallay, J., & Schalk, I. J. (2005). Binding of iron-free siderophore, a common feature of siderophore outer membrane transporters of *Escherichia coli* and *Pseudomonas aeruginosa*. *Journal of Biological Chemistry*, 280(21), 20222–20230.
- Horstmann, U., & Soria-Dengg, S. (1995). Ferrioxamines B and E as iron sources for the marine diatom *Phaeodactylum tricornutum*. *Marine Ecology Progress Series*, 127, 269–277. <http://www.int-res.com/articles/meps/127/m127p269.pdf>
- Hutchins, D A, Franck, V. M., Brzezinski, M. A., & Bruland, K. W. (1999). Inducing phytoplankton iron limitation in iron-replete coastal waters with a strong chelating ligand. *Limnol. Oceanogr*, 44(4), 1009–1018.
- Hutchins, David A., & Bruland, K. W. K. W. (1998). Iron-limited diatom growth and Si: N uptake ratios in a coastal upwelling regime. *Nature*, 393(June), 65–68. <https://doi.org/Doi 10.1038/31203>
- Jeong, J., Cohu, C., Kerkeb, L., Pilon, M., Connolly, E. L., & Guerinot, M. Lou. (2008). Chloroplast Fe (III) chelate reductase activity is essential for

seedling viability under iron limiting conditions. *Proceedings of the National Academy of Sciences*, 105(30), 10619–10624.

Johnson, K. S., Chavez, F. P., & Friederich, G. E. (1999). Continental-shelf sediment as a primary source of iron for coastal phytoplankton. *Nature*, 398(6729), 697–700. <https://doi.org/10.1038/19511>

Jones, G. J., Palenik, B. P., & Morel, F. M. M. (1987). Trace metal reduction by phytoplankton: the role of plasmalemma redox enzymes. *Journal of Phycology*, 23(2), 237–244. <http://onlinelibrary.wiley.com/doi/10.1111/j.1529-8817.1987.tb04131.x/abstract>

Karas, B. J., Diner, R. E., Lefebvre, S. C., McQuaid, J., Phillips, A. P. R., Noddings, C. M., Brunson, J. K., Valas, R. E., Deerinck, T. J., Jablanovic, J., Gillard, J. T. F., Beerli, K., Ellisman, M. H., Glass, J. I., Hutchison III, C. a., Smith, H. O., Venter, J. C., Allen, A. E., Dupont, C. L., ... Weyman, P. D. (2015). Designer diatom episomes delivered by bacterial conjugation. *Nature Communications*, 6, 1–10. <https://doi.org/10.1038/ncomms7925>

Katoh, K., & Standley, D. M. (2013). MAFFT multiple sequence alignment software version 7: improvements in performance and usability. *Molecular Biology and Evolution*, 30(4), 772–780.

Kazamia, E., Sutak, R., Paz-Yepes, J., Dorrell, R. G., Vieira, F. R. J., Mach, J., Morrissey, J., Leon, S., Lam, F., Pelletier, E., Camadro, J., Bowler, C., & Lesuisse, E. (2018). Endocytosis-mediated siderophore uptake as a strategy for Fe acquisition in diatoms. *Science Advances*, 4(5), eaar4536. <https://doi.org/10.1126/sciadv.aar4536>

Keeling, P. J., Burki, F., Wilcox, H. M., Allam, B., Allen, E. E., Amaral-Zettler, L. A., Armbrust, E. V., Archibald, J. M., Bharti, A. K., Bell, C. J., Beszteri, B., Bidle, K. D., Cameron, C. T., Campbell, L., Caron, D. A., Cattolico, R. A., Collier, J. L., Coyne, K., Davy, S. K., ... Worden, A. Z. (2014). The Marine Microbial Eukaryote Transcriptome Sequencing Project (MMETSP): illuminating the functional diversity of eukaryotic life in the oceans through transcriptome sequencing. *PLoS Biology*, 12(6), e1001889. <https://doi.org/10.1371/journal.pbio.1001889>

Kelly, L. A., Mezulis, S., Yates, C., Wass, M., & Sternberg, M. (2015). The Phyre2 web portal for protein modelling, prediction, and analysis. *Nature*

Protocols, 10(6), 845–858. <https://doi.org/10.1038/nprot.2015-053>

- Kersey, P. J., Allen, J. E., Allot, A., Barba, M., Boddu, S., Bolt, B. J., Carvalho-Silva, D., Christensen, M., Davis, P., Grabmueller, C., Kumar, N., Liu, Z., Maurel, T., Moore, B., McDowall, M. D., Maheswari, U., Naamati, G., Newman, V., Ong, C. K., ... Yates, A. (2018). Ensembl Genomes 2018: An integrated omics infrastructure for non-vertebrate species. *Nucleic Acids Research*, 46(D1), D802–D808. <https://doi.org/10.1093/nar/gkx1011>
- Kim, Y., Yun, C. C., & Philpott, C. C. (2002). Ferrichrome induces endosome to plasma membrane cycling of the ferrichrome transporter, Arn1p, in *Saccharomyces cerevisiae*. *The EMBO Journal*, 21(14), 3632–3642.
- King, A., & Barbeau, K. (2007). Evidence for phytoplankton iron limitation in the southern California Current System. *Marine Ecology Progress Series*, 342, 91–103. <https://doi.org/10.3354/meps342091>
- King, A. L., & Barbeau, K. A. (2011). Dissolved iron and macronutrient distributions in the southern California Current System. *Journal of Geophysical Research: Oceans*, 116(3), 1–18. <https://doi.org/10.1029/2010JC006324>
- Kominek, J., Doering, D. T., Ofulente, D. A., Shen, X.-X., Zhou, X., DeVirgilio, J., Hulfachor, A. B., Groenewald, M., Mcgee, M. A., & Karlen, S. D. (2019). Eukaryotic acquisition of a bacterial operon. *Cell*, 176(6), 1356–1366.
- Kraemer, S. M. (2004). Iron oxide dissolution and solubility in the presence of siderophores. *Aquatic Sciences*, 66(1), 3–18.
- Kraemer, S. M., Butler, A., Borer, P., & Cervini-Silva, J. (2005). Siderophores and the dissolution of iron-bearing minerals in marine systems. *Reviews in Mineralogy and Geochemistry*, 59(1), 53–84.
- Krewulak, K. D., & Vogel, H. J. (2008). Structural biology of bacterial iron uptake. In *Biochimica et Biophysica Acta - Biomembranes* (Vol. 1778, Issue 9, pp. 1781–1804). <https://doi.org/10.1016/j.bbamem.2007.07.026>
- Kustka, A. B., Allen, A. E., & Morel, F. M. M. (2007). Sequence Analysis and Transcriptional Regulation of Iron Acquisition Genes in Two Marine Diatoms. *Journal of Phycology*, 43(4), 715–729.

<https://doi.org/10.1111/j.1529-8817.2007.00359.x>

Laglera, L. M., & van den Berg, C. M. G. G. (2009). Evidence for geochemical control of iron by humic substances in seawater. *Limnology and Oceanography*, *54*(2), 610–619. <https://doi.org/10.4319/lo.2009.54.2.0610>

Lartillot, N., Lepage, T., & Blanquart, S. (2009). PhyloBayes 3: a Bayesian software package for phylogenetic reconstruction and molecular dating. *Bioinformatics*, *25*(17), 2286–2288.

Lesuisse, E., & Labbe, P. (1989). Reductive and non-reductive mechanisms of iron assimilation by the yeast *Saccharomyces cerevisiae*. *Journal of General Microbiology*, *135*(2), 257–263. <https://doi.org/10.1099/00221287-135-2-257>

Lesuisse, Emmanuel, Blaiseau, P. L., Dancis, A., & Camadro, J.-M. M. (2001). Siderophore uptake and use by the yeast *Saccharomyces cerevisiae*. *Microbiology*, *147*(2), 289–298. <https://doi.org/10.1099/00221287-147-2-289>

Leventhal, G. E., Ackermann, M., & Schiessl, K. T. (2019). Why microbes secrete molecules to modify their environment: the case of iron-chelating siderophores. *Journal of The Royal Society Interface*, *16*(150), 20180674. <https://doi.org/10.1098/rsif.2018.0674>

Lis, H., Shaked, Y., Kranzler, C., Keren, N., & Morel, F. M. M. (2014). Iron bioavailability to phytoplankton: an empirical approach. *The ISME Journal*, 1–11. <https://doi.org/10.1038/ismej.2014.199>

Lommer, M., Specht, M., Roy, A.-S., Kraemer, L., Andreson, R., Gutowska, M. a, Wolf, J., Bergner, S. V, Schilhabel, M. B., Klostermeier, U. C., Beiko, R. G., Rosenstiel, P., Hippler, M., & LaRoche, J. (2012). Genome and low-iron response of an oceanic diatom adapted to chronic iron limitation. *Genome Biology*, *13*(7), R66. <https://doi.org/10.1186/gb-2012-13-7-r66>

Maldonado, M. T., & Price, N. M. (2001). Reduction and transport of organically bound iron by *Thalassiosira oceanica* (Bacillariophyceae). *Journal of Phycology*, *37*(2), 298–309. <https://doi.org/10.1046/j.1529-8817.2001.037002298.x>

Maldonado, M T, & Price, N. M. (1999). Utilization of Fe bound to strong

organic ligands by phytoplankton communities in the subarctic Pacific Ocean. *Deep-Sea Research II*, 46, 2447–2473.
[https://doi.org/10.1016/S0967-0645\(99\)00071-5](https://doi.org/10.1016/S0967-0645(99)00071-5)

Maldonado, Maria T., Allen, A. E., Chong, J. S., Lin, K., Leus, D., Karpenko, N., & Harris, S. L. (2006). Copper-dependent iron transport in coastal and oceanic diatoms. *Limnology and Oceanography*, 51(4), 1729–1743.
<https://doi.org/10.4319/lo.2006.51.4.1729>

Maldonado, Maria T., & Price, N. M. (1999). Utilization of iron bound to strong organic ligands by plankton communities in the subarctic Pacific Ocean. *Deep-Sea Research Part II: Topical Studies in Oceanography*, 46(11–12), 2447–2473. [https://doi.org/10.1016/S0967-0645\(99\)00071-5](https://doi.org/10.1016/S0967-0645(99)00071-5)

Maldonado, Maria T., Strzepek, R. F., Sander, S., & Boyd, P. W. (2005). Acquisition of iron bound to strong organic complexes, with different Fe binding groups and photochemical reactivities, by plankton communities in Fe-limited subantarctic waters. *Global Biogeochemical Cycles*, 19(4).
<https://doi.org/10.1029/2005GB002481>

Malmstrom, R. R., Rodrigue, S., Huang, K. H., Kelly, L., Kern, S. E., Thompson, A., Roggensack, S., Berube, P. M., Henn, M. R., & Chisholm, S. W. (2013). Ecology of uncultured Prochlorococcus clades revealed through single-cell genomics and biogeographic analysis. *The ISME Journal*, 184–198.
<https://doi.org/10.1038/ismej.2012.89>

Marchetti, A., Schrueth, D. M., Durkin, C. A., Parker, M. S., Kodner, R. B., Berthiaume, C. T., Morales, R., Allen, A. E., Armbrusta, E. V., & Armbrust, E. V. (2012). Comparative metatranscriptomics identifies molecular bases for the physiological responses of phytoplankton to varying iron availability. *Proceedings of the National Academy of Sciences*, 109(6), E317–E325.
<https://doi.org/10.1073/pnas.1118408109>

Marschner, H., Treeby, M., & Römheld, V. (1989). Role of root-induced changes in the rhizosphere for iron acquisition in higher plants. *Zeitschrift Für Pflanzenernährung Und Bodenkunde*, 152(2), 197–204.

Martinez, J. S., Haygood, M. G., & Butler, A. (2001). Identification of a natural desferrioxamine siderophore produced by a marine bacterium. *Limnology and Oceanography*, 46(2), 420–424.
<https://doi.org/10.4319/lo.2001.46.2.0420>

- Martinez, J S, Zhang, G. P., Holt, P. D., Jung, H.-T., Carrano, C. J., Haygood, M. G., & Butler, A. (2000). Self-assembling amphiphilic siderophores from marine bacteria. *Science*, *287*(5456), 1245–1247.
- Martinez, Jennifer S, & Butler, A. (2007). Marine amphiphilic siderophores: marinobactin structure, uptake, and microbial partitioning. *Journal of Inorganic Biochemistry*, *101*(11–12), 1692–1698.
- Maumus, F., Allen, A. E., Mhiri, C., Hu, H., Jabbari, K., Vardi, A., Grandbastien, M.-A., & Bowler, C. (2009). Potential impact of stress activated retrotransposons on genome evolution in a marine diatom. *BMC Genomics*, *10*(1), 624.
- Mawji, E., Schlitzer, R., Dodas, E. M., Abadie, C., Abouchami, W., Anderson, R. F., Baars, O., Bakker, K., Baskaran, M., Bates, N. R., Bluhm, K., Bowie, A., Bown, J., Boye, M., Boyle, E. A., Branellec, P., Bruland, K. W., Brzezinski, M. A., Bucciarelli, E., ... Zimmer, L. A. (2015). The GEOTRACES Intermediate Data Product 2014. *Marine Chemistry*, *177*, 1–8.
<https://doi.org/10.1016/j.marchem.2015.04.005>
<<http://dx.doi.org/10.1016/j.marchem.2015.04.005>> , hdl:10013/epic.46232
- McCormack, P., Worsfold, P. J., & Gledhill, M. (2003). Separation and detection of siderophores produced by marine bacterioplankton using high-performance liquid chromatography with electrospray ionization mass spectrometry. *Analytical Chemistry*, *75*(11), 2647–2652.
<https://doi.org/10.1021/ac0340105>
- McDaniel, L. D., Young, E., Delaney, J., Ruhnau, F., Ritchie, K. B., & Paul, J. H. (2010). High Frequency of Horizontal Gene Transfer in the Oceans. *Science*, *330*(6000), 50. <https://doi.org/10.1126/science.1192243>
- McKie, A. T., Barrow, D., Latunde-Dada, G. O., Rolfs, A., Sager, G., Mudaly, E., Mudaly, M., Richardson, C., Barlow, D., & Bomford, A. (2001). An iron-regulated ferric reductase associated with the absorption of dietary iron. *Science*, *291*(5509), 1755–1759.
- McQuaid, J. B., Kustka, A. B., Oborník, M., Horák, A., McCrow, J. P., Karas, B. J., Zheng, H., Kindeberg, T., Andersson, A. J., Barbeau, K. A., & Allen, A. E. (2018). Carbonate-sensitive phytotransferrin controls high-affinity iron uptake in diatoms. *Nature*, *555*(7697), 534–537.

<https://doi.org/10.1038/nature25982>

Miethke, M., & Marahiel, M. A. (2007). Siderophore-Based Iron Acquisition and Pathogen Control. *Microbiology and Molecular Biology Reviews*, 71(3), 413–451. <https://doi.org/10.1128/MMBR.00012-07>

Miethke, Marcus, Hou, J., & Marahiel, M. A. (2011). The siderophore-interacting protein YqjH acts as a ferric reductase in different iron assimilation pathways of *Escherichia coli*. *Biochemistry*, 50(50), 10951–10964.

Mock, T., Samanta, M. P., Iverson, V., Berthiaume, C., Robison, M., Holtermann, K., Durkin, C., BonDurant, S. S., Richmond, K., Rodesch, M., Mock, T., Kallas, T., Samanta, M. P., Robison, M., Sussman, M. R., Holtermann, K., BonDurant, S. S., Huttlin, E. L., Cerrina, F., ... Rodesch, M. (2008). Whole-genome expression profiling of the marine diatom *Thalassiosira pseudonana* identifies genes involved in silicon bioprocesses. *Proceedings of the National Academy of Sciences*, 105(5), 1579–1584. <https://doi.org/10.1073/pnas.0707946105>

Moore, J. K., Doney, S. C., & Lindsay, K. (2004). Upper ocean ecosystem dynamics and iron cycling in a global three-dimensional model. *Global Biogeochemical Cycles*, 18(4), 1–21. <https://doi.org/10.1029/2004GB002220>

Moosburner, M. A., Gholami, P., McCarthy, J. K., Tan, M., Bielinski, V. A., & Allen, A. E. (2020). Multiplexed Knockouts in the Model Diatom *Phaeodactylum* by Episomal Delivery of a Selectable Cas9. *Frontiers in Microbiology*, 11(January), 1–13. <https://doi.org/10.3389/fmicb.2020.00005>

Muller, G., & Raymond, K. N. (1984). Specificity and mechanism of ferrioxamine-mediated iron transport in *Streptomyces pilosus*. *Journal of Bacteriology*, 160(1), 304–312. <https://doi.org/10.1128/jb.160.1.304-312.1984>

Nguyen, M., Ekstrom, A., Li, X., & Yin, Y. (2015). HGT-finder: A new tool for horizontal gene transfer finding and application to *Aspergillus* genomes. *Toxins*, 7(10), 4035–4053. <https://doi.org/10.3390/toxins7104035>

Nymark, M., Sharma, A. K., Sparstad, T., Bones, A. M., & Winge, P. (2016). A CRISPR/Cas9 system adapted for gene editing in marine algae. *Scientific*

Reports, 6(April), 24951. <https://doi.org/10.1038/srep24951>

Ohgami, R. S., Campagna, D. R., Greer, E. L., Antiochos, B., McDonald, A., Chen, J., Sharp, J. J., Fujiwara, Y., Barker, J. E., & Fleming, M. D. (2005). Identification of a ferrireductase required for efficient transferrin-dependent iron uptake in erythroid cells. *Nature Genetics*, 37(11), 1264.

Patel, P., Song, L., & Challis, G. L. (2010). Distinct extracytoplasmic siderophore binding proteins recognize ferrioxamines and ferricoelichelin in *Streptomyces coelicolor* A3 (2). *Biochemistry*, 49(37), 8033–8042.

Philpott, C. C., & Protchenko, O. (2008). Response to iron deprivation in *Saccharomyces cerevisiae*. *Eukaryotic Cell*, 7(1), 20–27.

Price, N. M., Harrison, G. I., Hering, J. G., Hudson, R. J., Nirel, P. M. V., Palenik, B., & Morel, F. M. M. (1989). Preparation and Chemistry of the Artificial Algal Culture Medium Aquil. *Biological Oceanography*, 6(5–6), 443–461. <https://doi.org/10.1080/01965581.1988.10749544>

Pruitt, K. D., Tatusova, T., & Maglott, D. R. (2006). NCBI reference sequences (RefSeq): a curated non-redundant sequence database of genomes, transcripts and proteins. *Nucleic Acids Research*, 35(suppl_1), D61–D65.

Raven, J. A., & Kübler, J. E. (2002). New light on the scaling of metabolic rate with the size of algae. *Journal of Phycology*, 38(1), 11–16.

Roberts, A. A., Schultz, A. W., Kersten, R. D., Dorrestein, P. C., & Moore, B. S. (2012). Iron acquisition in the marine actinomycete genus *Salinispora* is controlled by the desferrioxamine family of siderophores. *FEMS Microbiology Letters*, 335(2), 95–103. <https://doi.org/10.1111/j.1574-6968.2012.02641.x>

Rue, E. L., & Bruland, K. W. (1995). Complexation of iron (III) by natural organic ligands in the Central North Pacific as determined by a new competitive ligand equilibration/adsorptive cathodic stripping voltammetric method. *Marine Chemistry*, 50(1–4), 117–138.

Schalk, I. J., Yue, W. W., & Buchanan, S. K. (2004). Recognition of iron-free siderophores by TonB-dependent iron transporters. *Molecular Microbiology*, 54(1), 14–22.

- Schallenberg, C., Davidson, A. B., Simpson, K. G., Miller, L. A., & Cullen, J. T. (2015). Iron(II) variability in the northeast subarctic Pacific Ocean. *Marine Chemistry*, *177*, 33–44. <https://doi.org/10.1016/j.marchem.2015.04.004>
- Shaked, Y., Kustka, A. B., Morel, F. M. M., & Erel, Y. (2004). Simultaneous determination of iron reduction and uptake by phytoplankton. *Limnology and Oceanography: Methods*, *2*(11), 137–145.
- Shaked, Y., & Lis, H. (2012). Disassembling iron availability to phytoplankton. *Frontiers in Microbiology*, *3*, 123.
- Singh, A., Kaur, N., & Kosman, D. J. (2007). The metalloreductase Fre6p in Fe-efflux from the yeast vacuole. *Journal of Biological Chemistry*, *282*(39), 28619–28626.
- Smith, S. R., Gillard, J. T. F., Kustka, A. B., McCrow, J. P., Badger, J. H., Zheng, H., New, A. M., Dupont, C. L., Obata, T., Fernie, A. R., Allen, A. E., Martin, J., Fitzwater, S., Kolber, Z., Barber, K., Coale, S., Fitzwater, S., Greene, R., Johnson, K., ... Allen, A. A. E. (2016). Transcriptional Orchestration of the Global Cellular Response of a Model Pennate Diatom to Diel Light Cycling under Iron Limitation. *PLOS Genetics*, *12*(12), e1006490. <https://doi.org/10.1371/journal.pgen.1006490>
- Stintzi, A., Barnes, C., Xu, J., & Raymond, K. N. (2000). Microbial iron transport via a siderophore shuttle: a membrane ion transport paradigm. *Proceedings of the National Academy of Sciences of the United States of America*, *97*(20), 10691–10696. <https://doi.org/10.1073/pnas.200318797>
- Strzepek, R. F., Maldonado, M. T., Hunter, K. A., Frew, R. D., & Boyd, P. W. (2011). Adaptive strategies by Southern Ocean phytoplankton to lessen iron limitation: Uptake of organically complexed iron and reduced cellular iron requirements. *Limnology and Oceanography*, *56*(6), 1983–2002. <https://doi.org/10.4319/lo.2011.56.6.1983>
- Sunda, W. G., Price, N. M., & Morel, F. M. M. (2005). Trace metal ion buffers and their use in culture studies. *Algal Culturing Techniques*, *4*, 35–63.
- Sunda, W., & Huntsman, S. (2003). Effect of pH, light, and temperature on Fe-EDTA chelation and Fe hydrolysis in seawater. *Marine Chemistry*, *84*(1–2),

35–47.

- Sutcliffe, I. C., & Russell, R. R. (1995). Lipoproteins of gram-positive bacteria. *Journal of Bacteriology*, *177*(5), 1123.
- Suzuki, N., Miller, G., Morales, J., Shulaev, V., Torres, M. A., & Mittler, R. (2011). Respiratory burst oxidases: the engines of ROS signaling. *Current Opinion in Plant Biology*, *14*(6), 691–699.
- Timmermans, K. R., Van Der Wagt, B., Veldhuis, M. J. W., Maatman, a., & De Baar, H. J. W. (2005). Physiological responses of three species of marine pico-phytoplankton to ammonium, phosphate, iron and light limitation. *Journal of Sea Research*, *53*, 109–120.
<https://doi.org/10.1016/j.seares.2004.05.003>
- Törönen, P., Medlar, A., & Holm, L. (2018). PANNZER2: a rapid functional annotation web server. *Nucleic Acids Research*, *46*(W1), W84–W88.
- Tovar-Sanchez, A., Sañudo-Wilhelmy, S. A., Garcia-Vargas, M., Weaver, R. S., Popels, L. C., & Hutchins, D. A. (2003). A trace metal clean reagent to remove surface-bound iron from marine phytoplankton. *Marine Chemistry*, *82*(1–2), 91–99.
- Traxler, M. F., Seyedsayamdost, M. R., Clardy, J., & Kolter, R. (2012). Interspecies modulation of bacterial development through iron competition and siderophore piracy. *Molecular Microbiology*, *86*(3), 628–644.
- Turnšek, J., Brunson, J. K., Deerinck, T. J., Horák, A., Bielinski, V. A., & Allen, A. E. (2019). Phytotransferrin endocytosis mediates a direct cell surface-to-chloroplast iron trafficking axis in marine diatoms. *BioRxiv*, 1–93.
- Vraspir, J. M., & Butler, A. (2009). Chemistry of marine ligands and siderophores. *Annual Review of Marine Science*, *1*, 43–63.
- Wells, M. L. (1999). Manipulating iron availability in nearshore waters. *Limnology and Oceanography*, *44*(4), 1002–1008.
<https://doi.org/10.4319/lo.1999.44.4.1002>
- Wells, M. L., & Trick, C. G. (2004). Controlling iron availability to phytoplankton

in iron-replete coastal waters. *Marine Chemistry*, 86(1–2), 1–13.
<https://doi.org/10.1016/j.marchem.2003.10.003>

Weyman, P. D., Beerli, K., Lefebvre, S. C., Rivera, J., McCarthy, J. K., Heuberger, A. L., Peers, G., Allen, A. E., & Dupont, C. L. (2015). Inactivation of *Phaeodactylum tricornutum* urease gene using transcription activator-like effector nuclease-based targeted mutagenesis. *Plant Biotechnology Journal*, 13(4), 460–470. <https://doi.org/10.1111/pbi.12254>

Xu, G., Martinez, J. S., Groves, J. T., & Butler, A. (2002). Membrane affinity of the amphiphilic marinobactin siderophores. *Journal of the American Chemical Society*, 124(45), 13408–13415.

Yoshinaga, R., Niwa-Kubota, M., Matsui, H., & Matsuda, Y. (2014). Characterization of iron-responsive promoters in the marine diatom *Phaeodactylum tricornutum*. *Marine Genomics*, 16(1), 1–8.
<https://doi.org/10.1016/j.margen.2014.01.005>

Yun, C. W., Bauler, M., Moore, R. E., Klebba, P. E., & Philpott, C. C. (2001). The Role of the FRE Family of Plasma Membrane Reductases in the Uptake of Siderophore-Iron in *Saccharomyces cerevisiae*. *Journal of Biological Chemistry*, 276(13), 10218–10223. <https://doi.org/10.1074/jbc.M010065200>

Zhang, X., Krause, K. H., Xenarios, I., Soldati, T., & Boeckmann, B. (2013). Evolution of the Ferric Reductase Domain (FRD) Superfamily: Modularity, Functional Diversification, and Signature Motifs. *PLoS ONE*, 8(3).
<https://doi.org/10.1371/journal.pone.0058126>